Computer Aided Optimization of Tube Hydroforming Processes

By

Pinaki Ray, B.Eng.

This thesis is submitted to Dublin City University as the fulfilment of the requirement for the award of the degree of

Doctor of Philosophy

Supervisor: Dr Bryan J. Mac Donald, B.Eng. M.Sc. Ph.D.

Centre for Intelligent Design Engineering Analysis and Simulation

School of Mechanical and Manufacturing Engineering
Dublin City University

March 2005

DECLARATION

I hereby certify that this material, which I now submit for assessment on the programme of study leading to the award of *Doctor of Philosophy*, is entirely my own work and has not been taken from the work of others save and to the extent that such work has been cited and acknowledged with in the text of my work.

Signed: Pinaki Ray Date: 21/04/05

Pinaki Ray
ID: 51178672

Acknowledgements

There are many individuals who have assisted me during my research study. I would like to thank you all.

In particular, I would like to acknowledge the contributions of Dr Bryan J. Mac Donald for his supervision, guidance, help and his constructive suggestions and comments. I am indebted to him for the moral support extended to me.

I would like to thank the academic staff for any help they gave me over the course of my work, especial thanks to Prof M S J Hashmi (Head of School, School of Mechanical and Manufacturing Engineering). I am especially grateful to Mr Liam Domnican and Mr Keith Hickey for their technical support and help throughout this work. I wish to thank all of my fellow postgraduate students with in Dublin City University for their support and friendship.

Special thanks are due to my parents Mr Bechu Ram Ray and Mrs Ina Ray, my sisters Ms Somali Ray, Dr Mrs Chaitali Ray, my brother-in-law Dr Amit Neogi and, my wife Mrs Panchali Ghosh for their endless encouragement and support during my studies, without which I may not have got this far.

Computer Aided Optimization of Tube Hydroforming Processes

Pinaki Ray B.Eng.

ABSTRACT

Tube hydroforming is a process of forming closed-section, hollow parts with different cross sections by applying combined internal hydraulic forming pressure and end axial compressive loads or feeds to force a tubular blank to conform to the shape of a given die cavity. It is one of the most advanced metal forming processes and is ideal for producing seamless, lightweight, near net shape components. This innovative manufacturing process offers several advantages over conventional manufacturing processes such as part consolidation, weight reduction and lower tooling and process cost. To increase the implementation of this technology in different manufacturing industries, dramatic improvements for hydroformed part design and process development are imperative. The current design and development of tube hydroforming processes is plagued with long design and prototyping lead times of the component.

The formability of hydroformed tubular parts is affected by various physical parameters such as material properties, tube and die geometry, boundary conditions and process loading paths. Finite element simulation is perceived by the industry to be a cost-effective process analysis tool and has the capability to provide a greater insight into the deformation mechanisms of the process and hence allow for greater product and process optimization. Recent advances in the non-linear metal forming simulation capabilities of finite element software have made simulation of many complex hydroforming processes much easier. Although finite element based simulation provides a better understanding of the process, trial-and-error based simulation and optimization becomes very costly for complex processes. Thus, powerful intelligent optimization methods are required for better design and understanding of the process.

This work develops a better understanding of the forming process and its control parameters. An experimental study of 'X' and 'T'-branch type tube hydroforming was undertaken and finite element models of these forming processes were built and subsequently validated against the experimental results. Furthermore these forming processes were optimized using finite element simulations enhanced with numerical optimization algorithms and with an adaptive process control algorithm. These new tools enable fast and effective determination of loading paths optimized for successful hydroforming of complex tubular parts and replace trial-and-error approaches by a more efficient customized finite element analysis approach.

Keywords: Tube hydroforming, Finite element analysis, LS-DYNA, Forming load paths, Optimization, Adaptive process control

Chapter 4: Part And Process Design Consideration Of Tube Hydroforming Components

Chapter 5: **Determine Loading Paths Using Finite Element Simulations and Optimization Technique**

Chapter 6: **Determination of Feasible Forming Loading Paths Using Adaptive Simulation Concepts**

Chapter 8: **Conclusions And Recommendation For Future Work**

Appendix A

Appendix B

Appendix C

Appendix D

Nomenclature

Symbol	Definition	Dimension
c	Sonic wave propagation velocity	m/s
l	Element characteristic length	m
t	Time	s
E	Young's modulus	N/m^2
ε	Strain	-
ρ	Density	Kg/m^3
ν	Poisson's ratio	-
σ_y	Yield strength	N/m^2
	(Used in Optimization Simulation)	
f	Objective function	-
F	Feed	mm
g	State variable	-
h	State variable	-
n	Number of design variable	-
P	Pressure	N/m^2
T	Simulation time	m-s
x	Design variable	-
w	State variable	-
α_i	Tolerance limit	-
β_i	Tolerance limit	-
γ_i	Tolerance limit	-
	(Used in Adaptive Simulation)	
f	Feed	mm
Δf	Incremental feed	mm
p	Pressure	N/m^2
Δp	Incremental pressure	N/m^2
t	Time	m-s
Δt	Incremental time	m-s
V_n	Normal velocity	mm/m-s
Δε	Strain difference	-

List of Figures

List of Tables

Chapter 1: Introduction, Research Problem Statement and Objective

1.1. Introduction

Hydroforming is a widely used industrial process, which uses hydraulic pressure to deform a metallic sheet or tube into complex shapes. Depending upon the forming process and its application, it can be classified into two categories.

1) Sheet Hydroforming
2) Tube Hydroforming

In sheet hydroforming process, a metallic sheet is forced into a female die cavity hydraulically under pressure from a pump or by press action. The hydraulic pressure on the sheet acts as a male punch, which deforms the sheet to the required shape of the part or the forming die cavity. Whereas in case of a tube hydroforming process, a metallic tube is subjected to internal forming pressure using some hydraulic fluid (water or oil) to deform it plastically to the shape of the forming die cavity. Depending upon application, the tube may be subjected to internal hydraulic pressure simultaneously with end axial feed to push the material in the deforming zone.

The research study detailed here deals with tube hydroforming processes and will be discussed in further detail. This process is a relatively new technology among all metal tube forming processes. It is a process of forming closed section, hollow parts with different cross-sections by applying an internal hydraulic pressure and sometimes additional axial compressive loads or axial feed to force a tubular blank to conform to the shape of a given die cavity. The main advantages of this process (fig 1.1.1) over conventional manufacturing processes such as stamping, bending, welding etc are:

a.) Reduction of the weight of a component efficiently by consolidation of parts
b.) Reduction in associated tools and process cost
c.) Reduction in number of secondary operations
d.) Reduction in scrap
e.) Significant reduction in spring back effects
f.) Increased structural stiffness
g.) Improvement in manufacturing repeatability and dimensional stability

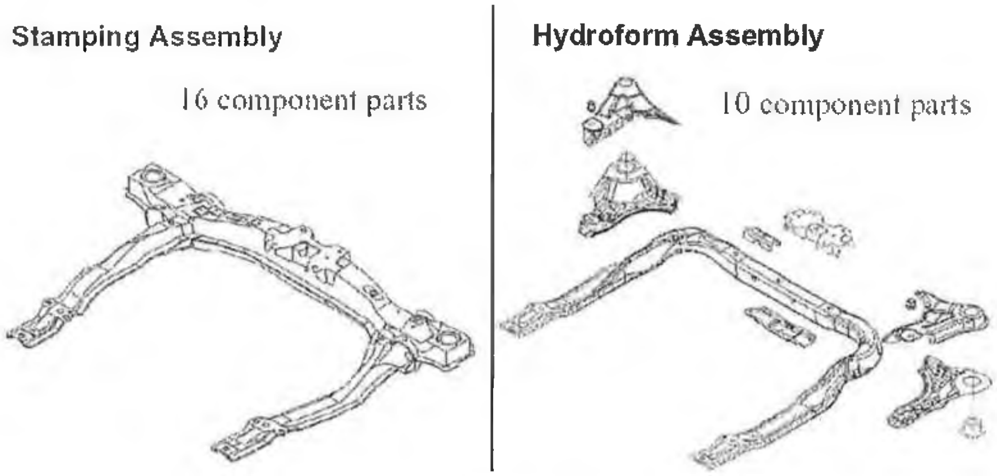

Fig 1.1.1 Advantages of hydroforming over conventional manufacturing process [1]

Due to the various advantages of this process over conventional manufacturing processes and with advancement in computer control and high-pressure hydraulic systems, it is now widely used in manufacture of various near-net shaped tubular components of different configurations such as T-branches, X-branches and various angular shapes, used in pharmaceutical industries and for household appliances. The major application of the process is in the automotive (fig 1.1.2) and aerospace industries for manufacture of components in automotive chassis systems, sub-frames, power trains (stepped hollow shafts, engine camshaft), exhaust systems (exhaust manifolds), and body structures.

Fig 1.1.2 Automotive application of hydroforming- A. roof headers, B. instrument panel support, C. radiator support, D. engine cradles, E. roof rails, F. frame rails [2]

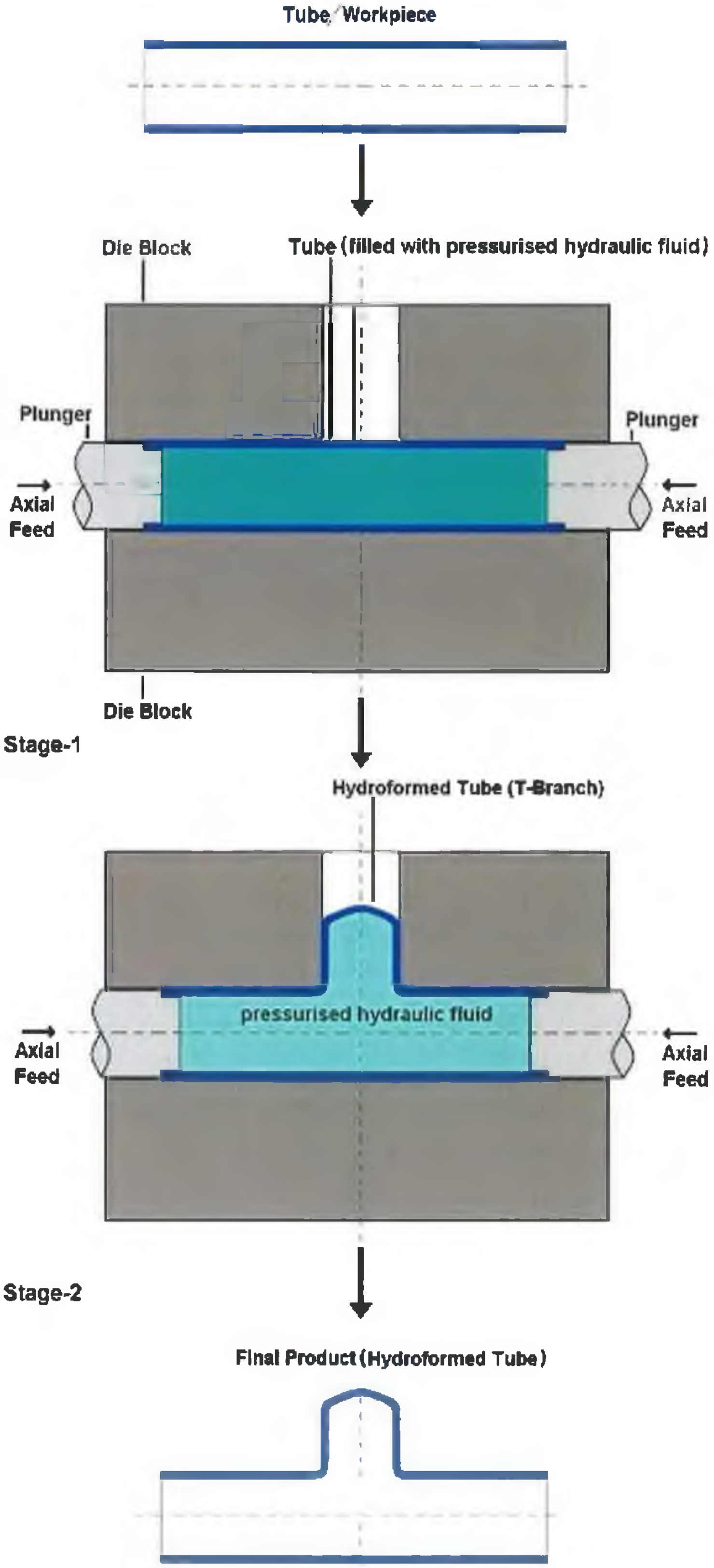

Fig 1.1.3 Setup of a typical tube hydroforming process with different stages of operation

Fig 1.1.3 shows a schematic diagram of a set-up of a simple tube hydroforming process with different stages of the process, which involves both internal hydroforming pressure and end axial feed. In this process (stage-1) a tubular blank (work piece) is placed between the two die halves (upper and lower dies), the dies are closed and the end plungers are advanced towards the tube, then the tube is filled with hydraulic fluid and the plungers are further advanced slightly to seal the tube ends. After this sealing, a controlled internal hydroforming pressure and end axial feeds are applied to deform the tube into the shape of the die cavity (stage-2).

In the process, if the pressure is to high with respect to the end axial feed, then there is a chance of excessive thinning of the tube wall resulting in bursting of the tube. Conversely, if the end axial feed is too high with respect to the internal pressure then there is a chance of formation of a wrinkle, which can subsequently lead to buckling of the tube. Thus, bursting, wrinkling and buckling are the main failure criteria for any tube hydroforming process. For a successful application of the process (i.e. without any kind of failure) the prior knowledge of the process parameters (i.e. the loading path- reltion between forming pressure and end axial feed) are of academic interest. Thus, an optimum loading condition that would avoid all these instabilities and failure criteria and which will enable higher deformations resulting in a more efficient process should be of interest.

The hydroforming process is a highly complicated process to analyse theoretically and hence, to date, theoretical analysis methods for plastic deformation of the process have resulted in limited understanding of the actual deformation mechanism of the process. Finite element simulation and numerical analysis have the potential to provide a much deeper understanding of the process and hence allow for better design of the process equipment, tools and end products.

1.1.1. Metal forming analysis using finite element methods

The finite element method came of age in the early 1960's with the replacement of analog with digital computers and the development of first commercial finite element analysis code. The introduction of the finite element method to plasticity problems dates back to late 1960's when an elastic – plastic constitutive equation was incorporated in the standard solution routine that had been used in the solution of elasticity problems. At this early stage, the application was confined to the contained elastic-plastic deformation where the plastic strain is of the order of 0.1%. The extension to the large strain regime was achieved in the late 1970's when limited nonlinear solvers were developed and made available. With the continuous development in computer technology, hardware and softwares in the subsequent years, today very advanced and robust implicit and explicit finite element analysis codes and packages are available, using which most complicated and complex engineering problems starting from simple linear structural analysis to complex non-linear vehicle crash problems can be analysed. One of the most important applications of these non-linear finite element codes is in analysis and in-depth study of various complex metal forming processes for which proper analytical solutions or deformation theories are not readily available. In the recent years computer aided engineering tools and computer simulations have been used for various aspects of metal forming processes, such as formability assessment, die design, product feasibility evaluation, material selection and process design. Apart from metal forming applications, computer aided engineering and simulation is also increasingly being used in hydroforming applications. Finite element simulations of most of the metal forming processes are quite complex as the processes are highly non-linear in nature. This is mainly due to their: physical (viscoplasticity, fracture), geometrical (large displacement and large deformation) and contact/friction factors which affects the process. Explicit finite element codes have much better capabilities to handle such kind of non-linear behaviours exhibited by the metal forming processes. Hydroforming operations usually involve complex process setup and multi-stage forming operations. Thus, with computer aided simulation and analysis, and by using some standard empirical metal forming and plasticity theories, a better understanding of the physical deformation mechanism of the process has resulted.

1.2. Research problem statement and objectives

The tube hydroforming process is a complex manufacturing process. As stated above, due to the large plastic deformation associated with the process and with existence of complex contact between the tube and die, the behaviour of the process is highly non-linear in nature. Due to these complexities the theoretical studies to date have produced limited understanding of its deformation mechanics and characteristics. To achieve better output, the process requires a proper combination of part design and selection of proper material and process boundary conditions (i.e. load paths- forming pressure vs. end axial feed, die and blank contact surface friction). In terms of hydroformability, the process is highly dependent on tube material properties, tube and die geometry, complex die-tube interface lubrication, and process parameters (i.e. loading paths). Finite element analysis along with experimental validation provides a better understanding of the process and its optimization. For successful application of the process, the proper knowledge and understanding of selection of suitable material, component and tool geometries, process boundary conditions and the loading paths, which are the major factors deciding the final performance of the process are quite important. The objectives of this research work are:

- To perform an experimental study of a typical tube hydroforming processes (T and X-branch forming) and its deformation mechanics and subsequently build finite element simulation models of the process using LS-DYNA explicit finite element code and hence validate the finite element simulation results against the experimental observations.

- To study the effects of varying geometric parameters of the die and blank, and the process control parameters on the tube hydroforming process performance.

- To develop methodologies for design and optimization of the loading paths by maximizing the part expansion, avoiding all failure modes. The methodologies will utilise a.) Systematic explicit finite element simulations and analysis enhanced with numerical optimization techniques based on 'sub-problem approximation optimization method' and, b.) Adaptive simulation method using a 'fuzzy logic' based control program coupled with the LS-DYNA finite element code.

1.3. Thesis Organization

The structure of this thesis is as follows:

Chapter 1: Introduction, Research Problem Statement and Objective

Chapter 2: Literature Survey (This chapter details the past research work and studies done on tube hydroforming processes)

Chapter 3: Experimental Study and Finite Element Analysis of 'X' and 'T'- Branch Tube

Hydroforming Processes (This chapter details experimental studies and finite element analysis of simple tube hydroforming processes using LS-DYNA 3D explicit finite element code)

Chapter 4: Part and Process Design Consideration of Tube Hydroforming Components. (This chapter details effects of various finite element parameters, physical geometric parameters and process parameters on the hydroforming process and their importance in design and analysis of the process)

Chapter 5: Determination of Optimal Loading Paths Using Finite Element Simulations and Optimization Technique. (This chapter details the use of an optimization tool to calculate an optimal load path of a tube hydroforming process)

Chapter 6: Determination of Feasible Forming Loading Paths Using Adaptive Simulation Concepts. (This chapter details a customized developed adaptive control program using fuzzy logic to calculate a feasible forming load path of any tube hydroforming process)

Chapter 7: Discussions

Chapter 8: Conclusions and Recommendation for Future Work

1.4. Summary of Chapter 1

This chapter introduces the tube hydroforming processes and its major application in engineering and automotive industries, and its advantages over conventional manufacturing process. It illustrates how further understanding of the process is required for better design, optimization and control of the process. The application of finite element methods for analysis and study of metal forming processes with an emphasis on the hydroforming process is also described.

Chapter 2: Literature Survey

2.1. Introduction

The objective of this chapter is to examine and highlight previous work, similar or related to this work done by various researchers and to develop a basic understanding of tube hydroforming processes. There are many experimental studies, theoretical studies based on empirical relations, thin shell theory and plasticity flow laws, and numerical/finite element simulation studies available on simple tube hydroforming processes. A limited number of studies on numerical optimization of the process parameters and development of the process control mechanism for models with simple geometric shapes have also been reported. However, more complex tube hydroforming processes, particularly hydroforming of asymmetric components, have received little attention.

2.2. Overview of development of bulge forming and tube hydroforming technology

Although the tube hydroforming process is relatively a new manufacturing technology, which has gained much importance in the manufacturing and automotive industries in recent years, the basic development of the process started at an early stage. In early 1939 Grey et al [3] described a tube hydroforming process for manufacture of seamless metal fittings with tube branches such as 'T' and 'X' shapes. The machine used for manufacture of the components, allowed control of the internal hydraulic pressure and tube end axial feed/load to avoid rupture of the tube blank. The process involved placing a tubular blank in-between two die halves, which were then clamped together and a compressive load was then applied to provide an axial feed to the tube ends via plunger, which entered through the two die holes. The internal hydroforming pressure was applied via a liquid through a drilled hole in one of the plungers. This combination of axial feed and internal pressure pushed the tube wall into the die recess thus forming the component. In subsequent years Crawford [4] described an applied process whereby components were formed by pouring a soft metal (a bismuth-lead-tin alloy) into a copper tube and subsequently applying an endwise pressure to both the filler material and the tube while they were restrained in a die. The process was different from the process described by reference [3] in the sense that the bulging medium in this case was solid. This process produced well-shaped components however had the disadvantage of requiring the filler material to be added before and removed after the process. This was more time consuming than using a liquid bulging medium, but had the advantage of a reduction in tooling costs due to the elimination of the need for hydraulic pumps, seals etc. An improvement in the process was patented by Stalter [10], which increased productivity of the process and removed the disadvantages caused by shrinking of the filler material on pouring. Further Remmerswaal and Verkaik et al [9] described a method of bulge forming axisymmetric conical products from deep drawn aluminium cylindrical blanks using internal hydraulic pressure and Ogura and Ueda [11] described procedures to form axisymmetric and asymmetric components by simultaneous application of axial compressive load and internal hydraulic pressure using carbon steel. Typical components formed were T-branch, X-branch, component with four branches and bicycle hubs.

In a separate development Al-Qureshi et al. [12] described an experimental process for axisymmetrically bulging thin walled metal tubes with a new solid bulging medium. A polyurethane rod was used to apply the internal pressure and the friction between the tube and the rod provided the axial load on the tube.

In the recent years various scholars have consolidated the details of the basics of tube hydroforming process and its industrial application. Dohmann and Hartl [40,42], Ahmetoglu and Altan [53], Koç and Altan [58], Lücke et al [59] detailed an overview of the fundamental principles of hydroforming processes and their variants with typical applications of the process for manufacture of automotive components and other household components, highlighting the typical failure modes of the process such as wrinkling, buckling and bursting and the effects of blank material properties, lubrication , process control on the product design and quality.

From the above studies, the main modes of failure were identified as:

- Failure due to bursting is caused due to excessive wall thinning
- Failures due to buckling and wrinkling are caused due to axial instability

2.3. Experimental and analytical studies

Further to the development of the process detailed in section 2.2, different researchers reported various experimental and analytical approaches to the process. Al-Qureshi [13] experimentally compared bulge forming using a polyurethane rod with hydraulic bulge forming. The observation showed that greater circumferential expansion and longitudinal drawing was possible with the use of polyurethane as the bulging medium. Woo [18] presented a numerical solution for analysing tube bulging under axial compressive load and internal hydraulic pressure assuming that the whole length of the bulged tube was in tension and effectively free bulging took place. Experimental results showed reasonable agreement with theoretical results when stress-strain properties used obtained from biaxial tests were used for calculations. Limb et al [14, 16] reported experimental analysis of tube hydroforming using combined axial load and internal hydraulic pressure for both axisymmetric and asymmetric (T-branch) components using various blank materials such as steel, annealed copper, aluminium and brass and with different blank geometries. The study detailed that the most satisfactory method of forming axisymmetric thin walled tubes was to increase the internal pressure as a step function with respect to the axial feed. In a separate presentation, Limb et al [15] also developed a theoretical analysis method for axisymmetric bulging of with axial force and indicated the manner in which the loading parameters i.e. the forming pressure should be applied during the process with respect to the axial load to obtain successful components. Fig 2.3.1 shows the geometry of the bulge and equation-1 states the relation between the forming pressure and geometric parameters of the bulge during forming.

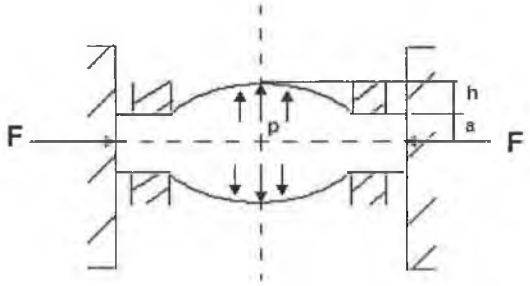

Fig 2.3.1 Geometry of the bulge [13]

$$\frac{pa}{Bt_0}=\left\{\ln\left(1+\frac{h}{a}\right)\right\}^n\left\{\frac{1}{2+{3nh}/{a}}+\frac{1}{1+n}\frac{\ln\left(1+{h}/{a}\right)}{\left(1+{h}/{a}\right)}\right\} \qquad (1)$$

Where, p is the internal forming pressure, B and n are constants, and t_0 is the initial tube wall thickness.

Further experimental work was reported by Kandil [17] in which brass, aluminium and copper tubes were axisymmetrically bulge formed under hydraulic pressure only. No axial compressive load was applied. The experimental results were used to derive empirical relationships between pressure, stress and the geometry of the die and tube. Sauer et al. [19] reported an experimental analysis of an axisymmetric tube bulging where both pressure and axial load was used. Further a computer program using a numerical technique, based on force equilibrium equations, stress-strain laws and buckling instability criteria for thin tubes was developed to determine the bulge shape where load increments (pressure and feed) were specified on a step-by-step basis for the forming operation. The study concluded that the results of the computer program and bulging experiments for 9 tube samples were in good agreement for axial forces, internal pressures and bulge radius. Woo and Lua [20] extended earlier theoretical work [18] by introducing anisotropy of the tube material and considering bulge forming using pressure load alone. In another work Woo [21] presented an experimental technique of bulge forming closed ended containers using combined axial load and internal hydraulic pressure from deep drawn tubular blanks, which in turn were formed out of circular sheet metal blanks.

Lukanov et al. [22] presented an experimental technique of bulge forming of a double T-branch from a singular tubular blank by combined axial compressive load and controlled internal hydraulic pressure. The experimental technique was quite similar to those described by Ogura and Ueda [11].

In a new development, Ragab [23] used a thermo-forming technique to form T-joint from tubular blanks of superplastic lead-tin alloy in which pressurised heated air was used to bulge the tubes in a specially made split die block. An approximate analysis was also given which enabled prediction of wall thickness of the formed component. This analysis was based on those applicable to the bulging of circular diaphragm into a cylindrical cavity and was found to be inadequate for predicting the thickness distribution around the branch of the T-joint.

Although in the early developments, tube hydroforming technique using liquid bulging medium was applied for manufacturing components with simple configuration, Ueda [25, 26] described a new method of manufacturing automotive differential gear casings from a straight tubular blank using hydroforming technology with a flexible tooling system. The forming process detailed was entirely different from conventional tube hydroforming process as in this case flexible dies (sliding dies) were used to apply the axial compressive loads. The details of the forming setup are shown in fig 2.3.2. The design had an advantage over the conventional forming method as in this case the frictional effects during the forming were minimum as there was no relative movement between the tube and die contact surfaces. In later years Dohmann and Klass [30] also described axisymmetric hydraulic bulging of tubes with sliding dies.

(a) *Conventional forming method*

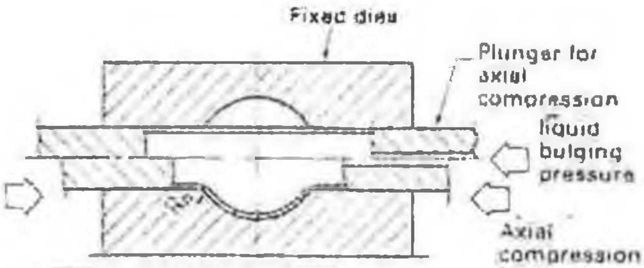

(b) *New bulge forming method*

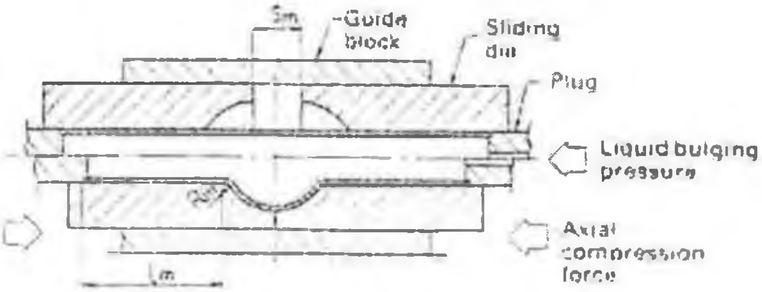

Fig 2.3.2 Flexible dies used for bulge forming [25, 26]

Hashmi [24] presented an approximate analysis for the prediction of wall thickness around the circumference (dome) for different branch heights of a T-branch component, formed due to internal hydroforming pressure and end axial compressive force. The analysis was developed based on the final geometry of the bulge (protrusion). For development of the theory it was assumed that the branch top at the final stage of forming maintain a constant radius of curvature, in other word the developed dome was assumed to be spherical in nature. The branch top thickness defined as a function of branch height was given as:

$$t = \frac{t_0}{\left[1+\left\{h\left(H^2-H_0^2\right)/H\left(H_0^2+R^2\right)\right\}\right]^2} \qquad (2)$$

Where, t is the final thickness, t_0 is the initial tube wall thickness, H and H_0 are the polar heights of the bulge at the final and initial stage, R is the internal radius of the tube (fig2.3.3 and fig 2.3.4)

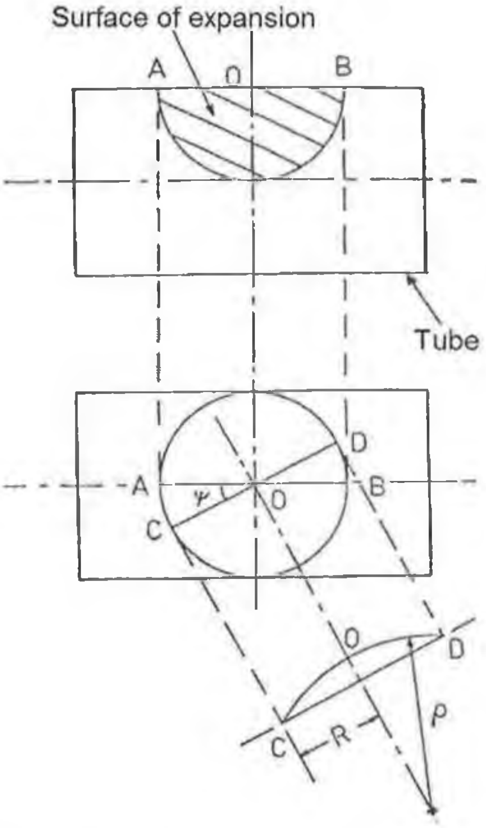

Fig 2.3.3 Part of the tubular blank subjected to bulge pressure [24]

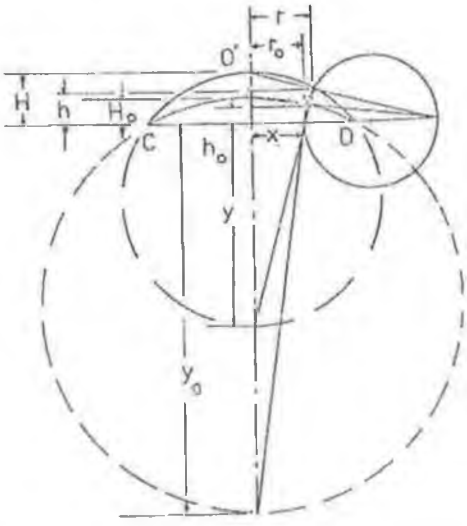

Fig 2.3.4 Geometrical mode of expansion during the initial stage of bulging [24]

In a separate presentation, Hashmi [27] reported an analytical method to predict height and thickness distributions of both axisymmetric and asymmetric (X-branch) hydroformed components. The analysis was based on the geometry of the formed bulge, however in the analysis an important process parameter (i.e. contact surface friction) was not considered which has a considerable effect on the final part expansion. Later, Hashmi and Crampton [29] compared experimental results with this analytical method and found that the analytical method generally overestimated the thickness of the formed components for the axisymmetric component and underestimated for the asymmetric component.

The use of a solid bulging medium such as polyurethane for tube hydroforming process described in section 2.2 is a relatively new bulge forming technique. Filho and Al-Qureshi [28] presented an experimental method of forming T-joints from straight tubes using a urethane rod. The deformation was achieved by using repetitive loading and unloading cycles and by varying the length of the urethane rod between cycles. A theoretical expression for total forming load prediction was also developed and compared with experimental results. Thiruvarudchelvan and Travis [33] described experiments to axisymmetrically bulge copper tubes using a urethane rod. Urethane rods of different hardness were used and the friction between the rod and tube was varied using different lubrication methods. Further, Thiruvarudchelvan [34,35] developed an approximate theory for predicting the initial yield pressure and final forming pressure required for bulging a metal tube using a urethane rod. The theory made use of experimentally determined friction characteristics and was compared with experimental results. Filho et al. [37] presented a theoretical analysis of bulge forming of a T-branch using an elastomer rod as the bulging medium. The equations were solved using the finite difference method to determine the axial compressive load required for the process.

Sheng and Tonghai [38] reported on experimental research on solid bulge forming of asymmetric components like T-branch using polyurethane. In addition to internal pressure and axial load, a counter pressure was used on the bulged section of the formed component. It was found that this method improved the stress state in the formed component. An upper bound analysis was used to estimate the total power requirements during the deformation process, which was basically the summation of plastic-deformation power, friction power, urethane-compression power and counter-pressure power.

2.3.1. Instabilities and failures in tube hydroforming

Due to the complex nature of the process, during bulge or hydroforming of tubes, an area of major concern is the onset of instability. Studies [42, 45,61,62] show that excessive amounts of either the pressure or axial loads relative to the other, causes instability of the process resulting in excessive thinning leading to bursting or on the contrary wrinkling and buckling. A great deal of research has been conducted in attempting to determine the onset of instability in tubes subjected to internal pressure and axial loads. Mellor [5] presented an analytical solution to determine the strain at instability of thin walled tubes subjected to internal pressure and independent axial compressive load. In the analysis, it was assumed that the circumferential to axial stress ratio remains constant and positive throughout the straining process and was shown that a material has greatest ductility when the ratio of the hoop stress to axial stress has the value one half. In a subsequent work, Jones and Mellor [8] experimentally showed that the theoretical solution in [5] was in good agreement with experimental results. Felgar [6] analysed instability of pressure vessels subjected to internal pressure and tensile axial load. Both thin and thick walled pressure vessels were examined for constant circumferential and axial stress ratio. When compared with experimental results, it was found that the theoretical prediction of instability pressure was accurate, but the predictions of instability strains were in disagreement with experimental results. Weil [7] theoretically analysed tensile instability of thin walled cylinders of finite length. The analytical results showed that burst pressures increases progressively as the length/diameter ratio of the cylinders is reduced from infinity to lower values.

The above instability studies were basically formulated on tensile instability of the tube. Various authors have also presented instabilities of tube subjected to compressive axial loads along with internal during forming of tube in case of hydroforming. The axial compressive load is one of the predominating factors, which initiate premature failures such as wrinkling and buckling in tube hydroforming processes. As indicated in section 2.3, the major failure modes in tube hydroforming processes are wrinkling, buckling and bursting (fig 2.3.5). Reliable failure detection methods for tube hydroforming processes are under investigation. However a reliable analysis method for the failure detection has not yet been established. Considering the bulging of thin walled tubes to be an example of sheet metal forming process [39], the failure detection methods used for sheet metal forming analysis (using forming limit diagram) can also be applied to hydroforming processes which gives an estimation of the failures [74].

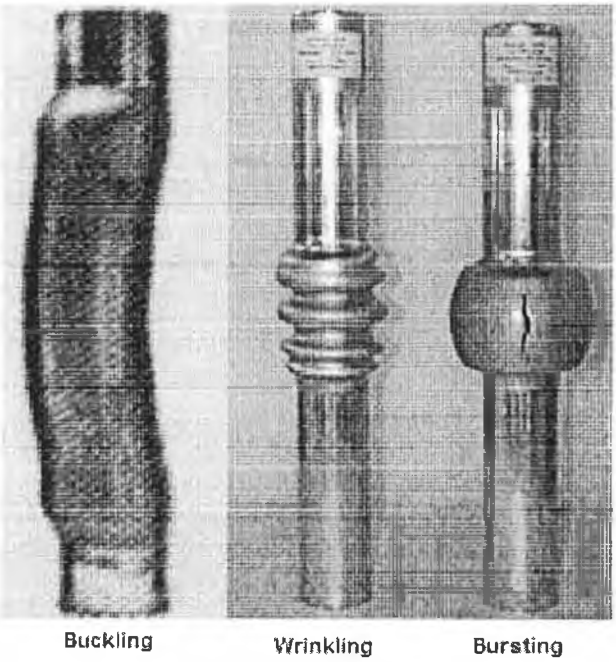

Fig 2.3.5 Failure modes of tube hydroforming processes [45]

The fracture mode of thin walled tube hydroforming processes can be well understood by considering the forming limit diagrams of sheet metal subjected to different stress conditions, which may be a combination of tensile and compressive stresses. Failure in sheet metal forming can be explained by considering the experimental strain analysis. Fig 2.3.6 shows a circular grid on a plane sheet, which is subjected to bi-axial stress (tensile) of different magnitude. Depending upon the magnitude of the stress the circle will deform to take the shape of an ellipse. Thus the principal strains developed on the sheet, assuming incompressibility can be defined as:

$$\varepsilon_1 = \ln\left(\frac{d_1}{d_0}\right),\ \varepsilon_2 = \ln\left(\frac{d_2}{d_0}\right),\ \varepsilon_3 = \ln\left(\frac{t}{t_0}\right) = -(\varepsilon_1 + \varepsilon_2) \qquad (3)$$

According to laws of pure proportional deformation, ε_2 can be defined in terms of ε_1, i.e. $\varepsilon_2 = -\beta\varepsilon_1$. From this different conditions of stretching of the sheet can be defined by considering various values of β (Fig 2.3.7). Further it can be shown how due to these different kind of loading the sheet will fail in different modes like shear fracture, tearing etc. [85]. Thus for various values of β there exist different points on the strain plots at which the sheet may fail, which is termed as the forming limit of the sheet, which is dependent on the initial thickness (t_0) of the sheet, strain hardening coefficient (n), anisotropic parameter (R) of the material [85]. For a sheet when all these points (forming limit) are joined together a resultant curve is formed which is termed as forming limit curve. Fig2.3.8 shows a typical forming limit curve on the same major and minor strain plot for a material with a set of material parameters (t_0, n, R).

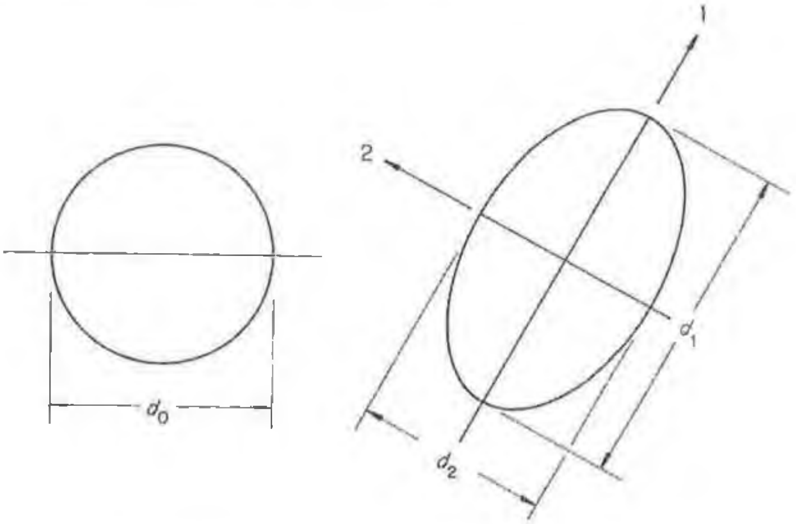

Fig 2.3.6 Deformation of a circle to an ellipse [85]

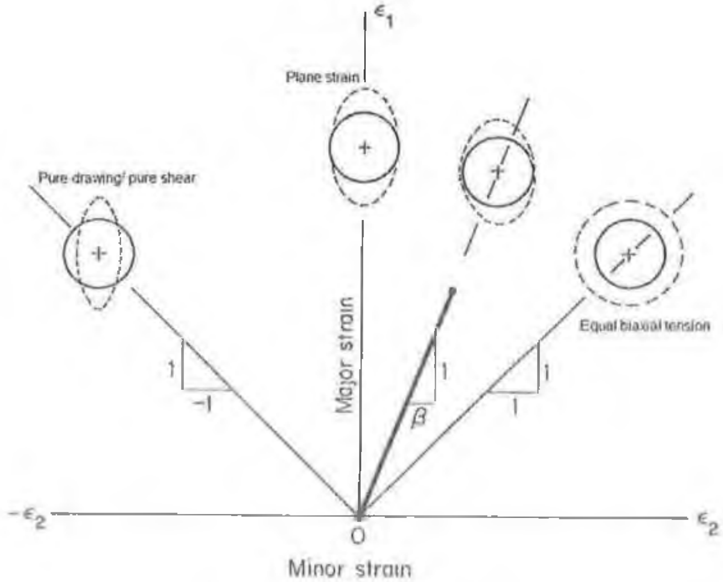

Fig 2.3.7 Graphical representation of pure, proportional large deformation in 2D strain space [85]

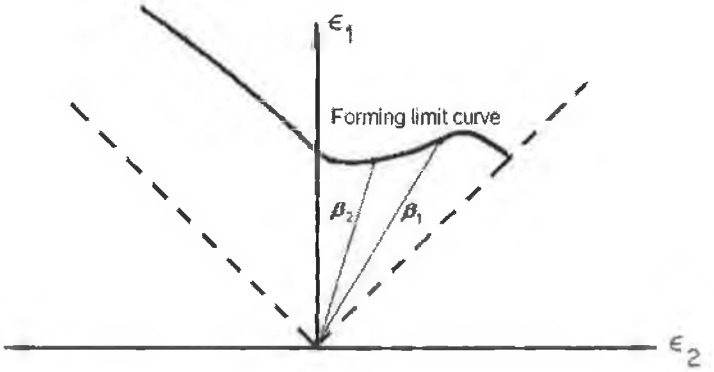

Fig 2.3.8 The forming limit curve [85]

On the forming limit diagram there exist spaces in which plastic deformation can be assumed to be safe. Fig 2.3.9 details a graphical representation of bi-axial major and minor true strains for thin walled sheet metal deformation with different regions with its failure types [85].

In a sheet metal forming process in order to detect the failure of the process it is important to first estimate the forming limit curve of the material in use for the forming process depending upon its material properties and wall thickness values. Thus for predicting the failure modes in a tube hydroforming process, the forming limit curve and forming limit diagram can be quite instrumental.

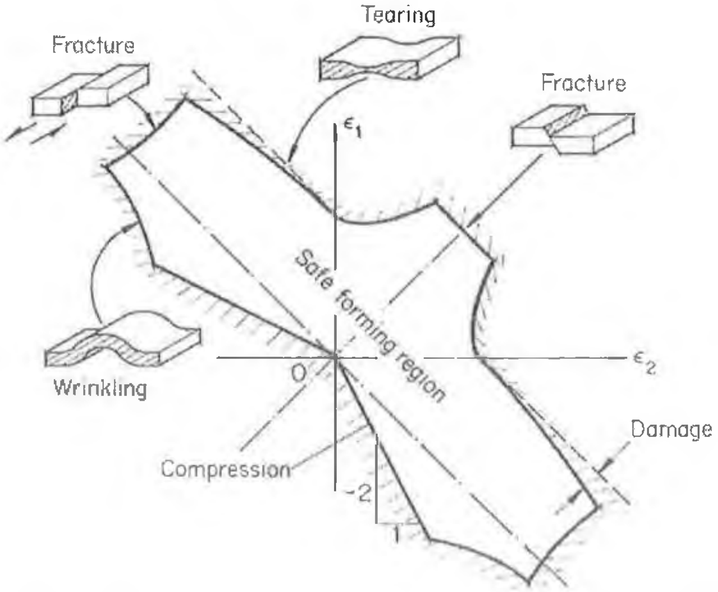

Fig 2.3.9 The various failure limits to a simple sheet forming (Forming limit diagram) [85]

Several authors [42, 45, 61, 62] have reported the typical failure modes of tube hydroforming processes such as wrinkling, buckling, bending, necking and bursting. Thus the knowledge of the feasible forming domain is of academic interest in design of tube hydroforming components and processes. Hutchinson et al [31, 32, 84] experimentally established a formability zone (fig 2.3.10) for forming of T and X-branches from three different blank materials-copper, steel and aluminium for different tube dimensions i.e. length, internal radius and wall thickness. Boudeau et al[68] used bulge tests to predict the bursting failure of a sheet subjected to hydraulic pressure, in a different presentation [74] the same authors used the concepts of forming limit diagram to predict bursting failure of copper brass tubes subjected to asymmetric expansion.

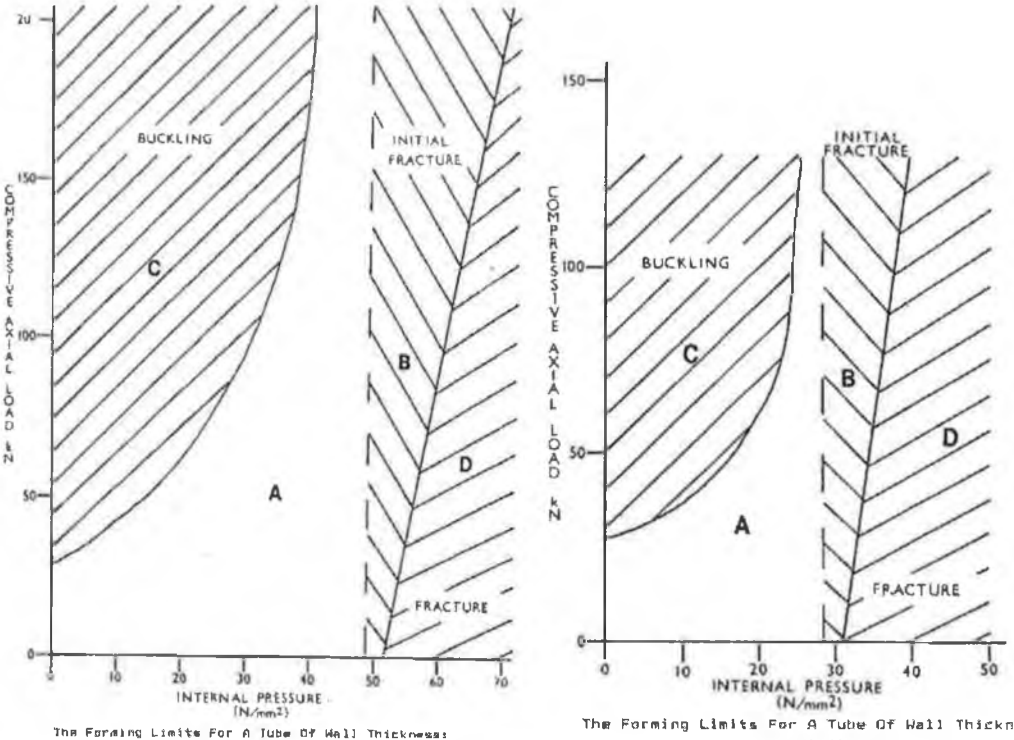

The Forming Limits For A Tube Of Wall Thickness: t_o = 1.32 mm.

The Forming Limits For A Tube Of Wall Thickness: t_o = 1.03 mm.

Fig 2.3.10 Forming limits of tubes with different wall thickness [84]

The process performance of a tube hydroforming depends on various factors which can be categorised as a.) process parameters, b.) material parameters, c.) tool parameters and, d.) process limits. The loading conditions represents the process parameters i.e. the effect of forming pressure and end feed, the material parameters are represented by the mechanical properties of the tube such as Young's modulus, yield strength and the anisotropic behaviour, the tool parameters are represented by the shape and dimensions of the die and the contact surface lubrication conditions and failure modes i.e. wrinkling, buckling and bursting represent the process limits. Thus for success of the process in other terms to avoid all failure modes it is important to have proper understanding of all these parameters and its effects on the process.

Tirosh et al. [39] described an upper bound analysis of axisymmetric bulging of tubes by combined internal pressure and axial compression. Using this formulation, the authors experimentally attempted to determine an optimum loading pattern to give maximum bulging strain without early failure by buckling or necking.

Nefussi and Combescure [67] highlighted the plastic instability and buckling failure criteria of an axisymmetric tube hydroforming and also analytically examined the possibility of plastic instability due to buckling. Koc and Altan [61] also analytically determined the forming limits of a tube hydroforming process using known plasticity, membrane and thin-thick walled tube theories. Using these theories, simple models to predict buckling, wrinkling and bursting were developed for an axisymmetric free forming condition with combined axial compressive loads and internal pressure. The critical axial compressive stress and force for wrinkling was formulated as:

$$\sigma_{cr} = \frac{1}{\sqrt{3\left(1-\nu^2\right)}} E_t \frac{t}{r} \qquad (4)$$

$$F_{cr} = \frac{2\pi}{\sqrt{3\left(1-\nu^2\right)}} E_t t^2 \qquad (5)$$

Where, E_t and ν are the tangent modulus and Poisson's ratio of the material, t is the wall thickness, r is the tube radius. It can be seen that the above equations were independent of the tube length, which is one of the critical factor for buckling. Similarly the critical or instability strain at bursting was given as:

$$\varepsilon = \frac{2n\sqrt{1-\alpha+\alpha^2}}{\left(1+\alpha\right)} \qquad (6)$$

Subjected to the plastic material-flow law is assumed to be $\sigma = K\bar{\varepsilon}^n$ (power law plasticity)

In a separate development Kim and Kim [62] developed analytical models to determine the forming limits of an axisymmetric tube hydroforming process and demonstrated how the loading path and material parameters such as strain hardening coefficient (n), anisotropic parameter (R) and tensile strength, influence the forming results. At different instability conditions, the critical bursting pressure (p_{cr}) was given by:

$$p_{cr} = \frac{\bar{\sigma}}{\bar{\varepsilon}_{\max}} \frac{t}{r} \left[\frac{n - 1/(R+1)\varepsilon_{l,\max}}{1 - \left(R/(1+R)\right)^2} \right] \qquad (7)$$

and critical stress at initiation of wrinkle was given by:

$$\sigma_{cr} = -\left(\frac{2t_0}{r_0\sqrt{3\left(1-\nu^2\right)}} \frac{\sqrt{n}}{\sqrt{n}+1} \right)^n \left[\frac{1}{1+R} \left\{ 1 + \frac{1}{\alpha^2} + R\left(1 - \frac{1}{\alpha}\right)^2 \right\} \right]^{(n-1)/2} \qquad (8)$$

2.3.2. Analytical estimation of loading parameters

As described in the section 2.3.1 all tube hydroforming processes are vulnerable to various instabilities, which is mainly due to the complex nature of the forming process. One of the major concerns for any tube hydroforming process design lies in selection of suitable loading condition (i.e. forming pressure and end feed), which can avoid these instabilities during the forming process. Although the process is quite complicated to be modelled analytically, however few attempts have been made by various researchers to calculate analytically and numerically feasible forming load paths for parts with axisymmetric shapes or part geometries.

Asnafi [45] developed analytical models for free forming of tubes with axisymmetric expansion using internal hydraulic pressure to show the forming limits. The analysis detailed the calculation of the yielding pressure and axial force required at the point of yielding of the tube subjected to internal pressure. The geometric model was similar as shown in Fig-1. The analysis was done using the formulas of thin walled tubes subjected to internal pressure and compressive axial loads with an assumption that the stress condition is bi-axial in nature (fig 2.3.11). Equation-9, 10 and 11, were derived for yield pressure (p_{iy}), compressive force (F_y) required to yield the tube at the beginning of the bulging and the force (F) required during the course of forming.

$$p_{iy} = \frac{R_{p0.2}}{\left(1-\alpha+\alpha^2\right)^{1/2}} \cdot \frac{2t_0}{\left(d_0-t_0\right)} \qquad (9)$$

$$F_y = p_i.\pi.\frac{\left(d_0-t_0\right)^2}{4}.\left(1-2\alpha\right) \qquad (10)$$

$$F = p_i\pi\rho_1^2\left(1-\frac{2\alpha}{1+\alpha.\rho_1/\rho_2}\right)+p_i\pi\left(\left(d_0-2t_0\right)/2\right)^2+\mu p_i\pi d_0\left(l_0-s\right) \qquad (11)$$

Where $R_{p0.2}$ is the yield strength, t_0 is the initial wall thickness, d_0 is the outer diameter of tube, α is ratio of the axial stress is to tangential stress, ρ_1 is minor radius of curvature, ρ_2 is major radius of curvature l_0 is initial contact length of the tube with the die surface and, s is the stroke.

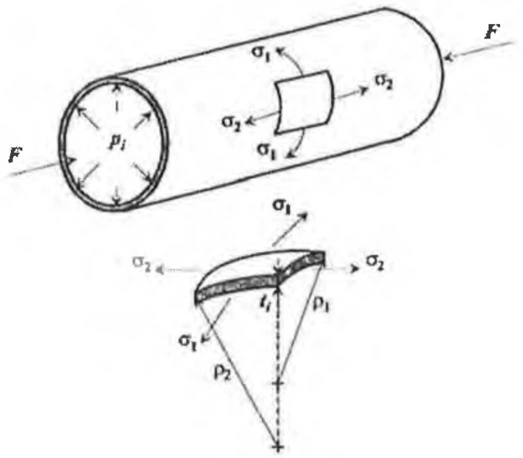

Fig 2.3.11 Bi-axial stresses acting on an element at the middle of the tube [45]

Rimkus et al [54] analytically estimated and designed the loading parameters of an axisymmetric tube hydroforming process and subsequently applied it for numerical simulation to study the process behaviour. In the work, methodologies were defined to derive and calculate load paths for internal pressure and axial force as a function of time. For calculation of the force curve, it was assumed that the total forming force consists of two parts, the first part is the force required for initial sealing and the second part is the force required to push material into the deforming zone. Even for the design of the pressure curve, the loading was assumed to be in two different phases. The first phase is for forming or expansion of the tube and the second phase is for calibrating the tube against the die corner radius. All these load curves were calculated using simple plasticity theory and with the geometry of the part expansion.

Koc and Altan [61] (refer section 2.3.1) in the same work reported analytical models to predict the free forming load such as internal pressure (p_i) and axial force (F_a) for similar axisymmetric geometry (fig 2.3.12) as used by Asnafi [45]. In the analysis same membrane theories (bi-axial stress-strain condition) were used to model the problem.

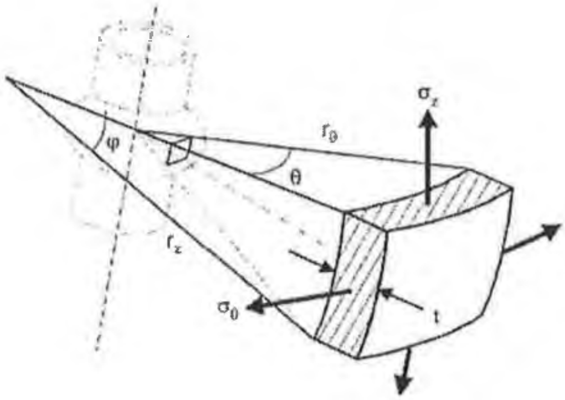

Fig 2.3.12 Bi-axial stresses on a thin tube subjected to combined axial load and internal pressure [61]

The load values were defined as:

$$p_i = K\frac{(\varepsilon_0+\varepsilon)^n}{(1-\alpha+\alpha^2)^{1/2}}.\frac{t_0}{r_0}.e_r^{-\varepsilon_\theta(2+\alpha)} \qquad (12)$$

$$F_a = \pi R_0 t_0 \sigma_{yp} + \pi (R_1 - t_1)^2 P_i + 2\pi R_1 d_a \mu P_i + 2\pi\left(R_1 - \frac{t_1}{2}\right) t_1 \sigma_z \qquad (13)$$

Where, α is the stress ratio (axial to hoop), t_0 is the initial wall thickness and, r_0 is the initial mean radius of the tube.

2.4. Numerical simulation studies

Considering the various experimental and analytical studies, it can be concluded that tube hydroforming is a relatively complex metal forming process to analyse theoretically. Thus is imperative to find an alternate solution methodology, three-dimensional (3D) finite element simulations with different formulations have helped a lot to understand the actual process and the deformation mechanism.

Numerical analysis of tube hydroforming has various advantages such as it assists design engineers finite to, a.) assess the manufacturability of parts at the design stage, b.) explore alternative design schemes, and eventually c.) arrive at an optimized design in a cost effective and timely fashion. With the aid of finite element simulation, the part quality control, and the design of the tube hydroforming process can be easily implemented and monitored. It also provide insights on the necessary process parameters/ loading paths (i.e. internal pressure and axial feed), part geometry, and part formability by analyzing the thinning, thickening, and stress-strain distribution in the deformed tube. A number of numerical simulation work concerned with analysis and optimization of simple to complex hydroforming processes have also been reported using various customised general-purpose or commercially available finite element codes. Until now a number of researchers have applied three-dimensional finite element simulation and analysis on several tube hydroforming processes, majority of which have been applied for simulation of axisymmetric geometries and few on relatively complex geometries such as automotive structural parts.

Structural finite element codes are basically available in two different formulation namely implicit and explicit formulations. Thus it is important to select the proper code prior to analysis of the problem. This can be explained by considering a typical cycle of a component manufactured by using tube hydroforming technology. For example tube a tube hydroforming process may have different phases of operation, such as in certain cases depending upon the final geometry of the component to be formed, the requirement may be to pre-bend the tube first and then hydraulically deform to the required die shape and further account for the spring back effects after the hydroforming operation. In this type of case it is important to select the proper formulation for analysis of each stage of the operation. With the availability of two different formulations (explicit and implicit) of finite elements codes, it has become relatively easy to simulate and analyse all these steps using these formulations. This can be explained considering the above case in which the entire process (pre-bending of tube – hydroforming – springback effects) the initial bending and hydroforming operation can be analysed by explicit codes whereas the spring back effects can be analysed by implicit codes. Again proper selections of the formulations are quite important and it purely depends on the process characteristics such as strain rate and velocities. Usually static analyses are done by implicit methods whereas dynamic analyses are done by explicit methods. Furthermore there are few processes which are quasi-static in nature, these processes can be analysed by either implicit or explicit formulation. Fig 2.4.1 details application of these two formulations for simulations of various physical phenomenons. Considering the low strain rates during the deformation of typical tube hydroforming, the deformation mechanism of the process can be categorized as a quasi-static deformation and different researchers [46, 49, 50, 55, 72] have taken this advantage to simulate the process with a reduced or scaled down simulation time with respect to the actual forming process time, which apparently results in a reduced computation time. Thus it is possible to simulate and analyse the process with both implicit and explicit formulations. However there exist intrinsic problems associated with the implicit finite element formulation such as convergence and long computation time, which have been detailed in later chapters. Therefore, implicit finite element formulations are normally not a good choice for analysis of tube hydroforming processes where large deformations are the predominating factors, thus explicit formulations are the best solution for these kinds of processes.

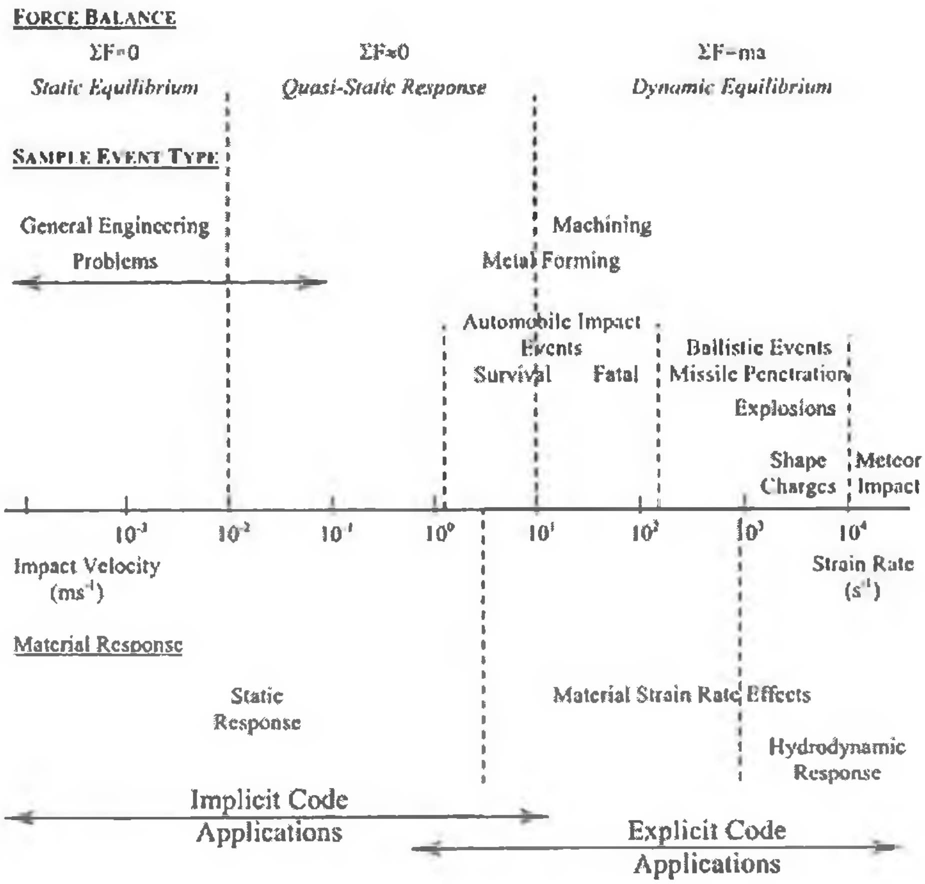

Fig 2.4.1 Application of implicit and explicit time integration methods [78]

Finite element analysis of a forming process has great advantages for understanding the process. However, for some of the processes depending upon the complex nature of the problem, or large model size and complex tool and blank contact interface, finite element simulation of such processes can be computationally expensive due to long computation time. Thus, the solid modelling and selection of element type are quite important. Where ever possible if the model is simplified in the solid and finite element modelling stage, for example certain 3D shapes can be defined in terms of 2D shapes (axisymmetric models or volume generated by surface of revolution, symmetric or partial models) it can be quite advantageous from computation cost of view. Ahmed and Hashmi [43] simulated circular cup bulge forming using the commercial implicit finite element code ANSYS. The finite element model used for the analysis was built with 2D quadrilateral solid elements with axisymmetric boundary condition to represent the entire 3D model of the circular cup. A bi-linear elasto-plastic material model was used and a semi-automatic contact algorithm with penalty function was employed to model the contact region between the die and the sheet. Two loading conditions were used in the simulation, a.) pressure loading only and, b.) combined pressure load with in-plane compressive load. It was shown that with combined pressure with in-place axial loading, the dome height developed was higher along with less wall thinning in comparison to the pressure only loading condition.

Koc and Altan [63] simulated a simple tube hydroforming process using 2D finite elements with axisymmetric boundary conditions. Due to the axisymmetric nature of the die surface, the actual 3D model was simplified to 2D model, which subsequently reduced the simulation time. The simulations were performed using commercial explicit finite element analysis codes DEFORM 2D and LS-DYNA 3D. For the simulation the forming load paths were obtained from experiments. The simulation results were in good agreement with their experimental results. This kind of simplified simulation approach with 2D elements is only possible for axisymmetric kind of expansion of tube blank.

Mac Donald and Hashmi [49] simulated a X-branch tube hydroforming (Fig 2.4.2) of copper tubes using LS-DYNA 3D explicit finite element code with 3D solid brick elements with two different loading conditions i.e. with a.) pressure only and, b.) combined pressure and end axial feed with multi step loading, to study the effect on final bulge height, stress, strain developments in the bulged region and the tube wall thickness change. Fig 2.4.2 shows the typical linear and piecewise linear load paths used for the analysis. Selection of the combined loading condition was done with an objective to avoid premature failure due to wrinkling or buckling. The model used for the analysis was a reduced one-eighth symmetric model (fig 2.4.2). Assuming the strain rate to be small, an approximate bi-linear plasticity model was used in the numerical model. In the analysis, effect of die and blank contact surface friction was also studied on the branch height development and wall thickness variation. From the analysis it was concluded that with combined loading (pressure and end feed, loading pattern-2), the branch height developed was much higher and the wall thinning at the branch top was much less in comparison to forming with pressure load only condition. Contact surface friction also had a significant effect on the branch height development and material flow during the process, with higher friction values the branch height development showed a decreasing trend and more thinning of the tube at branch top and thickening at the tube end. Thus, it is very important that in the process the friction should be kept as low as possible.

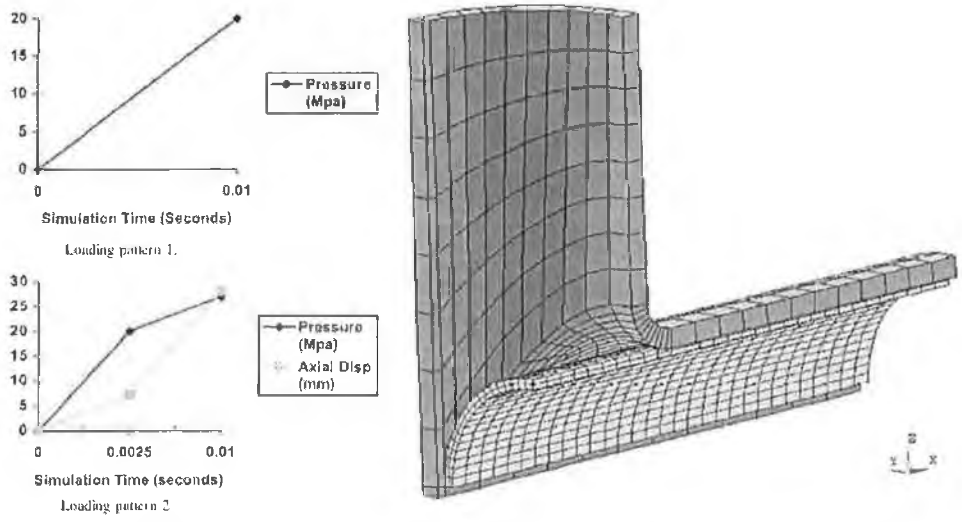

Fig 2.4.2 Load paths, One-eighth symmetric 3D finite element model for a typical X-branch forming [49]

Further to the development of analytical models by Asnafi [45] in a separate work Asnafi et al [48] presented numerical study of free forming of axisymmetric tubes using LS-DYNA 3D. In the study the load paths (relation between pressure and axial feeds) were calculated analytically [45] and were used for the simulations. In the finite element model the dies were modelled as rigid body as it was assumed that there will be no deformation of the die and the deformable tube blank was modelled with transversely anisotropic elastic plastic material law with true stress strain values obtained by tensile tests. From the analysis the forming limit curve for the material was determined and was compared with the experimental forming limit curve. It was concluded that the numerical results (forming limit curve) underestimated the experimentally obtained forming limit curve.

Ahmetoglu et al [52] presented an overview of application of explicit finite element formulations INDEED, LS-DYNA 3D and PAM-STAMP for simulation and analysis of manufacture of tubular axisymmetric components from low carbon steel and aluminium alloys and concluded that for successful application of the process and to avoid failures due to wrinkling proper control of pressure and feed are required during the process.

Various studies have been conducted with LS-DYNA for analysis of tube hydroforming process, in one of the studies Chen et al [69], reported process and material sensitivity study (effects of friction, end feed, anisotropic factor R-value, and pressure loading) on the part expansion and die corner filling of a component with square cross-section with corner radius (fig 2.4.3) subjected to combined internal pressure and end axial feed. The model was built with 3D shell elements. From the study it was concluded that, end feeding along with reduced friction improves forming significantly. Higher end feeding increases the formability however at the risk of formation of wrinkle or buckling of the tube. With increase of R-value the part expansion was poor, and with higher forming pressure the part expansion was better with decrease in final tube corner radius (i.e. better filling near the die corner radius).

Fig 2.4.3 3D finite element model of the tube and die [69]

In a separate study Kridli et al [75] reported a material sensitivity study on a similar model as above. The simulation study detailed the effects of material properties and geometry on the selection of hydroforming process parameters and discussed the effects of the strain hardening exponent, initial tube wall thickness, and die corner radii on corner filling and thickness distribution of hydroformed tube. The study was conducted using ABAQUS explicit finite element code with a two-dimensional plane strain finite element model (fig 2.4.4). The study detailed that the final wall thickness distribution is a function of die corner radius and strain hardening behaviour of the material, i.e. with larger corner radius the wall thinning was less and with lower strain hardening value higher thinning was observed.

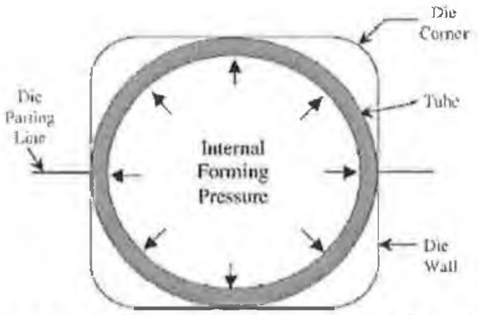

Fig 2.4.4 2D model of the tube and die [75]

In one of the simulation studies using LS-DYNA, Manabe et al [65] simulated and studied the factors effecting wall thickness distribution of the hydroformed tube and compared the simulation results with experimental findings for a steel tube. The process model was similar to the model as stated above (fig 2.4.3) subjected combined internal pressure and end axial feed. For the analysis the factors, coefficient of friction, hardening coefficient (n) and anisotropic parameters (R) were considered. In this case also, the finite element model was built using shell elements and the die contact surface was modelled as rigid surface. The tubular blank material model was modelled with both isotopic and anisotropic elastoplastic materials obeying power law plasticity model. From the analysis of the simulation results, it was also shown that fracture location depends upon the process conditions and material properties and axial loading and better lubrication conditions improve the thickness distribution of the product and with decrease of R-values, smaller axial displacement is required in order to expand up to the same formed profile as obtained by higher R-values at the cost of excessive wall thinning and finally it was concluded that in order to obtain hydroformed parts with uniform wall thickness, tubular material with high n-value and R-value should be selected with good lubrication condition.

From the different literatures available on tube hydroforming it was observed that most of the studies reported were on simple axisymmetric or asymmetric geometries with a very little attention was given to design and analysis of structures with complex geometries. Lei et al [51] reported a design and analysis of manufacture of an automobile rear axle with a relatively complex geometry using tube hydroforming process. The process was analysed using a custom developed finite element code HydroFORM 3D. Different failure conditions, caused due to different die set up, loading and boundary conditions were also analysed for the manufacture of the part. Using the custom finite element code the authors determined the potential failure types and the failure zones for the part, and also compared them with their experimental study. The results obtained from the simulations were found to be in good agreement with the experimental results. In another review Ahmed and Hashmi[46] reported simulation of hydroforming of an elbow with square cross section (box type) from pre-bent circular tube. In the simulation only internal forming pressure was used without any axial feed and the stress strain distribution, final wall thickness variation and the springback effects were studied. The simulation basically highlights the industrial application of the process for manufacture of components or structures with complex shapes and geometries.

The choice or selection of element type in simulation of a particular model or problem has different effects on the simulation process in terms of computation time and final wall thickness prediction. Depending upon the solid model of the problem to be analysed the choices lies in selecting either 3D brick or 3D shell elements. Ahmed and Hashmi [55] and Mac Donald and Hashmi [49] simulated T and X branch components with various loading conditions using 3D solid elements (brick) for the finite element model using LS DYNA3D explicit finite element code to study the deformation mechanism, stress strain development, part expansion during the process. However, there are few limitations associated with the use of brick elements, which have been discussed in detail in subsequent chapters.

Different researches have reported on effects of material properties, friction and loading condition on the process and for all the analysis it was assumed that the initial wall thickness of the tube is constant or uniform throughout, but for practical application the situation may not be so due to various reasons such as manufacturing inconsistencies etc, Shirayori et al [72] presented an experimental study along with finite element simulation for the deformation behaviour of tubes for free bulge forming with initial wall thickness variation along the circumferential direction of the tube (fig 2.4.5), or in other words, a tube with eccentricity in the internal and external tube diameter. In the work, influence of the initial thickness deviation of the tube wall on the deformation behaviour during free hydraulic bulging was studied. The results show that the cross-section i.e. the outer and inner circles of the tube cross section remain circular until fracture of the tube during the expansion. This was independent of the amount of initial deviation or eccentricity between the inner and outer circle of the cross-section.

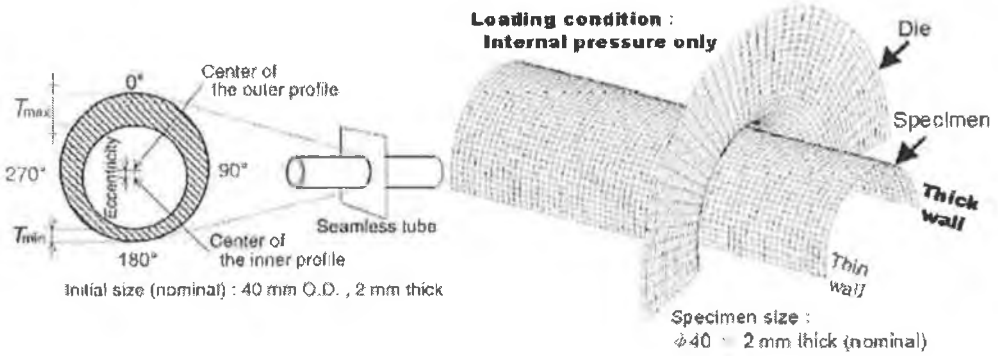

Fig 2.4.5 Tube with eccentricity and the corresponding half-symmetric finite element model with thickness variation [72]

In general, most hydroforming processes use either water or oil as the incompressible bulging or pressurising medium, some researchers [12, 28, 33, 34, 35] have also used a solid bulging medium such as polyurethane. The advantage of using a solid bulging medium is, only axial feed is required for the deformation, thus eliminating use of costly hydraulic systems. Use of a solid bulging medium can be suitable for manufacture of small components with relatively soft blank material. Mac Donald and Hashmi [64] presented a simulation study of bulging of X-branch with a solid bulging medium (polyurethane) and compared the results with a similar model with hydraulic bulging [49]. The study concluded that, use of solid bulging medium allows for greater branch height, less thinning of the branch top and less stress in the formed component when compared to hydraulic bulging process.

Most of the research work done in this filed are primarily on hydroforming of components from straight tubes with open ends. Very few works have been reported on closed tube hydroforming. Teng et al [56] presented experimental investigation and numerical simulation of hydroforming of toroidal structures (closed tube) with different initial structures or cross-sections such as hexagonal cross-section and non-symmetrical cross-section with the upper part resembling octagonal shape and the lower part with hexagonal shape. In the study these closed sections structures were subjected to internal forming pressure to finally deform then into toroids. The study was basically conducted to investigate the effect of the initial structure on formation of toroidal shells. This was done with an objective to avoid wrinkle formation in the final formed toroid or elbow, which occurs mainly due to development of large compressive strains in the inner part of the toroid during the forming process. The process was also simulated using LS-DYNA explicit finite element code and the simulation results were compared with the experimental results. The occurrence of wrinkle and its cause was explained with the finite element simulation. The study concluded that no wrinkle occurred on the toroidal shell with an octagonal cross-section, however the tiny wrinkles were observed on the toroidal shell with a hexagonal cross-section and the formed shape was better was octagonal cross-section in comparison to shell with hexagonal cross-section.

2.4.1. Selection of loading paths and initial blank/ die dimensions

From different studies presented in section 2.3.1, 2.3.2 and 2.4 it can be concluded that proper loading conditions plays a major role in tube hydroforming process. Koc [71] presented the effect of loading path and variation in material properties on the robustness of the tube hydroforming process and final part requirement i.e. the final wall thickness. In the study, guidelines for the use of loading paths schemes were basically obtained from the finite element simulation of few simple geometries (axisymmetric expansion), and the developed guidelines were further applied experimentally for manufacture of automotive structural frame parts. These simple guidelines can help for further development or refinement of the new load path for the component as per its part expansion requirement. Fig 2.4.6 shows the two typical assumed load paths used for simulation of a T-branch component to study the feasibility of the process and part-thinning characteristic. The approximate load paths were calculated from the analytical model (for axisymmetric expansion) developed by Koc and Altan [61] illustrated in section 2.3.2. From the simulation result it was observed that corresponding to case-2, the developed bulge height was higher with the same level of wall thinning as of case-1.

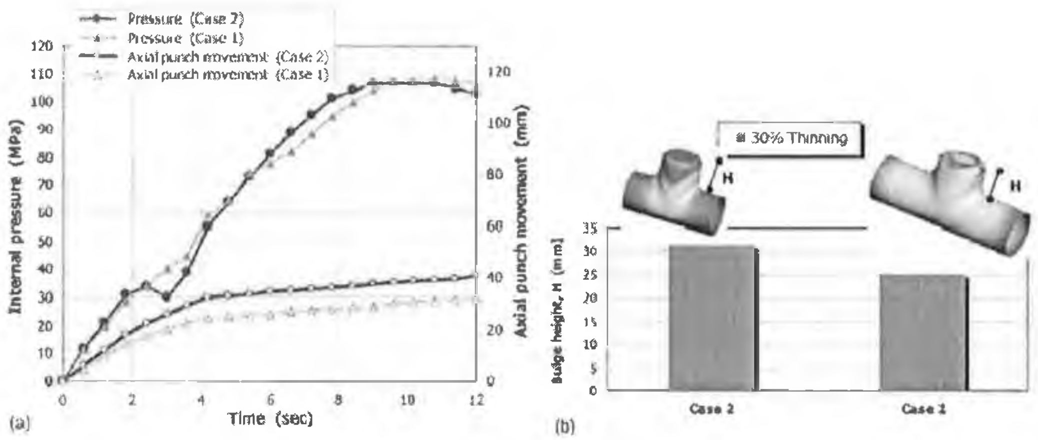

Fig 2.4.6 Effect of loading path design on final part properties (bulge height and wall thinning) [71]

Apart from loading paths the initial blank and die dimensions are also quite important in establishing the final part expansion features. This has been demonstrated by one of the studies by Koc et al [50]. In the study it was shown how variation of blank length and die corner radius of a T-branch forming affects the final part expansion (i.e. the protrusion height). Basically in the study finite element analysis was used along with design of experiments to establish a relationship between various dimensional parameters (length of tube, die corner radius, diameter of the die cavity in the section where expansion takes place- fig 2.4.7) of the tube blank and die with the protrusion height of the T-branch. For the study, the authors developed a design of experiment technique, 'Low Cost Response Surface Method' and were used to predict and optimize the

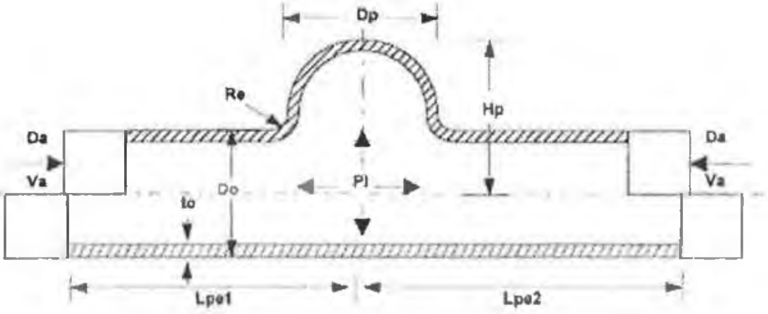

Hp	Height of Feature
Lpe1	Distance between Feature and Edge
Lpe2	Distance between Feature and Edge
Do	Initial Outer Diameter of Tube
Dp	Outer Diameter of the Feature (i.e., protrusion)
Re	Fillet (Entry) Radius of Feature
to	Initial Tube Wall Thickness

Fig 2.4.7 Geometrical parameters for a T-shape part in hydroforming process [50]

protrusion height as a function of geometrical parameters subjected to acceptable thinning 25% of the wall thickness at the protrusion region. For the design of experiment, the preliminary data were obtained from the finite element simulations of the process using a finite element model, which was being validated with the experimental results.

The results of the design of experiment show (fig 2.4.8) the protrusion height increases with the decrease in the tube length, with the increase in the die corner radius and protrusion cavity die diameter. In the study any wall thinning above 25% was treated as failure of the tube.

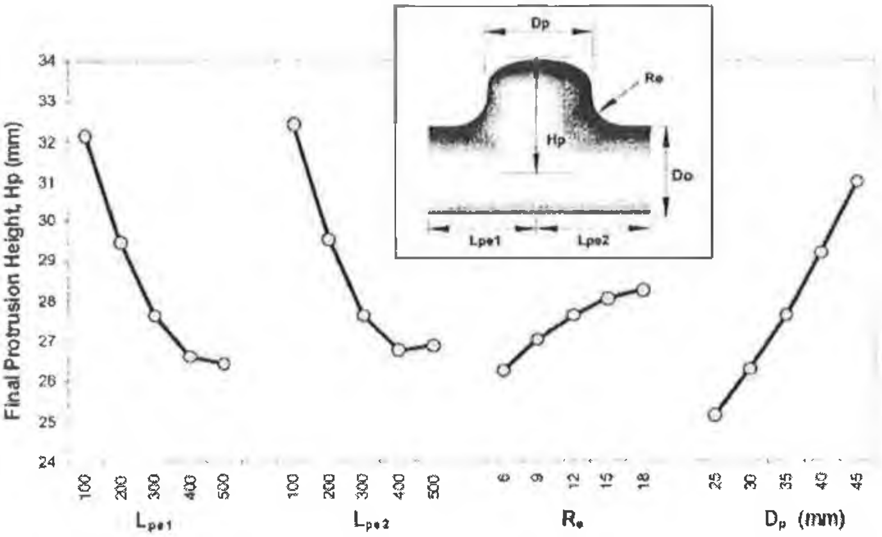

Fig 2.4.8 Effects of the geometrical parameters on the protrusion height [50]

2.4.2. Numerical process optimization, control and estimation of loading paths

From the various experimental, analytical and numerical studies done on tube hydroforming process, it can be concluded that for a successful application of the process without any failure due to wrinkle, buckling and bursting, it is quite important to design the process and its parameters in advance. With the selection of proper material properties of the blank, geometry of the blank and die, lubrication condition, the next bottleneck comes in the selection of proper loading paths or loading conditions (i.e. selection of internal pressure and axial feed curves). The selection of proper loading paths can be done by using empirical methods, analytical methods, or numerical methods. Empirical methods, which are usually developed use simple guidelines and may be suitable to approximately estimate the process parameters for simple hydroforming part geometries. However for complex geometries this does not hold good. Analytic methods are developed based on plasticity theories and flow laws. Most of the analytical models available or developed are for tube hydroforming processes with axisymmetric geometries and cannot be applied to determine the load paths for other complex or asymmetric geometries. However, for simple part geometries (axisymmetric) the available analytical models can be of much use. For general cases, numerical simulations using finite element methods are very practical and widely applied in the industry.

In numerical simulation there exists two options i.e. either select trial-and-error method or apply intelligence to the program to calculate the loading condition. Trial-and-error simulations using finite element method for the process design (i.e. design of pressure and feed load curves) can be very time consuming. In this approach, an approximate pressure and axial feed curves versus time are selected to conduct a simulation. If the results are not satisfactory, the input curves are modified by intuition and the simulation are run again until satisfactory results are obtained.

Fortunately, this iterative simulation of the process using finite element analysis method can be done systematically and automatically with kinds of optimization. For example, determination of the loading paths can be treated as a classical optimization problem. By this way the resultant loading paths can be optimized to maximize the part formability or part expansion. Alternative approach is to add intelligence to the finite element program so that the loading parameters can be calculated with in the numerical simulations. In the recent past few researchers have come up with different concepts for either to optimize or develop adaptive control strategies of the loading parameters.

Ghouati et al [47] suggested an optimization technique to control the process (i.e. to control or minimize the final part wall thinning) simultaneously determining the optimal process parameters of tube hydroforming processes. The method used for optimization was based on coupling of an optimization technique and the finite element method. The control of the process was mathematically formulated by the classical optimization concept with as a non-linear mathematical programming problem, which can be defined as:

$$\min S_0(p,u) \quad \text{subjected to} \qquad (14)$$

$$h_j(p,u) \le 0 \qquad 1 \le j \le n_{ic} \qquad (15)$$

$$g_j(p,u)=0 \qquad 1\le j\le n_c \qquad (16)$$

Where n_{ic} is the number of inequality constraints and n_c is the number of equality constrains, p represents the vector of process parameters and u the calculated displacement field and S_0 is the objective function, which gives a measure of the process performance. The formulation was applied to a tube hydroforming simulation in which the objective function (S_0) takes account of the nodal thickness variation during the process and was defined as:

$$S_0=\left(\sum_{i=1}^{N}\left|\frac{h_i-h_0}{h_0}\right|^q\right)^{\frac{1}{q}} \qquad q=1,2 \text{ or } \infty \qquad (17)$$

Where N is the total number of nodes, h_0 is the initial thickness and h_i is the final thickness of node *i*.

The constraint function g represents the distance from the desired shape for the final product and was expressed in two different forms:

$$g_1(p)=\left(\sum_{i=1}^{N}(d_i)^q\right)^{\frac{1}{q}} \qquad \text{or} \qquad g_2(p)=1-\frac{Vol_{piece}}{Vol_{tgt}} \qquad (18)$$

Where d_i is the distance of node i to the tool, Vol_{piece} is the inner volume of the final product and Vol_{tgt} inner volume of desired (depending on the tool/die). There process parameters used were the inner forming pressure $p(t)$ and the end feed $u(t)$. For the optimization an initial approximate load path is required which initiates the simulation and subsequently the optimization algorithm determine the optimal load path from subsequent simulation runs. In a separate presentation Gelin and Labergere [70] applied the above optimization technique to determine the optimal load paths with an objective to minimize the part wall thinning simultaneously adhering to the final shape of the die for asymmetric components such as T-branch expansion.

As mentioned above for optimization of the loading path using optimization algorithm coupled with finite element simulation, requires an initial approximate load path, whose control points are used as design variable by the optimization program. The selection of the initial load path may be simple straight line as used by [70] or complex curves, Yang er al [60] in their work used the above optimization concept [47] and used cubic B-spline functions with equi-distant control points to define the initial load path (fig 2.4.9) and calculated an optimal load path by minimizing the part wall thinning for an axisymmetric type tubular expansion using a gradient based optimization technique. In another work Fann and Hsiao [76] used a conjugate gradient method with LS-DYNA finite element simulations to calculate the optimal load paths for a T-branch expansion with the same objective as used by previous researchers i.e. to minimize the tube wall thinning.

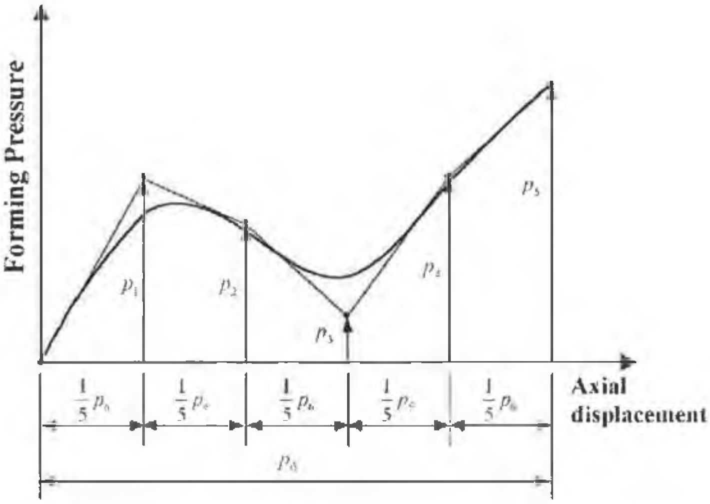

Fig 2.4.9 B-spline curve for internal pressure and axial feed (initial load path) [60]

In one of the recent presentations a similar approach of optimization as mentioned above was used by Jirathearanat and Altan [79] along with general optimization code PAM-OPT integrated with PAM-STAMP finite element solver to optimize loading paths for various tube hydroforming components such as a Y-shape and a complex structural part. For the process optimization, the loading paths were represented by piecewise-linear curve functions of which the control points were the design variables. In the optimization the objective and constraints functions were formulated to express the desirable qualities of the final part such as uniform part thickness distribution and part dimensional accuracy (i.e. no part wrinkles).

For optimization of the tube hydroforming process most of the researchers have used traditionally available standard optimization tools or algorithms integrated with the finite element codes. In a recent development Abedrabbo et al [80] used a heuristic method i.e.

used genetic algorithm (GA) search method integrated with LS-DYNA simulation to maximize formability of a tube hydroforming component. The GA search used usually tries to identify the optimal internal hydraulic pressure and feed rate so that the final part expansion is maximized simultaneously maintaining the final strains values (major and minor true strains) of the tube with in the safe limits of the forming limit diagram of the material.

Other than the use of optimization tool coupled with finite element simulations, few researchers have suggested adaptive control methods to calculate feasible load path and control the process numerically. Doege et al [44] developed an adaptive control method to find a suitable forming load path for simple axisymmetric tube hydroforming processes. An algorithm was used in the finite element simulation, which avoids failure of the tube by adjusting the end axial force and pressure boundary conditions. The algorithm was implemented in the finite element program ABAQUS/Explicit via user subroutines. The algorithm basically recognises wrinkle growth during the finite element simulation and correspondingly adjusts the process parameters, i.e. the internal pressure and the axial force. The developed control algorithm was used to simulate and obtain load paths (relation between axial force and internal pressure over the simulation time) for simple axisymmetric geometries. However the developed algorithm had certain limitations, such as, it cannot determine the failure due to excessive tube wall thinning.

In one of the presentation Manabe et al [73] described the application of fuzzy adaptive process control technique for control of axial feeding simultaneously eliminating the failure due to buckling and improve the bulge height of a T-branch tube hydroforming process. In the forming process simulation, only the axial feeding was controlled using the adaptive control whereas the forming pressure was applied as a free forming pressure.

In a recent development, Johnson et al [81] developed a numerical control algorithm that predicts the end axial feed and internal pressure loads to give maximum formability of circular tubes during hydroforming. The controller used the stresses, strains and mechanical response of the incremental finite element solution results to estimate the proper incremental load values for the next step. The algorithm was used to simulate hydroforming of cylindrical aluminium tubes with axisymmetric configuration.

2.5. Summary of Chapter 2

From the literature cited and described the following points can be noted:

Most of the experimental studies were conducted on relatively simple geometries of axisymmetric nature with limited studies done on asymmetric components such as T and X-branch components.

Very few finite element simulation studies were found on tube hydroforming of asymmetric components. In particular limited studies have been reported on simulation of T and X-branch type components.

Structural instabilities and failure due to wrinkling, buckling and bursting are the major concern for all tube hydroforming processes. Analytical process failure theories (for bursting, wrinkling) were developed on the assumption that the part expansion is axisymmetric in nature, thus they hold good for simple axisymmetric geometries. However these developed equations are not valid for relatively complex asymmetric geometries like T and X-branch, as in these cases, due to the nature of the part expansion (asymmetric), the strain conditions are expected to be different at different regions of the bulge. Thus numerical simulations coupled with plasticity flow laws can aid in approximate detection of these failures well in advance.

Geometrical parameters of tube blank and die/tool also have effects on the final part expansion and wall thickness distribution, however limited studies have been reported on the effect of these parameters on the forming process.

In order to avoid premature failures due to wrinkling, buckling and bursting and for successful application of the process, prior estimation of well-balanced loading paths (internal forming pressure and end axial feed curves) are quite important. Few analytical solutions for calculation of loading paths have been developed for simple axisymmetric geometries assuming the final shape, geometry and part expansion. These theories hold good for part expansion with axisymmetric geometries and cannot be used for calculation of loading paths for part expansion with complex asymmetric geometries. Further attempts were made to develop adaptive control techniques coupled with numerical simulations, which can calculate the feasible loading paths, however until now a limited achievement have been made in this area.

Chapter 3: Experimental Study and Finite Element Analysis of 'X' and 'T'-Branch Tube Hydroforming Processes

3.1. Introduction

The tube hydroforming process is a relatively complex manufacturing process, the performance of this process depends on various factors and requires proper combination of part design, material selection and boundary conditions. Experiments can provide better understanding of the process, however it is not possible to study every process experimentally due to high cost involved in the tooling and process design. Due to the complex nature of the process, the best method to study the behaviour of the process is by using numerical techniques and with advanced explicit finite element codes. In this work, X and T-branch components (fig 3.1.1) were formed using a tube hydroforming machine and the experimental load paths (relation between internal forming pressure and end axial feed) were obtained for the processes, which were further used for numerical simulation and analysis.

This chapter details the experimental machine setup with the automation and upgradation details from the old to new machine setup, the physical forming process of X and T-branches with experimental results and observation, and further numerical study of the processes using LS-DYNA 3D explicit finite element code. For the finite element simulation the exact or similar experimental boundary and process conditions, solid model geometric dimensions and material properties were used. The simulation results were compared with experimental results for branch height development and the final wall thickness distribution of the formed parts (i.e. X and T-branches).

Fig 3.1.1 X and T-branch components

3.2. The hydraulic tube hydroforming machine

The basic equipment required for a tube hydroforming process with end axial feed is a hydraulic press and two axial pistons. The press is used to clamp the upper and lower forming die halves together during the forming process and ensures that the deformation of the blank does not force the dies apart. The two axial pistons are used to seal the tube filled with hydraulic oil and provide necessary axial feed during the process.

The setup consists of a hardened steel die set with lower and upper die halves with X or T-branch cavities, which are clamped using a hydraulic ram attached to the upper die holder and the lower die is fixed to the rigid machine base. The tube blank is placed on the straight cylindrical die cavity of the lower die, after the dies are closed the two end axial tapered plungers are pushed inward simultaneously using two horizontal hydraulic pistons and the tube ends are sealed. After this sealing the tube is filled with hydraulic oil and bleeding is done to remove any trapped air pockets from the sealed tube filled with hydraulic oil. Simultaneous controlled forming pressure on the inner surface of the tube and axial feed on the tube ends are applied to deform the tube blank into the shape of the die cavity.

The hydroforming machine used for the experiments in this study was upgraded and partially automated from an old setup with manual controls with few functional modification of the control system. This was done with an objective to control the forming loads (internal forming pressure and end feed) and also to register the actual forming loading path (i.e. build up of internal forming pressure and axial displacement of the plunger) during the operation. The machine was built in 1986 by Barlow [83] subsequently modified by Hutchinson [84] and partially automated by Mc Donnell [89], fig 3.2.1, fig 3.2.2 and, fig 3.2.3 show the detail machine setup. The original controls for activation and application of sealing pressure, forming pressure and end axial feeds were manual in nature.

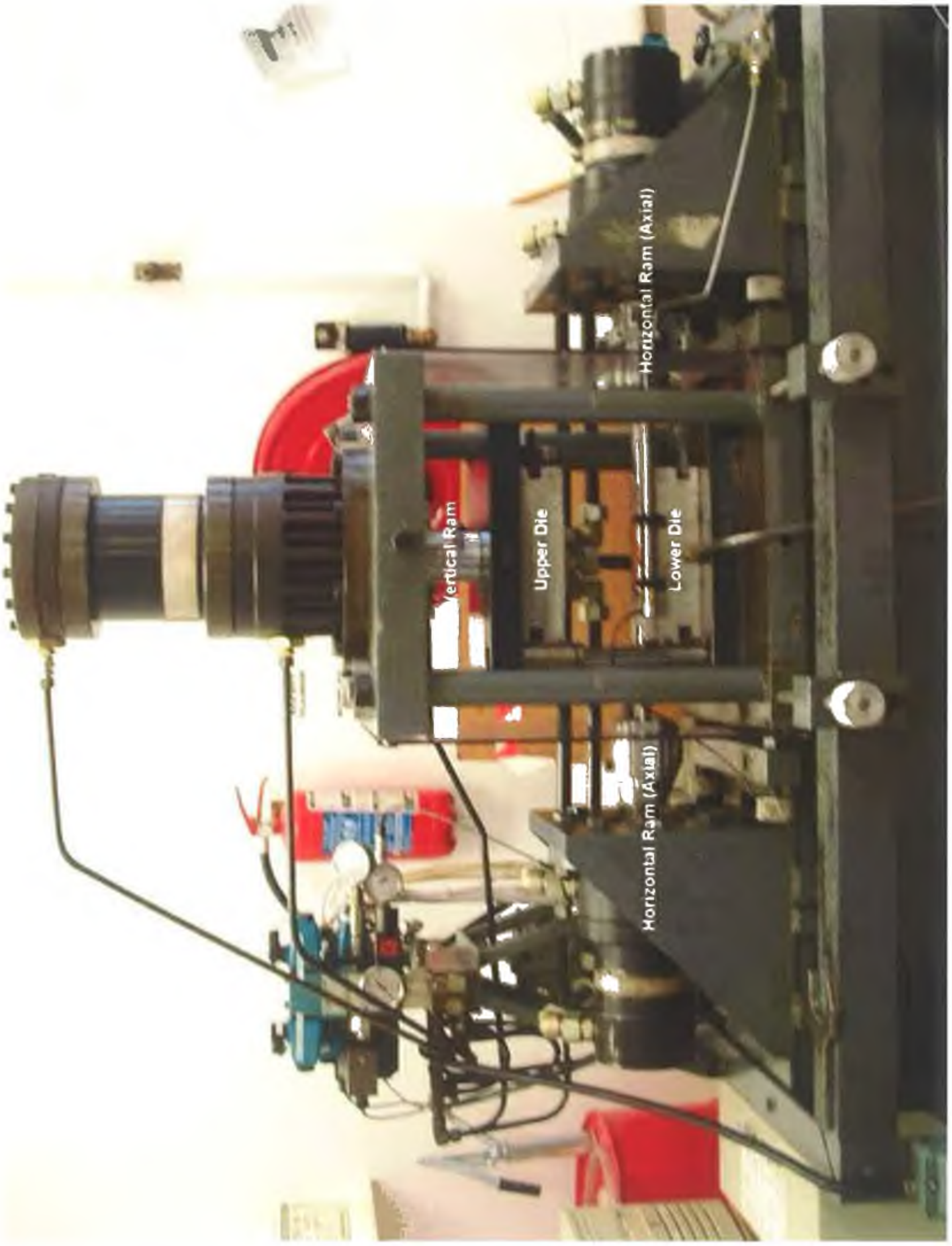

Fig 3.2.1 Tube hydroforming machine

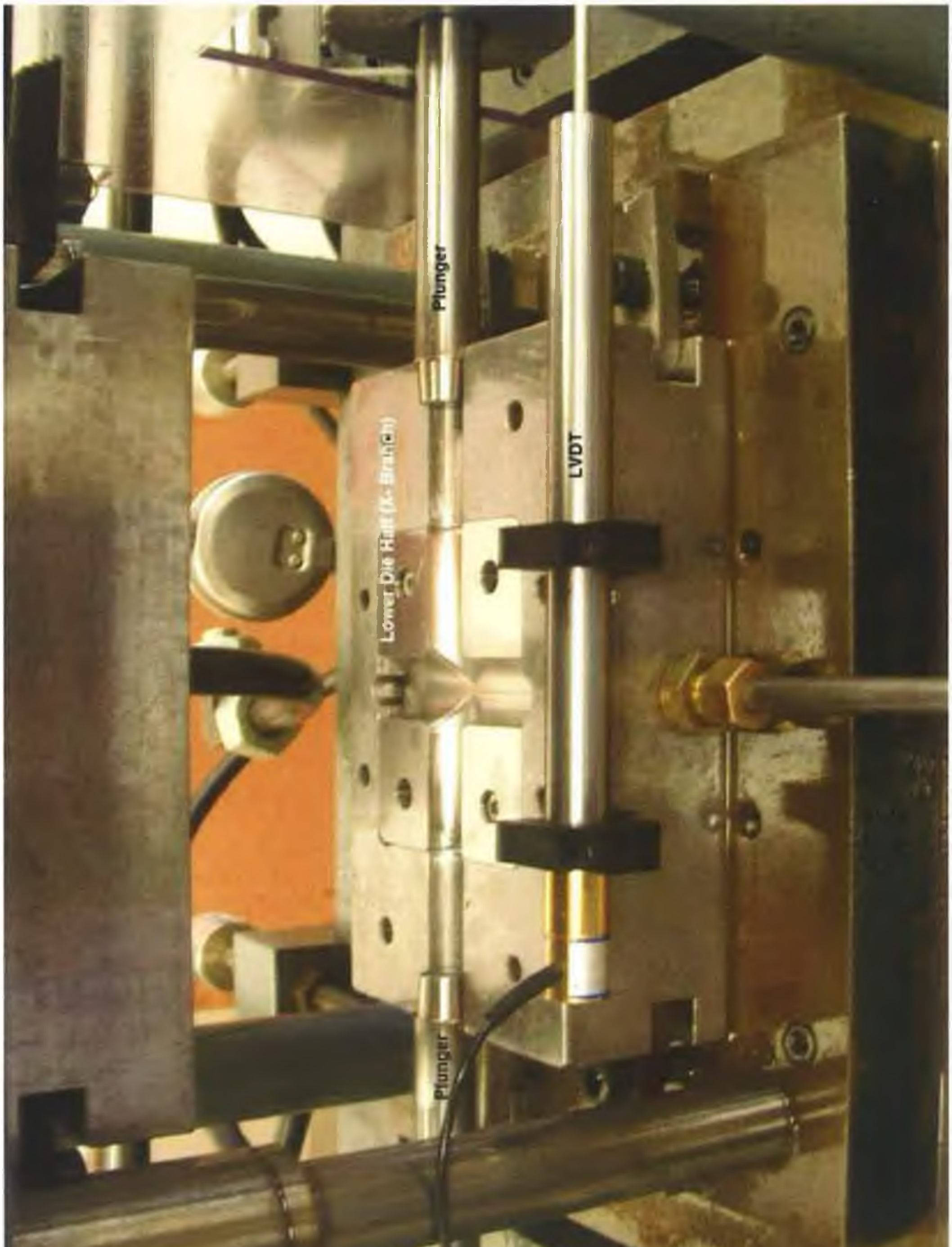

Fig 3.2.2 Magnified view of a die setup, with X-branch die and axial plungers

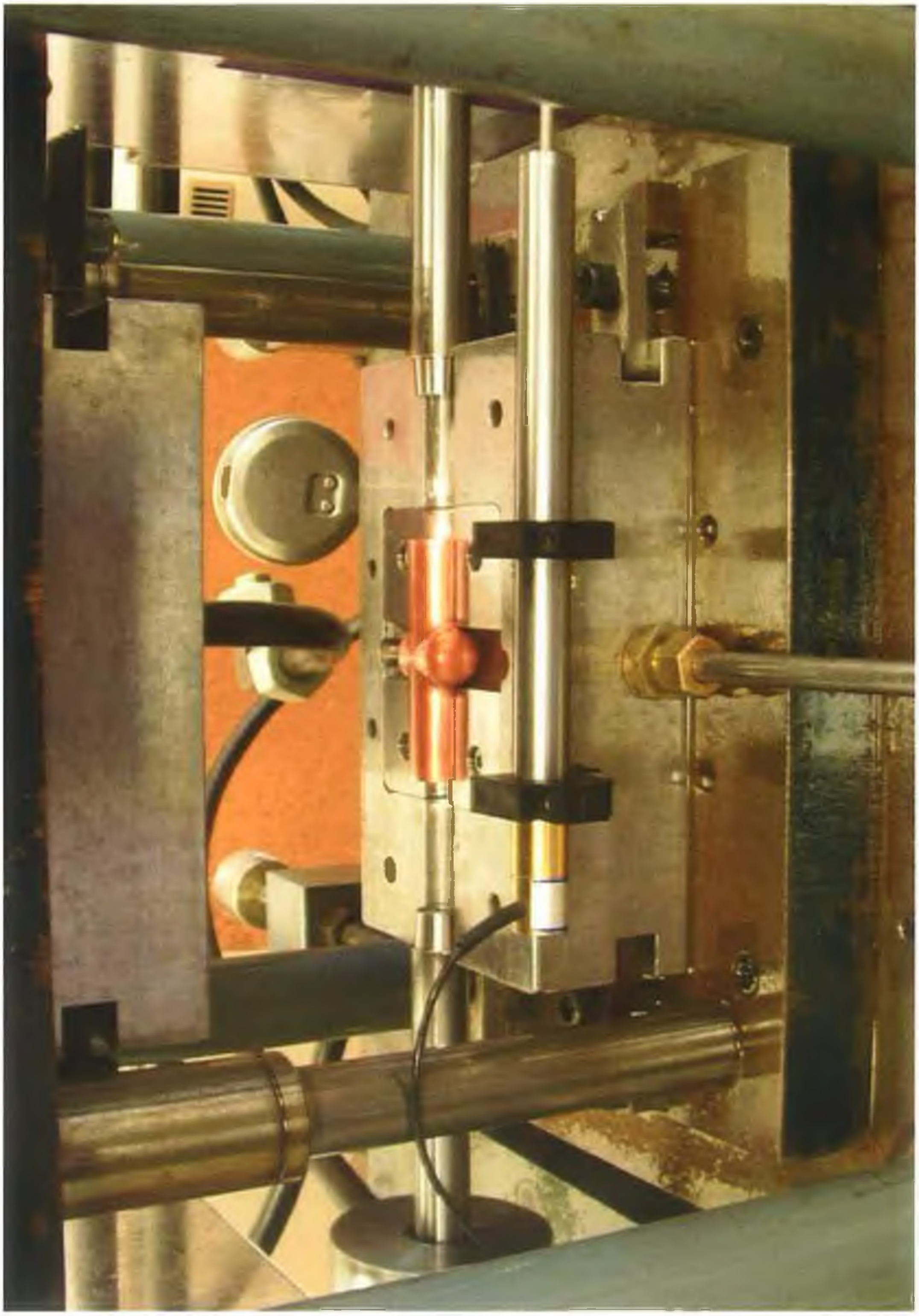

Fig 3.2.3 X-branch hydroformed component (sample of the formed tube in the die cavity)

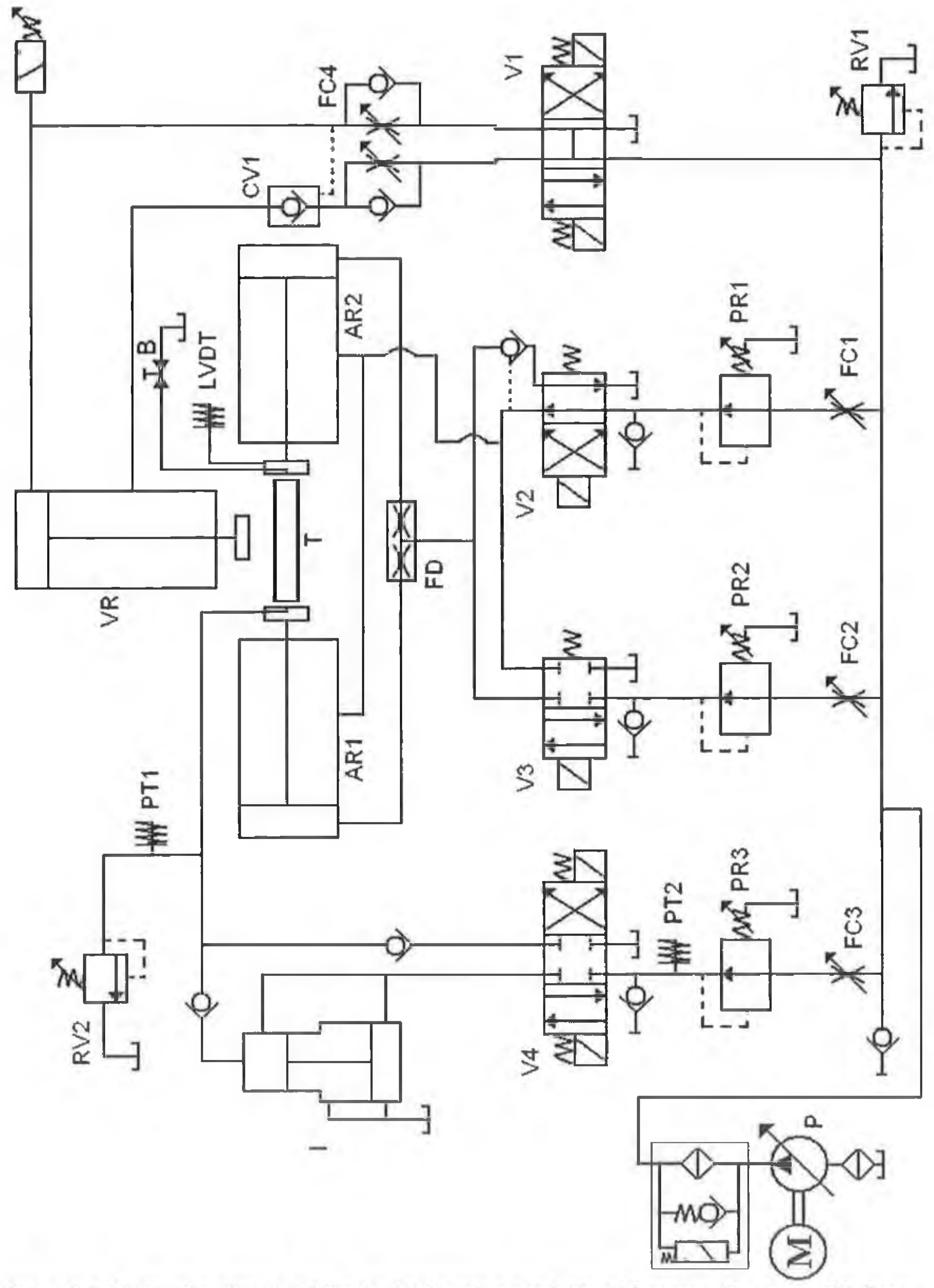

Fig 3.2.4 Hydraulic circuit of the hydroforming machine (M-motor, P-pump, FC-flow feed control valve, PR- pressure reducing valve, V- 2 way/ 3 way flow valve, RV- relieve valve, CV- check valve, B- bleed valve, FD- flow divider, PT- pressure transducer, LVDT-linear variable displacement transducer, I- intensifier, AR- axial ram, VR- vertical ram, T- tube blank)

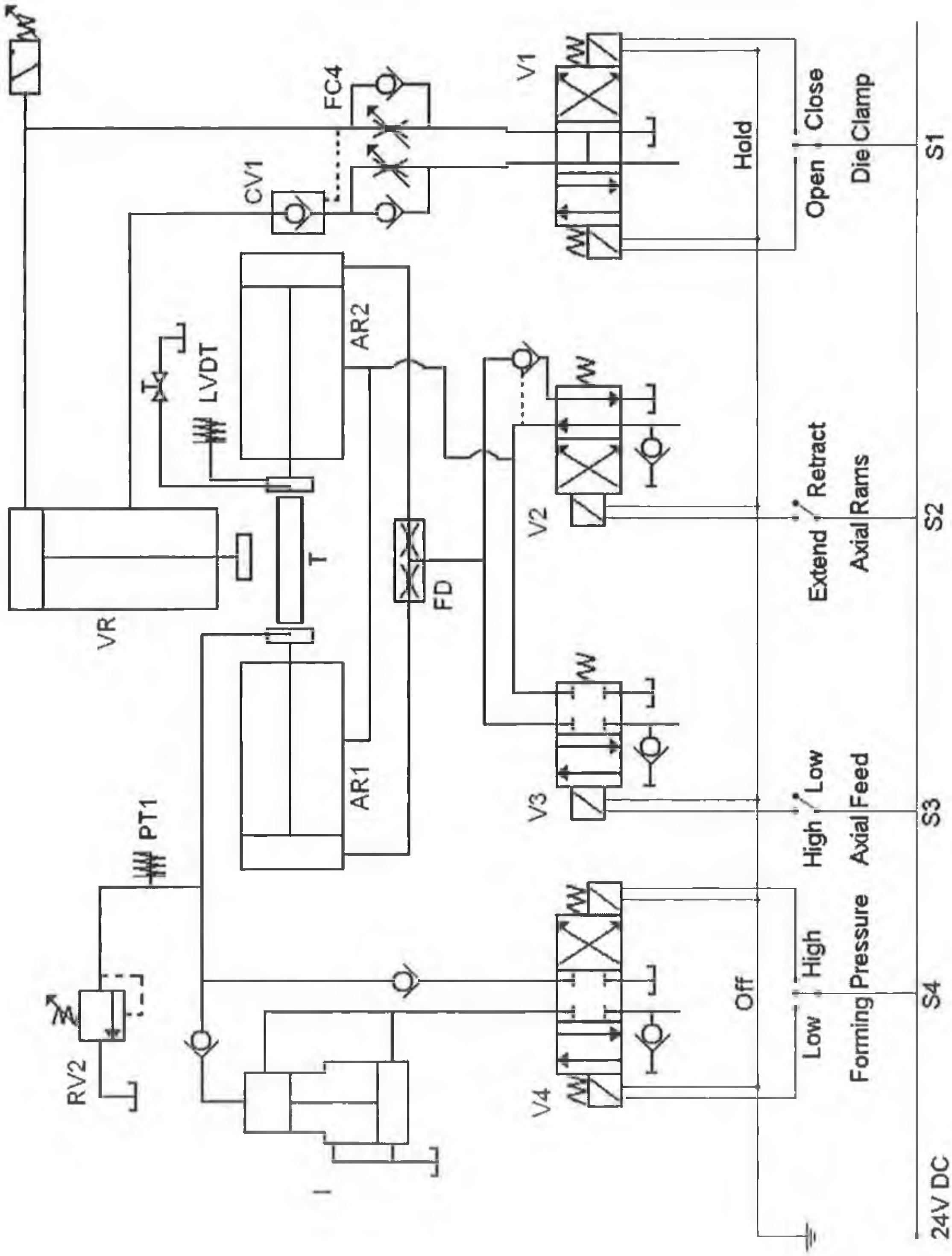

Fig 3.2.5 Solenoid switch connections with manual controls of the hydroforming machine

3.2.1. The hydroforming machine specification

The specification details of the hydroforming machine are after the partial automation of the system. Fig 3.2.4 shows the detail hydraulic control circuit of the machine and fig 3.2.5 shows the switches and control of the machine.

The hydraulic components

1. **Hydraulic supply pressure**

A maximum internal pressure of 0.069GPa is available for the forming process, which is being obtained by using a main circuit pressure of 0.0175GPa, which is further increased to the necessary forming pressure through a 6.5:1 pressure intensifier (I).

2. **The hydraulic cylinders applying axial load**

In order to provide axial feed to the tube during the forming operation, two axial hydraulic cylinders each with a diameter of 125mm and stroke of 100mm are used. These hydraulic cylinders solve two different purposes, the tapered step plungers attached with the cylinders initially seals the tube ends and also simultaneously applies the necessary end feed to the tube ends during the forming operation. The initial settings for the axial sealing pressure and maximum axial feed pressure are controlled by the pressure reducing valves PR1 and PR2 respectively.

3. **The vertical clamping hydraulic cylinder**

The function of the vertical hydraulic cylinder is to extend and retract the upper die and firmly clamp the upper and lower dies so that the tube blank is firmly placed in the die cavity during the operation, this facilitates proper metal flow during the operation so that the blank takes the shape of the die cavity. In addition, the high clamping pressure ensures that the dies are not parted apart during the forming operation incase there is bursting of the tube due to high forming fluid pressure.

4. **The hydraulic pump and electric motor**

The power source for the hydraulic system is a variable displacement piston pump driven by a 7.5KW electric motor. The pump is capable of operating at maximum pressure of 0.021GPa, but it is set at an operating pressure of 0.0175GPa for the current working setup.

3.2.2. Machine control and data recording system

1. Manual control setup

Prior to partial automation, all the controls of the machine were manual in nature. The machine had two sets of two-way control switches and two sets of three-way control switches that controlled the entire process. Table 3.2.1 below illustrates the action of all the manual switches (S1, S2, S3 and S4).

Table 3.2.1 Hydroforming machine switch configuration

S1- Vertical Clamp	S2- Axial Rams	S3- Axial Feed	S4- Forming Pressure
Open	Retract	Low Feed	Low Pressure
Hold			No internal pressure
Close	Extend	High Feed	High Pressure

2. Automated control setup

The manual control setup was kept intact and additionally, all these controls (i.e. the opening and closing of the vertical clamp, horizontal movement of the axial rams and application of internal forming pressure with the help of solenoid controlled flow valves) were automated using a LabView data acquisition control card where all these functions could be controlled using a centralised PC. With the automated control system, it was possible to control all the functions in a chronological order along with simultaneous application of the forming pressure and end axial feed pressure. Further to record the build-up of internal forming pressure, an online electronic pressure transducer with a pressure range of.0.0GPa to 0.06GPa was used, and for actual end feed measurement a linear variable displacement transducer with a displacement range of 0mm-120mm was used.

3.2.3. Operation procedure

The operation of the machine requires the clamping of a tube blank in the die-blocks with the subsequent application of internal forming pressure and end axial feeds. However the combination and the order in which the internal forming pressure and end axial feeds are applied determine the final shape of the component.

The actual operation can be best explained by referring to the manual control of the machine (fig 3.2.5). Assuming the machine is pressurized by turning on the main control switch and the pump motor and the switch S1 at 'hold', S2 at 'retract', S3 at 'low' and S4 at 'off' positions respectively. The actual forming operation follows these sequential stages.

1. Open the die by moving switch S1 to the 'open' position from the 'standby /hold' position. This operation is being controlled by the 3-way flow control valve 'V1'.
2. Place the tube blank firmly on the lower die, with axis of the tube coinciding with the axis of the plungers.
3. Close the die-block by moving the switch S1 to the 'close' position.
4. Move switch S2 to 'extend' position to move the horizontal hydraulic cylinders (axial rams) inside, and bring the taper stepped plungers into contact with the tube blank to seal the tube ends. This operation is being controlled by the 2-way flow valve 'V2' and the pressure reducing valve 'PR2', the value of the sealing pressure can be preset within the range of 0.0020GPa to 0.0025GPa so that there is no leakage of forming hydraulic fluid from the tube blank.
5. After the sealing, fill the tube blank with the forming hydraulic fluid by moving the switch S4 to 'low' position simultaneously opening the bleed valve 'B' to remove any air pockets trapped inside the tube blank. After this bleeding, close the bleed valve so that an initial very low internal pressure is generated in the tube blank.
6. After the above five preparatory stages, now the actual forming process can be started by moving the switch S4 to 'high' and S3 to 'high' positions simultaneously to apply high forming pressure and axial feeds. With this, the forming process is completed. These operations are controlled by the flow valves 'V4' and 'V3' and the pressure reducing valve 'PR4' and 'PR3'. The pressure reducing valve 'PR4' can be preset for applying maximum forming pressure whereas the valve 'PR3' can be preset for applying the maximum axial feed pressure.
7. After the completion of the operation, in order to remove the formed component from the die-blocks, the system pressure is lowered/neutralised first by moving the switch S4 to 'off' and then moving switch S3 to 'low' positions respectively. Finally, retract the axial ram back and open the die blocks by moving the switch S2 to 'retract' and switch S1 to 'open' positions respectively.

The above sequence of the process can be controlled either manually or by using the automation program with the LabView card.

3.3. Experimental forming of ‘X’ and ‘T’-branch components

Experiments were conducted on the tube hydroforming machine to form X and T-branch components for different values of final forming pressure and end axial feed with an objective to study the physical behavior of the process and to obtain the actual forming load paths (relation between internal forming pressure and end axial feed). Further these experimental load paths were used as the loading conditions in the finite element simulation models, which were built to simulate and analyze the process numerically for its deformation behavior and part expansion characteristics. The subsequent section details the experimental setup and the outcomes.

Annealed copper tubes blanks with 121+/-0.5mm in length, 24+/-0.1mm outer diameter and 1.30+/-0.05mm thickness were used for the experiments, with physical properties- Young’s modulus = 119.86GPa, Yield-strength = 0.116GPa, Poisson’s ratio = 0.31 and Density = 8900Kg/m^3. The die halves used (fig 3.2.2, fig 3.3.1, fig 3.3.2) were 120mm in length (parallel to the tube axis), 100mm width (perpendicular to the tube axis), 3mm die corner radius (at the blending region of X or T) and, 24.12mm tube cavity diameter. The diameter of the branches was same as the main tube cavity diameter.

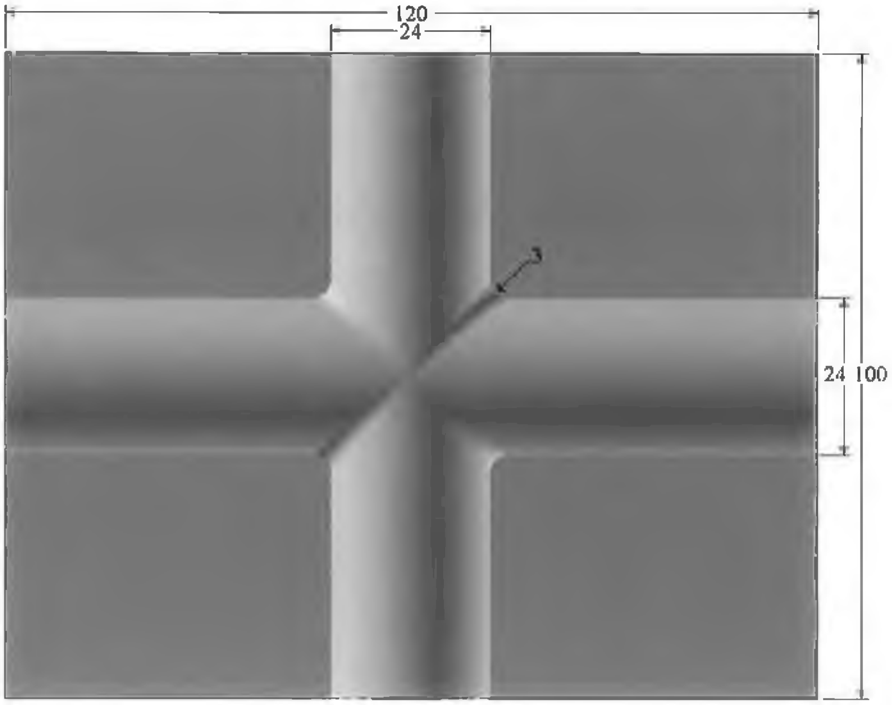

Fig 3.3.1 CAD model of X-branch die (all dimensions are in mm)

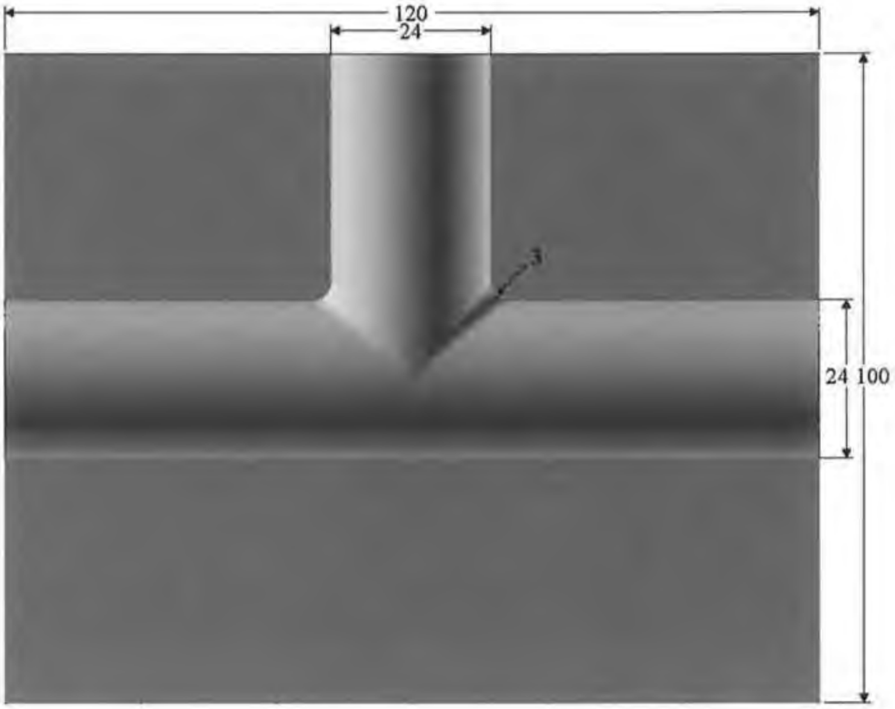

Fig 3.3.2 CAD model of T-branch die (all dimensions are in mm)

The basic operation procedure of the machine has been detailed in the previous section. In order to produce sound components (without defects such as wrinkle growth, buckling and excessive wall thinning) simultaneous controlled internal forming pressure (on the inner surface of the tube) and end axial feed pressure (on the tube ends) were applied to deform the tube blank into required shape of the die cavity (X or T shapes).

The LabView data acquisition system along with other electronic controls (i.e. variable potentiometer for control relief valves controlling the axial feed pressure and internal forming pressure) were used to set the limiting axial sealing pressure, maximum internal forming pressure and the maximum end axial feed pressure. The basic layout of the controls is shown in fig 3.3.3. The instantaneous change in the internal pressure was recorded with the electronic pressure transducer and the end axial feed values with the linear variable displacement transducer (LVDT). Further these forming pressure and end axial feed/ displacement data were fed to the LabView data acquisition system, which finally converted the electronic signals into a text database. Furthermore, this data was used for calculation of the experimental forming load paths (i.e. pressure as a function of end axial feed). As described above, the load values for the forming process was recorded in terms of internal forming pressure and end axial feed, but for practical application and for design of the process (load paths) and associated tooling, compressive force acting on the tube ends are of equal importance. The present capability of the machine does not allow recording of the end feed force value.

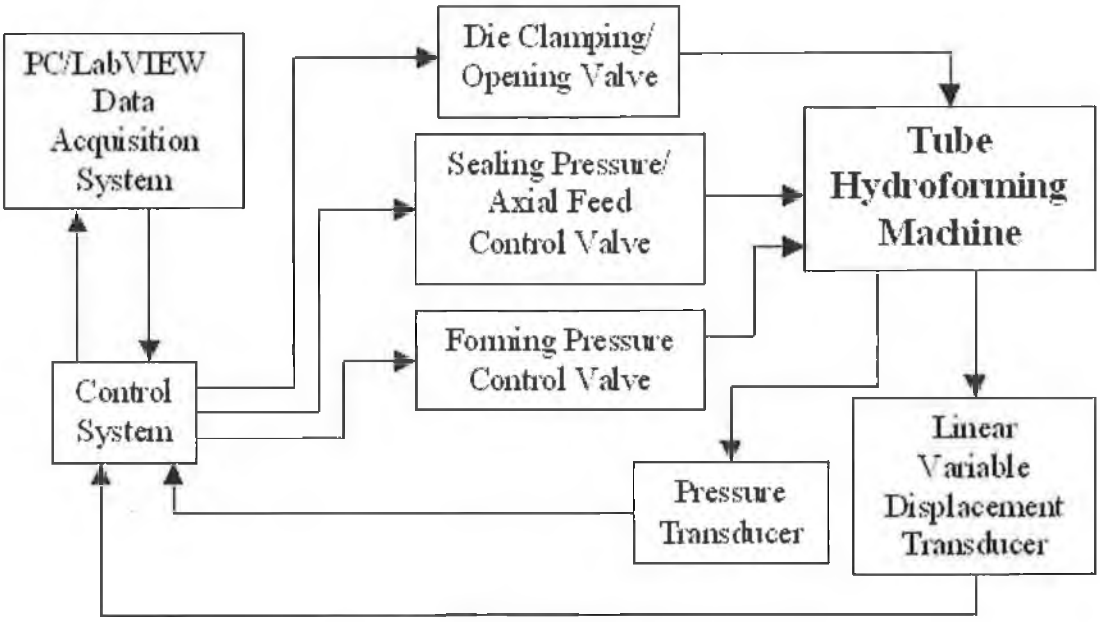

Fig 3.3.3 Process set-up with control and recording systems

3.3.1. Study of machine consistency and repeatability

In order to start the detail experimental study and further develop the corresponding finite element simulation models of the components and validate the simulation results against the experimental results, for this it was important to consider certain factors, such as consistence and repeatability of the component produced by the hydroforming machine. This was required to ensure that the machine is capable of producing identical or consistent components at a preset loading condition (i.e. for a fixed variation of forming pressure with respect to end axial feed). This was established by conducting few sets of repetitive tests with a sample size of five for each set at different loading conditions. To obtain sound components (without any wrinkle growth) from all the tests, the initial rate of increase of pressure was kept relatively higher with respect to the end axial feed. In other word there was a steep build-up of the forming pressure in the initial stage of forming and the pressure was maintained throughout with simultaneous application of end axial feeds. This type of loading conditions were assumed, as it was seen from results of previous simulations and experiments done by many researchers [84,86,88] on X and

T-branch components where it has been shown that if the initial forming pressure is relatively high with respect to the end axial feed then the part expansion is relatively good. Finally from the formed components different response parameters (i.e. actual axial feed, branch height and percentage wall thinning at branch top- fig 3.3.4) were measured. Three sets of X-branch and one set of T-branch repetitive tests were conducted. Table 3.3.1 details the experimental test data with different responses for various X and T-branch tests.

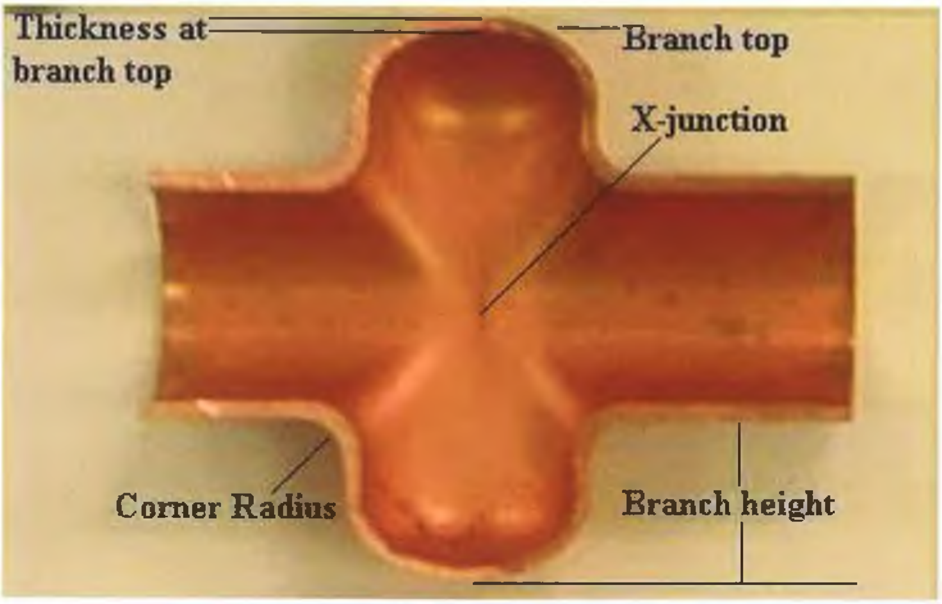

Fig 3.3.4 X-branch formed component with different parameter details

Table: 3.3.1 Experimental test data and results for repetitive tests

Type of test – X branch			
Setting-1 (maximum axial feed pressure-0.011GPa, maximum internal forming pressure-0.0387GPa.)			
Test	feed (mm)	branch height (mm)	% wall thickness reduction at the branch top
1	36.25	29.25	11.22
2	36.25	29.15	11.20
3	36.25	29.00	11.05
4	36.15	28.90	11.01
5	36.15	29.10	11.07
Spread (Max-Min)	0.10	0.35	0.21
Mean	36.21	29.08	11.11
% deviation from the mean value	0.14	0.60	0.94

Setting-2 (maximum axial feed pressure-0.005GPa, maximum internal forming pressure-0.0387GPa.)			
Test	feed (mm)	branch height (mm)	% wall thickness reduction at the branch top
1	17.60	14.40	11.11
2	17.55	14.10	11.10
3	18.05	14.50	11.15
4	18.00	14.15	11.01
5	17.55	14.05	10.98
Spread (Max-Min)	0.50	0.45	0.17
Mean	17.75	14.24	11.07
% deviation from the mean value	1.40	1.58	0.76

Setting-3 (maximum axial feed pressure-0.005GPa, maximum internal forming pressure-0.0308GPa.)			
Test	feed (mm)	branch height (mm)	% wall thickness reduction at the branch top
1	15.50	11.65	6.18
2	15.90	12.00	6.05
3	15.50	11.75	6.10
4	15.45	11.80	6.17
5	15.55	12.20	6.03
Spread (Max-Min)	0.45	0.30	0.15
Mean	15.58	11.81	6.10
% deviation from the mean value	1.44	1.27	1.22

Type of test – T branch			
Setting-1 (maximum axial feed pressure-0.011GPa, maximum internal forming pressure-0.0387GPa.)			
Test	feed (mm)	branch height (mm)	% wall thickness reduction at the branch top
1	36.25	25.00	14.12
2	36.12	25.10	14.01
3	36.22	25.00	14.55
4	36.00	24.70	13.92
5	36.10	24.90	13.98
Spread (Max-Min)	0.25	0.40	0.20
Mean	36.13	24.94	14.11
% deviation from the mean value	0.34	0.80	0.70

From the above table, considering the maximum spread and percentage deviation from the mean value, for the final axial feed, branch height and percentage wall thinning, it can be concluded that the machine is capable of producing consistent components or parts at a fixed load settings with a minor deviation and hence a single experiment with any of the load settings can be assumed to be reasonable good for study of the process in further detail.

3.3.2. Experimental design

Many researchers [42, 45, 49, 54, 61, 62] have shown that loading paths play a substantial role in tube hydroforming processes (i.e. part expansion, wall thickness distribution, wrinkle growth etc). Thus in this study, the effects of different load settings on the part expansion (branch height development) characteristic, wall thickness reduction and degree of wrinkle growth of a X-branch type expansion were studied experimentally for a X-type expansion. The experiments were designed with different load settings (forming pressure and end axial feed) to study the above effects. From previous literature review [50, 65] it was also observed that several geometric factors such as length of the tube, die corner radius, boundary conditions and process variables such as friction, forming pressure and feed have different effects on the process (i.e. final part expansion, wall thickness variation and development of wrinkle etc.). In the present experimental study and analysis the geometric factors (length and thickness of the tube, die corner radius) and friction conditions were kept constant. Thus only two process variables (forming pressure and end feed) were varied to study the different responses (i.e. branch height development, percentage wall thinning and wrinkle depth). For the experiments three different levels (low, medium and high) of forming pressure and end feed were selected i.e. the pressure levels were maintained at 0.0265GPa (low), 0.0308GPa (medium) and 0.0387GPa (high) respectively, and feed levels were maintained at 7.5mm (low), 15.50mm (medium) and 36.25mm (high) respectively. It was ensured that the minimum value of the pressure level was much above the yielding pressure of the tube, which was calculated by using the thin tube formula equation-1 (i.e. thin tubes subjected to internal pressure). Although the formula does not hold good for this kind of part geometry (X-expansion) however it gives an approximate estimation of the yielding pressure.

$$P_y = \frac{2\sigma_y t}{D-t} \qquad (1)$$

Where P_y is the minimum yielding pressure, σ_y (0.116GPa) is the yield strength of the material, D (22.8) and t (1.3mm) are the mean diameter and wall thickness of the tube. The above formula indicates that the minimum pressure (i.e. yielding pressure) to initiate the forming should be above 0.013GPa for the tube.

The experiments were conducted with all possible combinations of forming pressure and end axial feed and the final branch height, percentage wall thickness reduction at the branch top and centre of the tube (X-junction) and wrinkle depth were measured. Fig 3.3.5, fig 3.3.6, fig 3.3.7 and fig 3.3.8 details the different responses (branch height, wall thinning and wrinkle height) with respect to the variation of forming pressure and end axial feed.

3.3.3. Experiment results

From different response surface plots of pressure/feed vs. branch height, pressure/feed vs. percentage wall thinning and pressure/feed vs. wrinkle height, it can be seen that the part expansion (i.e. the branch height) is maximum when both forming pressure and end feed are maximum without any wrinkle growth, however there is a considerable wall thinning both at the branch top and at the X-junction, whereas with lower forming pressure and high axial feed the wrinkle height was the highest. As mentioned above in section 3.3.1 all the experiments were conducted with a loading path where the initial build-up of pressure was relatively high with respect to axial feed. Thus the wrinkle growth is not so prominent for any of the cases except for tests with low forming pressure and high axial feed, where a minor distortion due to wrinkle growth was observed at the X-junction. It has been shown in further detail in the later part of this chapter (section 3.4.6) and in Chapter 4, how different loading paths can affect the process considerably in terms of wall thickness reduction and wrinkle growth.

To allow a better understanding of the process (i.e. final part expansion, wall thickness distribution, failure modes due to different loading conditions), further experimental results have been presented in the subsequent sections of this chapter along with the finite element simulation results, and systematic comparisons have been made between these two results.

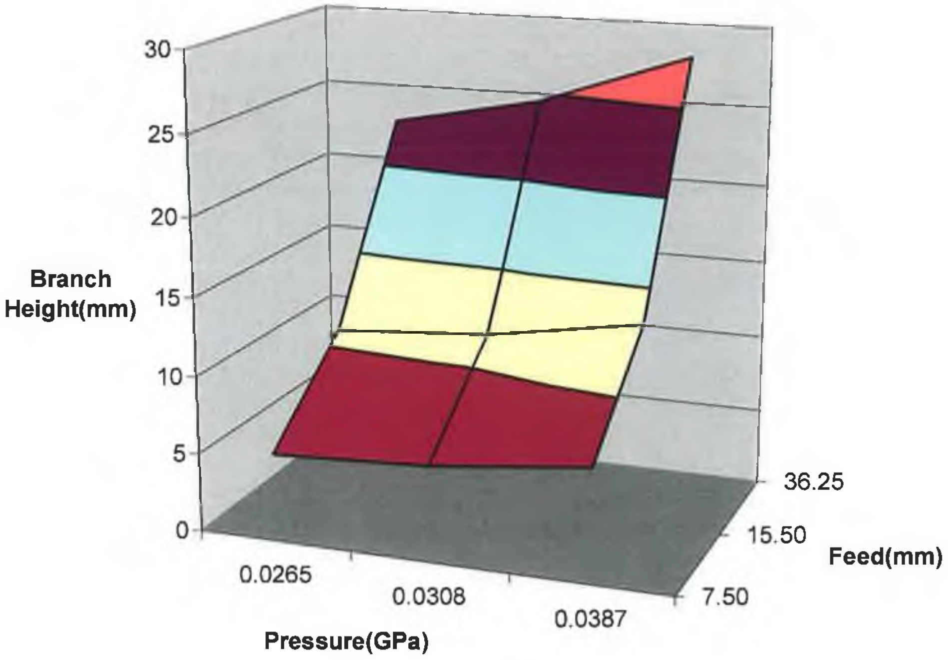

Fig 3.3.5 Variation of branch height with respect to forming pressure and end axial feed (X-branch forming)

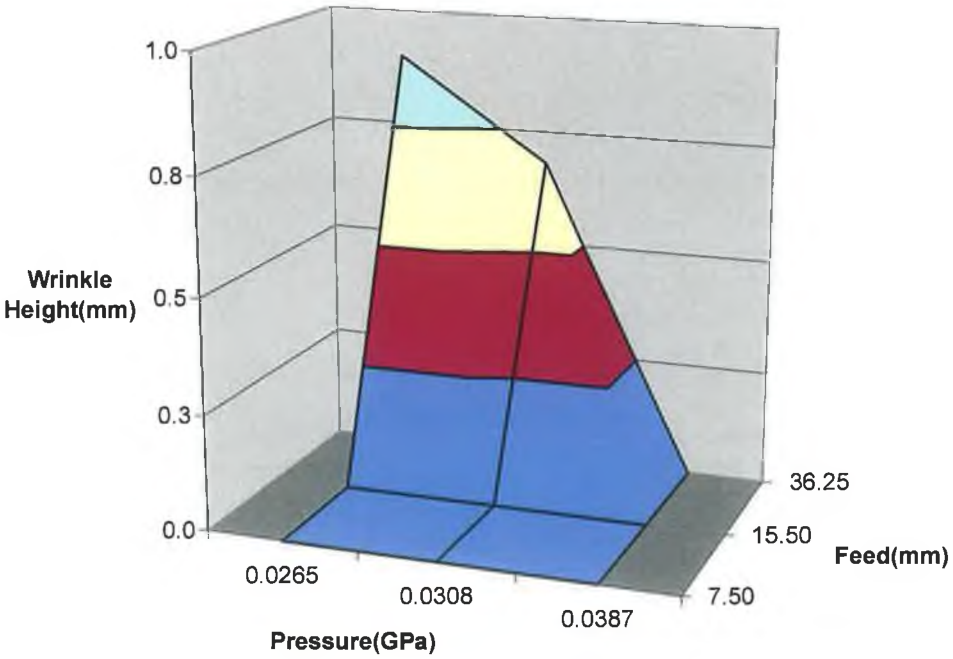

Fig 3.3.6 Variation of wrinkle height with respect to forming pressure and end axial feed (X-branch forming)

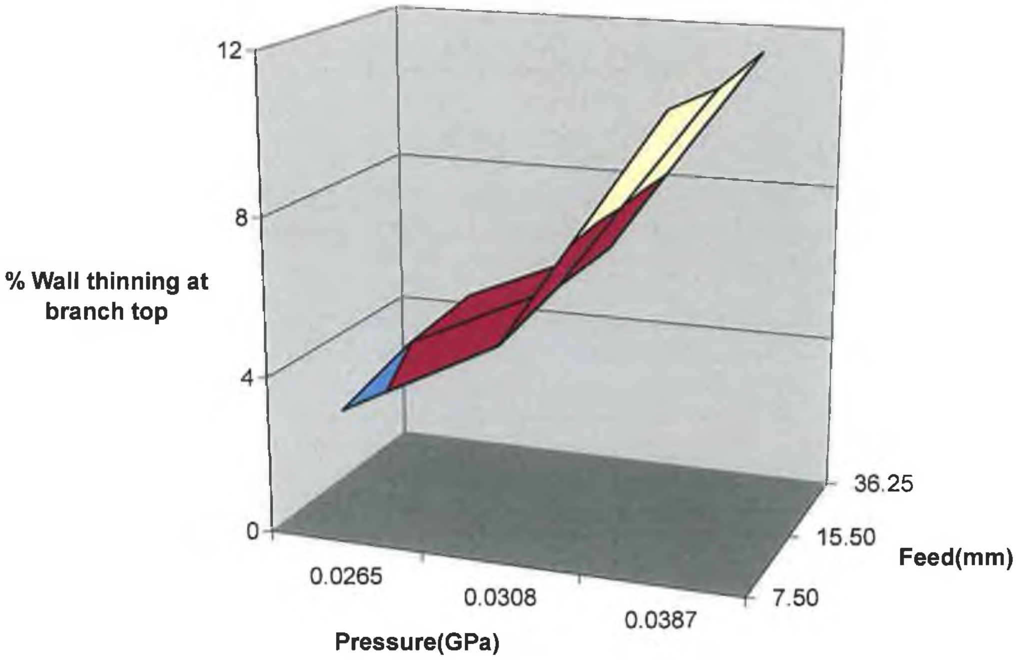

Fig 3.3.7 Variation of percentage wall thinning at the branch top with respect to forming pressure and end axial feed (X-branch forming)

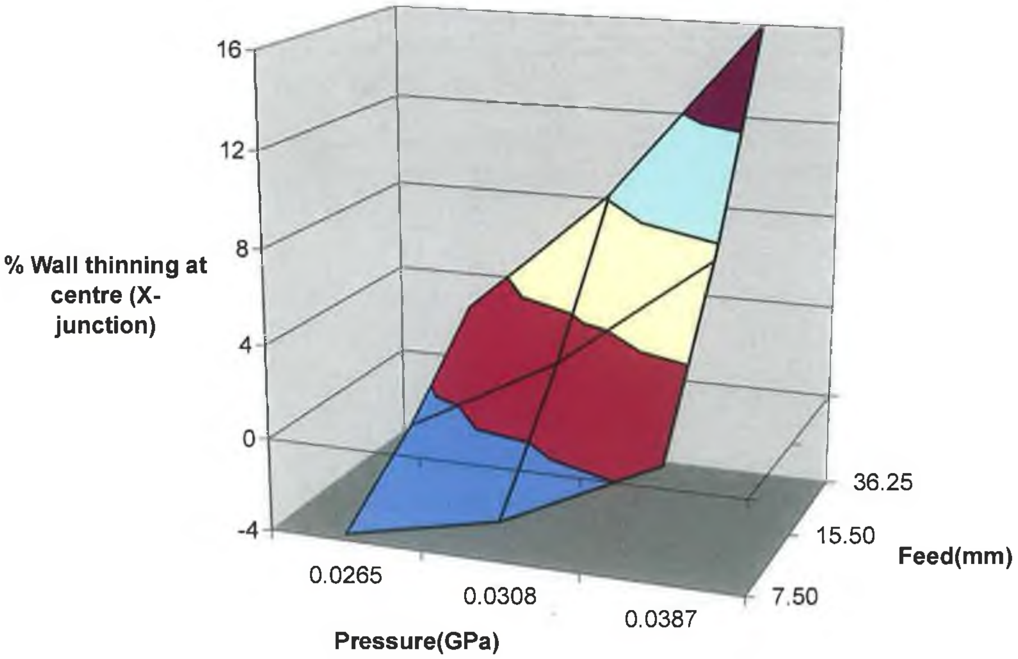

Fig 3.3.8 Variation of percentage wall thinning at centre (X-junction) with respect to forming pressure and end axial feed (X-branch forming)

3.4. Finite element simulation of X and T-branch components

In the recent years various 3D finite element analysis codes of dynamic explicit non-linear formulation such as LS-DYNA, DYTRAN, MARC, ABAQUS, PAM-STAMP have been widely used for simulations of various non-linear dynamic problems such as automotive crashworthiness and occupant safety, impact problems, dynamic vibration analysis, turbine blade containment, drop testing etc. However, it has been shown that these dynamic explicit codes can also be used for simulation of quasi-static problems as well as sheet metal forming processes [57, 77]. Furthermore these explicit finite element analysis codes have also been used extensively by many researchers for simulation of hydroforming processes [46, 49, 55, 56, 69, 72, 73].

This section discusses the finite element simulation of the process using LS-DYNA 3D finite element analysis code which includes, building the simplified CAD model, defining the material properties and attributes, finite element meshing, defining the contact interface parameters, finite element constraints, boundary and loading conditions, and solution control parameters. Finally different results of the simulations are presented, analyzed and compared with the corresponding experimental results so as to validate the developed finite element models against the experimental results.

Finite element simulation models of X and T-branch were built keeping a.) the solid model geometrical dimensions, the same as the experimental blank dimensions and the profile of the die curved surface area in contact with the blank and, b.) the simulation boundary conditions, the same as the experimental boundary conditions. This was done with the objective to study the forming process in further detail and to compare the finite element simulation results with the experimental results so as to set a bench mark for finite element modeling of X and T-branch type hydroforming processes which can reflect the actual physical process.

3.4.1. CAD and Finite element modelling

The most important step in any finite element simulation is the idealization and modelling of the problem. For metal forming simulations and analysis, which involves complex boundary conditions and contact interfaces, good modelling of the deforming body as well as the tooling is of most importance in order to achieve a realistic solution.

In order to properly represent the problem and to able to obtain better results, simultaneously detecting any unusual deformations such as wrinkling, folding and buckling a three-dimensional analysis is required. Furthermore, when building the preliminary CAD model it is important to identify first the element type to be used for meshing in the finite element simulation and as per that the CAD modelling should be done i.e. a CAD model for finite element analysis which will use 3D solid brick element will differ from a CAD model for finite element analysis which will use shell elements. In this case, the ANSYS pre-processor was used to build the 3D CAD and as well as the finite element models and the LS-DYNA 3D explicit solver was used for the forming analysis. The details of the finite element modelling are explained in the subsequent sections.

Simulations were conducted to hydroform X and T-branches from annealed copper tubes with 121mm length, 24mm outer diameter and 1.3mm wall thickness. The diameter of the branches was equal to that of the main tube. The geometry of the die and the tube were modelled to be consistent with the geometries of the experimental die and blank. In the present analysis only the deformation behaviour of the blank was studied, so the portion of die surface in contact with the blank and the portion of the plunger surface in contact with the blank were modelled as 3D surfaces (areas) and were meshed with 3D shell elements. The models were built in three parts a.) flexible tube blank, b.) rigid die and, c.) rigid taper plunger. By taking advantage of symmetry [49, 66], one-eighth portion of the X-branch (fig 3.4.1) and one-fourth portion of the T-branch (fig 3.4.2) were modelled.

The blank was modelled with four node LS-DYNA 3D explicit thin shell elements with fully integrated advanced Belytschko Wong Chiang shell element formulation. The shell thickness change option was activated in the simulation model, which allows the change of the shell thickness during the deformation process. Although the computation cost for this advanced element formulation is relatively high, however it is very suitable and highly recommended for simulation of sheet metal forming processes [91] as it avoids warping and hourglassing deformation modes during the course of the finite element simulation. The deformable blank portion (i.e. tube) of X and T-branches were modelled with 990 and 1980 quadrilateral mapped meshed elements respectively.

3.4.2. Contact definition

Proper contact definition is a very important aspect in metal forming analysis as it ensures the level of penetration and the friction to be maintained between the blank and the tool during the deformation process. In the finite element model, the sliding interfaces between the tube and die, and the tube and plunger, were modelled with an advanced automatic surface-to-surface contact algorithm with an elastic coulomb friction law, with an assumed coefficient of friction of 0.15 between the tube-contact (slave) and die-target (master) surfaces [88], exponential decay coefficient of 0.5 (default value of the finite element code), calculated viscous damping friction coefficient of 0.067 (default value of the finite element code) and viscous damping coefficient of 20 (default value of the finite element code). The values were calculated by the finite element program using empirical relations [91]. Apart form these two contact pairs, a third contact parameter was defined with single surface contact entity. This was defined on the blank surface with the purpose that in case there is formation of a wrinkle due to excessive axial feed, in such case this contact definition would take care of self-surface contact (crush) of the tube blank due to wrinkle or buckling. The purpose of using these advanced contact options in the model is to avoid any spurious results due to contact problems and large deformation usually encountered in sheet metal forming simulations.

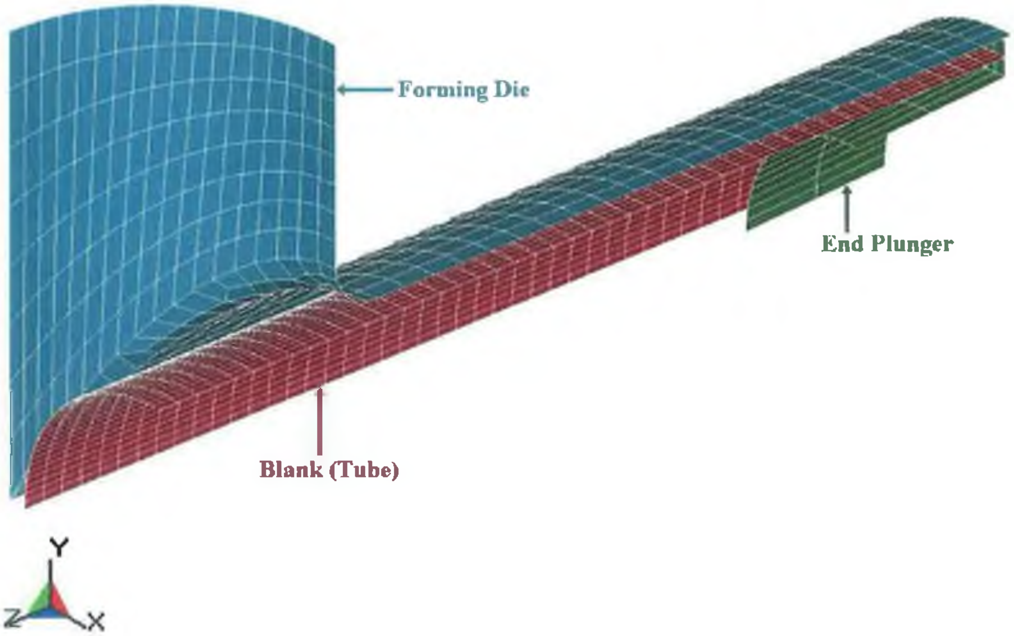

Fig 3.4.1 Finite element model of X-branch (one-eighth symmetric)

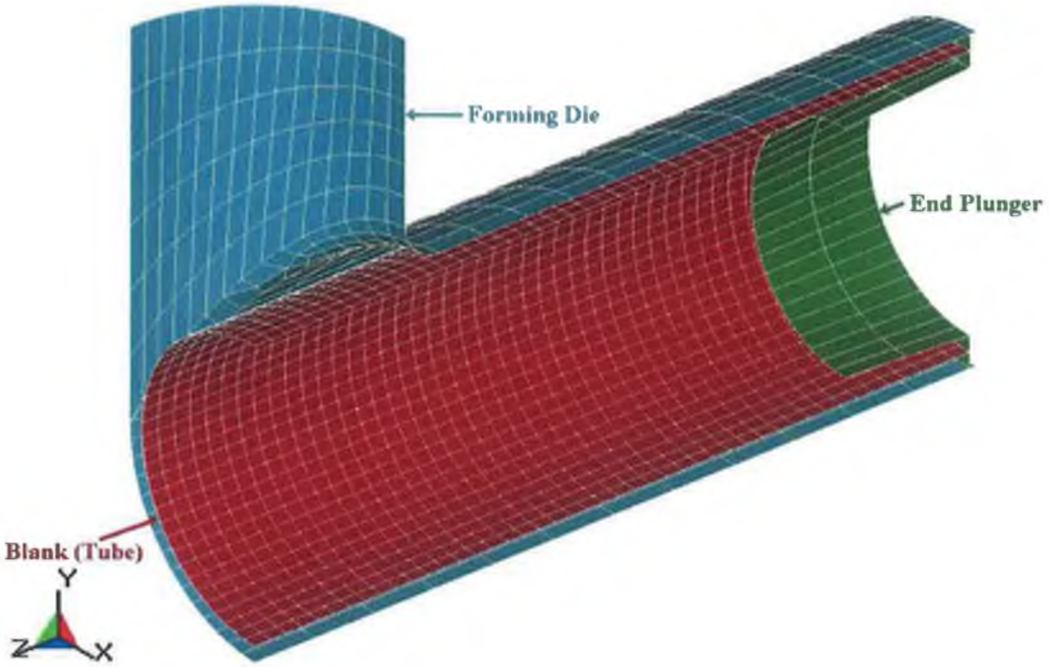

Fig 3.4.2 Finite element model of T-branch (one-fourth symmetric)

3.4.3. Material model

It is well known that most metal alloys show some anisotropic behaviour, however for this analysis an isotropic material model was assumed. Many researchers [19, 24] have reported that the exponential stress-strain laws (power law plasticity model) hold good for plasticity analysis of material with high ductility. Thus in the present analysis a power law plasticity model ($\sigma = 0.4257\varepsilon^{0.2562}$ GPa) representing the true stress-strain relation for the material was used for the simulation with strength coefficient (k=0.4257GPa) and hardening exponent (n=0.2562), and the other material properties (i.e. Young's modulus, yield strength, Poisson's ratio and density) were assumed to be same as mentioned above in the work specimen details (refer section 3.3). The material plastic flow properties (engineering stress-strain data) were obtained using a uniaxial tensile test of a standard flat copper specimen taken from the tube used for the experiment and the true stress-strain relation was derived from the engineering stress-strain value and subsequently a power law relation was fitted to it. Although in hydroforming the metal deformation is usually considered as bi-axial in nature (for thin tube hydroforming) [45, 61] however, for analytical study or for numerical simulation, the uniaxial stress-strain values of the deforming material equally holds good [61, 65].

The rigid die and the plunger were not fully modelled, only the surfaces in contact with the blank were modelled with 3D thin shell elements. The material properties used were of EN21 hardened tool steel for both die and plunger [88] with Young's modulus=210GPa, Poisson's ratio=0.3 and Density =7900Kg/m^3. Although the die and the plunger were assumed to be rigid, realistic material properties were defined as these values are used by the LS-DYNA finite element code for calculation of the contact stiffness.

3.4.4. Boundary conditions, constraints and loading

Since one-eighth portion of the X-branch and one-fourth portion of the T-branch were modelled for the simulation, by taking advantage of symmetry, the nodes at the symmetric edges of the tube were restrained in the appropriate directions and the nodes attached to tube end were kept free for all degrees of freedom. The pressure load was applied as a surface load on the shell elements with the normal directing outward assuming the pressure is acting on the tube inner surface and the axial load was applied as a prescribed displacement of the nodes at the edge of the tube end which was applied via the plungers. In the finite element model, the actual axial displacements were applied to the plungers. The die was assumed to be rigid, hence it was constrained for all degrees of freedom (i.e. translation and rotation) whereas the tapered rigid end plunger was constrained for all degrees of freedom except for Z- translation, i.e. it was allowed to move along the axis of the tube (fig 3.4.1, fig 3.4.2).

The load paths (plot of forming pressure vs. axial feed) used for the simulations were matched with the load paths obtained from the experiments. The experimental and simulation load paths for different experiments are shown in fig 3.4.3 to fig 3.4.14 in section 3.4.6 for X and T-branch respectively. In the simulation, the forming pressure and end axial feed were applied with respect to the time, however, due to the quasi-static nature of the process [46, 49, 50, 55, 72], it is more logical to represent the load-path plot as, forming pressure as a function of axial feed where the process is not time dependent. In the experimental pressure readings, it was observed that initially the pressure increased steadily but in the later part of the process it kept varying or fluctuating which was due to the dynamic nature and high sensitivity of the pressure intensifier, thus in the finite element simulation, the pressure variation was averaged in the fluctuating zone.

3.4.5. Finite element solution control parameters

For all the simulations, an average simulation termination time of 3.8msec was used. Due to the use of advanced, fully integrated shell element formulation with hourglass control, with relatively small element size of the mesh and large value of Young's modulus of the material blank as well as die, the LS-DYNA calculated solution time step size was very small, this resulted in a long simulation time. To overcome this problem, mass-scaling was used in the model to increase the time step size resulting in reduction of the total computation time (CPU). The LS-DYNA time step size Δt of the simulation depends on the smallest element characteristic length, which is given by equation-2.

$$\Delta t = \frac{l}{c} \qquad (2)$$

Where l is the characteristic element length. The l and c are calculated in a different manner depending on the type of element concerned in the finite element simulation. For shell elements, l is the smallest distance between two neighbouring nodes of the smallest element in the model and c is the velocity of sound wave propagation in the material. The sound wave propagation speed is given by equation-3.

$$c = \sqrt{\frac{E}{(1-\nu^2)\rho}} \qquad (3)$$

Where E is the Young's modulus, ν is the Poisson's ratio and ρ is the mass density of the material.

Furthermore during the simulation of the forming process, some of the elements are subjected to large deformation (compressive) due to which there is a drastic decrease in overall characteristic length of these deformed elements, this leads the code to assign new time step size whose values are further smaller in nature in comparison to the initial time step size. This results in drastic increase of the overall computation time. Thus to avoid such kind of situation a fixed time step size or mass-scaling was used as explained above. Further the quasi-static deformation nature of the process can be further justified by considering the flow strain rate of the deformation. This was established by simulating the process (X-branch test-d, refer table 3.4.1) with an actual forming time of 3.8sec and the strain rates for highly deformed elements were studied. It was found that the strain rates of the highly stretched or deformed elements were of the order of 0.01/sec-0.05/sec. This proves that the overall process can be considered as a low strain rate deformation process and hence the assumption of quasi-static deformation holds good for the numerical simulation of the process (refer fig 2.4.1), thus a reduced or scaled down simulation time of 3.6msec to 3.8msec was used for all successive simulation where the actual forming time (experimental) was usually of the order of 3.5sec to 4.0sec. As in the simulation time step size was kept constant by incorporating mass-scaling in the solution process, thus the ratio of process kinetic energy over the total internal energy was checked and ensured that it was as low as possible (i.e. of the order of 10^{-4}) to ensure that there was no dynamic or inertial effect in the entire solution period.

Also the results (branch height, wall thinning and thickening) of a part simulated with an actual process time of 3.8sec was compared with, a.) the experimental results and, b.) with finite element simulation model with a reduced/scaled simulation time of 3.8msec. The results show that the part expansion and wall thinning and thickening behaviour were almost identical with the results of the finite element simulation model with reduced/scaled down simulation time and were also in good agreement with the experimental results. However it was observed that the overall computation time with actual process simulation time (3.8sec) was approximately 120hours with a finite element model mesh density of 990 elements (X-branch forming), without time step sizing.

3.4.6. Results and analysis

For better understanding of the finite element simulation results, the experimental and simulations results are presented in parallel. The simulation results, a.) the forming load path, b.) developed branch height, and c.) final tube wall thickness variation at various planes, are presented for both X and T-branch forming with different loading conditions and are compared with the experimental results.

1. Load path comparison

As mentioned in the previous section the load paths used for the simulation were matched with the actual dynamic load path recorded by the LabView data acquisition system during the forming operation. Fig 3.4.3 to fig 3.4.14 details the load paths for all the test conditions (internal forming pressure vs. end axial feed) for X and T-branch experiments and represents the actual load path trend (variation) during the entire forming operation. All the load paths follow similar trend (i.e. initial rise in forming pressure with respect to end axial feed) except for the cases where failure due to wrinkle was observed (refer section 4).

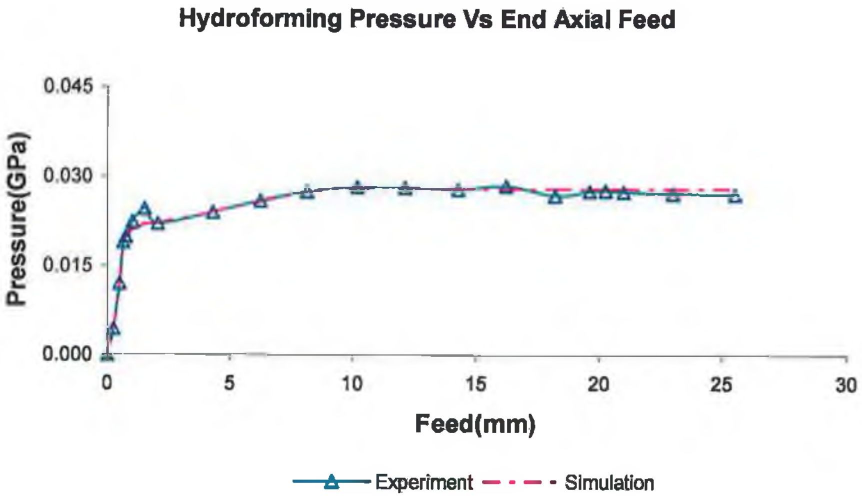

Fig 3.4.3 Experimental and simulation load paths-(Test-a, X-branch hydroforming)

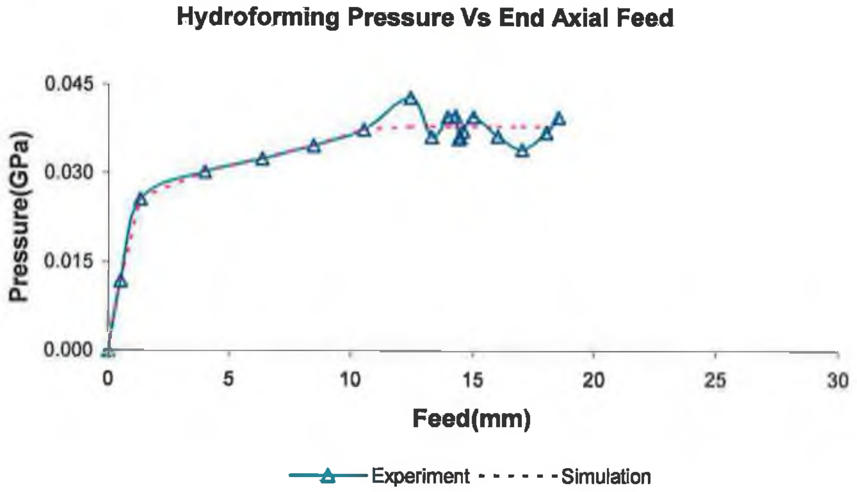

Fig 3.4.4 Experimental and simulation load paths-(Test-b, X-branch hydroforming)

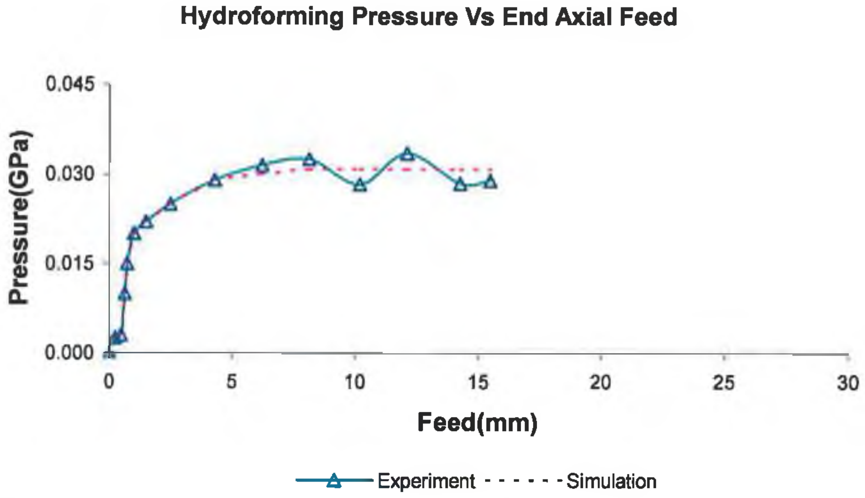

Fig 3.4.5 Experimental and simulation load paths-(Test-c, X-branch hydroforming)

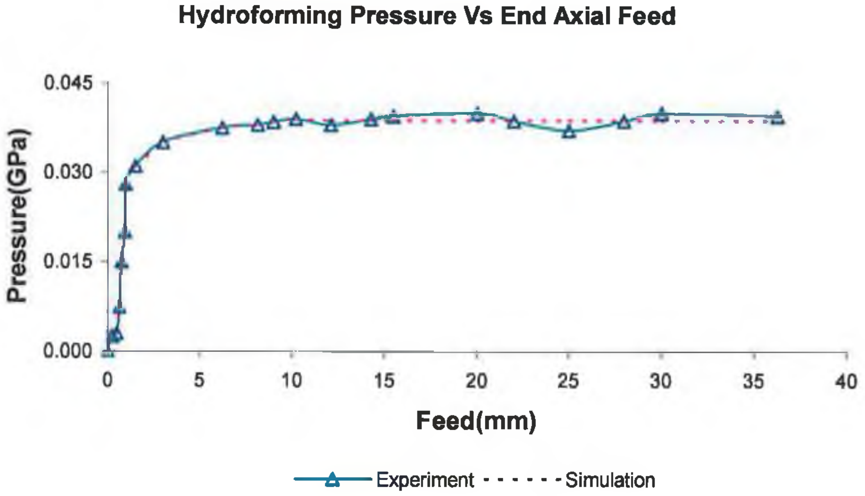

Fig 3.4.6 Experimental and simulation load paths-(Test-d, X-branch hydroforming)

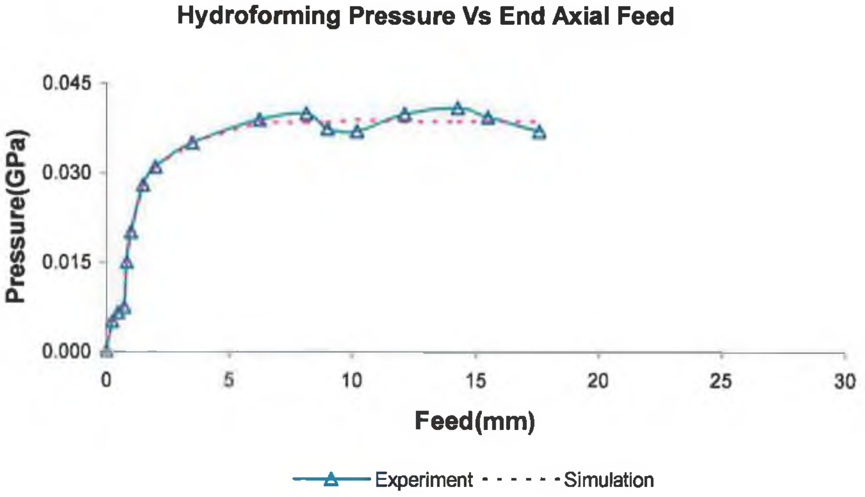

Fig 3.4.7 Experimental and simulation load paths-(Test-e, X-branch hydroforming)

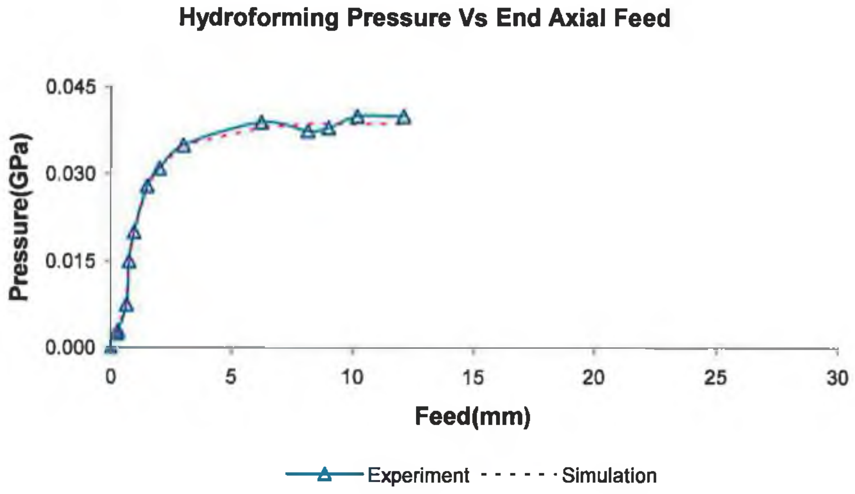

Fig 3.4.8 Experimental and simulation load paths-(Test-f, X-branch hydroforming)

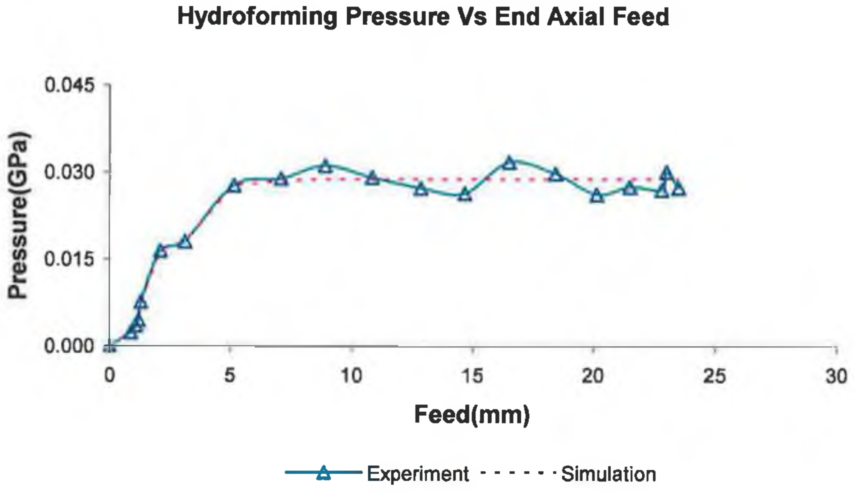

Fig 3.4.9 Experimental and simulation load paths- (Test-a, T- branch hydroforming)

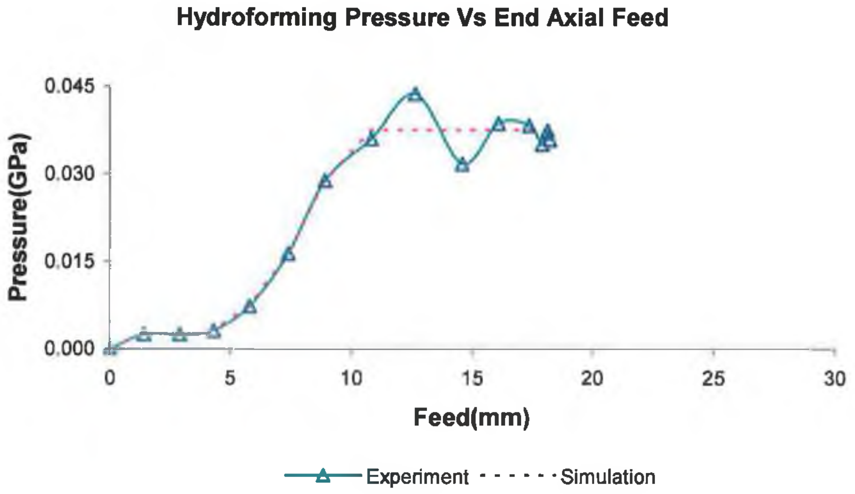

Fig 3.4.10 Experimental and simulation load paths- (Test-b, T- branch hydroforming)

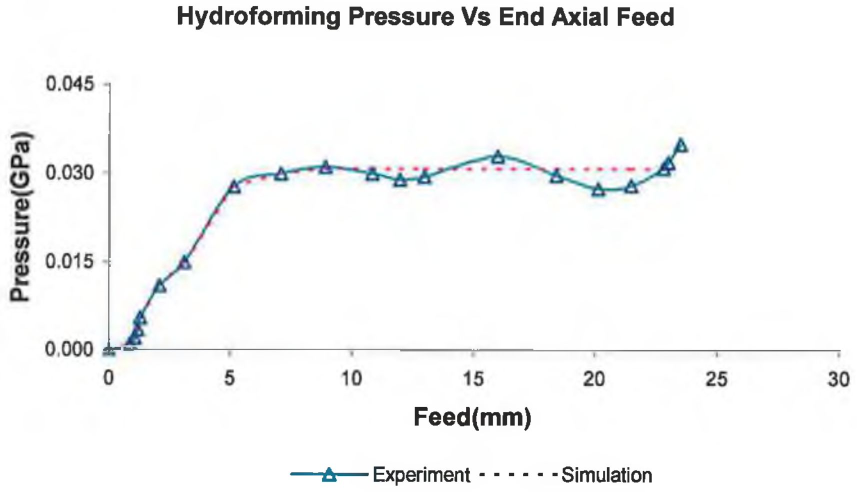

Fig 3.4.11 Experimental and simulation load paths- (Test-c, T- branch hydroforming)

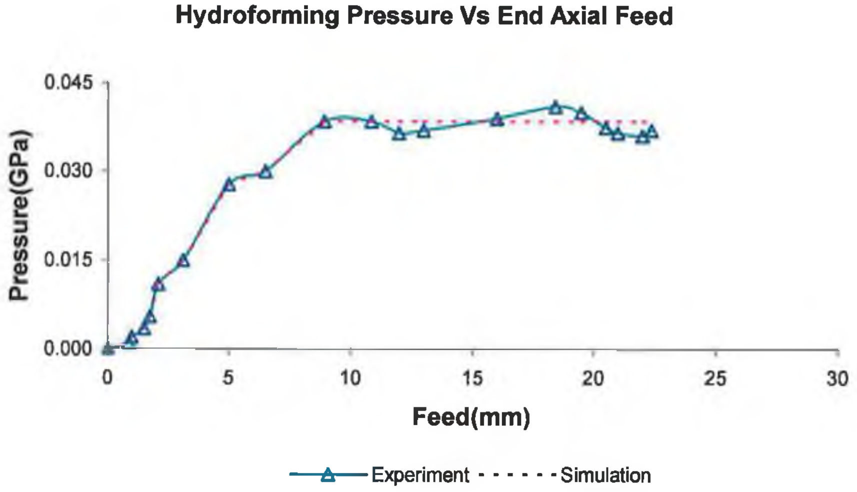

Fig 3.4.12 Experimental and simulation load paths- (Test-d, T- branch hydroforming)

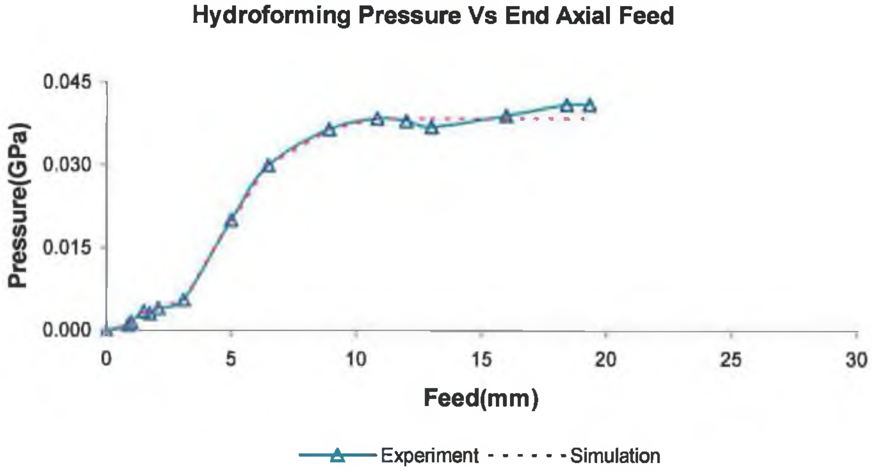

Fig 3.4.13 Experimental and simulation load paths- (Test-e, T- branch hydroforming)

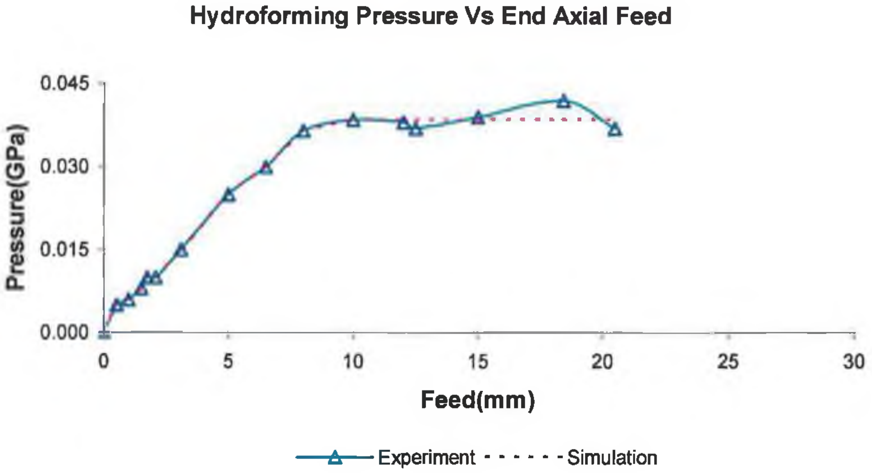

Fig 3.4.14 Experimental and simulation load paths- (Test-f, T- branch hydroforming)

For the initial stage of the simulation, the load paths were kept as it is, however for the later part or the fluctuating and unstable zone, the values were averaged and a smooth value was used. Separate sets of simulations were also conducted with the exact fluctuating experimental load paths to check if the fluctuation in pressure has any considerable effects on the part expansion. It was observed that both the experimental (fluctuating) load path and simulation (pressure value averaged over the fluctuating zone) load path yield similar result for the maximum developed branch height with a maximum deviation of 0.05%. Thus it can be concluded that the averaged or simplified simulation load paths gives a good approximation of the experimental load paths.

Depending upon the machine settings, (i.e. the pressure settings of the pressure reducing valves), it was observed that the load paths varied for different types of forming operation. For X-branch forming, the pressure increased rapidly to the maximum value whereas for T-branch forming a more gradual increase was noticed. This inconsistence was mainly due to the unsteady nature of the pressure build-up in the system during the forming operation.

2. Branch height comparison

The final branch heights (H- i.e. from the top surface of the tube to the maximum protrusion height of the bulged section-fig 3.4.16, fig 3.4.18), for the X and T-branch

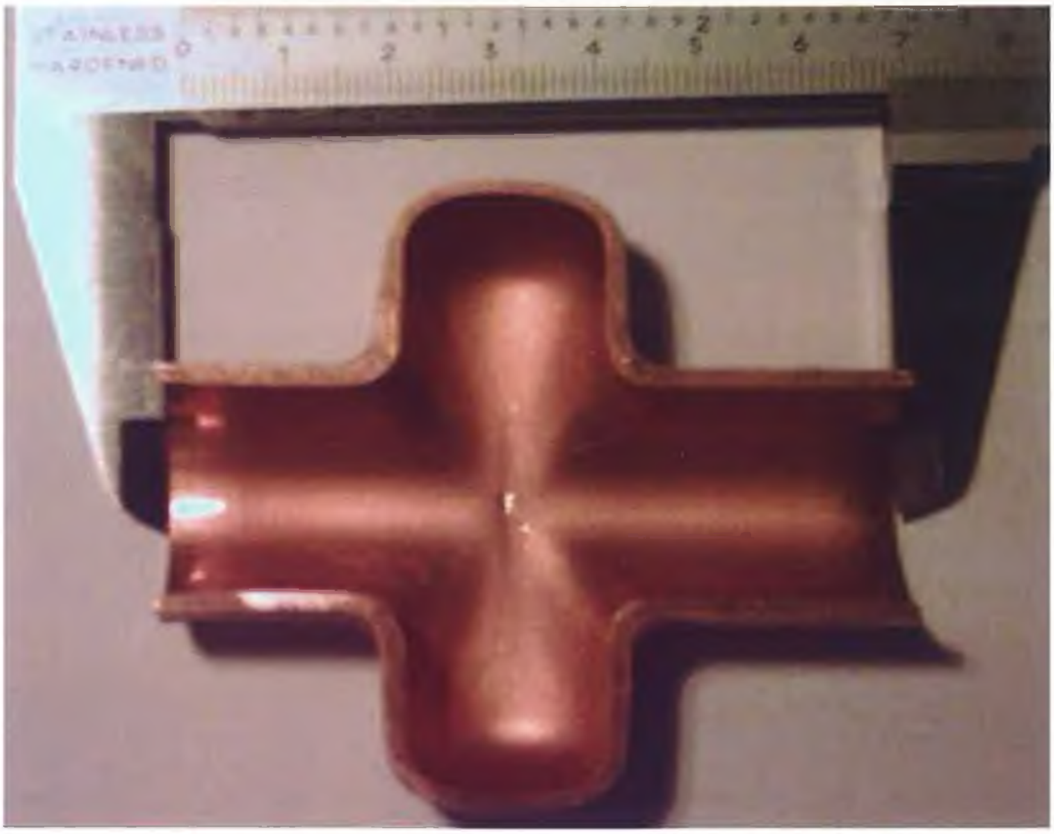

Fig 3.4.15 Experiment sample (test-a- X-branch)

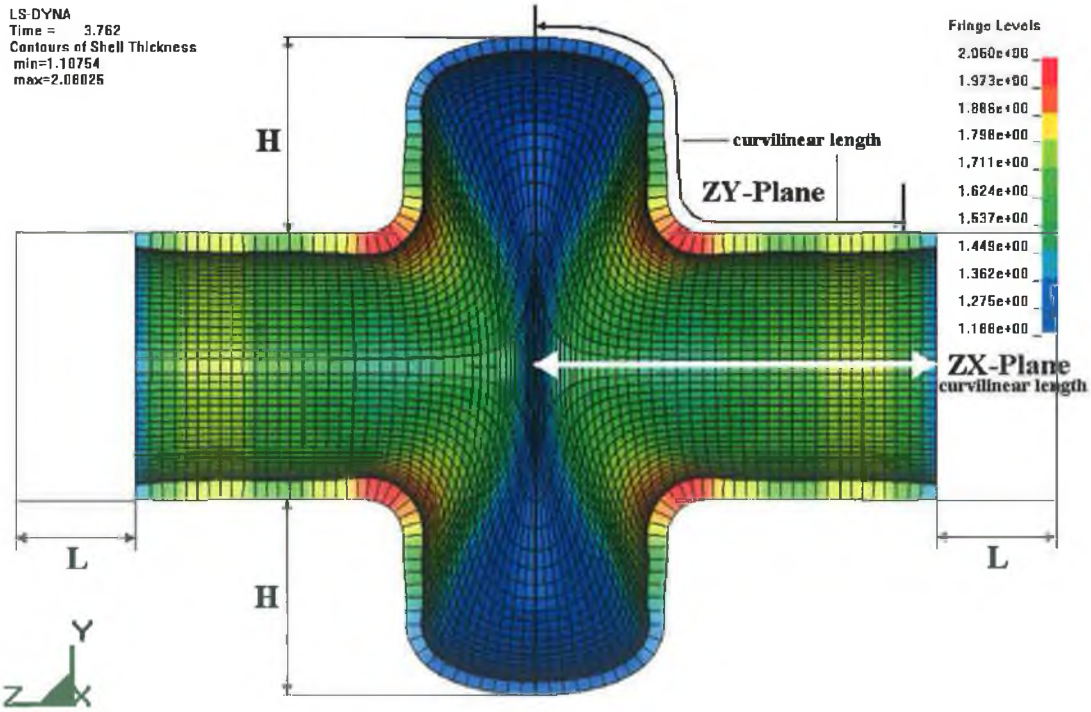

Fig 3.4.16 Simulated model of X-branch (test-a)

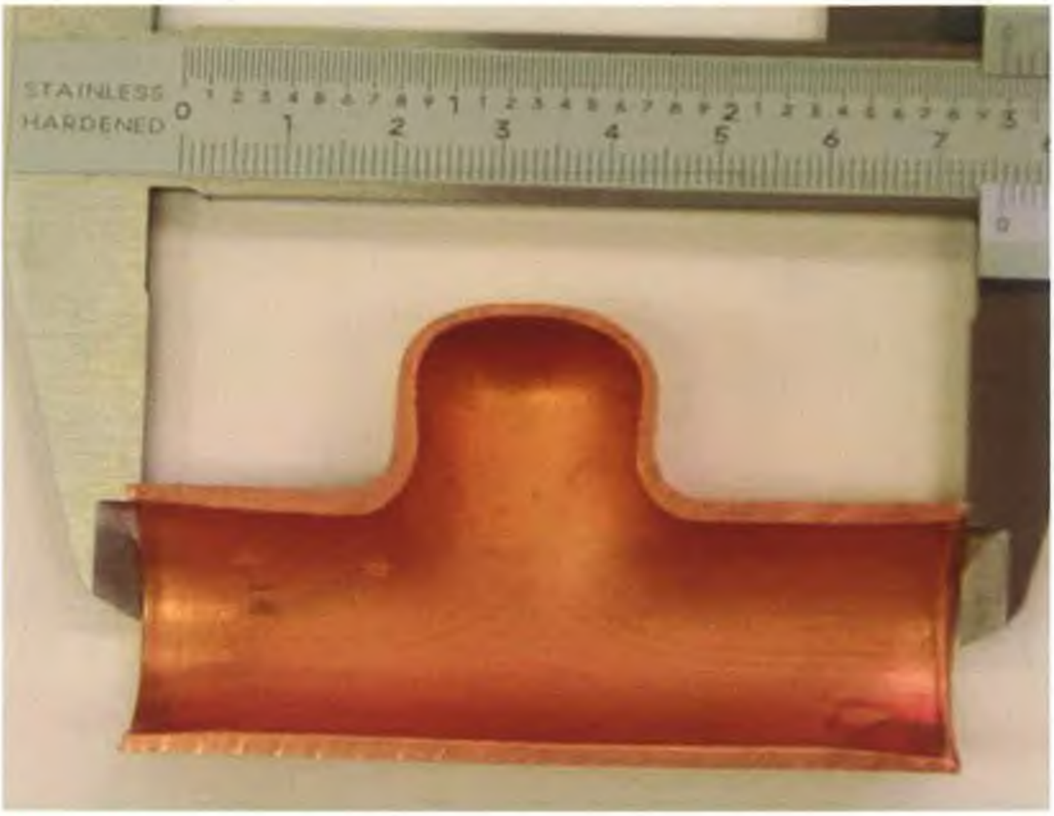

Fig 3.4.17 Experiment sample (test-a- T-branch)

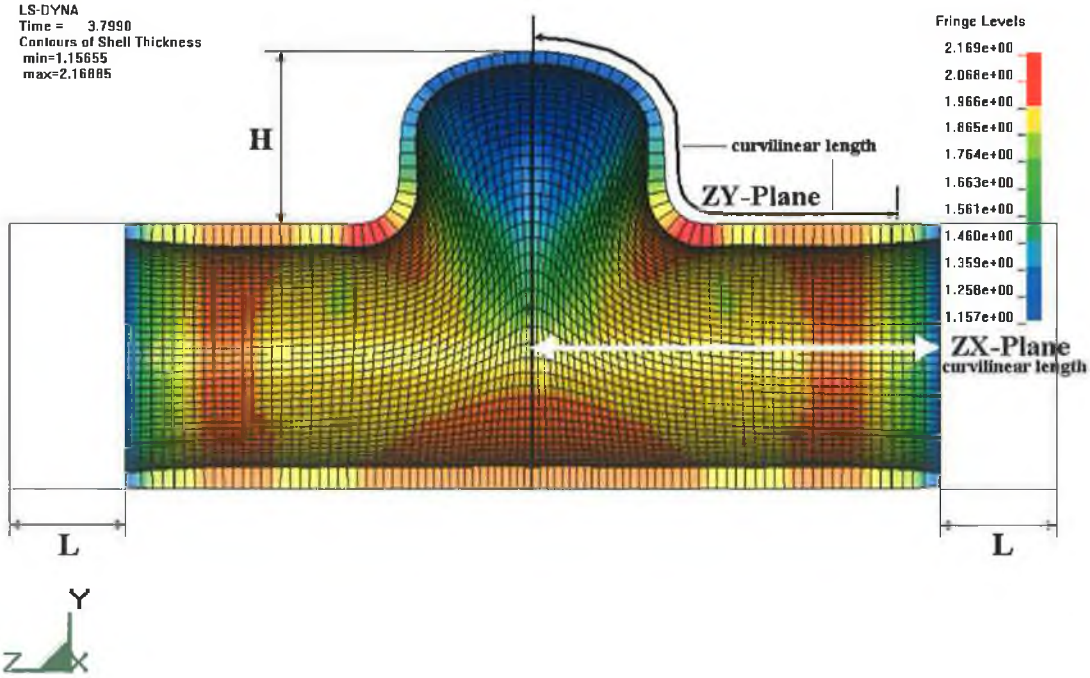

Fig 3.4.18 Simulated model of T-branch (test-a)

were measured from the hydroformed experimental samples (fig 3.4.15, fig 3.4.17) and were compared with the simulation results. Table 3.4.1 shows the results of the final branch height development with percentage deviation of simulation results with respect to the experimental results for twelve different tests with different load settings (maximum forming pressure i.e. the average value of the pressure at the unsteady or fluctuating zone of the load path and, total end axial feed) for X and T-branch forming. The maximum deviation in the branch height obtained from simulation was within +/- 5.30 % of the experimental value.

Table 3.4.1 Branch height comparison–experiment and simulation results

Branch type	Maximum-internal pressure (GPa) (average value at the fluctuating zone)	Total-feed (L) (mm)	**Branch height (H) (mm) (Experiment)**	**Branch height (H) (mm) (Simulation)**	Percentage deviation (Simulation results w.r.t Experiment)
X-Test-a	0.0284	25.50	**17.75**	**17.82**	-0.39
X-Test-b	0.0370	18.50	**14.75**	**15.44**	-4.67
X-Test-c	0.0308	15.50	**11.75**	**11.54**	+1.78
X-Test-d	0.0387	36.25	**29.15**	**27.93**	+4.18
X-Test-e	0.0387	17.60	**14.05**	**14.53**	-3.41
X-Test-f	0.0387	12.25	**10.75**	**10.79**	-0.37
T-Test-a	0.0294	23.50	**17.70**	**17.08**	+3.50
T-Test-b	0.0375	18.22	**12.70**	**12.32**	+2.99
T-Test-c	0.0308	24.25	**16.50**	**17.13**	-3.81
T-Test-d	0.0385	22.36	**19.50**	**18.58**	+4.71
T-Test-e	0.0385	19.35	**15.50**	**15.77**	-1.74
T-Test-f	0.0385	20.50	**17.30**	**16.39**	+5.26

3. Wall thickness distribution

To study the material flow characteristics in the final formed components, the wall thickness distributions were plotted along different planes. Fig 3.4.19 to fig 3.4.30 show the wall thickness plots of experimental and finite element simulation results in two different planes (zy and zx planes) along the curvilinear length of the tube (fig 3.4.16 and fig 3.4.18) from the center of the tube to tube end. Due to the presence of tapered punch (which was also modelled in the simulation) the wall thickness at the tube end has decreased in comparison to the straight portion of the tube. Thus, in the wall thickness plots the thickness at the tube end was ignored.

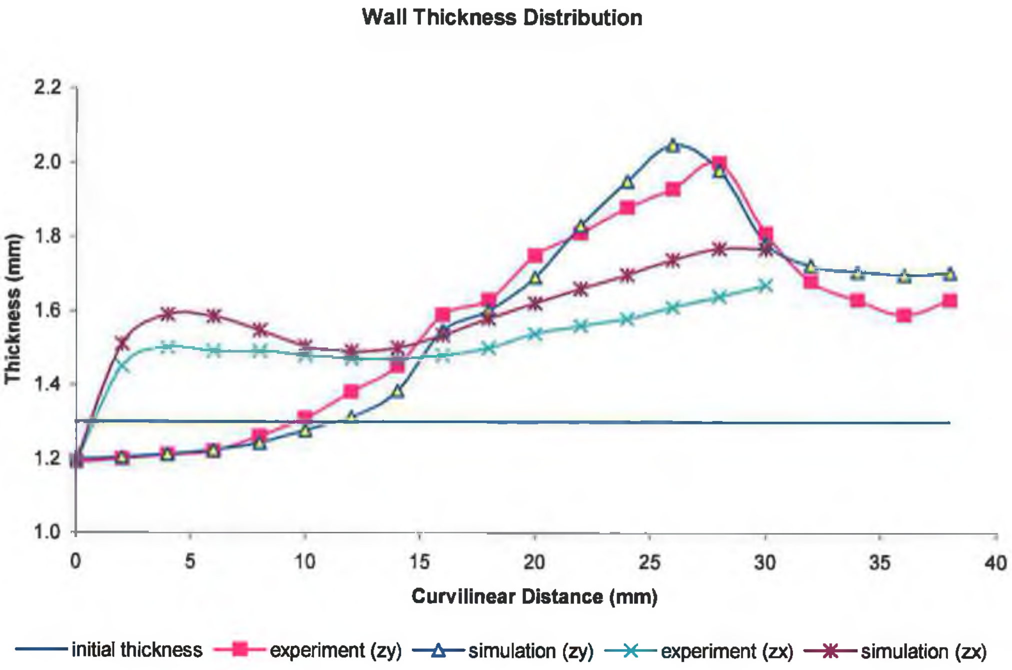

Fig 3.4.19 Wall thickness distribution along the curvilinear length, from tube centre to tube end along planes, zx and zy- X-branch (test-a)

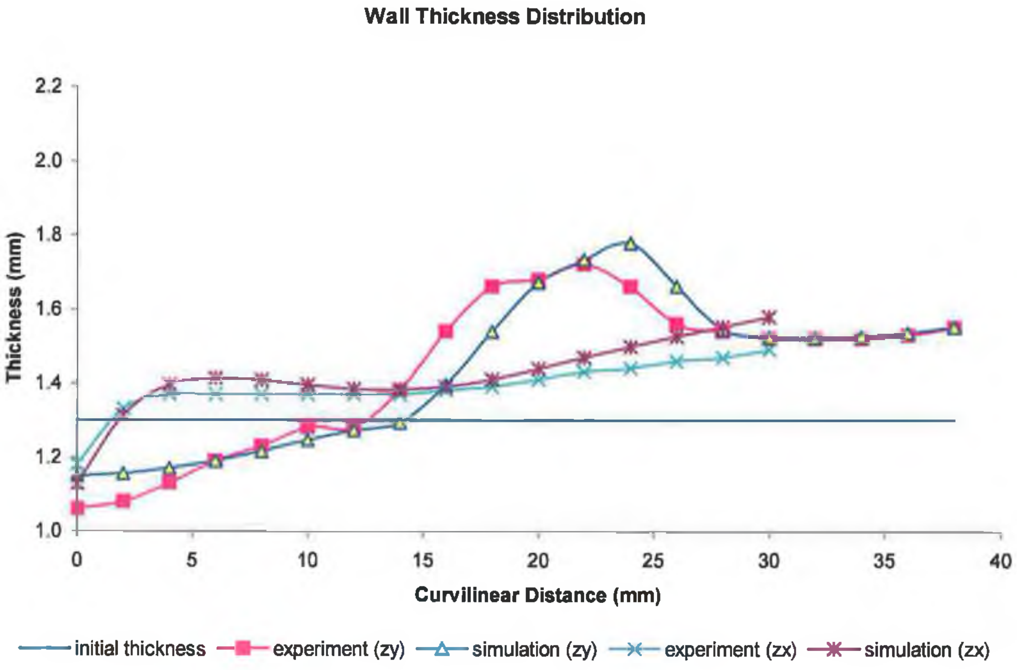

Fig 3.4.20 Wall thickness distribution along the curvilinear length, from tube centre to tube end along planes, zx and zy- X-branch (test-b)

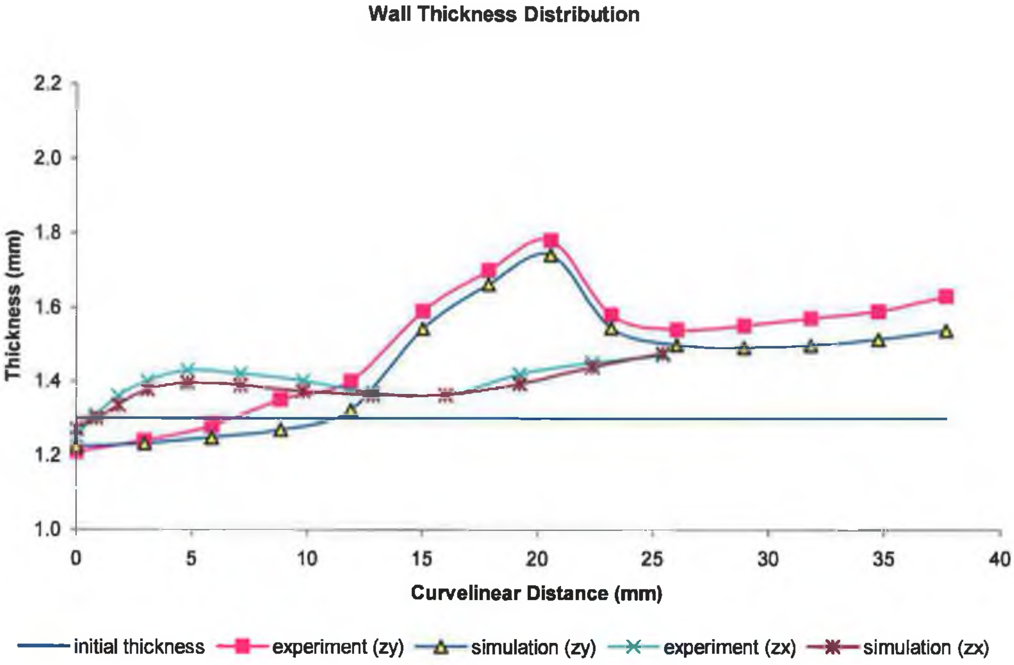

Fig 3.4.21 Wall thickness distribution along the curvilinear length, from tube centre to tube end along planes, zx and zy- X-branch (test-c)

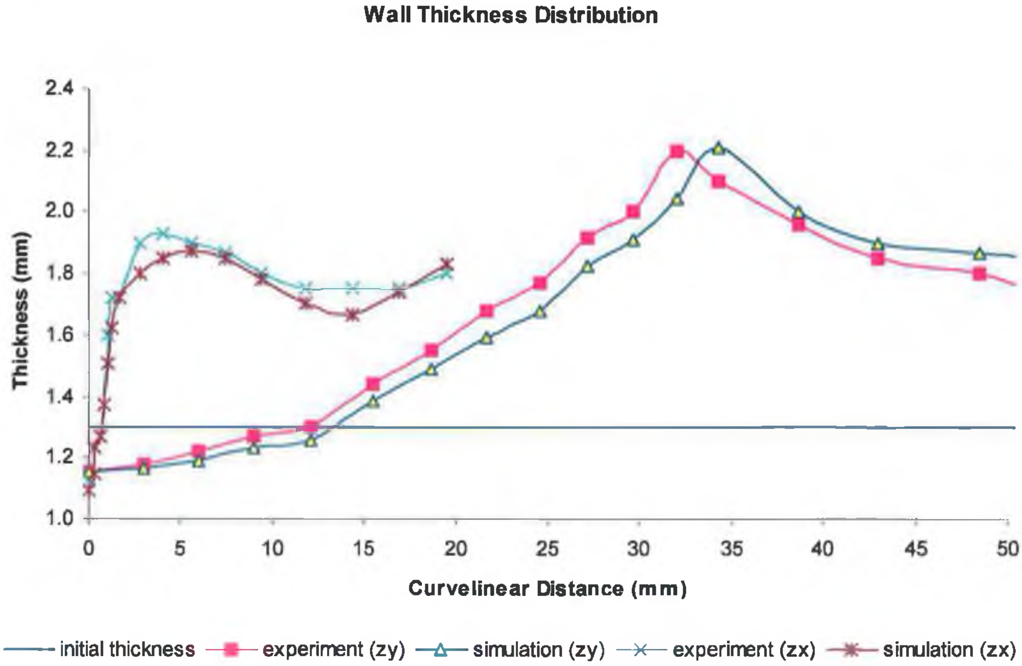

Fig 3.4.22 Wall thickness distribution along the curvilinear length, from tube centre to tube end along planes, zx and zy- X-branch (test-d)

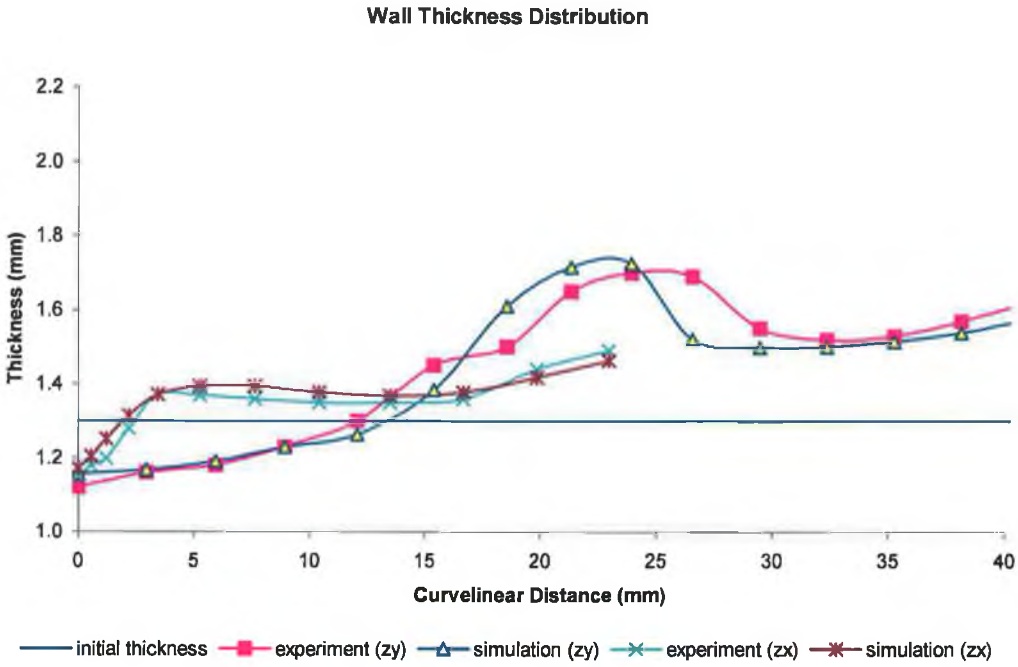

Fig 3.4.23 Wall thickness distribution along the curvilinear length, from tube centre to tube end along planes, zx and zy- X-branch (test-e)

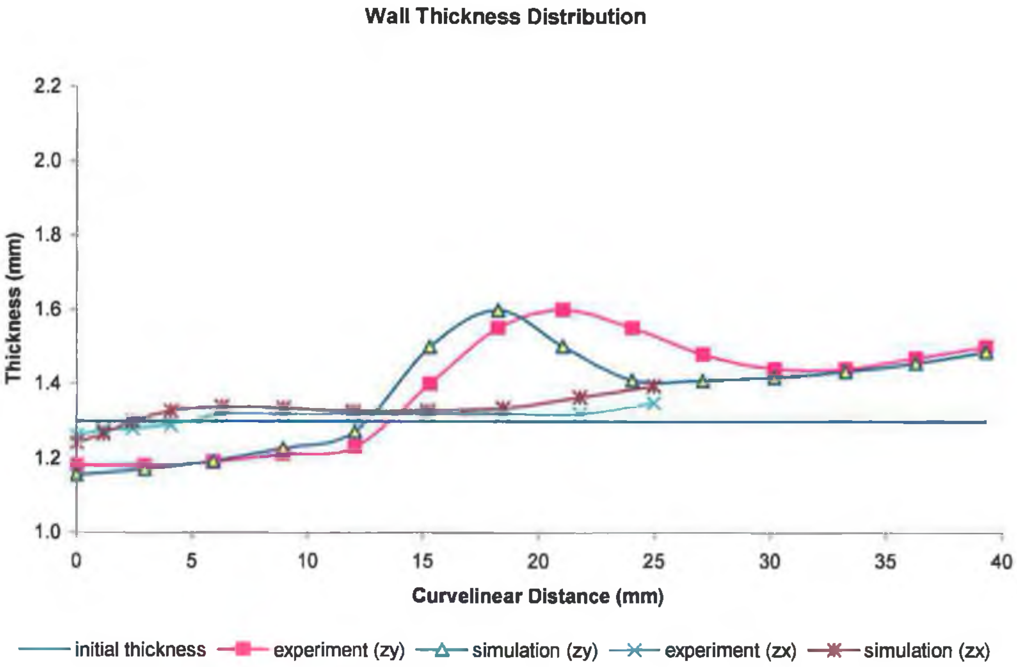

Fig 3.4.24 Wall thickness distribution along the curvilinear length, from tube centre to tube end along planes, zx and zy- X-branch (test-f)

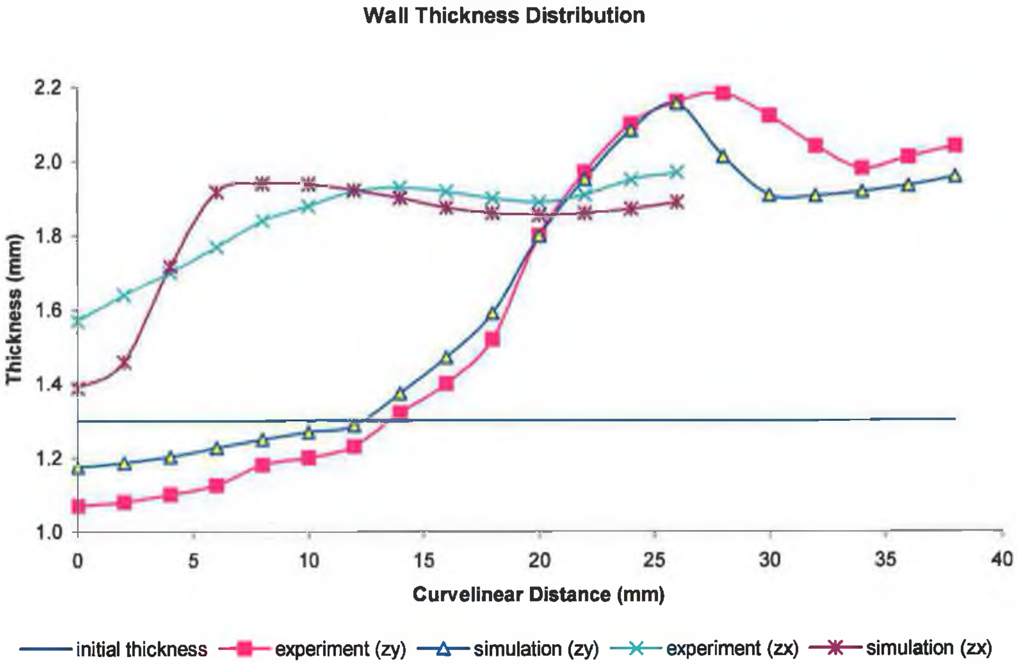

Fig 3.4.25 Wall thickness distribution along the curvilinear length, from tube centre to tube end along planes, zx and zy- T-branch (test-a)

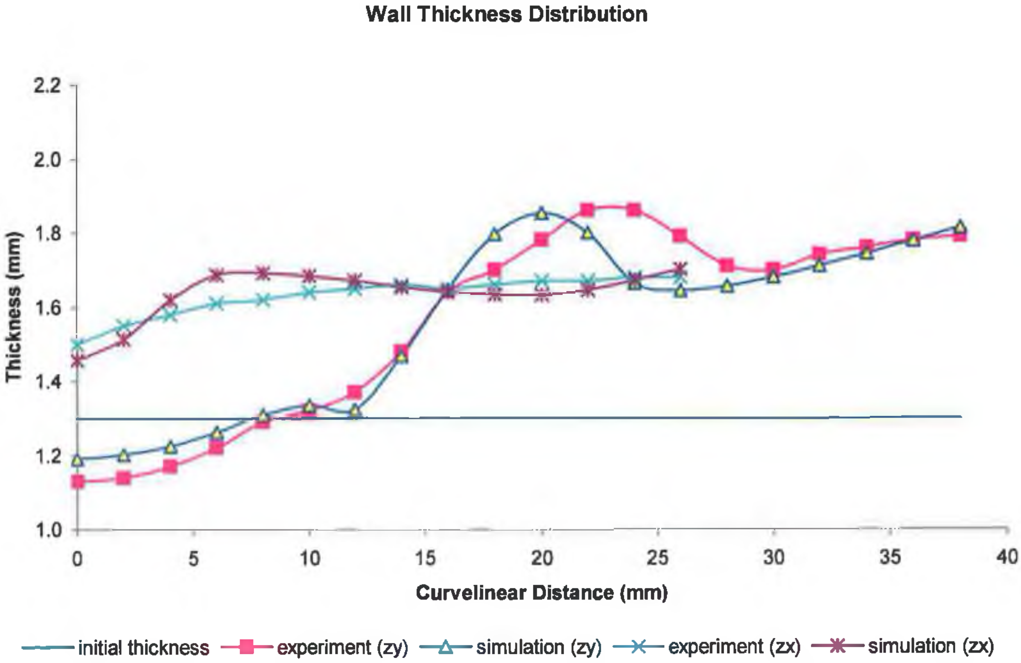

Fig 3.4.26 Wall thickness distribution along the curvilinear length, from tube centre to tube end along planes, zx and zy- T-branch (test-b)

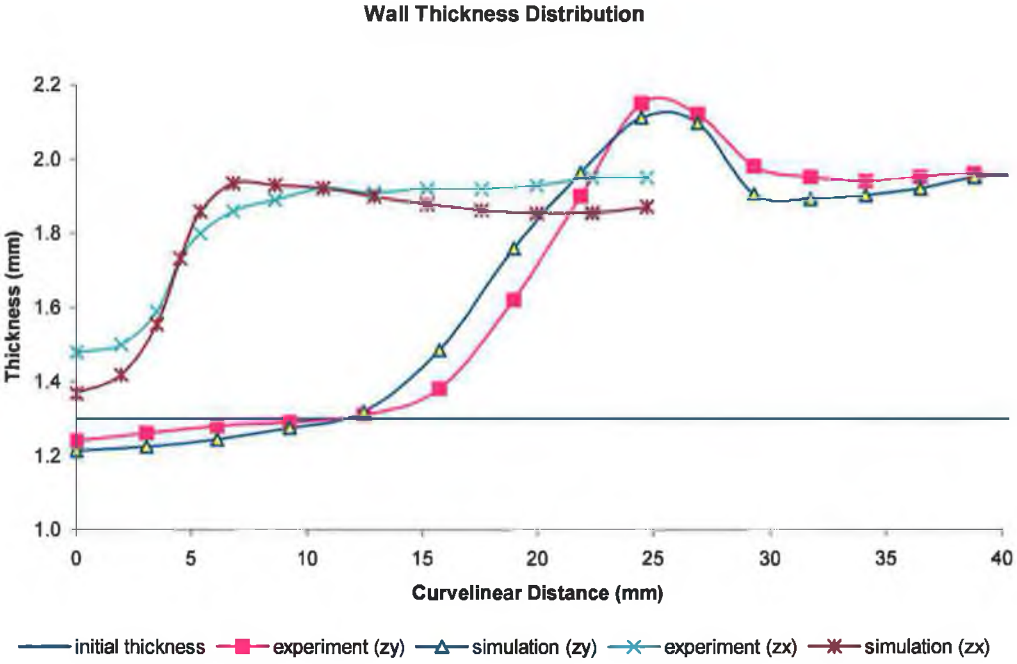

Fig 3.4.27 Wall thickness distribution along the curvilinear length, from tube centre to tube end along planes, zx and zy- T-branch (test-c)

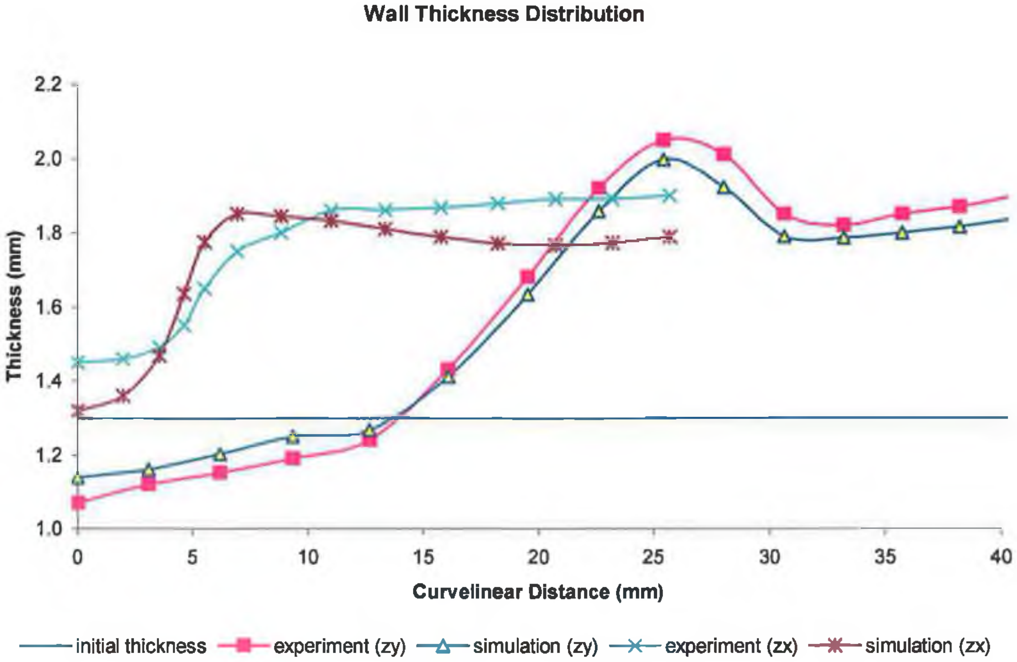

Fig 3.4.28 Wall thickness distribution along the curvilinear length, from tube centre to tube end along planes, zx and zy- T-branch (test-d)

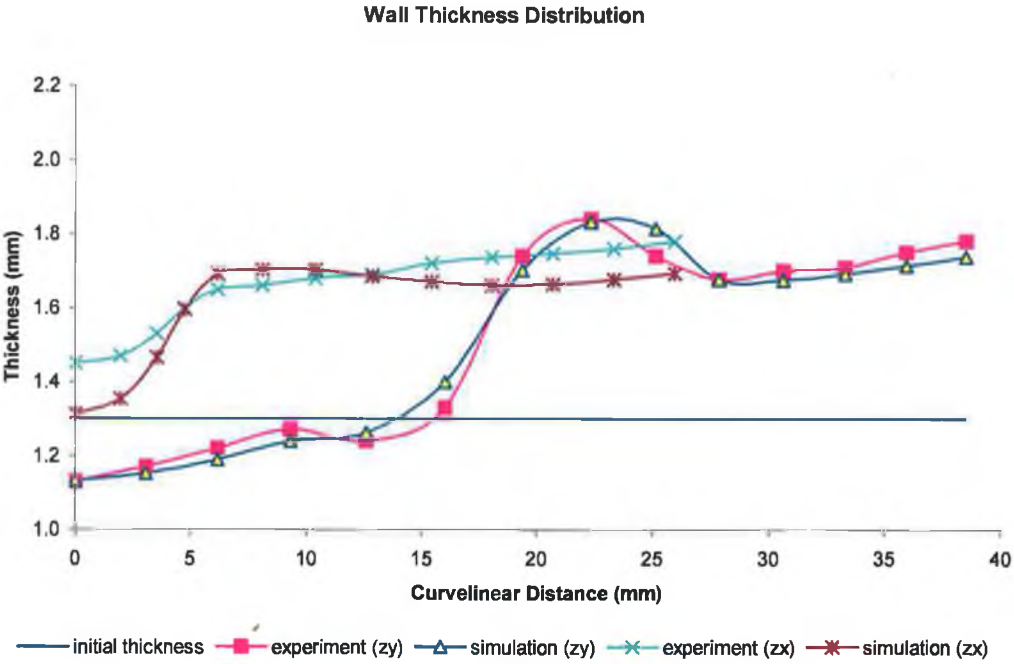

Fig 3.4.29 Wall thickness distribution along the curvilinear length, from tube centre to tube end along planes, zx and zy- T-branch (test-e)

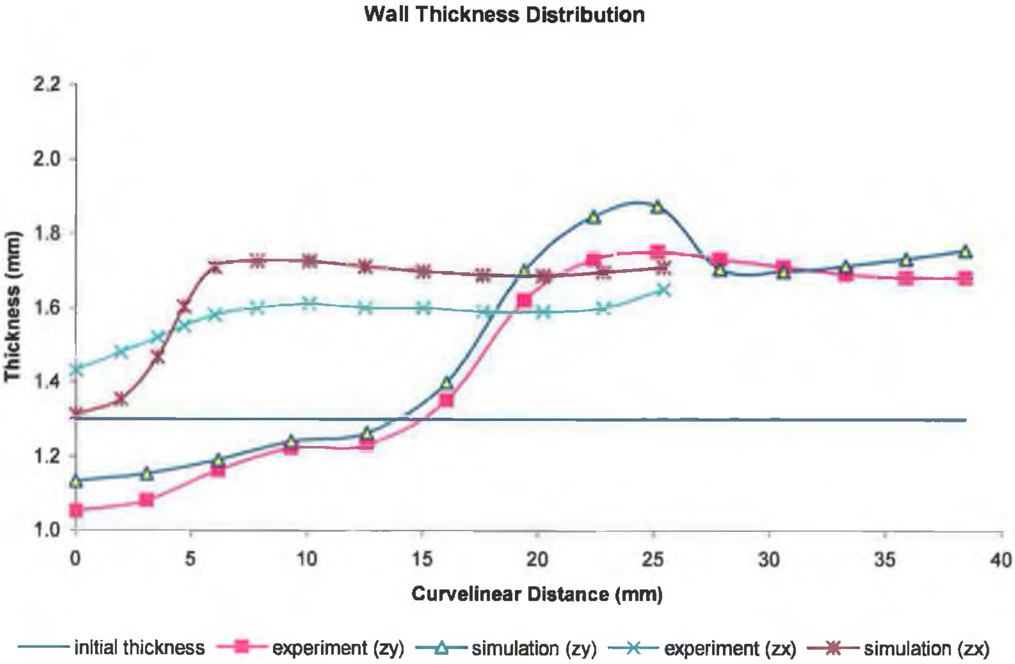

Fig 3.4.30 Wall thickness distribution along the curvilinear length, from tube centre to tube end along planes, zx and zy- T-branch (test-f)

From the wall thickness plots it was observed that the simulation and the experimental wall thickness distributions and variation trend were in good agreement for both the planes (zx and zy), the maximum variation in the simulation result was with in +/-10 % with respect to the experimental wall thickness values. The variation in the simulation result may be due to various factors, a) accuracy of finite element modelling b) frequently changing boundary and friction conditions during the process, c) error in measurement of the wall thickness, d.) anisotropic material properties of the tube blank, e.) variation in the initial wall thickness of the tube due to inconsistent manufacturing.

4. Process failure analysis

Finite element analysis provides a better understanding of the physical process and can determine various failure conditions (bursting / crack, wrinkling / buckling) caused due to excessive wall thinning (high forming pressure with respect to axial feed) or due to axial instability (high axial feed with respect to forming pressure). To study the various failure conditions such as formation of wrinkles due to large end axial feed or bursting due to excessive wall thinning, formability diagrams of the process can provide a better understanding of all these failure conditions. Fig 3.4.32 details an unstable forming condition (X-branch forming) with an occurrence of a wrinkle at the central portion of the tube. The finite element simulations along with formability diagram and forming limit curve were used to detect and analyse the failure (wrinkle growth). In this case also, for the finite element simulation, the boundary conditions and loading path used were approximately similar to the experimental conditions. Fig 3.4.31 details the simplified loading condition used in the simulation along with the actual experimental load path. From the simulation it was observed that, in the initial stage of the simulation (i.e. when axial feed was in the range of 4.5mm to 6mm), due to high feed has resulted into growth of a wrinkle, which could not be suppressed irrespective of the pressure rise in the final stage. For failure analysis using finite element simulation results, formability diagram (fig 3.4.33) was plotted for the component. The formability diagram used here was plotted with an assumed safety margin of 20% of the forming limit curve (default value of the post processor), with an allowable wall thinning of 0.275mm (as acceptable wall thinning for tube hydroforming processes can be assumed to be of the order of 25% of the initial tube wall thickness [50]) and wall thickening of 0.25mm (maximum wall thickening for this case was 13% of the initial value) for the tubes with an initial wall thickness of 1.30mm. As the material was assumed to be isotropic in nature, thus the coefficient of anisotropic hardening factor (R) was assumed to be 1, and the hardening exponent (n) of 0.2562 obtained from uniaxial tensile test of the sample.

Fig 3.4.34 details the element true strains (major and minor) values in the different regions (wrinkles, good or safe zone and zone with inadequate stretch) on the forming limit diagram. From the finite element simulation results the depth of the wrinkle (or height of wrinkle) obtained was 3.45mm and the branch height of 5.5mm were in close agreement with the experimental failed sample where the wrinkle depth was found to be approximately 3.5mm with a maximum branch height of 5.78mm.

Further analysis of other samples of X and T branches were done to study the different zones of the component susceptible to development of wrinkle or crack. Fig 3.4.35 and fig 3.4.36 show details of the formability diagram for X and T branch expansion pertaining to test-a. In these cases also the formability diagrams were plotted with an assumed safety margin of 20% of the forming limit curve, with an allowable wall thinning of 0.275-0.30mm and wall thickening of 0.75mm (as maximum tube wall thickening was observed to be in the range 0.70-0.75mm) of the final formed parts.

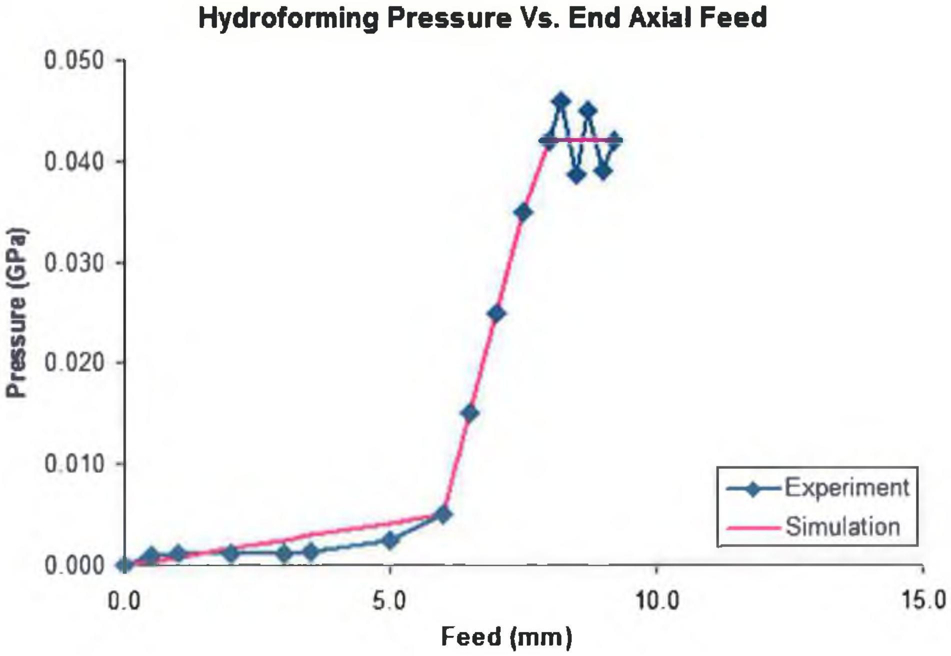

Fig 3.4.31 Load path leading to wrinkle growth (X-branch forming)

Fig 3.4.32 Wrinkle growth at the centre of the tube for a X-branch expansion

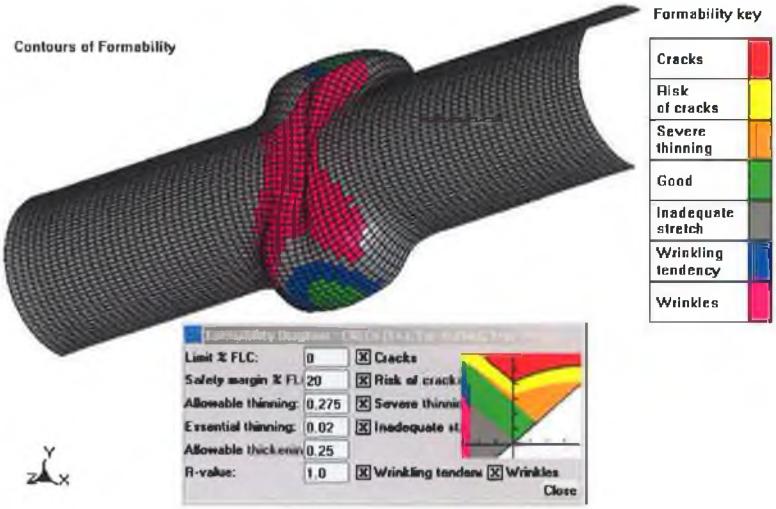

Limit % FLC: 0
Safety margin % FL 20
Allowable thinning: 0.275
Essential thinning: 0.02
Allowable thickenin 0.25
R-value: 1.0

☒ Cracks
☒ Risk of crack
☒ Severe thinni
☒ Inadequate st
☒ Wrinkling tendenc ☒ Wrinkles

Fig 3.4.33 Formability diagram of the X-branch expansion subjected to wrinkle

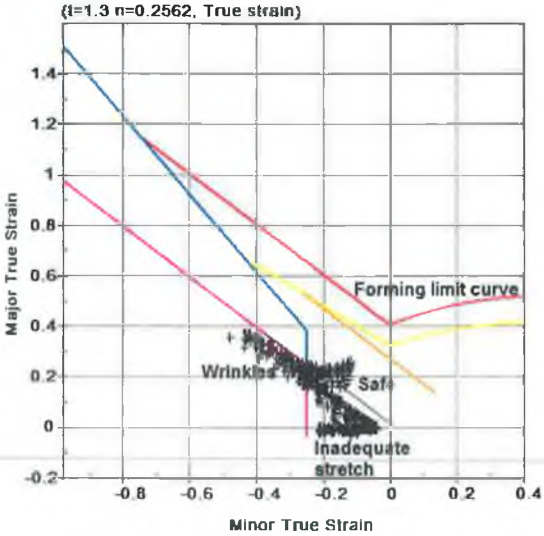

Fig 3.4.34 Element strain plots (major and minor strains) in different zones of the forming limit diagram (X-branch forming- see fig 3.4.33)

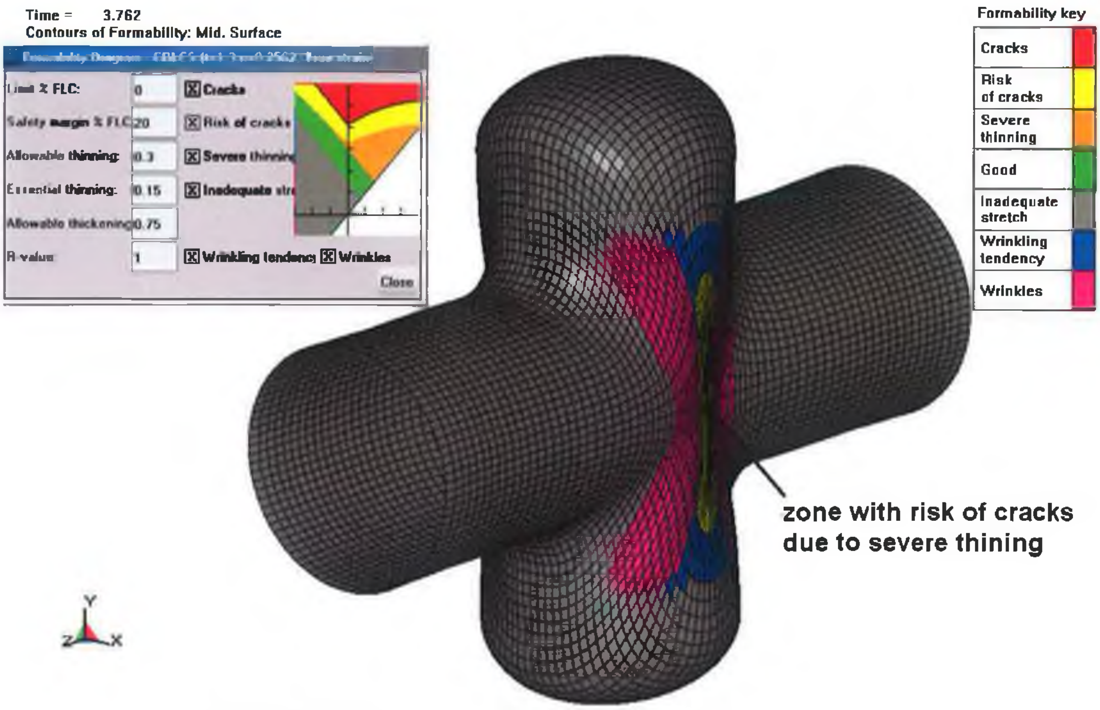

Time = 3.762

Contours of Formability: Mid. Surface

Formability Diagram - CALCS (t=1.3 n=0.2562 True strain)

Limit % FLC: 0

Safety margin % FLC: 20

Allowable thinning: 0.3

Essential thinning: 0.15

Allowable thickening: 0.75

R-value: 1

☒ Cracks

☒ Risk of cracks

☒ Severe thinnin

☒ Inadequate str

☒ Wrinkling tendency ☒ Wrinkles

Close

zone with risk of cracks due to severe thining

Fig 3.4.35 Formability diagram of X- branch (for test-a)

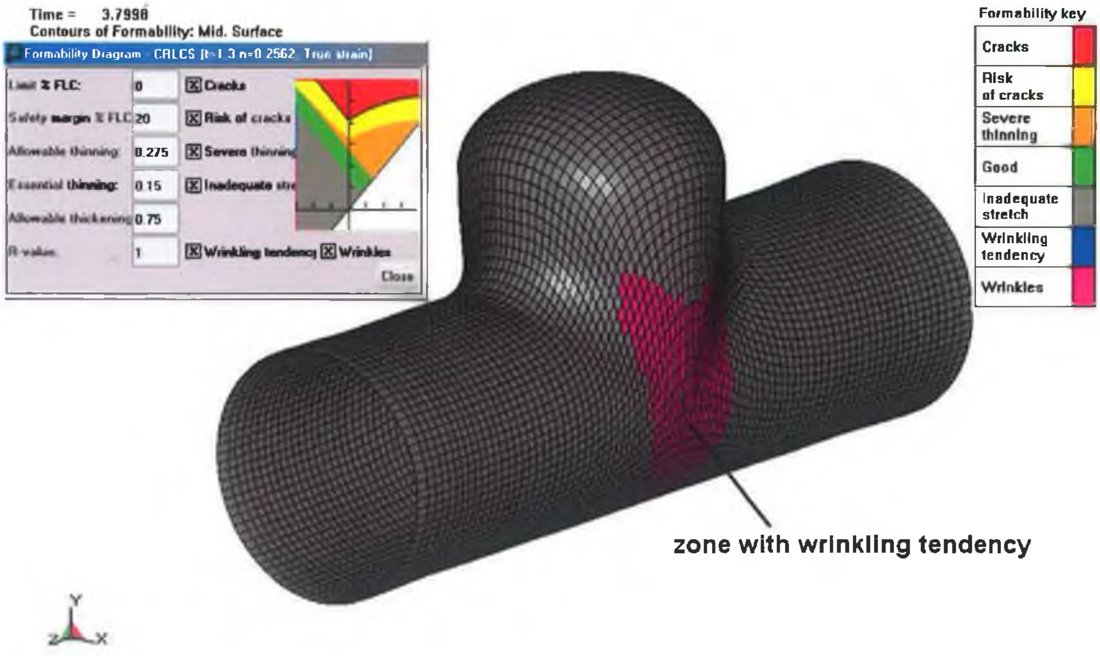

Time = 3.7998

Contours of Formability: Mid. Surface

Formability Diagram - CALCS (t=1.3 n=0.2562 True strain)

Limit % FLC: 0

Safety margin % FLC: 20

Allowable thinning: 0.275

Essential thinning: 0.15

Allowable thickening: 0.75

R-value: 1

☒ Cracks

☒ Risk of cracks

☒ Severe thinnin

☒ Inadequate str

☒ Wrinkling tendency ☒ Wrinkles

Close

zone with wrinkling tendency

Fig 3.4.36 Formability diagram of T- branch (for test-a)

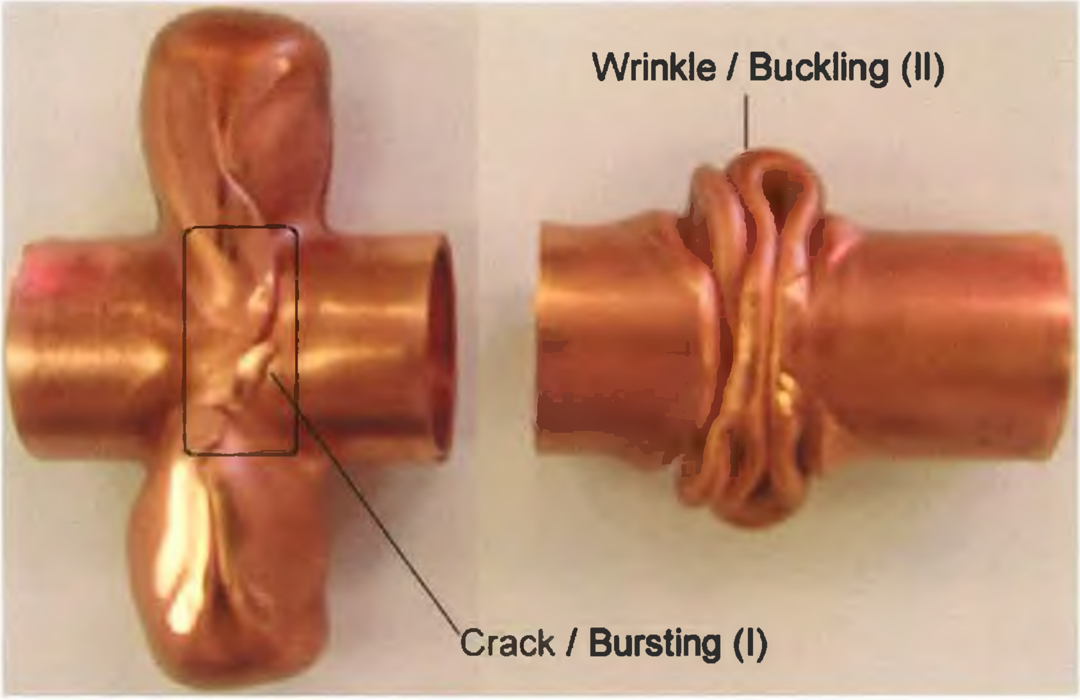

Fig 3.4.37 Failure due to crack/bursting (I) at the X-junction and, due to wrinkle / buckling (II) of a X-branch hydroforming

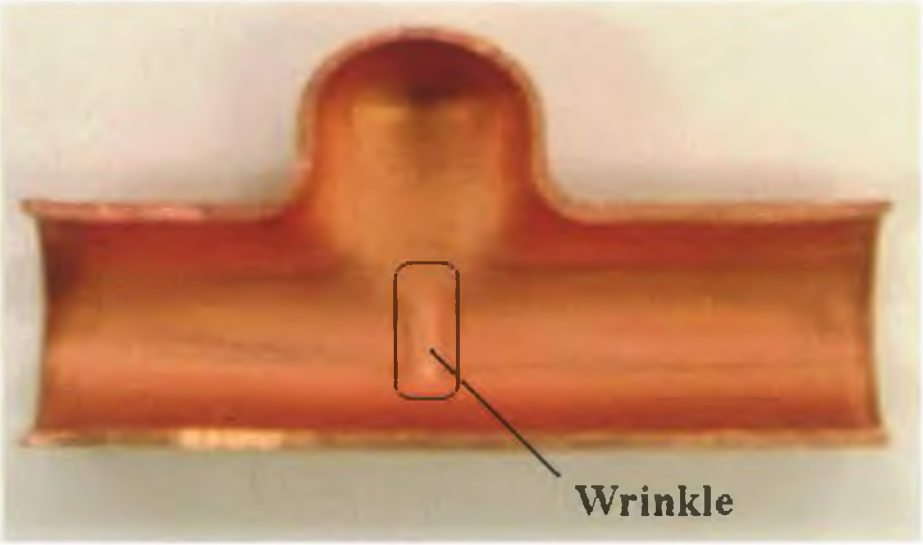

Fig 3.4.38 Wrinkle growth at the T-junction (T-branch hydroforming)

It can be seen that the tube wall near the X or T-junction was susceptible to wrinkle formation and also, in the case of X-branch this region has thinned substantially and was highly strained. This can lead to development of a crack, subsequently leading to tearing or shear failure (fig 3.4.37) of the wall. The branch top has also thinned substantially but the stretching was uniform along the plane, thus it can be assumed that this region was subjected to pure stretching. Further it can be seen from the wall thickness plot fig 3.4.19 (for X-branch formed tube), the wall thickness at the X-junction (centre of the tube) in the zx-plane has reduced substantially from its original value. Thus the wall thickness plot as well as forming limit diagram of X-branch justifies that the possible failure (for this type of expansion subjected to loading path shown in fig 3.4.3) will occur at the X-junction (fig 3.4.37 failed sample). Similarly fig 3.4.38 shows a T-branch expansion with a wrinkle growth at the centre of the T-junction, which is in good agreement with the wrinkle zone predicted by the formability diagram of a similar T-branch (fig 3.4.36) expansion. Thus from the above study it can be concluded that for tube hydroforming processes the formability diagram can provide a better understanding of the possible failure zones with different process failure modes.

3.5. Summary of Chapter 3

In this chapter the hydroforming of asymmetric X and T-branch, type tube hydroforming processes were studied experimentally and using explicit finite element simulations. Simplified finite element simulation models were built for these X and T-branch parts and the simulation results were compared with the experimental results. This was done to validate the simulation models and to set a standard for building the finite element analysis model for further analysis and optimization of the process parameters.

Chapter 4: Part and Process Design Consideration of Tube Hydroforming Components

4.1 Introduction

In the previous chapter hydroforming of X and T-branch components were simulated using the explicit finite element code LS-DYNA 3D and, the finite element modelling of the components were discussed in details. For a reliable prediction of results from the finite element simulations, it is important that all the finite element analysis parameters affecting calculations of the metal forming process as well as the geometrical and process factors which affect the behaviour of the process and metal flow be understood properly. This section discusses several important aspects of finite element analysis process modelling using LS-DYNA 3D (which was used in conducting the tube hydroforming simulations for the major part of this work) and the effects of various physical parameters on the final process performance.

4.2 Consideration in finite element modelling of tube hydroforming processes

4.2.1 Types of finite element formulations

Usually all sheet metal forming processes have multistage forming conditions and, for proper analysis of the process, dynamic explicit and quasi-static implicit are the two main types of finite element formulations which can be used. Due to various well known distinct advantages of explicit finite element formulation [77] over implicit finite element formulation such as, a.) gives better results for dynamic as well as quasi-static type problem , b.) fast changing boundary conditions due to contact and dynamic loading can be steadily simulated , c.) buckling and formation of wrinkles do not cause numerical instability during the simulation and, d.) relatively less computation time is required in comparison to implicit finite element code formulation, thus it is being widely used for sheet metal forming simulation. The tube hydroforming process is generally categorized as a sheet metal forming operation thus, the explicit finite element formulation is very suitable for its numerical analysis and study. This has been well demonstrated in various published literature [48, 49, 52, 55, 56, 63, 65, 69, 75].

4.2.2 Types of Finite Elements

Most finite element analyses of sheet metal or tube hydroforming processes adopt shell elements to model the work piece with an assumption that the shell elements follow the membrane theory (i.e. thin-shell theory). Closed-shell structures are usually analysed using thin shells theories if the tube wall thickness to the smallest radius (internal radius of tube) ratio is smaller than 1/10 (=0.1). With the lightweight driven design in the automotive industry, this thin-shell assumption is valid for most tube hydroformed automotive parts, which have thin walls compared to relatively large tube diameter. In this work the simulations were also conducted using shell elements.

Apart from application of tube hydroforming processes in the automotive industries, it is also being used for non-automotive applications such as medical, sanitary, pipefittings and other household applications. Components manufactured using this process (for non-automotive applications) usually have a much smaller radius as compared to automotive components, whereas the wall thickness is more or less the same. In other words, the ratio of wall thickness to the tube radius becomes much higher, which may not be suitable for analysis using thin shell theory. In such cases, brick elements can be used to model the tube if accurate thickness predictions are to be obtained [86,88]. Appendix-A details the simulation of X and T- branch tube hydroforming processes using solid brick elements with an implicit finite element code. Although use of solid brick elements in tube hydroforming simulation yields better thickness prediction, however it is associated with few drawbacks such as, a.) to obtain better results, multiple layers of elements across the wall thickness are usually used, in such cases for both implicit and explicit formulation, the computation time is usually much longer compared to that of shell elements, which is due to the increase in size of the finite element model, b.) adaptive meshing cannot be used with brick elements, and c.) the LS-DYNA code does not support formability and forming limit diagram plots for brick elements. These are the main reasons why solid elements are not used for sheet metal simulation. Table-4.2.1 highlights a basic comparison of computation time for implicit and explicit hydroforming simulation with 3D shell and solid elements on a standard finite element model with full integration, with total simulation time of 3msec, program calculated time step size and identical boundary and, loading conditions on a standard processor (Intel Pentium 4, 2.0GHz).

Table 4.2.1 Computation time comparison for various element type formulations

Solver/ Version	Element type/ Finite element formulation type/ Number of layers- for tube	Mesh type/Number of elements (mapped meshed) –for tube	Number of elements – die/contacts interface	Computation (CPU) time
LS-DYNA 970	Shell /Explicit	Surface (LxW) / 30x20=600	250	7min 32 sec
LS-DYNA 970	Solid /Explicit- 1 layer	Volume (LxWxT)/ 30x20x1=600	246	5min 40 sec
LS-DYNA 970	Solid /Explicit- 2 layers	Volume (LxWxT)/ 30x20x2=1200	246	15min 48 sec
ANSYS 8.1	Solid /Implicit- 1 layer	Volume (LxWxT)/ 30x20x1=600	848	20min 41 sec

Although a single layer solid element model resulted in lower computation time as compared to multilayer solid elements or single layer shell elements, however it must be noted that for predicting accurate results, single layer of solid elements are not recommended rather more than two layers are usually used [49,55] where wall thickness change is of prime importance. Further it can be seen that the computation time for implicit formulation was highest, this is mainly due to the large number of iterations the program has to do for search of the convergence for this kind of complex non-linear phenomenon (i.e. non-linear plastic deformation and complex contact interfaces). Furthermore when working with tube hydroforming with thin and thick walled parts, the proper choice of finite element type depends on the result prediction accuracy (i.e. wall thickness, part expansion etc.) demanded by the metal forming problem. Thus the above facts it can be concluded that explicit shell elements are always a good choice for simulation of thin walled tube hydroforming processes.

4.2.3 Element size

Element size plays an important role in tube hydroforming process simulation. One of the major problems encountered in tube hydroforming is buckling of the tube or formation of a wrinkle subsequently leading to buckling. This is mainly caused due to structural instability of the forming process, which may be either due to the geometrical irregularities of the tube blank or due to unbalanced loading conditions. The size of elements plays an important role in prediction of wrinkle, stress, strain and realistic thickness distribution. Simulations were conducted with different mesh densities of the tube blank with mapped finite element mesh size (i.e. length X breadth) 0.85mm X 0.85mm, 1.25mm X 1.25mm and 1.50mm X 1.50mm to study the wrinkle growth characteristic (depth of wrinkle) for an unstable (i.e. subjected to wrinkles) X-branch hydroforming process. The unstable load path used for the simulation is shown in fig 4.2.1.

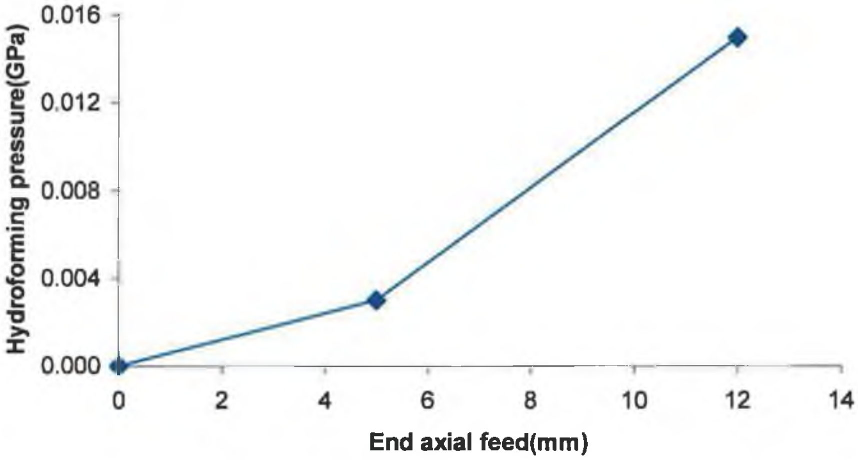

Fig 4.2.1 Unstable load path used for the simulation (wrinkle formation)

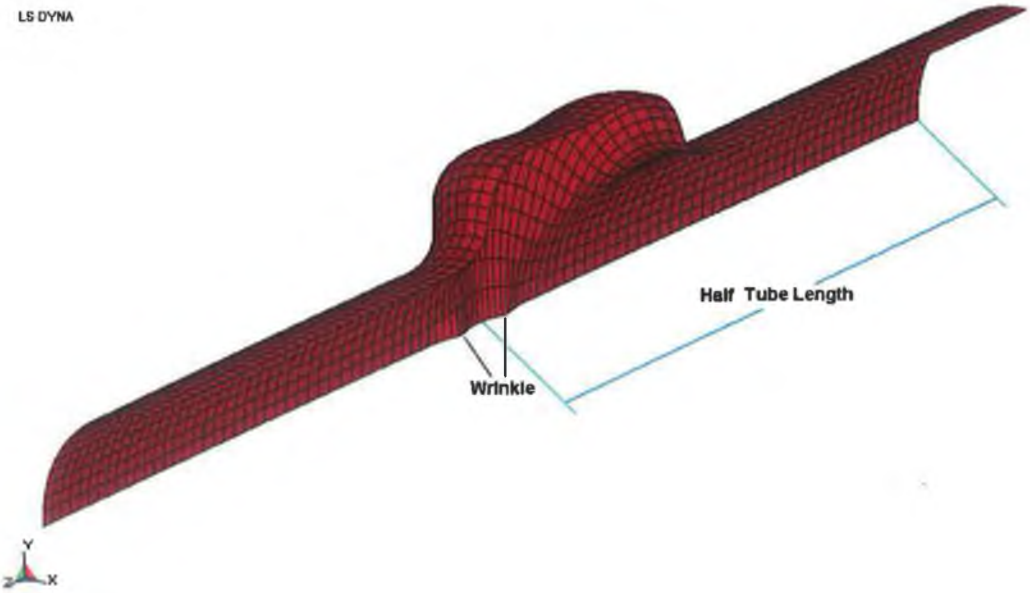

Fig 4.2.2 One-fourth symmetric model of X-branch hydroformed tube (with wrinkles in the central portion of the tube)

Fig 4.2.2 shows a one-fourth symmetric model of a X-branch component after a wrinkle formation in the central portion of the tube and fig 4.2.3 and fig 4.2.4 show the comparison of the wrinkle height predicted by different finite element mesh size, the values are plotted for half tube length from centre of the tube to tube end as shown in fig 4.2.2.

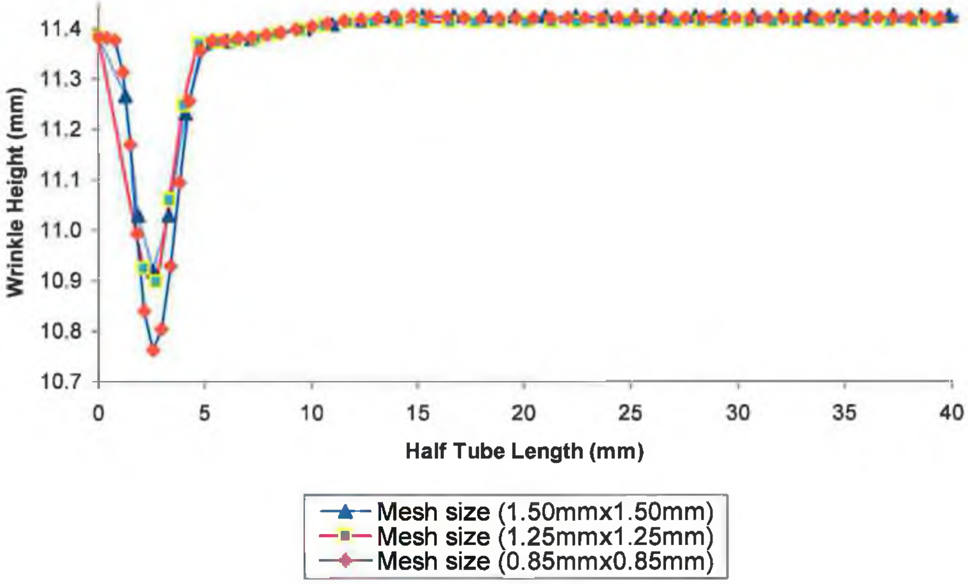

Fig 4.2.3 Depth of wrinkle from centre of the tube, to tube end (along zx-plane see fig 5.2.2)

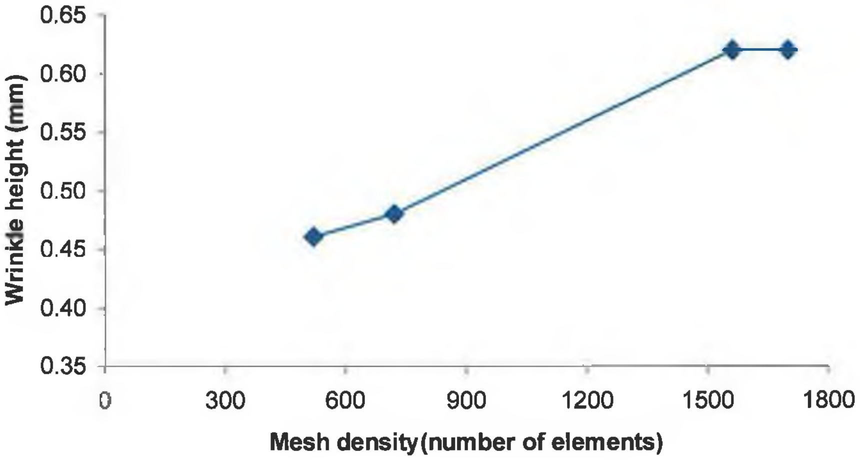

Fig 4.2.4 Variation of maximum wrinkle height with respect to mesh density (for one-eighth X-branch model)

It was observed that the wrinkle is best predicted with the finest element mesh size, as finer meshes usually define better profile and shape of the deformed structure, but the problem associated with use of a finer mesh is with the increase in total computation time. As explained earlier (in Chapter 3), the explicit computation time depends upon the characteristic length of the element, thus with increase of mesh density (i.e. number of elements) the element characteristic length also decreases simultaneously, resulting in longer simulation time. Thus, for these types of simulations where a reasonable result is desired a certain trade-off has to be made in element mesh size selection and total computation time.

4.3 Factors affecting the hydroformability characteristics of the process

The final geometric features of a components manufactured by tube hydroforming process depends upon various factors which can be broadly classified as a.) geometric factors and, b.) process control factors.

4.3.1 Geometric factors

The component geometry as well as its forming die geometry can greatly affect the component formability. Therefore, hydroformability of the component should be considered early in the component and its die/tool design stage. In tube hydroforming process, the initial geometry of the tube blank and the die have different effects on the final part expansion. Depending upon application, most of the tube hydroforming processes use either normal or preformed straight or bent tubes with different lengths and cross-sections. Thus, parameters like the initial tube wall thickness, length of the tube, initial diameter of the tube, die bend and blend radius (i.e. die corner radius), all play important roles in manufacture of a sound component and have different effects on the final part expansion.

In this section, the effects of the geometric parameters a.) initial tube length, b.) initial tube wall thickness and, c.) die radius, on hydroformability and branch height development are studied. The analysis is done on a X-branch tube hydroforming with a fixed boundary and loading conditions. The loading condition is judiciously selected so that there is no failure due to buckling or wrinkling. The finite element model used for the simulation is the same as that used for experimental validation. A partial load path resembling 'test-b' of X-branch as illustrated in Chapter 3, with a total end axial feed of 14mm, and forming pressure of 0.037GPa was used for all the simulations. The piecewise load path used for simulations is shown in fig 4.3.1. Other geometric parameters such as length of the tube, initial tube wall thickness and die radius were varied with in a specified range as per the simulation study requirement.

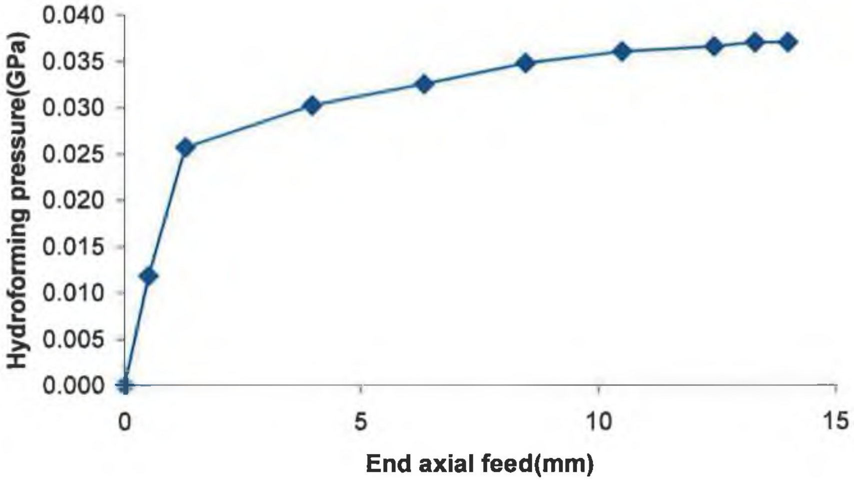

Fig 4.3.1 Simulation load path

4.3.1.1 Effects of initial tube length (spline length)

Simulations were conducted with total tube lengths ranging from 64mm to 124mm and the final branch height development and wall thickness variations at different points were studied for the part expansion and wall thickness variation. This knowledge is particularly useful when working with long automotive structural parts whose part geometrical features such as bulges, protrusions, and bends are located along the part axis. Fig 4.3.2 shows the variation of final branch height developed with initial half tube length. The results shows that the part expansion and material flow characteristics are much better with shorter initial tube length. The reason for greater branch height development can be explained by considering the effect of frictional forces acting on the tube during the process, tubes with longer spline length have greater contact surface area, and because of this the tube is subjected to relatively high contact frictional forces, which resist the flow of material during the process.

Fig 4.3.3, fig 4.3.4 and fig 4.3.5 show the variation of wall thickness at the branch top, at the centre of the X-junction and along the die radius (see fig 3.3.4 –in Chapter 3). The plots show that wall thinning is minimum at the branch top, whereas it is maximum at the

X-junction and wall thickening is maximum around die radius for tube with minimal length and it is just opposite with the maximum length.

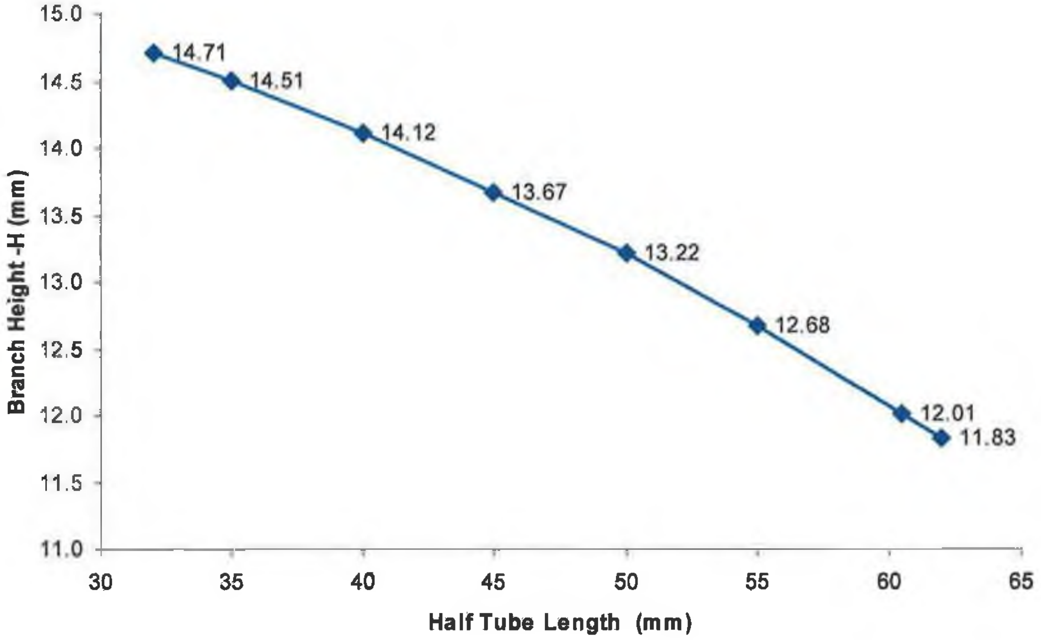

Fig 4.3.2 Variation of final branch height with respect to initial half tube spline length

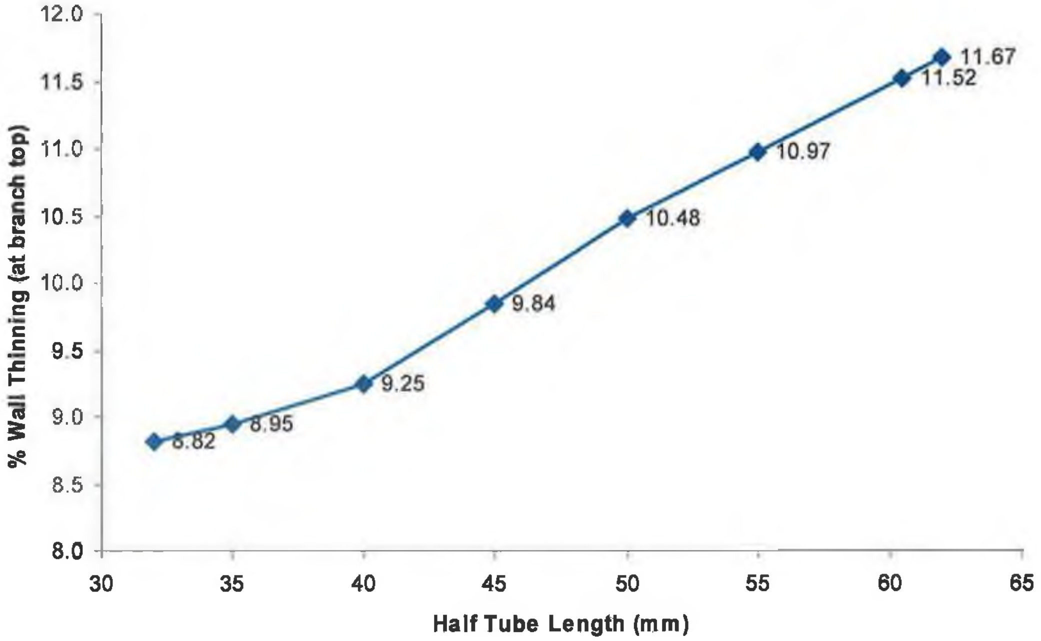

Fig 4.3.3 Percentage thinning of tube wall at tube branch top with respect to initial half tube spline length

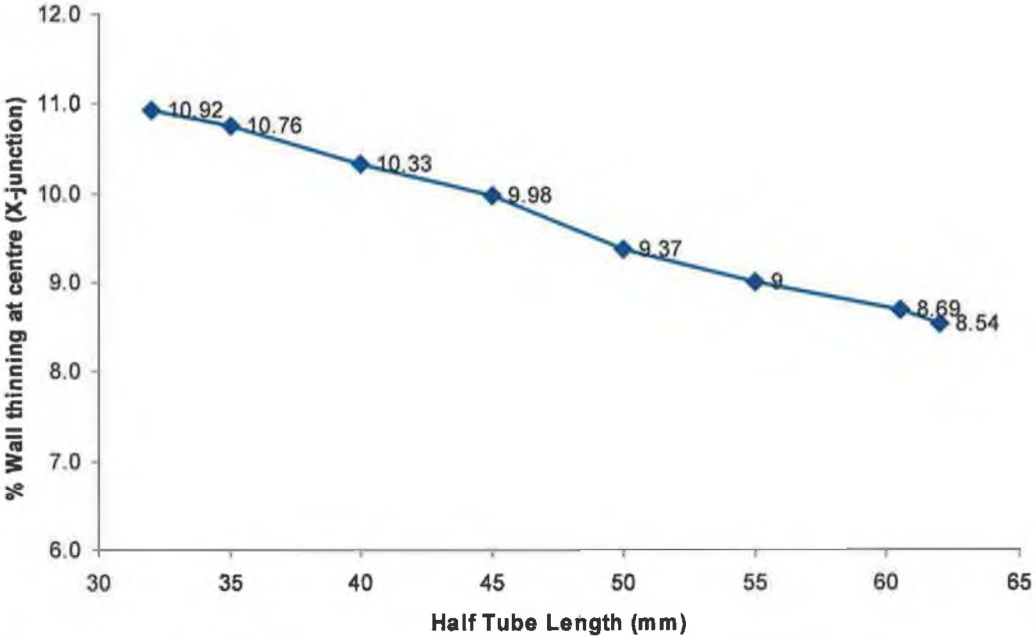

Fig 4.3.4 Percentage thinning of tube wall at tube centre (X-junction) with respect to initial half tube spline length

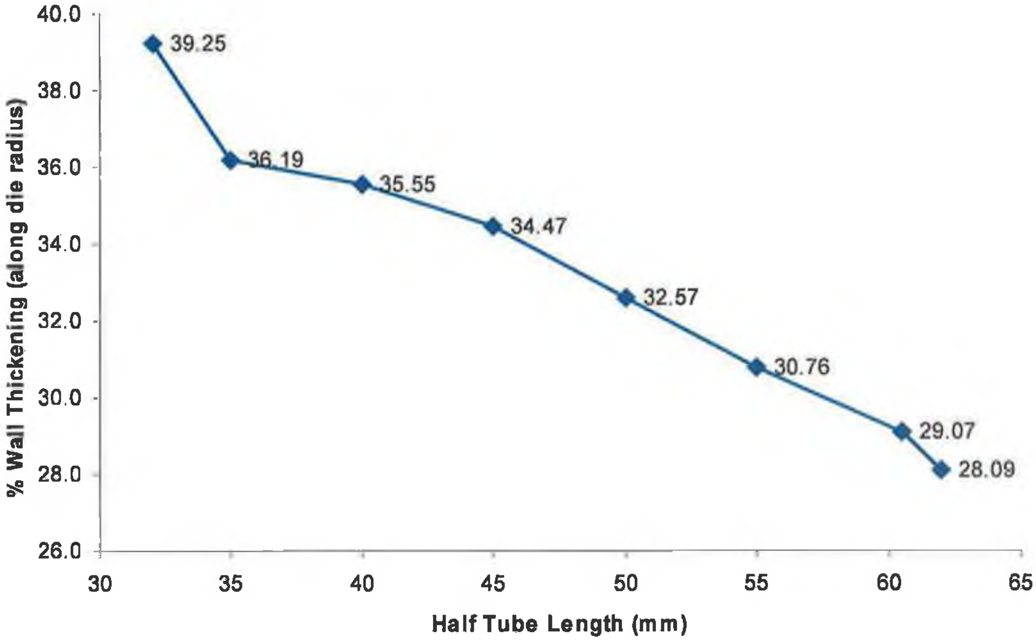

Fig 4.3.5 Percentage thickening of tube wall at bending of the tube along die radius with respect to initial half tube spline length

Thus, it can be concluded from this study that for better part expansion and to avoid excessive part wall thinning (i.e. to maintain a balance in wall thinning at various regions) the tube length used for the manufacture of the component should be selected judiciously.

4.3.1.2 Effects of initial tube wall thickness

In a different set of simulations, the spline length was fixed at 121mm and the initial tube wall thickness was varied from 1.0mm to 1.6mm keeping the outer tube blank radius fixed, and the effect on part expansion was studied. It was observed that for the tube with minimum wall thickness (fig 4.3.6), the part expansion was maximum at the cost of maximum wall thinning at the branch top (fig 4.3.7). This is not a desirable quality of any tube hydroforming process, thus it is important that the initial tube wall thickness should be selected judiciously depending upon the degree of expansion required in the final formed component.

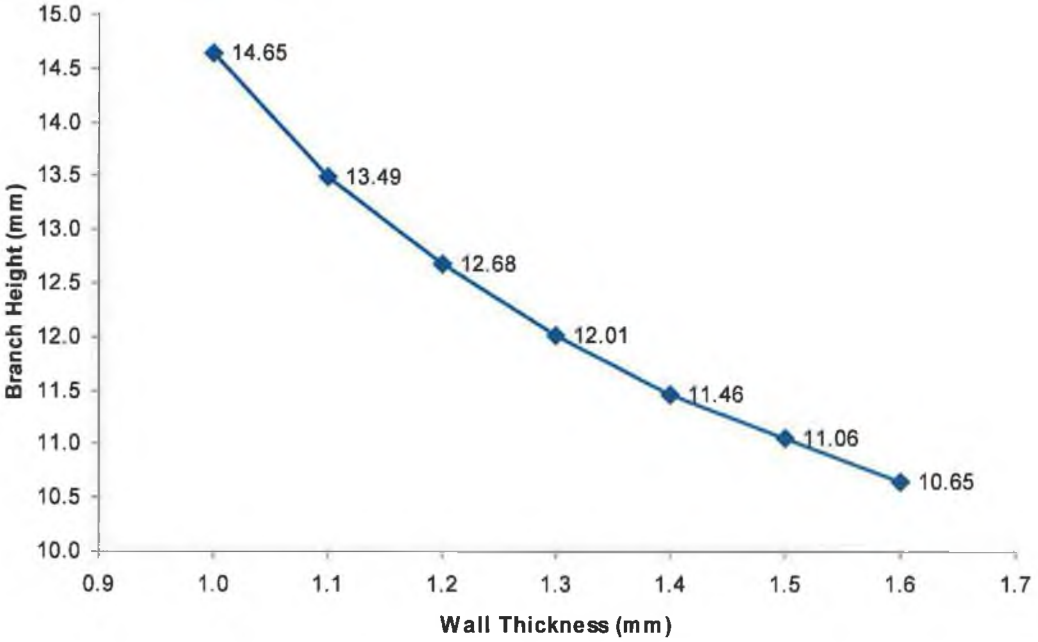

Fig 4.3.6 Variation of final branch height with respect to initial tube wall thickness

4.3.1.3 Effect of die radius

In this case the simulations were conducted with a spline length of 121mm and the effect of change in die blend radius on the final branch height development was studied for the radius range from 1.0mm to 4.5mm, the results (fig 4.3.8) shows that the branch height and part expansion was maximum for die with largest radius. Larger dies blend radius helps in better movement and plastic flow of material in the developed branch.

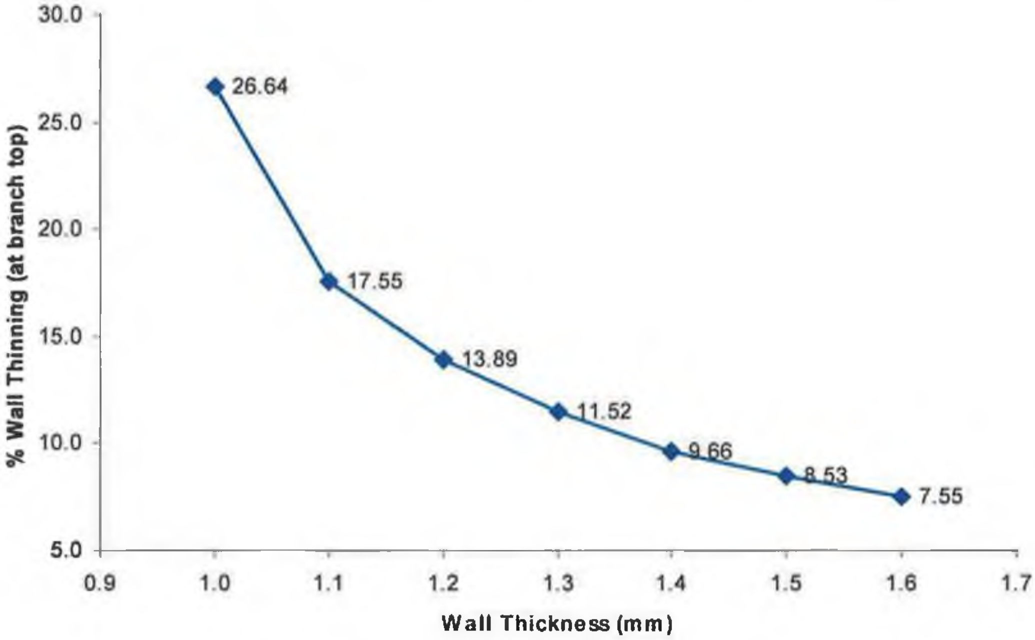

Fig 4.3.7 Percentage thinning of tube wall thickness at tube branch top with respect to initial tube wall thickness

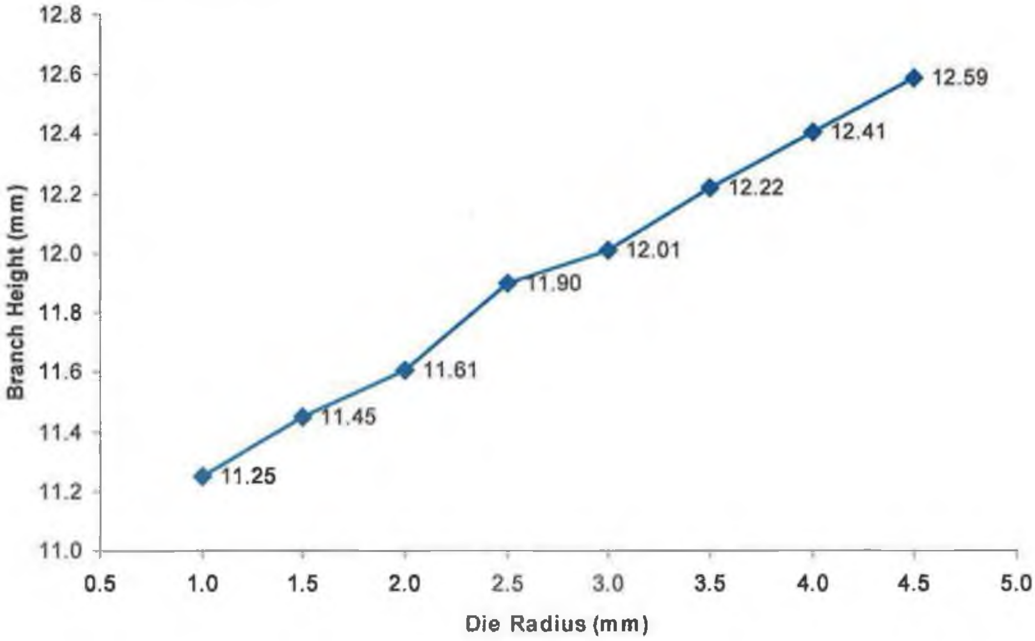

Fig 4.3.8 Variation of final branch height with respect to die radius

4.3.2 Process parameters

For tube hydroforming processes with end axial feeding, the chances of failure due to wrinkle or buckling are much higher in comparison to normal expansion due to pressure only loading where the normal failure mode is usually due to bursting or rupture of the tube wall due to excessive wall thinning. For this kind of process a proper balance of forming pressure and end axial feed is required to avoid the failures. Thus, the actual forming load path plays an important role in the entire process. Other than the load path the contact surface friction condition also plays an important role in the part expansion and failure of the process. The frictional forces acting during the process determine the amount of material flow during the plastic deformation. In the previous section, it was shown that at a fixed loading condition (i.e. variation of forming pressure with respect to axial feed), with the increase in spline length the effective part expansion decreased substantially, where the coefficient of friction was assumed to be constant. This was mainly due to the change in the effective frictional contact surface area with change in the spline length. In the subsequent section, the effects of change in frictional conditions and variation in the loading conditions on the final part expansion will be analysed.

4.3.2.1 Effects of friction

Simulations were conducted with different values of static and dynamic coefficient of friction ranging from a minimum value of 0.00 to a maximum value of 0.17 and the effects on final branch height development and part thickness change were studied. In all the simulations, values for both the static and dynamic coefficient of friction were assumed to be identical and also the tube spline length was kept constant (121mm). The load path used for the simulations is the same as shown in fig 4.3.1. The results show that there is a substantial effect of friction on both final branch height development and part thinning. It was observed that with higher values of friction, the final part expansion reduced (fig 4.3.9) simultaneously increasing the chances of wall thinning (fig 4.3.10) at the branch top on the contrary with lower values of friction the final branch height was maximum however at the cost of higher wall thinning at the X-junction (fig 4.3.11). Thus here also a trade-off has to be made to select the proper lubrication condition so that the final wall thinning can be almost uniform throughout the highly stretched regions of the part.

For the wall thickness at the tube bend along the die corner radius (fig 4.3.12), the plot shows that in the initial stage the tube wall thickness showed an increasing trend with increase of friction coefficient whereas in the later part it started decreasing after attaining the peak value.

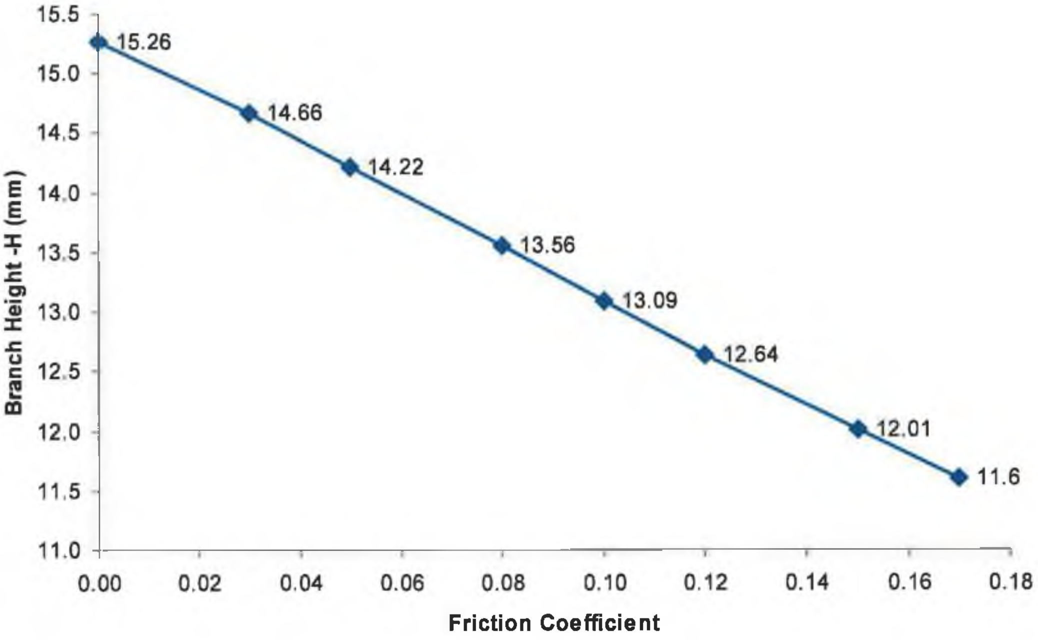

Fig 4.3.9 Variation of final branch height with respect to friction coefficient

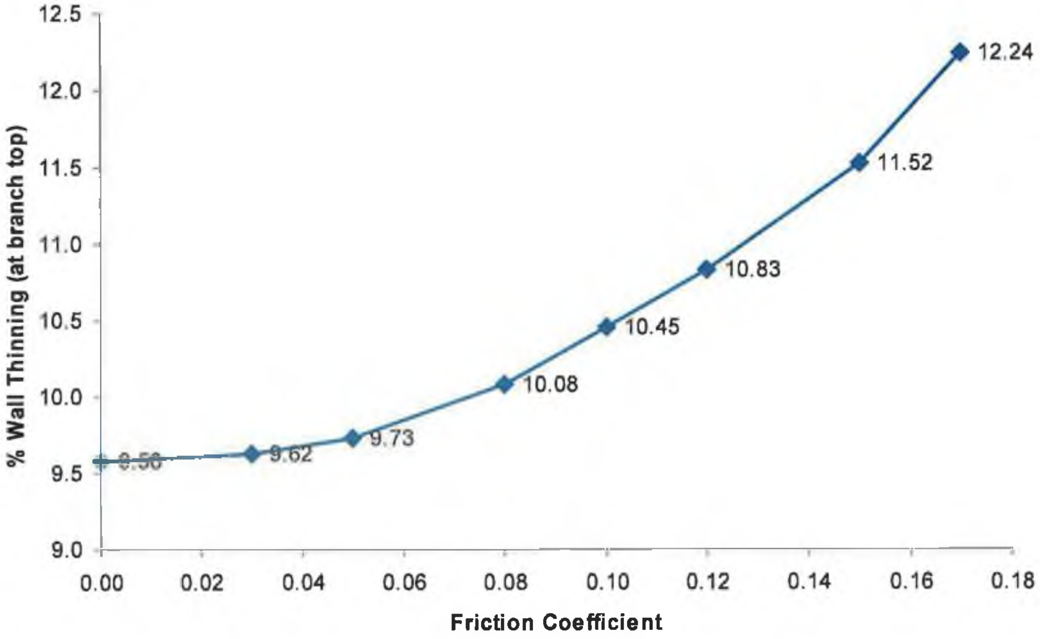

Fig 4.3.10 Percentage tube wall thinning at branch top with respect to friction coefficient

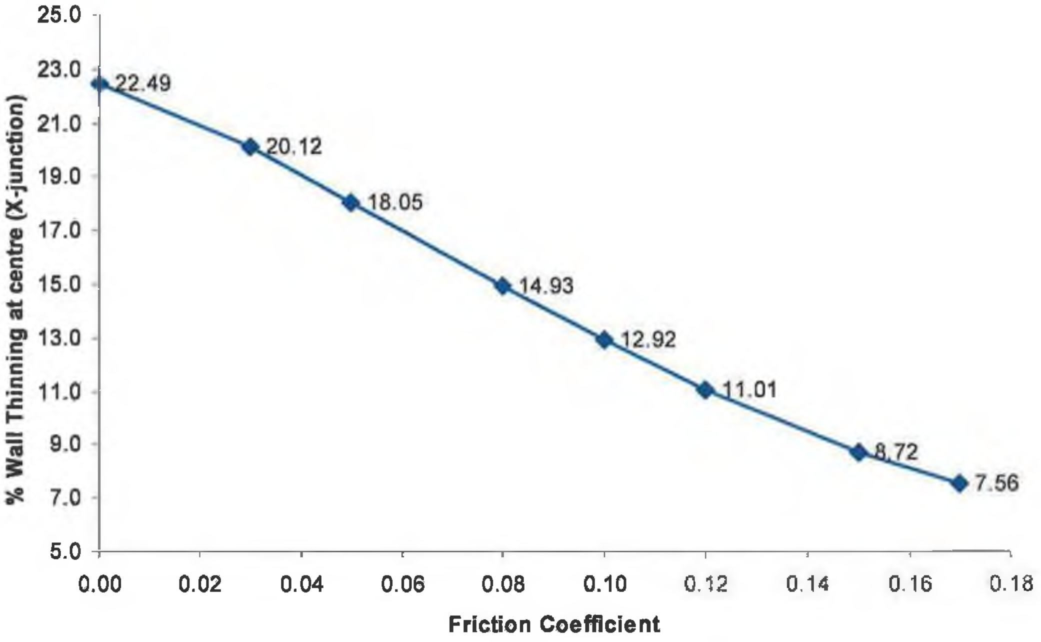

Fig 4.3.11 Percentage tube wall thinning at centre (X-junction) with respect to friction coefficient

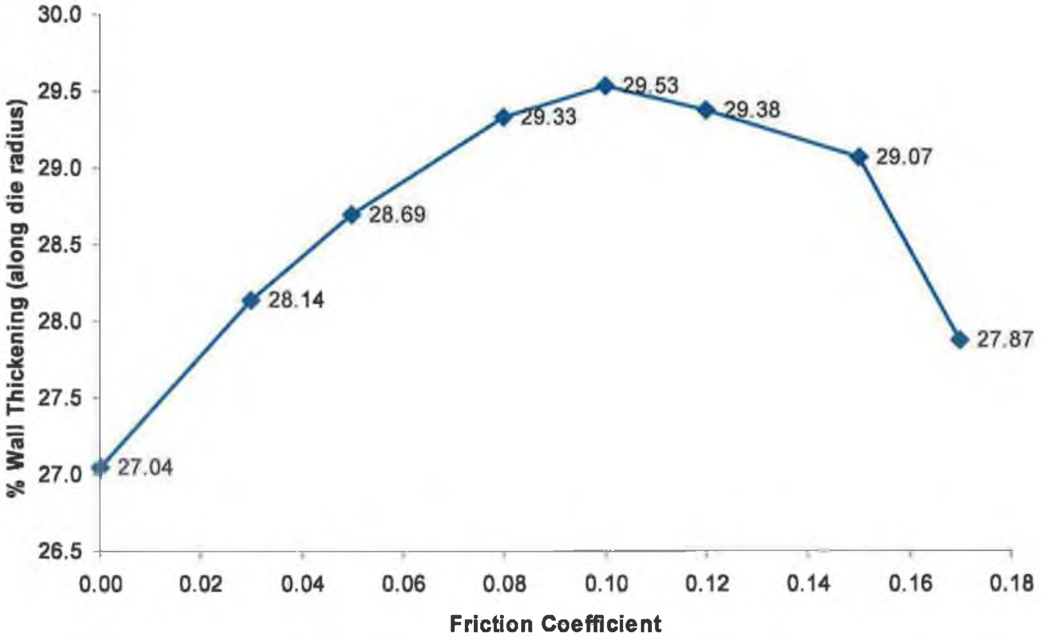

Fig 4.3.12 Percentage thickening of tube wall thickness at bending of the tube along die radius with respect to friction coefficient

4.3.2.2 Effects of loading paths

In Chapter 3, it was shown how an unstable loading condition (forming pressure with respect to axial feed) and result in formation of wrinkle (fig 3.4.23, fig 3.4.24– in Chapter 3). With such kind of loading (i.e. high axial feed with respect to forming pressure in the initial stage of the forming process) it is usually possible for the tube to buckle subsequently when further axial feeds are applied (fig 3.4.29– in Chapter 3) Similarly on the contrary it is also possible that if the initial forming pressure is too high with respect to the axial feed this would result in excessive wall thinning resulting in bursting or cracking of the tube wall (fig 3.4.29– in Chapter 3). In this section, a detail analysis of the effects of various load paths on the process is presented detailing the extent of part expansion, failure due to wrinkle, buckling and bursting with different loading conditions.

Simulations were carried out with various pressure values as a function of axial feed (load paths fig 4.3.13) with a maximum forming pressure of 0.036GPa, maximum end axial feed of 12mm, coefficient of friction of 0.15 and spline length of 121mm for all the cases. The simulation results for all the cases show that the final part expansion (i.e. branch height) was different for all the loading conditions with occurrence of failure due to wrinkle formation in certain cases, irrespective of the final fixed maximum pressure and end axial feed. The simulation results depicts that there was development of wrinkle with load paths corresponding to '1', '2' and '3' where the rate of increase of forming pressure was relatively low than the end axial feed. It was also observed that the degree of wrinkle and subsequent buckling is also dependent upon the load path. The wrinkle height developed with load path '1' was the highest with a poor part expansion (i.e. branch height), whereas the part expansion or developed branch height was reasonably good with load paths '4', '5', '6' and '7' without any wrinkles. However, the wall thinning (at branch top and the centre of the tube i.e. the X-junction) was maximum for load path '7', this shows that the chances of failure of the component due to excessive wall thinning and subsequent bursting or rupture is maximum for this kind of loading condition where in the initial phase of the process there is a steep rise of pressure with relatively low axial feed. Fig 4.3.14 shows a comparison of final branch height developed, wall thinning (at branch top and at X-junction) and degree of wrinkle

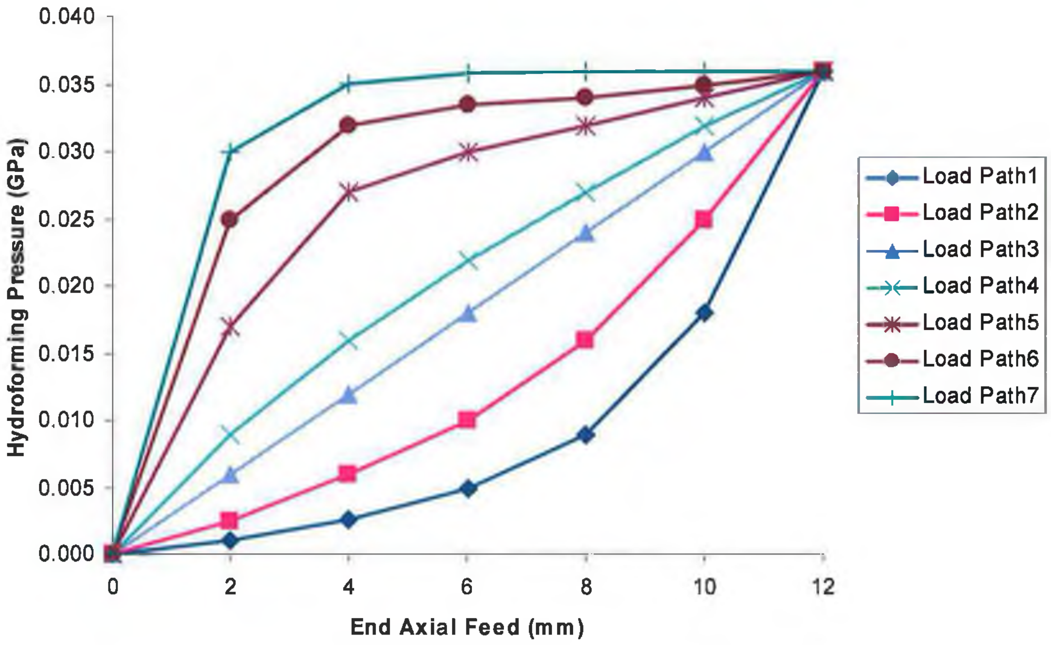

Fig 4.3.13 Forming load paths (hydroforming pressure as a function of end axial feed)

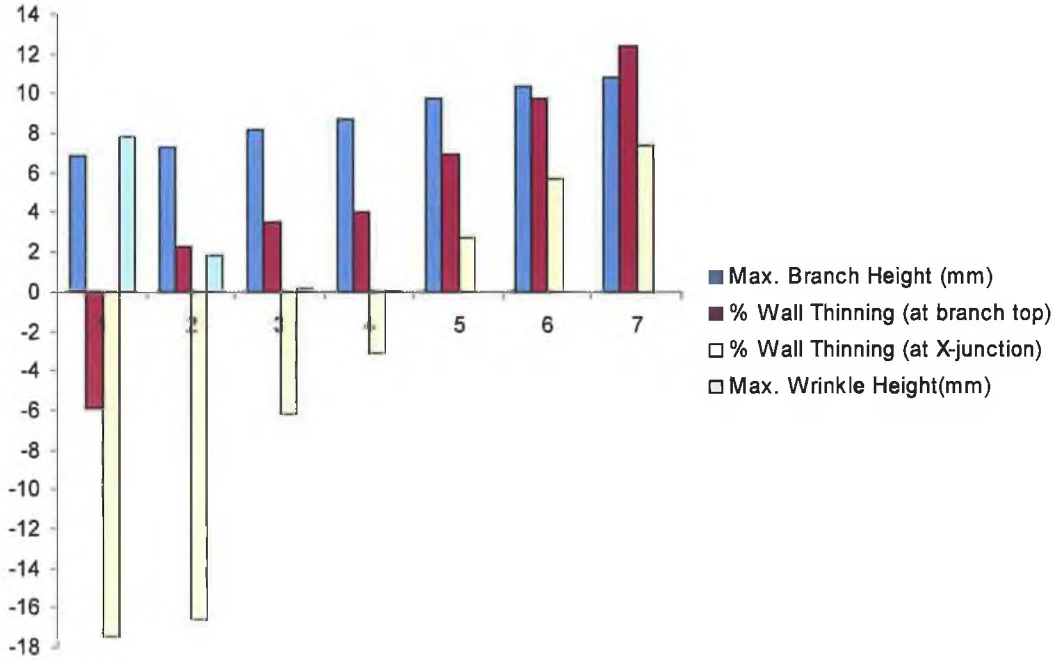

Fig 4.3.14 Comparison of maximum branch height, percentage wall thinning (at branch top and at X-junction) and maximum wrinkle height for load paths

formation or wrinkle height for all the load paths. Fig 4.3.15 illustrates the two different phases of the process, a.) at 50% axial feed and, b.) at 100% axial feed, corresponding to forming load path '2'. The figure shows the development of a wrinkle in the later part of the process. It was observed that with initiation of wrinkle the process becomes unstable and as a result of which the wrinkle growth rate becomes much faster with further axial feed irrespective of the pressure rise. Out of all the load paths, load paths '4' and '5' can be considered as the best from design point of view, as for these two load paths the overall part expansion was better, with average wall thinning and almost negligible wrinkle. Thus, from all the simulations with different load paths, it can be concluded that the actual part expansion, wrinkle growth and wall thinning is highly dependent upon the actual physical forming loading conditions.

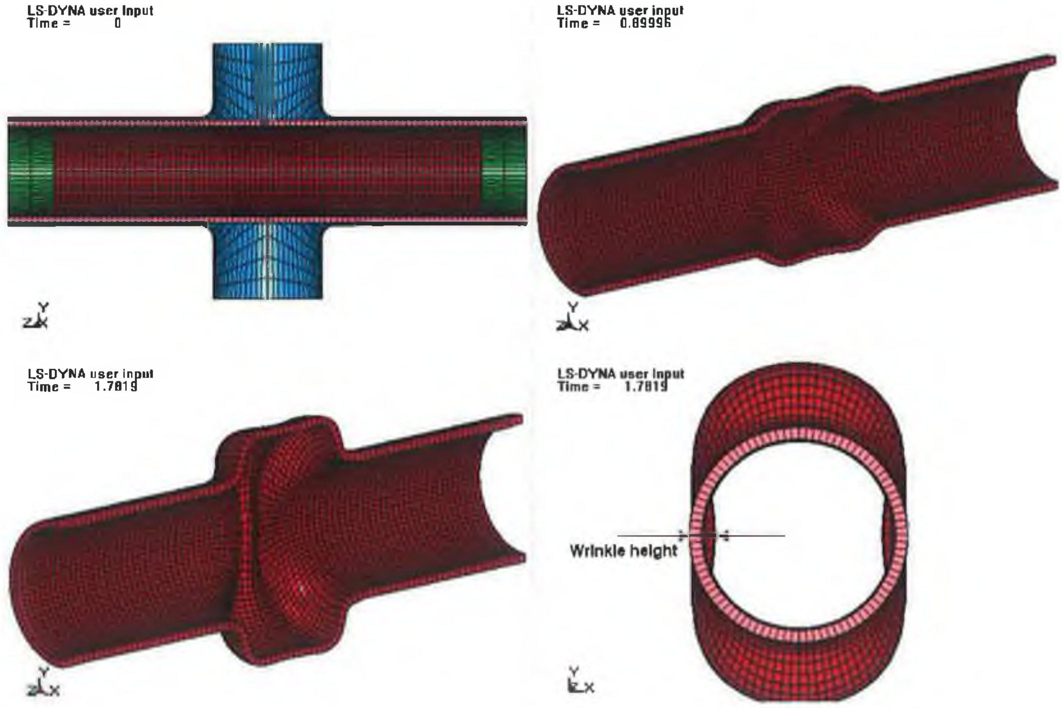

Fig 4.3.15 Part expansion and formation of wrinkle (load path 2) at different simulation time steps, illustrating development of wrinkles at the centre of the tube

For successful application of tube hydroforming processes, which involves end axial feed, the actual successful forming zone in the forming pressure vs. axial feed graph is very narrow in nature. Fig 4.3.16 shows in general approximate different forming zones with possibilities of various categories of failure for tube hydroforming process subjected to combined internal forming pressure and axial feed. Although, the plot does not represent the exact failure zones limits, it represents the possible areas of failure.

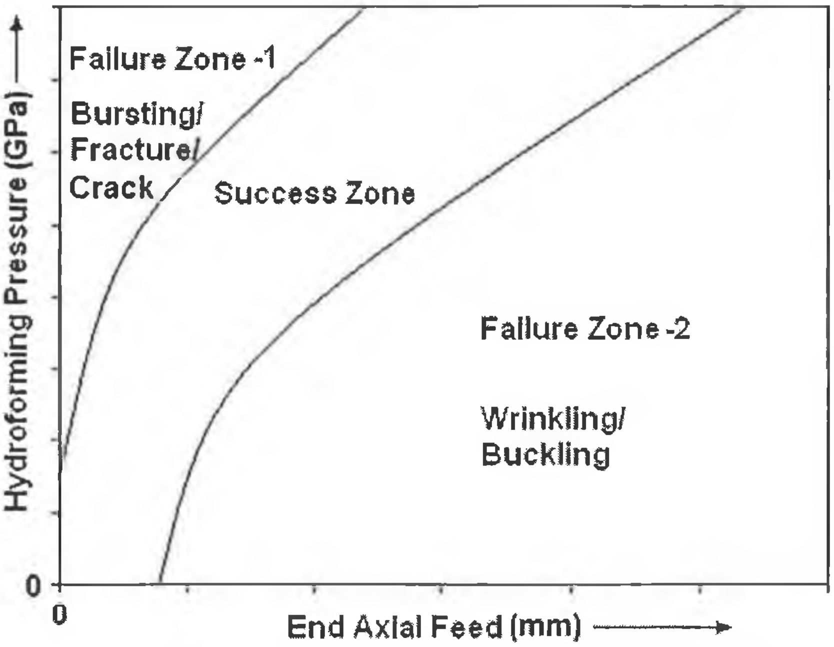

Fig 4.3.16 Successful and failure forming zones for a tube hydroforming process [73]

4.4 Experimental verification

In order to verify some of the simulation results where possible, further experiments were conducted. Tubes with different lengths were used to form X-branch with a fixed loading path (variation of forming pressure with respect to axial feed) with a maximum pressure of 0.038GPa and maximum end axial feed of 14.2mm. Although the experimental load path as well as the maximum forming pressure, total axial feed values and tube lengths used for the experimental study were different from the simulation study, however the results obtained from the experiments are in good agreement with the result trends shown by simulations for the branch height, wall thinning at the branch top, wall thinning at the X-junction and, wall thickening along the corner radius. Fig 4.4.1 details the experimental samples with the initial tube lengths and fig 4.4.2, fig 4.4.3, fig 4.4.4 and fig 4.4.5 details the branch height, wall thinning and thickening trends at different regions of the tube. A comparative study of the simulation and experimental result plots show that the branch heights (fig 4.4.2) in both the cases decreased with increase in tube length, similarly the wall thinning at the branch top (fig 4.4.3) shows an increasing trend whereas wall thinning at the X-junction (fig 4.4.4) and wall thickening along die corner radius (fig 4.4.5) show a deceasing trend with increase in the tube length. This validates the simulation findings (i.e. the variation trends) of the effects of tube length on the final part feature characteristics. The minor variation in the values can be accounted for by

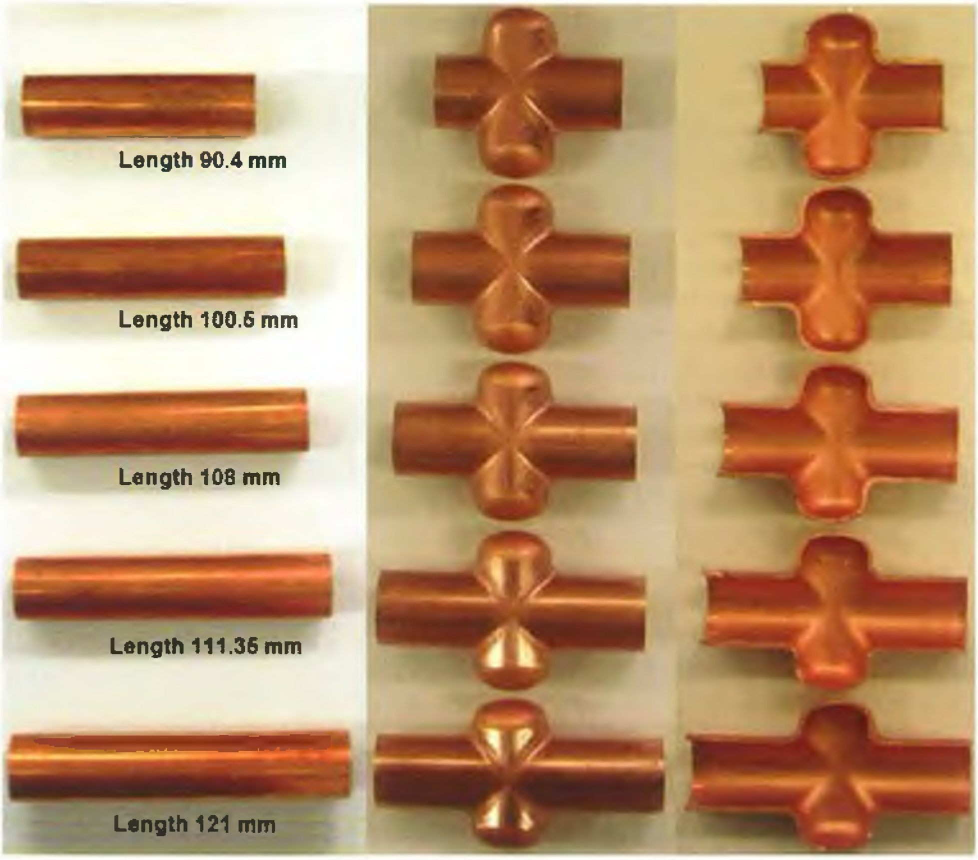

Fig 4.4.1 Experimental samples with different tube lengths

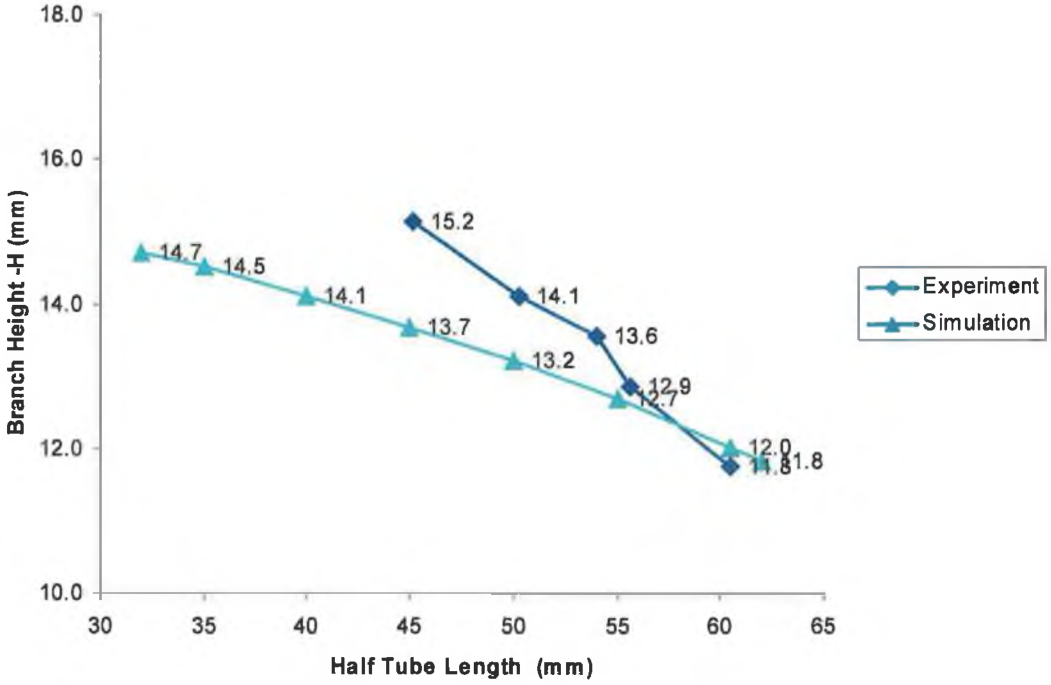

Fig 4.4.2 Variation of branch height with respect to half tube length

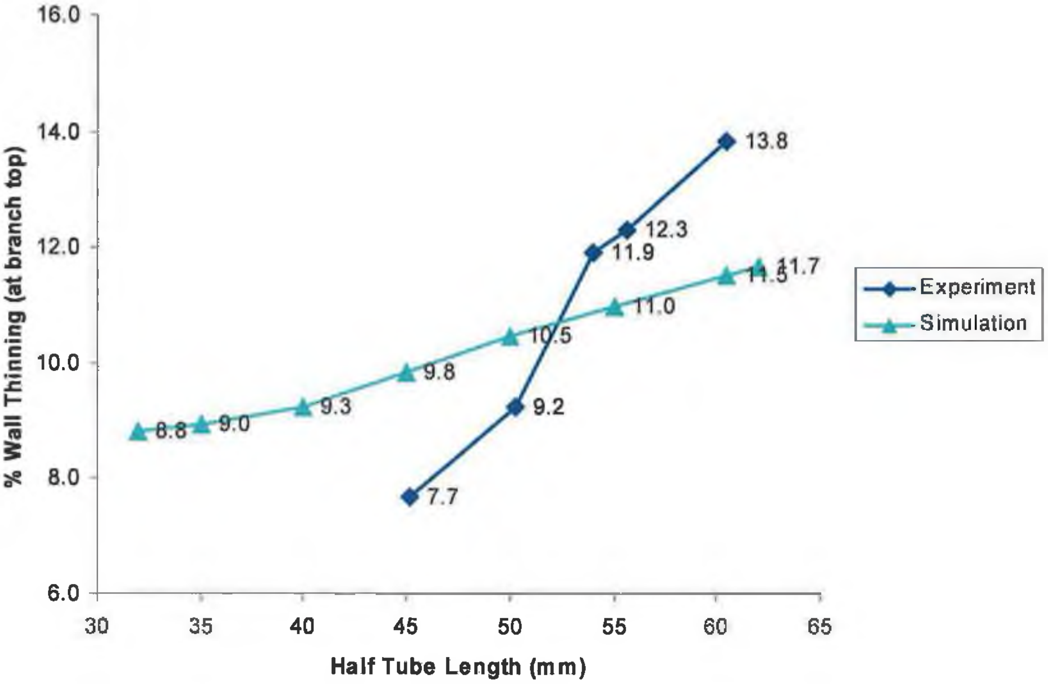

Fig 4.4.3 Variation of percentage wall thinning (at branch top) with respect to half tube length

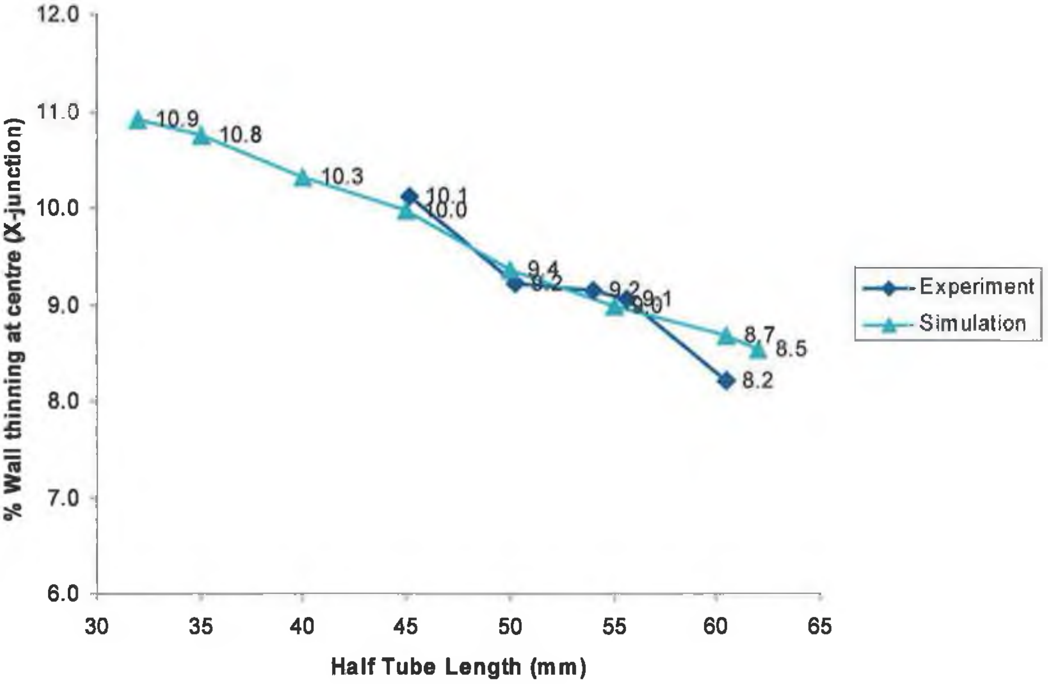

Fig 4.4.4 Variation of percentage wall thinning (at X-junction) with respect to half tube length

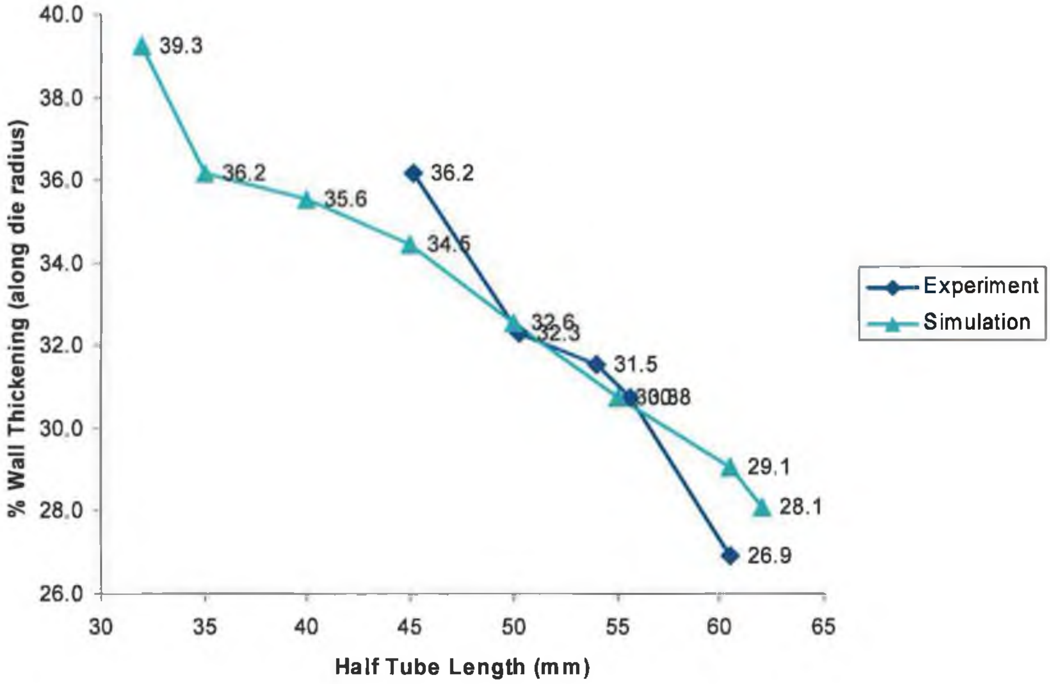

Fig 4.4.5 Variation of percentage wall thickening (along corner radius) with respect to half tube length

considering the variation in the load paths used for simulation and experiments, maximum forming pressure and total end axial feed. For experiments the maximum forming pressure as well as total end feed used were slightly higher in comparison to simulation values, thus it can be seen that the branch height values obtained from experiments are relatively higher in comparison to simulation findings. Similar findings have also been reported earlier [50] for T-branch expansion. Where it has been shown that with increase in tube lengths, the effective protrusion height (branch height) decreases and, similarly with increase in die corner radius the effective protrusion height increases.

4.5 Summary of Chapter 4

This chapter illustrates the effects of various geometric (initial length of tube, initial tube wall thickness and die blend radius), and the process parameters (contact surface friction and loading paths) on a X-branch type tube hydroforming. The information can be used for further analysis of the process and can be used as a design guideline for processes with similar geometric features.

Chapter 5: Determination of Optimal Loading Paths Using Finite Element Simulations and Optimization Technique

5.1. Introduction

In Chapter 3 and Chapter 4 it was shown, how forming load paths can affect the final part expansion, wrinkle growth and part thinning behaviour of a typical X-branch type hydroformed component. This is also valid for almost all type of tube hydroforming processes except for free forming cases, where only internal pressure is applied without any axial feeding for forming of the component [29]. In such cases, excessive part thinning is the only bottleneck of the process [29, 43, 46], whereas for cases with combined loading, wrinkling and bursting are the main bottleneck of the process. Thus, for a successful application of the process a feasible load path has to be calculated in advance which can avoid the failure conditions. Furthermore this feasible load path can be optimized so as to maximize the part expansion simultaneously conforming to the geometrical requirement of the part to be formed and, as well as avoid all failure modes such as excessive wall thinning and wrinkling. With development of high speed computers and robust finite element codes integrated with various optimization algorithms and tools, it has now become relatively easy to calculate and predict an optimal loading condition in advance depending upon the part quality and expansion requirement.

This chapter discusses a new approach to automatically determine feasible and optimal tube hydroforming load paths using an optimization algorithm coupled with finite element simulation. Here a subproblem optimization method will be used along with ANSYS /LS-DYNA pre-post processor interface and LS-DYNA 3D explicit solver to determine the optimal load paths subjected to design constraints such as wall thinning and wrinkle growth for asymmetric components such as X and T-branch. In the recent years similar optimization works have been reported by few researchers [47, 60, 70, 76, 79] on axisymmetric part expansion where the basic objective was to calculate an optimal load path (relation between forming pressure and end feed or relation between forming pressure and end compressive force) so that desired part characteristics (i.e. part expansion, uniform wall thickness distribution, avoid failures such as wrinkling, buckling and excessive wall thinning) can be achieved. In most of the work, finite element simulations coupled with inbuilt optimization tools were used for the optimization to predict the optimal load paths.

5.2. Overview of the optimization process

Formulation of optimization in engineering designs can be very different from one problem to another depending on the design objective, the associated design parameters and constraints. Consequently, there is no universally applicable formulation of optimization that can be applied to all the engineering design problems. Depending upon the problem and the application, an appropriate set of design variables, state variables, constraints and mathematical definitions of the optimization problem must be developed. In this study, typical tube hydroforming processes were optimized with different objectives. Thus, depending upon the application and type of expansion, the objective functions may be different and process dependent i.e. in certain cases simple part expansion of the process may be important and in certain cases the final profile of the component would be of much importance. In general, most non-linear constrained optimization problems can be defined mathematically as follows:

Minimize:
Objective function $f(x)$ (1)

Subject to:
Inequality constraint functions $g_i(x) \leq c_i$ (i=1,2,3… ,I) (2)
Equality constraint functions $h_j(x) = 0$ (j=1,2,3… ,J) (3)
Design variable limits $a_k \leq x_k \leq b_k$ (k=1,2,3… ,K) (4)
Where, design variables $x_l = [x_1, x_2, \ldots . x_l]$ (5)

The optimization solution method involves searching for the optimum design variable vector $\hat{x}$ that minimizes the objective function $f(\hat{x})$, while the optimum design vector $\hat{x}$ is bounded in the feasible set defined as:

$$S = \left\{ \hat{x} \geq \middle| \forall i : g_i(\hat{x}) \leq c_i .\&. \forall k : a_j \leq \hat{x}_k \leq b_k \right\} \tag{6}$$

For the present optimization study and analysis this was expressed as:

Branch Height = $f\{pressure, feed\}$ subjected to *Wrinkle* and *Wall Thinning* constraints.

Where, height branch is the protrusion height of X or T branch and the relation between the pressure and feed is the loading path.

The details of the optimization algorithm used in this work are explained in the later part of this chapter (section 5.3). In general, there is a common procedure in creating mathematical models for most optimization problems (fig 5.2.1). According to the procedure, the very first step in formulation of an optimization problem is to realize the need for using optimization in a specific design problem (i.e. to find the objective, what is to be optimized and what results are expected out of the optimization). Then the important design parameters associated with the design problem are to be identified. Then, some or all of these design parameters are to be chosen as optimization design variables depending on the interested design goal. The formulation of optimization problems requires some other important components such as constraint functions, objective functions, and variable limits. The procedure, (fig 5.2.1) usually goes from top to bottom. However, very often, all the steps are interrelated. Therefore, some iterations in the formulation procedural steps are necessary.

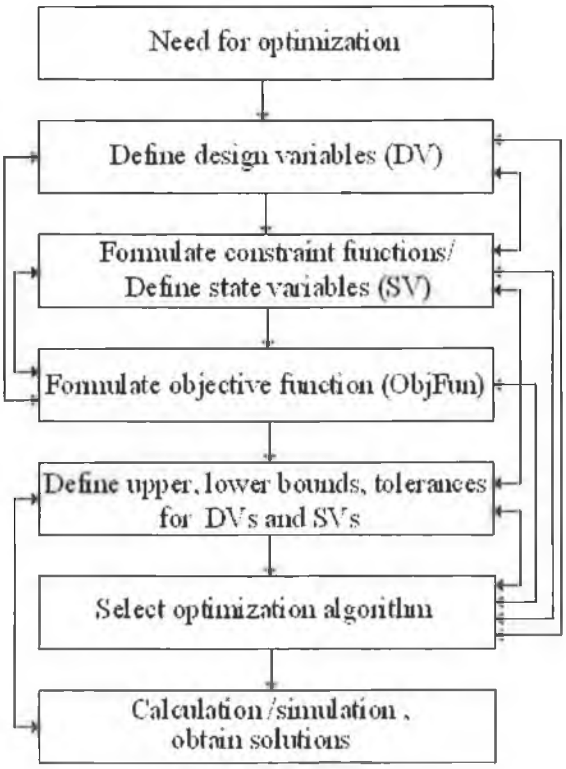

Fig 5.2.1 Flow chart depicting a typical optimization setup with interlinking between different parameters [87]

The optimization technique used in this study can be considered as a part of a design optimization process where the design parameters, here termed as process parameters i.e.

pressure and feed values are optimized for best performance of the process with an objective to maximize the part expansion. To run the optimization program along with the finite element code, one of the main important requirements is to define the model parametrically where all the design parameters can be defined numerically in a parametric form. Thus, in this case the finite element model was built parametrically using 'ANSYS parametric design language' (APDL) script and the design variables (pressure and feed) were defined parametrically for the initial run and in the course of the subsequent optimization runs (for the search of the maximum bulge height), the values of the parametrically defined design variables are reassigned by the program which are derived from the internal optimization calculations.

The optimizations of the processes were carried out using the 'sub-problem approximation' optimization algorithm, which is a gradient-based optimisation tool. Fig 5.2.2 shows the integration of the optimization tool and the flow of information during an optimization analysis using ANSYS/LS-DYNA simulation. In the optimization run, the program performs a series of analysis-evaluation-modification cycles. That is, an

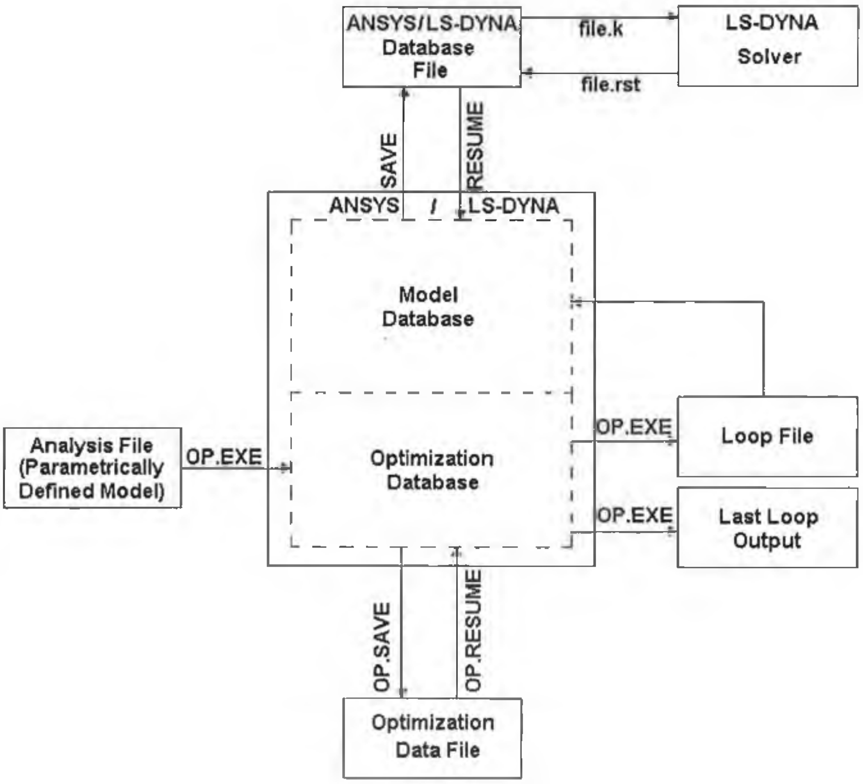

Fig 5.2.2 Optimization Data Flow – integration of optimization program with ANSYS/LS-DYNA finite element code [90]

analysis of the initial design is performed, the results are evaluated against specified design criteria, and the design is modified as necessary. This process is repeated until all specified criteria are met. In the final stage of optimization simulation runs, sets of design data are obtained of which one is the best design set with optimum values of design parameters.

The following section explains the detail of the optimization method and its application for determination of the optimized and feasible load path.

5.3. Theory of optimization

The basic numerical formulation of optimization was explained in the previous section. This section will outline the theory involved in the optimization tool drawing particularly from reference [90]. The optimization module used here is a universal and an integral part of the ANSYS Multiphysics program which can be used both with the ANSYS implicit solver and the LS-DYNA3D solver and can be employed to determine the optimum or the best design for a particular structural optimization problem. In this analysis, the goal will be to calculate the optimal process parameters (i.e. relation between forming pressure and end axial feed), by maximising the branch expansion (i.e. branch height) while keeping the tube wall thickness and wrinkle depth within the specified safety limits.

The optimization routines used in the program employ three types of variables that characterize the optimization process: a.) Design variables (DV), b.) State variables (SV) and, c.) The objective function or the goal (Obj.Fun.). The independent variables in an optimization analysis are the design variables. The vector of design variables is indicated by equation-(7). Design variables are the most relevant parameters for proper working of the design, the objective function and the constraint functions or the state variables depends on them.

$$x = [x_1, x_2, \ldots x_n] \qquad (7)$$

Design variables are subject to 'n' constraints with upper and lower limits, that is,

$$\underline{x}_i \le x_i \le \overline{x}_i \qquad \text{where i=1,2,3...n} \qquad (8)$$

Where 'n' is the number of design variables.

The design variable constraints are often referred to as side constraints and define what is commonly called feasible design space. Typically, an initial set of the design variables is specified, which is updated iteratively. These updated new design variables remains bound with in the feasible design space. For better optimization efficiency the total number of the design variables should be kept as minimum as possible. More design variables can be added to the optimization if necessary.

The next step in the optimization process is to minimise the objective function defined as

$f = f(x)$ (9)

subject to design constraints

$g_i(x) \leq \bar{g}_i$ (i=1,2,3... m_1) (10)

$\underline{h}_i \leq h_i(x)$ (i=1,2,3... m_2) (11)

$\underline{w}_i \leq w_i(x) \leq \overline{w}_i$ (i=1,2,3....m_3) (12)

where:

f, is the objective function to be minimized, and

g_i, h_i, w_i are termed as state variables containing the design, with underbars and overbars representing lower and upper bounds respectively

$m_1 + m_2 + m_3$ = number of state variables constraints with various upper and lower limit values

These design constraints are normally expressed in functions of the design variables to satisfy certain physical limitations of the design problems. This is to ensure that the optimization results are not just simply numerically possible but also realistically applicable or in other word, the optimization runs generate results (maxima or minima of the objective function- based on the optimization problem requirement), which can be physically applied for forming of the component and should satisfy the design constraints or limits imposed on the component model. Therefore, the design variables, while being varied iteratively, should satisfy the constraint functions, which restrict the design variables to a certain region of the design space. The state variables can also be referred to as dependent variables in that they vary with the vector 'x' of design variables. The objective function 'f' expresses specific design intentions that need to be minimized (or maximized). In other words, the objective function is a performance measure of whatever the design problem intends to optimize. There are primarily two types of objective functions: a.) function to be minimized and, b.) function to be maximized. The optimization tool used for the analysis by default finds the minima, thus for finding a maxima a minor modification in the objective function is required so that effectively the maxima is the final out come of the optimization run. This can be done by modifying the maximization problems to minimization problem by either subtracting the function to be maximized from a large positive integer (*f'*=C-*f*, where C is an arbitrarily chosen large positive integer) or taking the reciprocal value (*f'*=1/*f*) and then minimizing the modified function (*f'*) traditionally by the optimization algorithm.

In the design optimization runs, the results are presented as sets of infeasible and feasible sets. Design configurations that satisfy all constraints are referred to as feasible designs. Design configurations with one or more violations of the constraints are termed as infeasible design set. In defining feasible design space, a tolerance is added to each state variable limit (for example default tolerance value used in the optimization program is 0.001 times of the state variable value this can be further relaxed depending upon the problem statement and solution convergence criteria). So if x* is a given design set defined as:

$$x^* = (x_1^* x_2^* x_3^* \ldots x_n^*) \qquad (13)$$

The design is considered to be feasible only if

$$g_i^* = g_i(x^*) \le \overline{g_i} + \alpha_i \qquad (i=1,2,3\ldots \mathrm{m}_1) \qquad (14)$$

$$\underline{h_i} - \beta_i \le h_i^* = h_i(x^*) \qquad (i=1,2,3\ldots \mathrm{m}_2) \qquad (15)$$

$$\underline{w_i} - \gamma_i \le w_i^* = w_i(x^*) \le \overline{w_i} + \gamma_i \qquad (i=1,2,3\ldots \mathrm{m}_3) \qquad (16)$$

where:

$\alpha_i, \beta_i,$ and γ_i are the ‘tolerances’ of the state variables

and

$$\underline{x_i} \le x_i^* \le \overline{x_i} \qquad (i=1,2,3\ldots \mathrm{n}) \qquad (17)$$

For the design variables, no tolerances are used.

5.3.1. Optimization Method -Subproblem approximation method

This method of optimization can be described as an advanced, zero-order method in that it requires only the values of the dependent variables (objective function and state variables) and not their derivatives. The dependent variables are first replaced with approximations by means of least squares fitting of the data points, and the constrained minimization problem described in the previous section is converted to an unconstrained problem using penalty functions, the details of which will be explained in the subsequent sections. Minimization is then performed in every iteration on the approximated, penalized function (called the subproblem) until convergence of the optimization run is achieved or termination is indicated. For this method, each iteration is equivalent to one complete analysis loop.

Since the method relies on approximation of the objective function and each state variable, a certain amount of initial data in the form of design sets (for this case pressure and feed values) is needed. Thus, an initial preliminary design data has to be defined prior to performing this method of optimization. If not defined, the method itself will generate design sets at random.

5.3.1.1. Function Approximations

The first step in minimizing the constrained problem expressed by equations-(19),(20),(21) is to represent each dependent variable by an approximation, represented by the ^ notation. For the objective function,

$$\hat{f}(x) = f(x) + \text{error} \qquad (18)$$

And similarly for the state variables,

$$\hat{g}(x) = g(x) + \text{error} \qquad (19)$$

$$\hat{h}(x) = h(x) + \text{error} \qquad (20)$$

$$\hat{w}(x) = w(x) + \text{error} \qquad (21)$$

The most complex form that the approximations can take on is a fully quadratic representation with cross terms. Using the example of the objective function,

$$\hat{f} = a_0 + \sum_{i}^{n} a_i x_i + \sum_{i}^{n} \sum_{j}^{n} b_{ij} x_i x_j \qquad (22)$$

The actual form of each fit varies from iteration to iteration and is determined by the program. A weighted least squares technique is used to determine the coefficient, a_i and b_{ij}, in equation-(22). For example, the weighted least squares error norm for the objective function has the form

$$E^2 = \sum_{j=1}^{n_d} \Phi^{(j)} (f^{(j)} - \hat{f}^{(j)})^2 \qquad (23)$$

where:

$\Phi^{(j)}$ = weight associated with design set j

n_d = current number of design sets

Similar E^2 norms are formed for each state variable. The coefficients in equation-23 are determined by minimizing E^2 with respect to the coefficients. The weights used above are computed in the following ways, a.) based on the objective function values, where design sets with low objective function values have high weight, b.) based on design variable values, where the design sets closer to the best design receive high weight, c.)based on feasibility, where feasible sets have high weight and infeasible sets low weights and, d.)based on a combination of the three weights described above.

All weight are unity: $\Phi^{(j)} = 1$, for all j.

As mentioned in section 5.3.1. a certain number of initial design sets must exist in order to form the approximations, otherwise the optimization program will generate random designs sets (initial design sets) until the required number is obtained. This can be expressed as

$n_d < n + 2 \rightarrow$ generate random design sets

$n_d \geq n + 2 \rightarrow$ form the approximations (24)

where:

n = number of design variables

n_d = number of design sets

As more data (design sets) is generated, the terms included in equation-(22) increases.

5.3.1.2. Minimizing the Subproblem Approximation

With function approximations available, the constrained minimization problem is redefined as follows.

Minimize:

$$\hat{f} = \hat{f}(x) \qquad (25)$$

subject to

$$\underline{x}_i \le x_i \le \overline{x}_i \qquad i=1,2,3,\ldots.n \qquad (26)$$

$$\hat{g}_i(x) \le \overline{g}_i + \alpha_i \qquad i=1,2,3,\ldots.n \qquad (27)$$

$$\underline{h}_i - \beta_i \le \hat{h}_i(x) \qquad i=1,2,3,\ldots.n \qquad (28)$$

$$\underline{w}_i - \gamma_i \le \hat{w}_i(x) \le \overline{w}_i + \gamma_i \qquad i=1,2,3,\ldots.n \qquad (29)$$

The next step is the conversion of equations-(25), (26),(27),(28) and (29) from a constrained problem to an unconstrained one. This is accomplished by means of penalty functions, leading to the following subproblem function.

Minimize:

$$F(x,p_k) = \hat{f} + f_0 p_k [\sum_{i=1}^{n} X(x_i) + \sum_{i=1}^{m_1} G(\hat{g}_i) + \sum_{i=1}^{m_2} H(\hat{h}_i) + \sum_{i=1}^{m_3} W(\hat{w}_i)] \qquad (30)$$

in which X is the penalty function used to enforce design variable constraints; and *G, H*, and *W* are penalty functions for state variable constraints. The reference objective function value, f_0, is introduced in order to achieve consistent units. It can be noticed that the unconstrained objective function (also termed a response surface), $F(x,p_k)$, is seen to vary with the design variables and the quantity p_k, which is a response surface parameter. A 'sequential unconstrained minimization technique' is used to solve equation-(30) in each design iteration. The subscript *k* above reflects the use of sub-iterations performed during the subproblem solution, whereby the response surface parameter is increased in value ($p_1 < p_2 < p_3$ etc.) in order to achieve accurate, converged results.

All penalty functions used are of the extended-interior type. For example, near the upper limit, the design variable penalty function is formed as

$$X(x_i) = \begin{Bmatrix} c_1 + c_2/(\overline{x} - x_i) & if & x_i < \overline{x} - \varepsilon(\overline{x} - \underline{x}) \\ c_3 + c_4/(\overline{x}_i - \overline{x}) & if & x_i \ge \overline{x} - \varepsilon(\overline{x} - \underline{x}) \end{Bmatrix} (i=1,2,\ldots.n) \qquad (31)$$

where:

c_1, c_2, c_3, and c_4 = constants that are internally calculated

ε = very small positive number

State variable penalties take a similar form. For example, again near the upper limit,

$$W(w_i) = \begin{Bmatrix} d_1 + d_2/(\overline{w} - \hat{w}_i) & if & \hat{w}_i < \overline{w}_i - \varepsilon(\overline{w}_i - \underline{w}_i) \\ d_3 + d_4(\hat{w} - \overline{w}) & if & \hat{w}_i \ge \overline{w}_i - \varepsilon(\overline{w}_i - \underline{w}_i) \end{Bmatrix} (i=1,2,\ldots.m_1) \qquad (32)$$

where:

d_1, d_2, d_3, and d_4 = constants that are internally calculated

and similarly for G and H.

The 'sequential unconstrained minimization technique' algorithm is employed to reach the minimum unconstrained objective function, $\tilde{F}^{(j)}$, at design iteration j; that is,

$$x^{(j)} \rightarrow \tilde{x}^{(j)} \text{ as } F^{(j)} \rightarrow \tilde{F}^{(j)} \qquad (33)$$

where:

$\tilde{x}^{(j)}$ = is the design variable vector corresponding to $\tilde{F}^{(j)}$

The final step performed each design iteration is the determination of the design variable vector to be used in the next iteration $(j+1)$. Vector $x^{(j+1)}$ is determined according to the following equation.

$$x^{(j+1)} = x^{(b)} + C(\tilde{x}^{(j)} - x^{(b)}) \qquad (34)$$

where:

$x^{(b)}$ = best design set constants

C=internally chosen to vary between 0.0 and 1.0, based on the number of infeasible solutions.

5.3.1.3. Convergence

Subproblem approximation iterations continue until either convergence of the problem (optimization run) is achieved or termination occurs. These two events are checked only when the current number of design sets, *nd*, equals or exceeds the number required for the approximations (equation-(24)). Convergence is assumed when either the present design set, $x^{(j)}$, or the previous design set, $x^{(j-1)}$, or the best design set, $x^{(b)}$, is feasible; and one of the following conditions is satisfied.

$$\left|f^{(j)} - f^{(j-1)}\right| \le \tau \qquad (35)$$

$$\left|f^{(j)} - f^{(b)}\right| \le \tau \qquad (36)$$

$$\left|x_i^{(j)} - x_i^{(j-1)}\right| \le \rho_i \qquad (i=1,2,\ldots,n) \qquad (37)$$

$$\left|x_i^{(j)} - x_i^{(b)}\right| \le \rho_i \qquad (i=1,2,\ldots,n) \qquad (38)$$

where:

τ and ρ_i = objective function and design variable tolerances

Equations-(35) and (36) correspond to differences in objective function values; equations-(37) and (38) to design variable differences. If satisfaction of equations-(35), (36), (37) and (38) is not realized, then termination can occur if either of the below two conditions is reached.

$n_s = N_s$ (39)

$n_{si} = N_{si}$ (40)

where:

n_s = number of subproblem iterations

n_{si} = number of sequential infeasible design sets

N_s = maximum number of iterations

N_{si} = maximum number of sequential infeasible design sets

In other words the above can be stated as, at the end of each optimization loop, a check for convergence (i.e. for termination of the optimization cycle) is made. The problem is said to be converged if the current, previous, or best design is feasible and any of the following conditions are satisfied:

a. The change in objective function from the best feasible design to the current design is less than the objective function tolerance.
b. The change in objective function between the last two designs is less than the objective function tolerance.
c. The changes in all design variables from the current design to the best feasible design are less then their respective tolerances.
d. The changes in all design variables between the last two designs are less than their respective tolerances.

5.4. Application of the optimization technique in tube hydroforming – Process Parameter Design

Most complex sheet metal forming processes such as deep drawing and tube hydroforming can be best analyzed numerically using finite element simulations. In formulating optimization problems of these sheet metal forming processes, proper optimization algorithms have to be selected and applied in conjunction with finite element simulations. Generally, part characteristics such as part/die dimensions, shape and weight are usually optimized for these processes. For example, optimization of deep drawing of sheets is performed to maximize or improve the part formability [82].

Similarly this numerical optimization can also be applied for selection of proper loading profiles [47, 60, 76, 79, 80], i.e. for optimization of process parameters such as nodal displacement, forces, pressures etc. In contrast to typical metal forming design optimization, where one searches for the optimal values of part characteristics, process optimization address the problem of determining the process variables that influence the form and quality, or in other terms the formability of the final part. In case of the tube hydroforming process, the loading path that minimizes part thickness variation, and maximizes part dimensional accuracy simultaneously eliminating or minimizing the possibility of buckling or wrinkling is usually searched [47, 79, 80]. This process optimization is very challenging because it involves a number of issues that are either not well understood or are computationally complex:

1. It is not clear that there is an obvious or universally applicable definition for the objective function to be optimized, and thus one needs to develop an appropriate metric to measure the quality of the part.

2. Given the large number of variables that could influence this measure of performance, one must identify the (relatively few) variables that have a sufficiently significant effect and separate these from the (relatively many) ones that have only a marginal effect. Moreover, these variables may not be independent from each other and there may be significant interactions between them.

3. Objective function evaluation is very time consuming since each such evaluation typically involves a call to the finite element program that conducts a detailed finite element analysis. The results of this analysis will then be used to arrive at a single number that captures the objective function value.

Thus considering the above issues and depending upon the part geometry to be considered for the optimization analysis, proper selection of objective function, design variables and constraints functions are quite important. Moreover the selection of these parameters depends upon the part geometry and shape. For example in case of X and T-branch type free expansion (i.e. without counter punch) subjected to combined loading (internal pressure and end compressive force or feed), for such cases the degree of part expansion can be roughly judged by considering the extent to which the branch height is developed. Thus, if the objective is to maximize the part expansion then in such case the protrusion height or bulge height can be considered as the objective function. This may not be valid for other geometries. Similarly in Chapter 4 it was shown how different process parameters (friction, loading paths i.e. forming pressure and end feed curve) affect the final part expansion, wall thinning and wrinkle growth. From the analysis it was observed that with varying friction there was a variation in the branch height and as well as wall thinning (process response), whereas with variation in loading path, apart from change in the branch height and wall thickness variation, an additional response factor i.e. wrinkle growth was of major concern. Thus, in comparison to friction coefficient, the loading paths have more influence on the process and are more significant from design and optimization point of view. Hence for optimization of the process, loading paths should be of prime importance in comparison to all other process variables.

The detailed formulation of design variables, constraint functions, and objective function for tube hydroforming processes are discussed next.

5.4.1. Design Variables and Design Limits

For a typical tube hydroforming process, usually the optimum pressure versus time curve and axial feed versus time curve is of importance. In the optimization framework, these curves can be represented by piece-wise linear curves, of which the control points are the design variables which can be represented as:

$$x = [PDV1, PDV2, ...PDVn | FDV1, FDV2, ...FDVm]$$

Where, PDV1, PDV2,...PDVn are the design variables of the pressure piece-wise linear curve, and FDV1,FDV2,...FDVm are the design variables of the axial feed piece-wise linear curve. The number of design variables is 'n' and 'm' for the pressure curve and axial feed curve respectively. As mentioned in section 5.3 the total number of the design variables (n+m) should be kept minimum because the efficiency of the optimization largely depends on the size of the design variables. The design variables are further bound by the design limits denoted by $[PDL1, PDL2, ...PDLn | FDL1, FDL2, ...FDLm]$. Fig 5.4.1 and fig 5.4.2 show the graphical representation of the curves with the design limits.

An approximate number of the design variables can vary depending on how well these control points can represent the shape of the process parameter curve of interest (i.e. profile of the pressure and feed load paths) [60, 79]. As shown in Chapter 2, Mac Donald [49] used a piecewise bi-linear (two straight lines) for the load path for the simulation study, however considering the complexity of the load paths, more than two or multi-linear piecewise straight lines can further represent the profile of the load path in a better way. In other word more the gradation or control points (i.e. number of piecewise straight lines) better is the curve representation, however from the optimization point of view this becomes a bottleneck (higher values of multi-linear piecewise load path) as number of design variables increases with the increase of number of control points. Thus a balance should be made to select the divisions, for the case studies presented in this chapter, maximum four sets of each pressure and feed design variables were considered (fig 5.4.1 and fig 5.4.2) with four fixed time intervals (T0-T1, T1-T2, T2-T3, and T3-T4) which were sufficient enough to capture approximate shapes of the process parameter curves (i.e. load paths as shown in Chapter 3 and Chapter 4). In other words the design points (four sets of pressure and feed values) were defined at fixed time i.e. at T1, T2, T3 and T4, where T4 is the end of the LS-DYNA simulation time.

The selection of the design variables (pressure and feed load paths) for the present hydroforming optimization (X and T- branch expansion) were done based on the experience of the type and nature of loading path which yield successful parts i.e. from the experimental and simulation work reported in Chapter 3 and Chapter 4, it was seen that load paths with high axial feed with respect to pressure rise at the initial stage of the process result in wrinkle growth, whereas with high forming pressure in the initial stage with respect to axial feed resulted in proper part expansion however with chances of higher wall thinning. Thus a balance has to be made in selection of the design variable limits. For simplicity of the problem equidistant points can be assumed, however with this kind of settings (equidistant points or design control limits) there are chances of failure of the optimisation run to maximize the branch height subjected to the fixed design constraints (wrinkles and wall thinning), thus in such situation it calls for adjustment of the design limits (i.e. reducing or increasing the range of design limits so that they are no more equidistant) to obtain better part expansions simultaneously satisfying the design constraints.

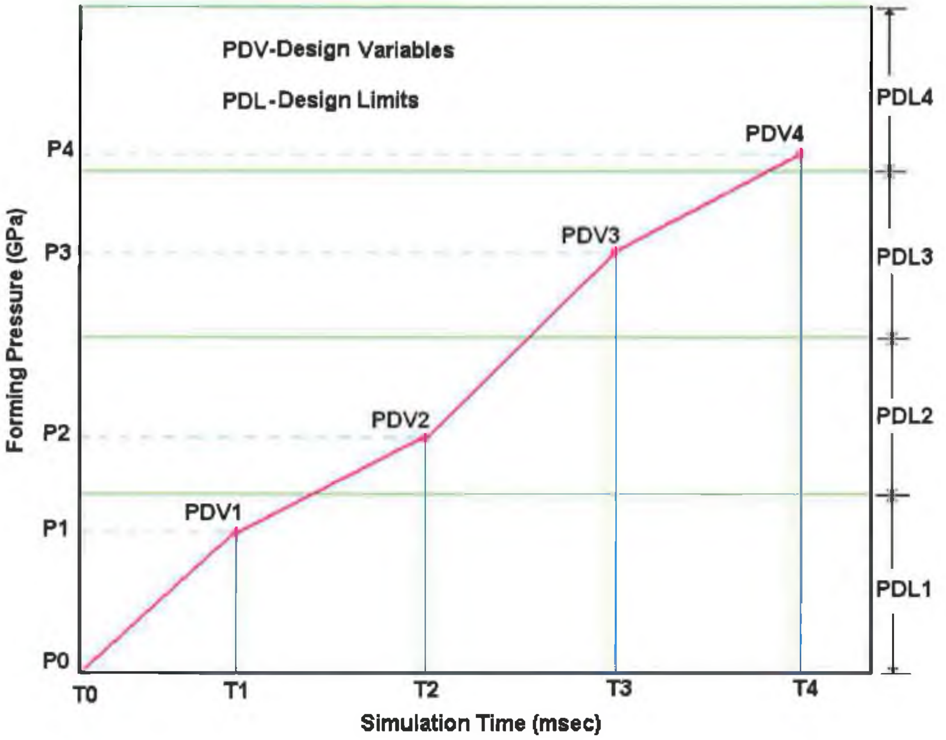

Fig 5.4.1 Piecewise linear pressure load curve (forming pressure as a function of simulation time) with design variable

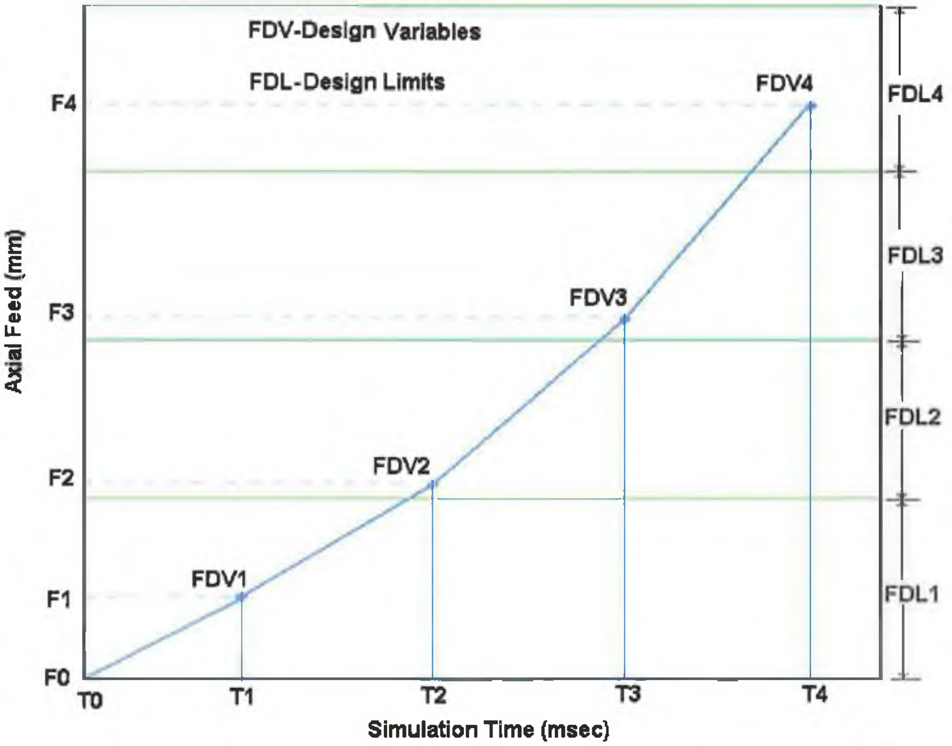

Fig 5.4.2 Piecewise linear axial feed load curve (end axial feed as a function of simulation time) with design variable

5.4.2. Objective Function

The main goal of optimization in any tube hydroforming process is to determine the best loading paths that would hydroform the given part with the most uniform part thickness distribution simultaneously maximizing the part expansion. The most common type of objective functions, which can be of practical importance are the following:

a.) Maximizing the final volume of the formed component:

In this type of objective function, the part expansion is assumed to be as function of final volume of the formed tube. In most of the hydroforming cases, the final volume (external curved surface area) of the tube increases and it takes the shape of the closed forming die. This type of objective function is used for components where the expansion is axisymmetric in nature or for cases where the final formed component expands so as to take the exact shape of the die without any wrinkle growth or excessive wall thinning. Examples of these kinds of expansions are forming of hollow shafts, chassis cross members or engine cradles.

b.) Maximizing the bulge height of the component:

This type of objective function can be used for maximizing the part expansion of X or T type of hydroformed components or its combination, where the part expansion can be assumed to be a function of the final bulge height of the component subject to no wrinkle formation or excessive wall thinning in any part of the tube. This type of objective function is only valid for the cases where a counter punch is not used to reshape the branch development i.e. the branch can grow freely within the X or T die cavity.

5.4.3. Constraint functions (State Variables)

Constraint functions or state variables are imposed in design optimization problems to ensure realistic results. The load curve obtained from the optimization should be such that it can be implemented in an automated hydroforming machine. For successful application of the process failures due to excessive wall thinning should be avoided thus, wall thickness reduction is one of the limiting conditions for tube hydroforming process. On the other hand, part dimensional accuracy is also important for certain formed components.

For certain cases, differentiating between the constraint function and the objective function is a little difficult task due to the fact that either of them can be defined as constraint function or objective function. For example, hydroforming of a difficult-to-form part requires that the part thickness distribution be as uniform as possible and also the part dimensions be highly accurate. Although, it is possible to achieve these two goals, by imposing multi-objective functions, but it is well known that in optimization problems with multi-objectives it is usually difficult to find converged solutions. To obtain part thickness uniformity it is important to have large axial feeds to push enough material into the zones susceptible to severe thinning. Unfortunately, this large amount of axial feed may lead to formation of a wrinkle in certain unstable zones, increasing the chances of inferior part dimension accuracy. Thus, it can be said that these two part qualities compete with each other. In such cases, the most important part quality should be used as the objective function and the rest should be imposed as constraint in the optimization problems. In this study as explained above the part expansion was considered for the objective function, so in that case part wall thickness variation is used as the constraint function with an additional design constraint i.e. wrinkling.

To increase the final part geometry adherence to the die shape and to avoid any wrinkle, the allowable wrinkle height was fixed to certain critical limit and the root-mean-square value of wrinkle height was used as the constraint function. Thus the wall thickness distribution and wrinkle height were defined as the state variables.

5.5. X and T-branch tube hydroforming (asymmetric expansion)

In section 5.3, the basic theory of sub-problem optimization method was explained in detail with the definition of optimization function, design and state variables. In this study, the optimization technique will be used to obtain an optimal and feasible load path for a X and a T-branch type asymmetric expansion with an objective to maximize the bulge height (part expansion), simultaneously keeping the tube wall thickness and the maximum wrinkle height with in the specified safety/cut-off limits. The load paths in this case are the relation between pressure versus simulation time and, axial feed versus simulation time, and finally it is presented as the pressure as a function of axial feed. In case of X or T type expansion, the degree of part expansion can be directly correlated with the developed branch height subjected to no buckling of the tube or wrinkle formation at any location. The finite element models of X and T-branch used for the simulations and optimization have been detailed in Chapter 4, where the models were validated against the experimental results for the part expansion and wall thickness distribution. For the present optimization study, 720 and 1440 finite shell elements were used for tube blank portion of X and T-branch respectively. In the optimization the bulge height (branch height) of the X and T-branch was defined as the objective function (Obj Fun), the minimum tube wall thickness (shell element thickness) at any point of the tube was defined as the first design constraint and the maximum wrinkle height along the line in the ZX plane (i.e. line generated by intersection of ZX plane along the global coordinate system with the tube) was defined as the second design constraint (i.e. the state variable- SV). The limiting value for the tube wall thinning was set at 1.17mm for both X and T-branch whereas the maximum allowable wrinkle height for X-branch was set at 0.095mm and for T- branch 0.2mm. Due to solution convergence difficulty (i.e. to obtain feasible design sets) with the T-branch simulation, the allowable wrinkle height was set a little higher (relaxation in design constraint limit) in comparison to X-branch forming. The limiting values for the allowable wall thickness change (allowable thinning 10% of the original wall thickness) and allowable wrinkle height were set very tight so as to ensure that there is minimum wall thinning and also the part adheres to the die shape (minimal wrinkle height) in other word there should not be any distortion in the final formed component.

The piecewise linear internal hydroforming pressures and end axial feeds were defined as the design variables (DV). The total number of design variables used was 8, 4 of which are for the pressure and 4 for the axial feed. As explained in section 5.4.1 in certain cases it requires an adjustment of the range of the design limits to obtain the best and optimal results (such as maximizing the branch height in the present case). In the present case initial trial optimizations were done with equidistant design range of the pressure and feed values (control limits), however it was observed that due to very rigid or tight design constraints (wall thinning and wrinkle height) imposed on the design, the optimization program failed to maximize the part expansion and all the calculated design sets were infeasible, thus minor adjustments were done in the design limit range to avoid this situation. The new design limit ranges for X and T-branch are detailed in table 5.5.1.

Further two different design constraints (i.e. state variables) were used on the optimization model, one of which is for the tube wall thickness distribution defines as the minimum cut-off wall thickness value and the second for the wrinkle height calculated as the root-mean-square value of deviation or separation of the tube nodes from the die geometry. The tolerance limits for these state variables were set at default values of the optimization program. The pressure and axial feed were applied in four discrete steps/stages. The lower and upper ranges for axial feed were defined in such a fashion and constrained, that in the entire simulation the axial feed values can either increase or remain steady. As in case of actual forming operation, the axial feed has to be always positive and should increase with the simulation time (i.e. forming time) whereas pressure can remain flexible i.e. it can either increase or decrease (vary) and adjust as per requirement. However, from the experience of the experimental studies, it was seen that pressure increased from zero (at the beginning of the process) to maximum value at the end of the process, thus for the optimization run the pressure was assumed to be increasing throughout the entire forming process. Thus, the lower and upper ranges of the pressure for all the design sets were defined in an increasing order similar to axial feeds.

The minimum wall thickness of the tube wall was calculated by using a small post-processing program which first sorts all the shell element thickness values of the tube and then sorts the minimum value of all the shell thickness. Similarly, the root-mean-square wrinkle height of any wrinkle if formed was calculated by another post-processing program, where the nodal displacements along X direction in the zx-plane for certain range of tube length was used to calculate the wrinkle height. The details of the parametric finite element models, post-processing of the results and integration of the finite element model with the optimization tool, developed using ANSYS parametric design language script are presented in Appendix–B.

For starting the optimization runs, the initial simulations were run by an arbitrarily chosen load path for the processes. 30 sets of simulations/iterations were set for optimization run to determine the optimal design set subject to the design constraints. In case of failure of the optimization program to calculate the optimal solution or if the solution did not converge or a feasible solution is not obtained then the design variable limits/bounds or constraint function limits have to be modified so that the program can calculate a feasible and optimal solution within the specified iterations. For optimization of the load path, the entire simulation model, the forming pressure, axial feed load functions and all the design parameters were defined parametrically. Table-5.5.1 shows the initial assumed design and state variables of the processes.

Table 5.5.1 Initial design and state variable parameters sets with design limits for X and T- branch with corresponding objective functions

Design Parameters	X-branch	Design Limits	T-branch	Design Limits
Wall THK. (SV)	1.286 mm	1.17 mm (min)	1.281mm	1.17 mm (min)
Wrinkle HT. (SV)	0.124 mm	0.095 mm (min)	0.144 mm	0.200 mm (min)
F1 (DV)	2.5 mm	0.05 mm-3.5 mm	2.5 mm	0.05 mm-3.5 mm
F2 (DV)	5.0 mm	3.5 mm-7.5 mm	5.0 mm	3.5 mm-7.5 mm
F3 (DV)	7.5 mm	7.5 mm-10.0 mm	7.5 mm	7.5 mm-12.0 mm
F4 (DV)	10.0 mm	10.0 mm-19.0 mm	14.0 mm	12.0 mm-19.0 mm
P1 (DV)	0.0085 GPa	0.005 GPa-0.015 GPa	0.0085 GPa	0.005 GPa-0.015 GPa
P2 (DV)	0.015 GPa	0.015 GPa-0.020 GPa	0.0150 GPa	0.015 GPa-0.020 GPa
P3 (DV)	0.020 GPa	0.020 GPa-0.025 GPa	0.0200 GPa	0.020 GPa-0.025 GPa
P4 (DV)	0.027 GPa	0.025 GPa-0.035 GPa	0.0280 GPa	0.025 GPa-0.035 GPa
T1	0.75 msec		0.75 msec	
T2	1.50 msec		1.50 msec	
T3	2.25 msec		2.25 msec	
T4	3.00 msec		3.00 msec	
Branch-Height (Obj Fn)	5.988 mm		8.462 mm	

5.5.1. Results

Table-5.5.2 and table-5.5.4 detail the results for all the simulations from initial design to final optimal or best design set (for maximized bulge height) for X and T-branch expansion respectively, subjected to the design constraint imposed on the forming process. The final developed bulge height, tube wall thickness distributions for the best design set were studied, and it was observed that for X-branch (fig 5.5.1) and T-branch (fig 5.5.8) the value of tube wall thinning and the maximum wrinkle height were below the specified safety/cut-off limits for the final feasible and optimal design set. Fig 5.5.2 and fig 5.5.9, fig 5.5.3 and fig 5.5.10, fig 5.5.4 and fig 5.5.11 show the optimal load paths (pressure and feed curves plotted against simulation time and plots with pressure as a function of feed) corresponding to the initial and the final (best design/optimal) sets for X-branch and T-branch formed tubes. It can be seen from the feed curves for both X and T-branch (fig 5.5.3, fig 5.5.10) that the final feed is relatively higher than the initial defined value. This can be explained, as in the optimization the main objective was to maximize the bulge height simultaneously keeping the wall thickness with in a specified limit, this can be only achieved by proper additional plastic flow of material in the deforming zones or in other terms there should be enough axial feeding of material. From the pressure curves (fig 5.5.2, fig 5.5.9) it can be observed that pressure has increased for all the design points with respect to the initial design set. This increase of pressure is required for proper expansion and calibration of the part against the die profile and also to suppress the growth of any wrinkle that may occur.

Fig 5.5.5 and fig 5.5.12, fig 5.5.6 and fig 5.5.13, fig 5.5.7 and fig 5.5.14 show evolution of the objective and constraint functions from the optimization runs (iterations) for X and T-branch respectively. A total of 12-13 optimization iterations were required to arrive at a converged solution with in the design space. For the X-branch, the optimization run converged after 12 design sets/iterations, whereas for the T-branch it converged after 13 design sets/iterations.

From the optimization results it can be seen that most of the design sets which were infeasible in nature did not satisfy the wrinkle constraint i.e. in all the infeasible sets the wrinkle height was above the cut-off limit of 0.095mm for X-branch and 0.2 for T-branch. The reason for this can be explained by considering the limit of the allowable wrinkle height, as it can be seen for both X and T-branch the wrinkle height limit was reasonably low. This low value of wrinkle height was set to eliminate even minor part distortion. Further while comparing the trend of the objective function (branch height) for all the design sets, it can be seen that the value kept changing (i.e. fluctuating) during the iteration, the reason being during the optimization run, the optimization algorithm used here searches for the global maxima within the design limits simultaneously satisfying the design constraints.

The initial load path (prior to optimization) and the optimal load path (fig 5.5.4, fig 5.5.11) for the X and T-branch were plotted for comparison between the first and last design sets. The optimal loading path obtained exhibits a typical tube hydroforming loading path shape (X-type) as shown in Chapter 4 (load paths 4,5 & 6) where the load path exhibits better control over wrinkle growth. The minimum wall thicknesses of the resultant parts for the optimal design set were also above the specified design constraint limit (fig 5.5.6, fig 5.5.13), this is one of the most desirable qualities of any tube hydroforming process. For the X-branch, the maximum tube wall thinning corresponding to the optimal design set was 7.3% of the initial wall thickness value whereas for the T-branch, it was 2.5% and the safety or allowable limits for both the cases were set at 10% of the original wall thickness value.

Table 5.5.2 X-branch- design sets (output) with iteration number

	SET	1	2	3	4	5	6	7	8	9	10	11	12*
Design variable		infeasible	infeasible	infeasible	infeasible	infeasible	infeasible	infeasible	infeasible	infeasible	infeasible	feasible	feasible
Wall THK (mm).	(SV)	1.286	1.278	1.274	1.264	1.282	1.260	1.261	1.280	1.241	1.256	1.224	1.205
Wrinkle HT (mm)	(SV)	0.124	0.201	0.229	0.129	0.271	0.165	0.122	0.314	0.116	0.207	0.063	0.061
F1 (mm)	(DV)	2.500	2.973	1.668	1.878	2.936	1.613	1.373	2.525	0.968	0.384	1.293	1.561
F2 (mm)	(DV)	5.000	5.329	4.781	7.458	3.973	6.872	3.738	5.095	7.128	6.263	4.292	3.697
F3 (mm)	(DV)	7.500	9.246	11.067	10.343	10.915	8.931	7.601	10.869	8.905	10.597	7.925	7.618
F4 (mm)	(DV)	10.000	16.231	15.239	11.358	16.423	15.527	14.190	17.782	14.370	14.282	17.557	18.621
P1 (GPa)	(DV)	0.0085	0.0104	0.0120	0.0127	0.0109	0.0128	0.0105	0.0051	0.0120	0.0135	0.0141	0.0148
P2 (GPa)	(DV)	0.0150	0.0181	0.0154	0.0178	0.0153	0.0185	0.0152	0.0181	0.0175	0.0151	0.0193	0.0198
P3 (GPa)	(DV)	0.0200	0.0242	0.0217	0.0224	0.0218	0.0205	0.0202	0.0225	0.0235	0.0217	0.0247	0.0249
P4 (GPa)	(DV)	0.0270	0.0250	0.0261	0.0330	0.0252	0.0308	0.0313	0.0264	0.0340	0.0272	0.0347	0.0349
OBJFUN	(OBJ)	5.988	10.075	9.365	7.355	9.849	10.059	9.413	10.773	9.812	9.082	12.641	13.544
(Branch Height-H)		Initial Design											Best Design

Further to ensure whether the optimization runs have converged to an optimal solution i.e. the branch height is maximized within the defined design space subjected to the design constraints, a new set of optimization was done with an entirely different initial sets design variables (control points) values for a X-branch type expansion. The final results obtained with the new optimization run were almost identical (maximum branch height) to the result obtained from the optimization run detailed above with a minor shift in the intermediate design variable positions (load paths). Table 5.5.3 details two

Table 5.5.3 Comparison of X-optimization run results for two different initial design sets

Design Variables		Initial Design (1)	Optimal Design (1)	Initial Design (2)	Optimal Design(2)
Wall THK (mm)	SV	1.286	1.205	1.283	1.230
Wrinkle HT (mm)	SV	0.124	0.061	0.16	0.061
F1 (mm)	DV	2.500	1.561	3.0	1.61
F2 (mm)	DV	5.000	3.697	6.0	3.671
F3 (mm)	DV	7.500	7.618	8.0	7.581
F4 (mm)	DV	10.000	18.621	12.0	18.582
P1 (GPa)	DV	0.0085	0.0148	0.010	0.0149
P2 (GPa)	DV	0.0150	0.0198	0.018	0.0196
P3 (GPa)	DV	0.0200	0.0249	0.022	0.0249
P4 (GPa)	DV	0.0270	0.0349	0.028	0.0348
(Branch Height-H)		5.988	13.544	7.534	13.129

different sets of optimization runs with initial (assumed) and final design (optimal) control points with the final wall thickness and wrinkle height for X-branch forming.

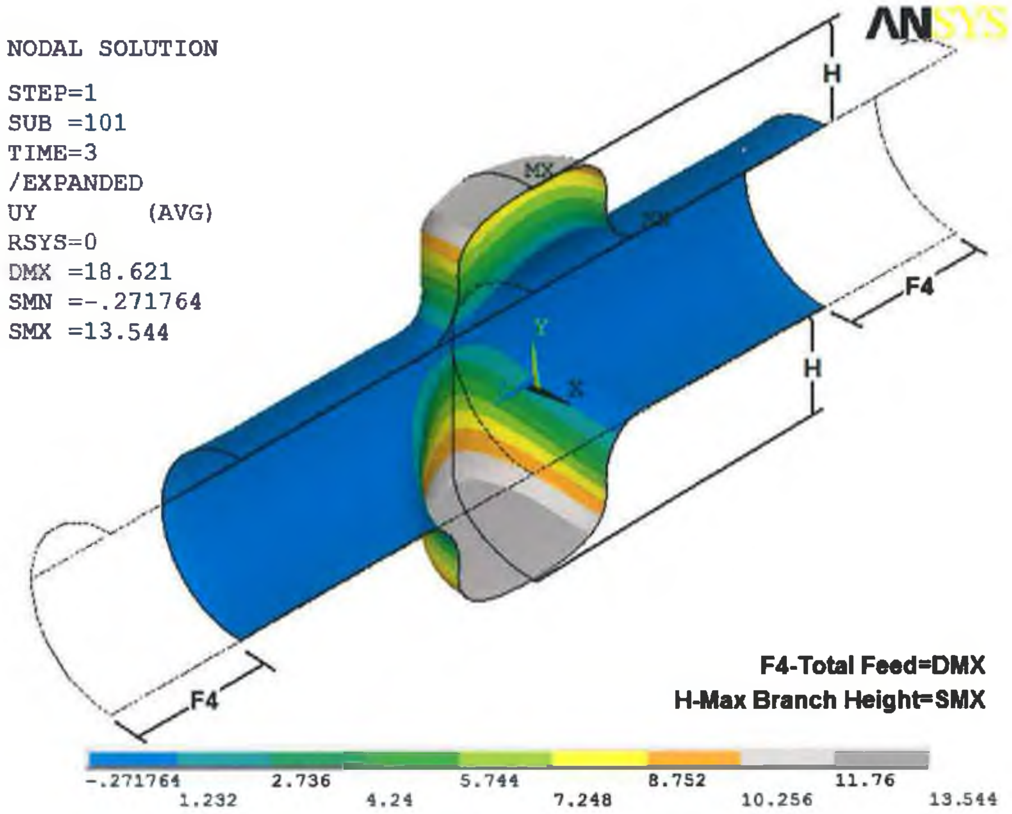

```
NODAL SOLUTION

STEP=1
SUB =101
TIME=3
/EXPANDED
UY          (AVG)
RSYS=0
DMX =18.621
SMN =-.271764
SMX =13.544
```

Fig 5.5.1 X-branch expansion corresponding to the optimal design set

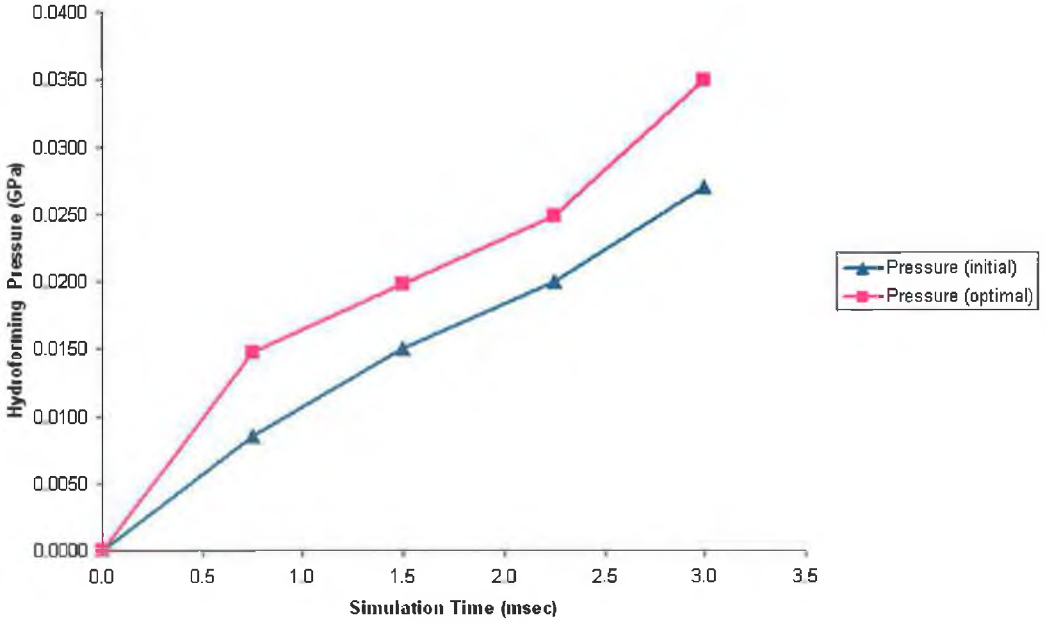

Fig 5.5.2 Pressure load curve for X-branch forming corresponding to the initial and final (optimal) design sets

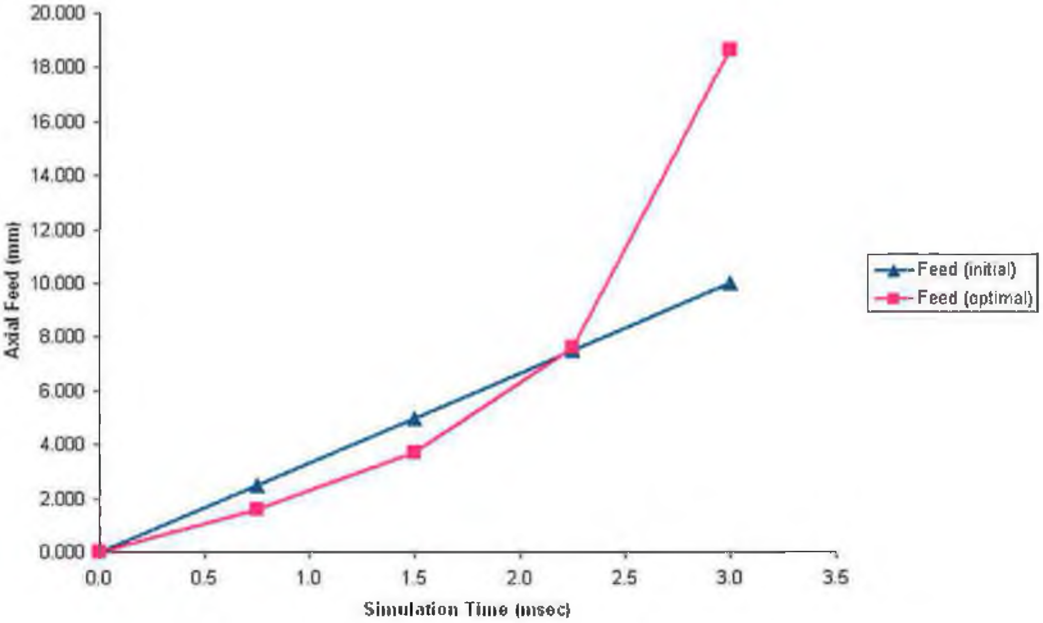

Fig 5.5.3 Axial feed curve for X-branch forming corresponding to the initial and final (optimal) design sets

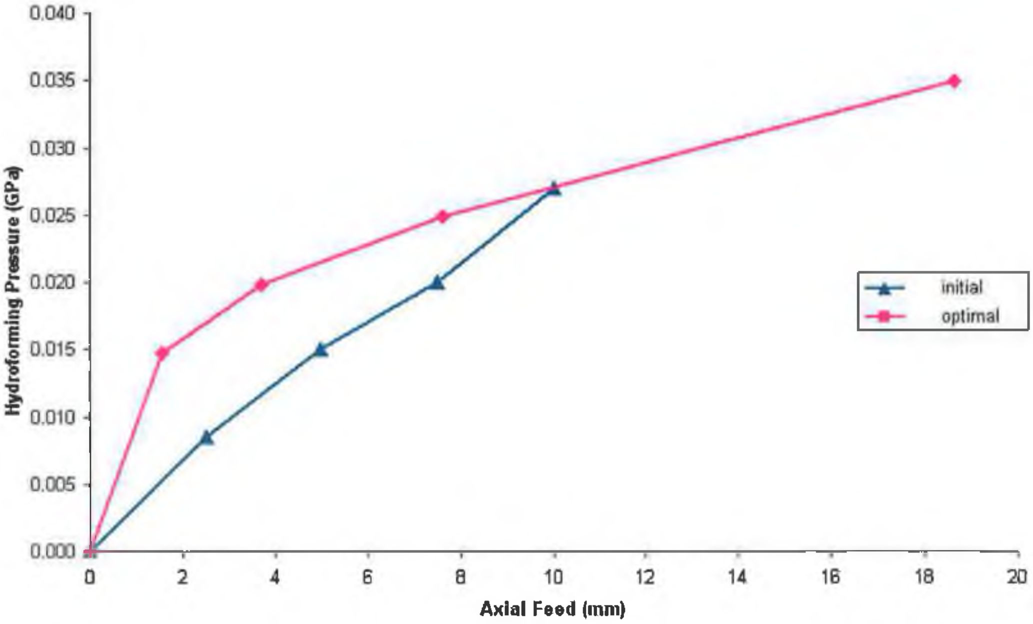

Fig 5.5.4 X-branch forming load path corresponding to the initial design and best design set (feasible and optimal load path)

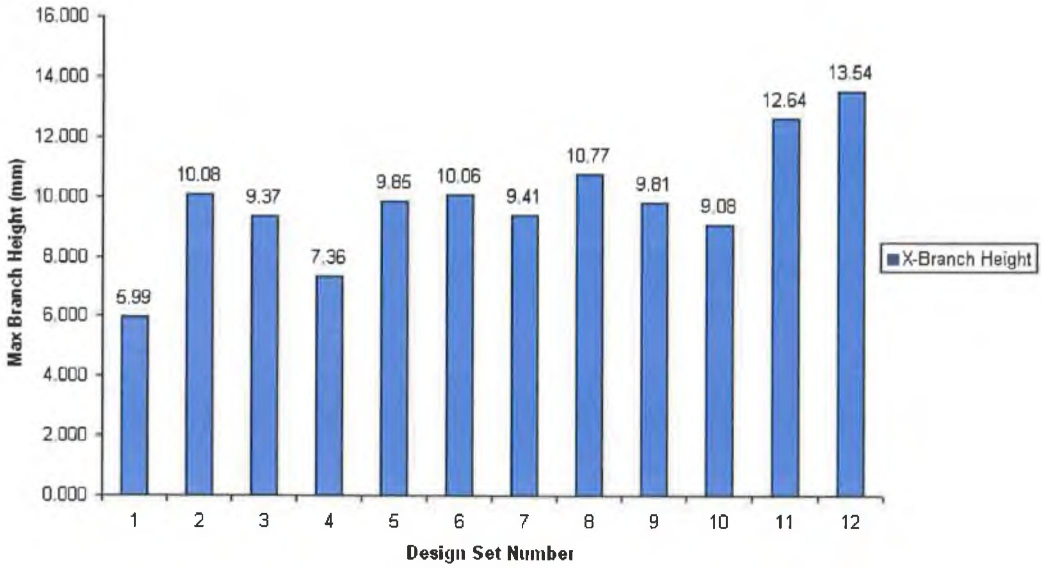

Fig 5.5.5 Maximum branch height (objective function) with respect to iteration number/design sets (X-branch)

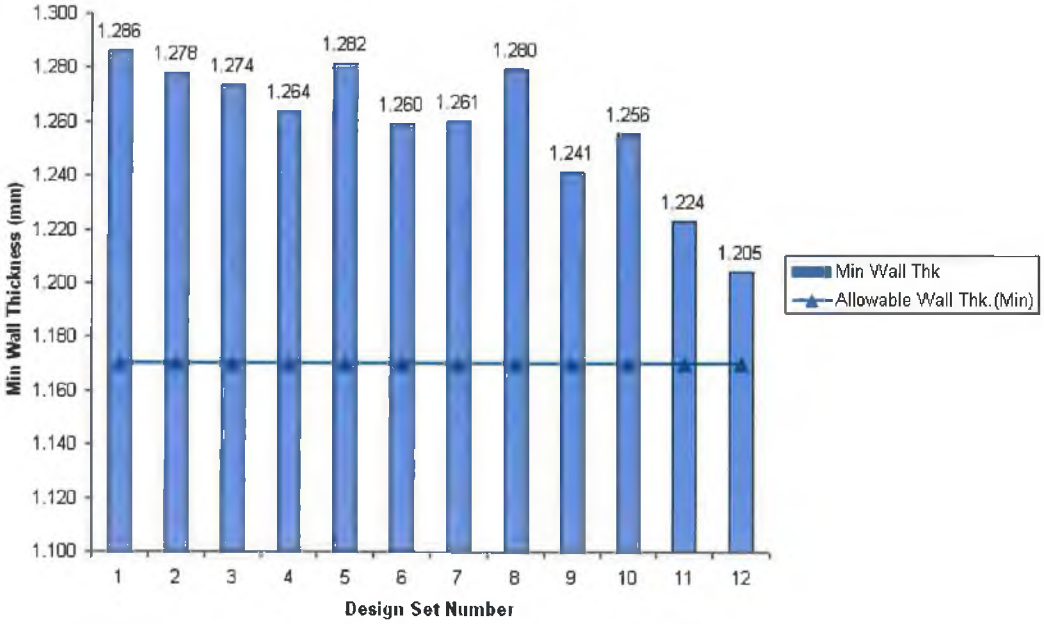

Fig 5.5.6 Minimum wall thickness distribution (design constraint/state variable) with respect to iteration number/design sets (X-branch)

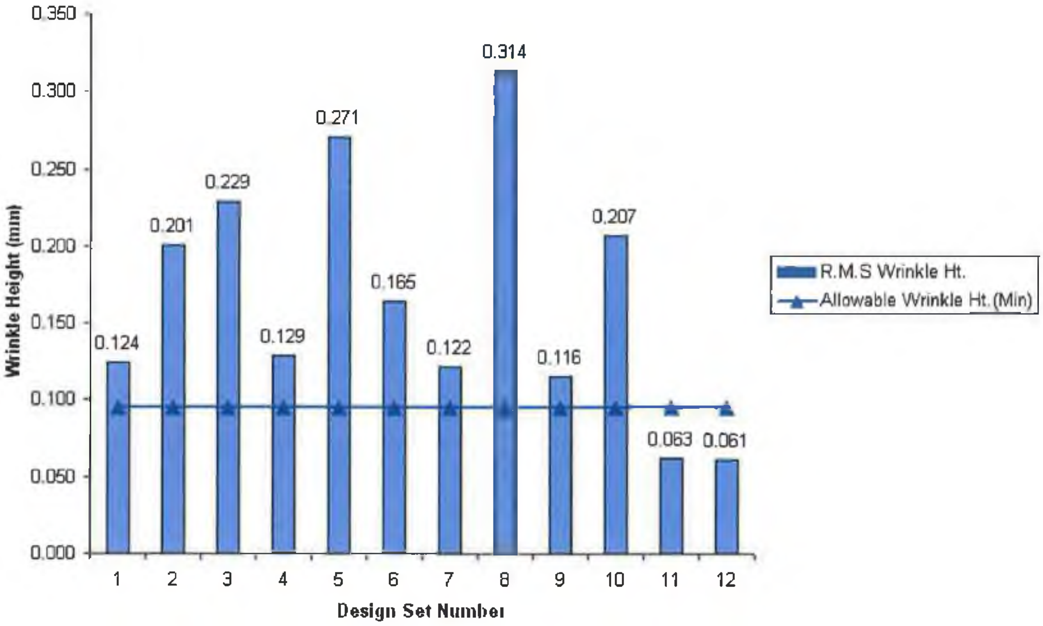

Fig 5.5.7 Maximum wrinkle height (design constraint/state variable) developed with respect to iteration number/design sets (X-branch)

Table 5.5.4 T-branch design sets (output) with iteration number

	SET	1	2	3	4	5	6	7	8	9	10	11	12	13*
Design variable		feasible	feasible	feasible	feasible	feasible	feasible	feasible	infeasible	feasible	feasible	infeasible	infeasible	feasible
Wall THK (mm)	(SV)	1.281	1.280	1.274	1.251	1.283	1.252	1.254	1.282	1.228	1.257	1.234	1.231	1.267
Wrinkle HT (mm)	(SV)	0.144	0.194	0.166	0.160	0.193	0.180	0.154	0.240	0.159	0.155	0.218	0.205	0.200
F1 (mm)	(DV)	2.500	2.973	1.668	1.878	2.936	1.613	1.373	2.525	0.968	0.384	0.813	1.231	2.541
F2 (mm)	(DV)	5.000	5.329	4.781	7.458	3.973	6.872	3.738	5.095	7.128	6.263	3.902	6.997	4.896
F3 (mm)	(DV)	7.500	9.246	11.067	10.343	10.915	8.931	7.601	10.869	8.905	10.597	8.027	7.993	8.717
F4 (mm)	(DV)	14.000	16.231	15.239	11.358	16.423	15.527	14.190	17.782	14.370	14.282	16.391	16.176	16.182
P1 (GPa)	(DV)	0.009	0.010	0.012	0.013	0.011	0.013	0.010	0.005	0.012	0.014	0.010	0.014	0.012
P2 (GPa)	(DV)	0.015	0.018	0.015	0.018	0.015	0.019	0.015	0.018	0.018	0.015	0.019	0.018	0.019
P3 (GPa)	(DV)	0.020	0.024	0.022	0.022	0.022	0.020	0.020	0.023	0.023	0.022	0.025	0.025	0.024
P4 (GPa)	(DV)	0.028	0.025	0.026	0.033	0.025	0.031	0.031	0.026	0.034	0.027	0.032	0.032	0.027
OBJFUN	(OBJ)	8.462	9.899	9.191	7.256	9.684	9.859	9.209	10.545	9.608	8.923	11.170	10.775	10.218
(Branch Height-H)		Initial Design												Best Design

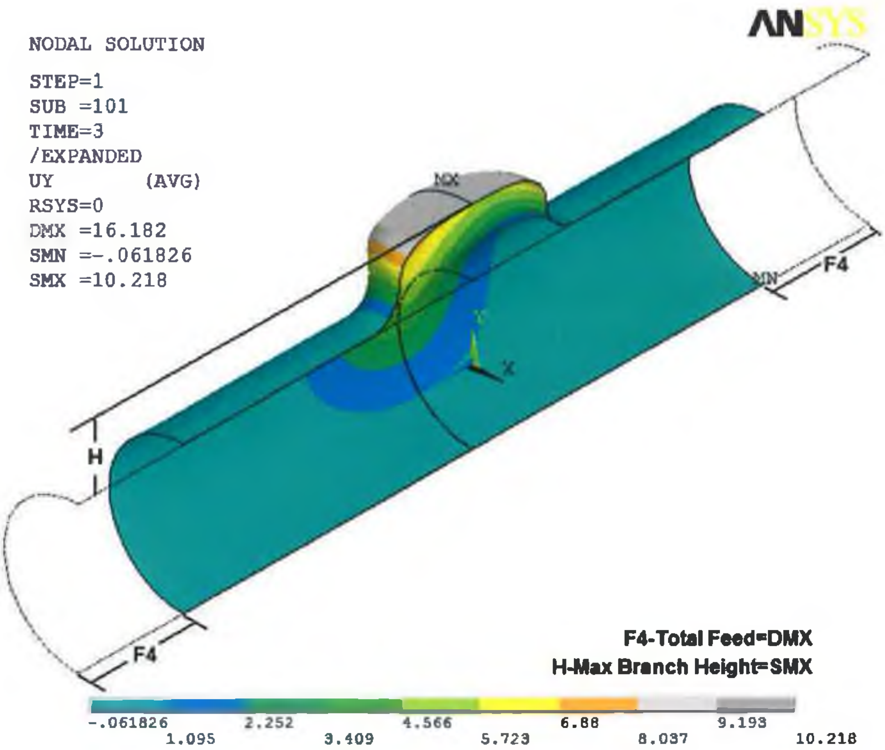

Fig 5.5.8 T-branch expansion corresponding to the optimal design set

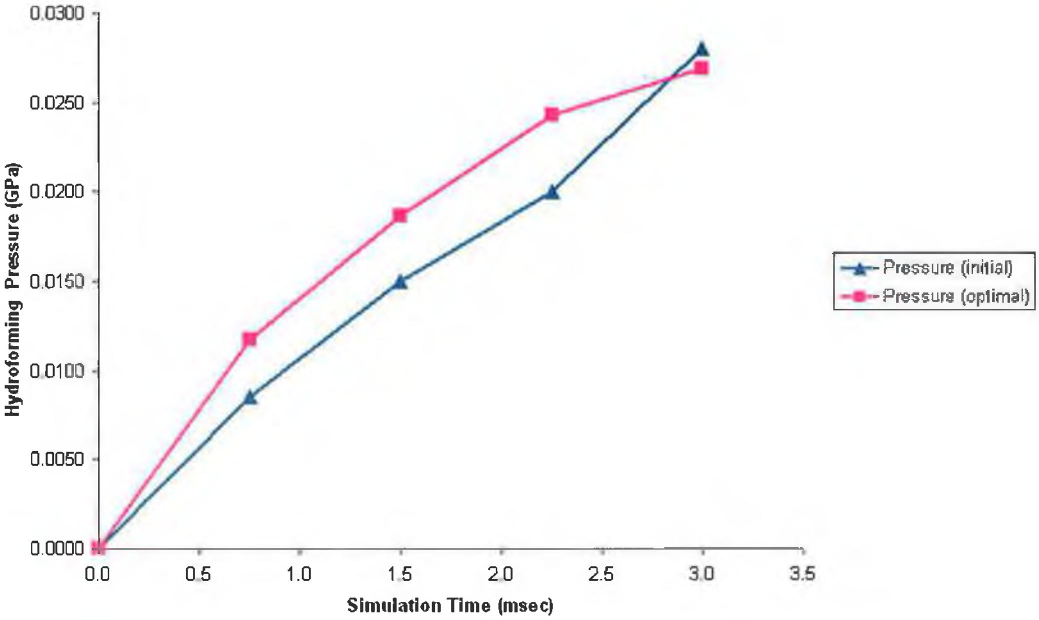

Fig 5.5.9 Pressure load curve for T-branch forming corresponding to the initial and final (optimal) design sets

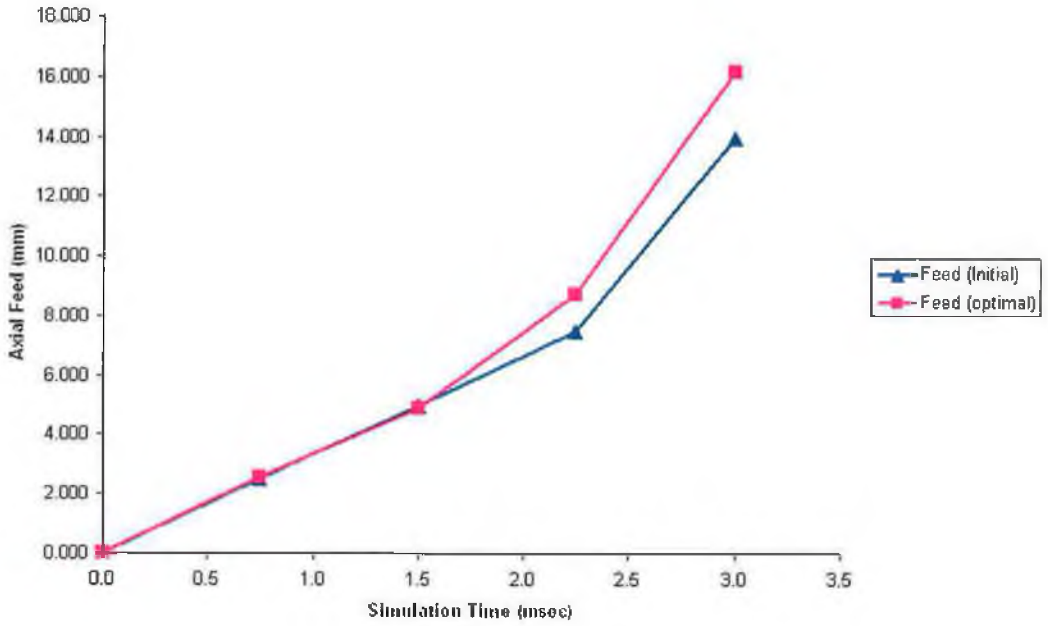

Fig 5.5.10 Axial feed curve for T-branch forming corresponding to the initial and final (optimal) design sets

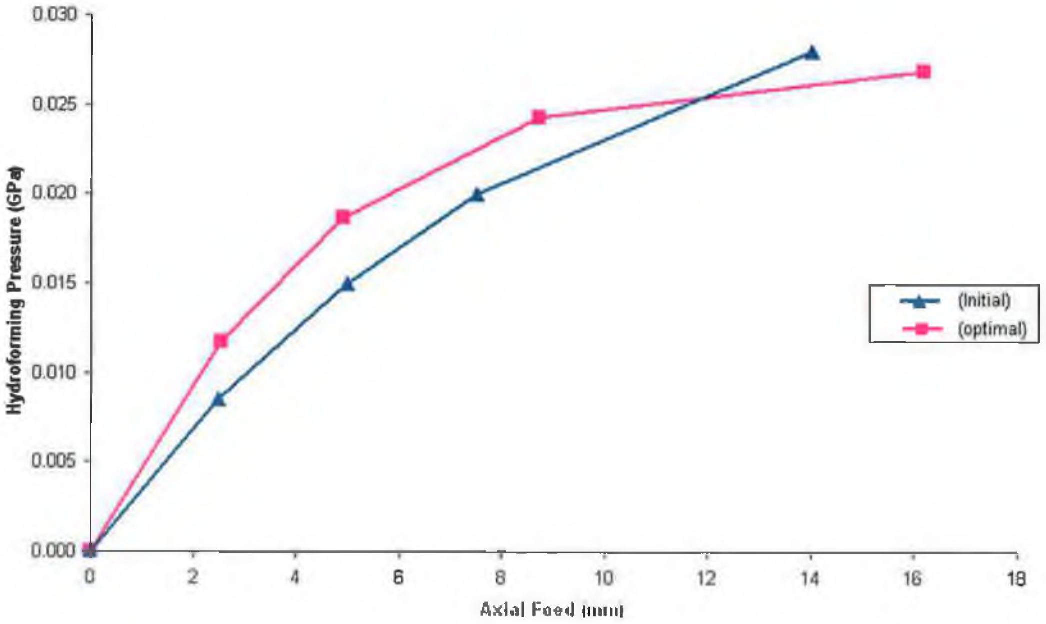

Fig 5.5.11 T-branch forming load path corresponding to the initial design and best design set (feasible and optimal load path)

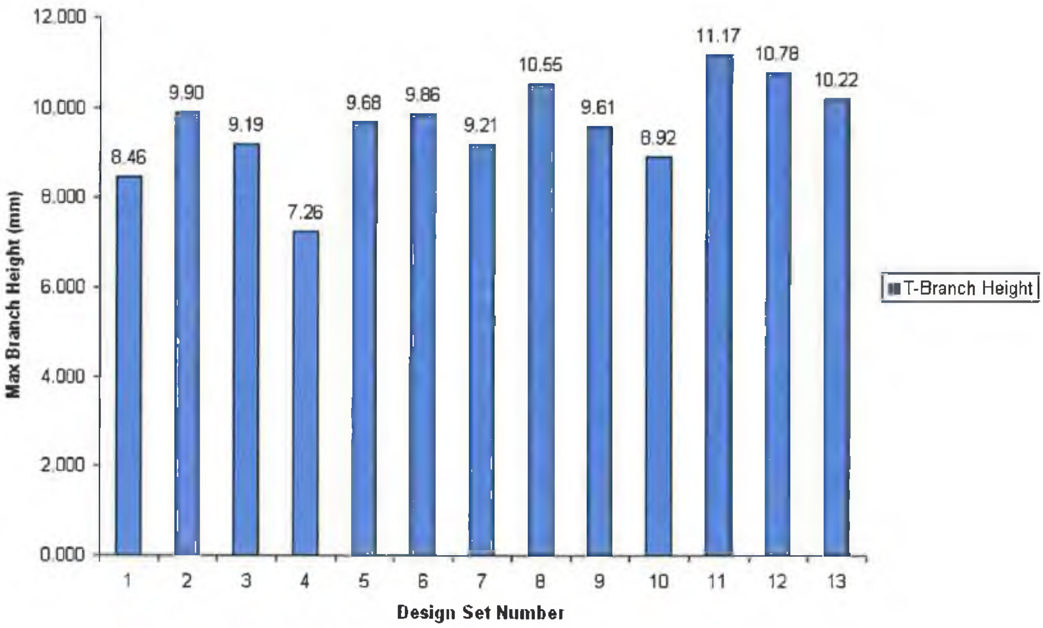

Fig 5.5.12 Maximum branch height (objective function) with respect to iteration number/design sets (T-branch)

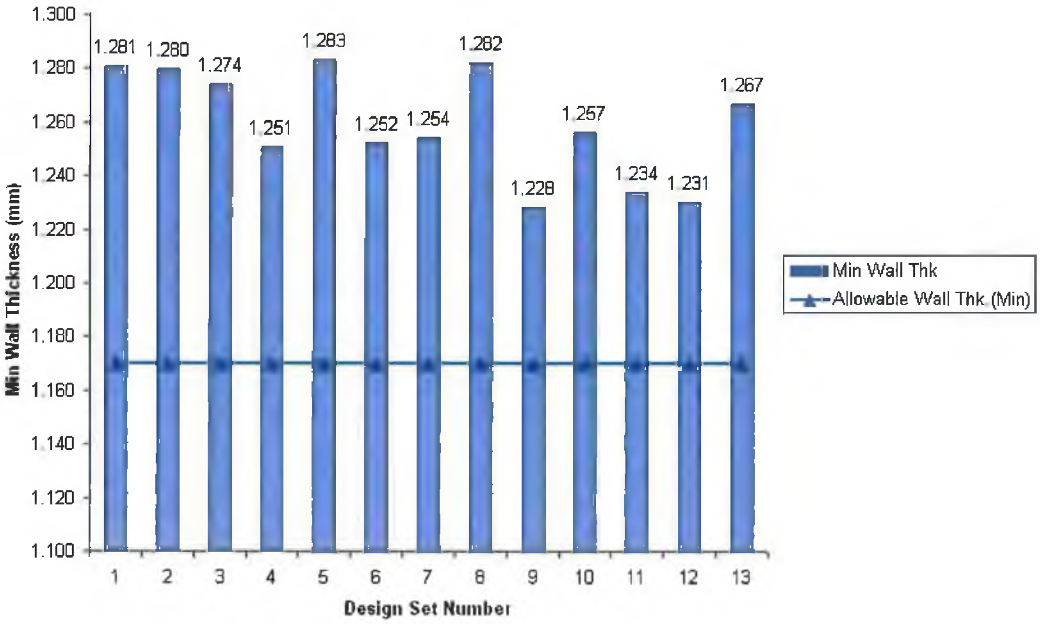

Fig 5.5.13 Minimum wall thickness distribution (design constraint/state variable) with respect to iteration number/design sets (T-branch)

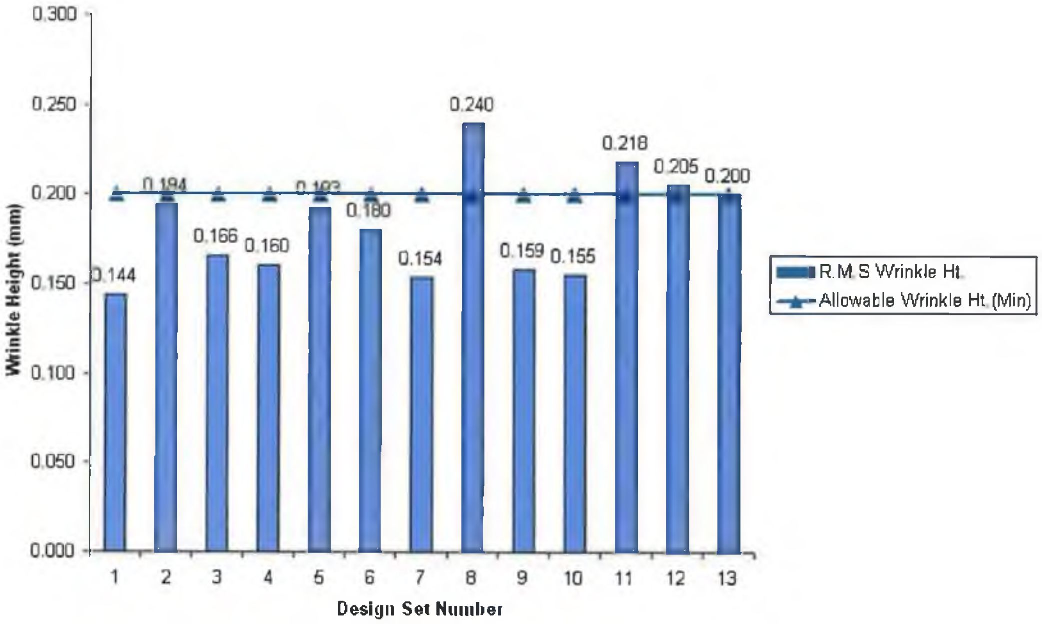

Fig 5.5.14 Maximum wrinkle height (design constraint/state variable) developed with respect to iteration number/design sets (T-branch)

5.6. Summary of Chapter 5

This chapter outlines details of subproblem approximation optimization method, its theory and its application in tube hydroforming processes, for process optimization (i.e. maximizing the part expansion simultaneously avoiding process failure) and determination of optimal load paths, which are of practical importance for successful application of the process.

Chapter 6: Determination of Feasible Forming Loading Paths Using Adaptive Simulation Concepts

6.1. Introduction

The attempt to develop methodologies for automatic determination of loading path continues further in this chapter. The simulation based optimization method, described in the last chapter, enables automatic determination of optimum process parameters curves (i.e. load paths) for tube hydroforming parts with asymmetric geometries. However the assumptions made to define the failure due to wrinkle formation, which is one of the main failure modes for most of the tube hydroforming processes, was very much shape dependent. In the simulation and optimization runs the formation of wrinkles were only considered at a certain localized zone of the tube, which was highly vulnerable to the formation of wrinkle. In this section the condition will be defined in a more general or global way, which will be suitable to determine the wrinkle growth at any point (i.e. at any weak and unstable zone) of the tube.

As discussed in Chapter 4, the output of a typical hydroforming process depends on certain parameters, which have significant effects on the process and part expansion. These parameters can be broadly categorized as a.) material property of the work piece, b.) geometric profile of the work piece and die and, c.) process or operating (loading) conditions and contact surface friction. Whereas the process limits (failure conditions) of any tube hydroforming process can be categorized as a.) bursting of the tube wall or development of crack, which is due to excessive wall thinning and, b.) formation of wrinkle or buckling due to structural instability.

In this chapter, a generalized condition for wrinkle development during the forming process will be used to develop an intelligent load control algorithm, which can automatically calculate the forming load curves avoiding the failure modes (i.e. wrinkle growth and excessive wall thinning) within the simulation process itself. A conceptual schematic diagram of an adaptive simulation procedure is shown in fig 6.1.1 and fig 6.1.2.

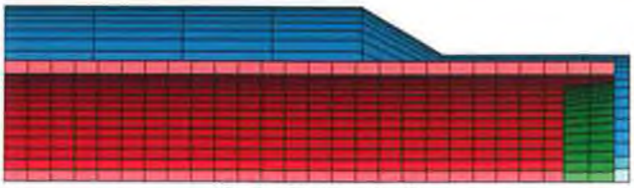

$t0=0, f0=0, p0=0$

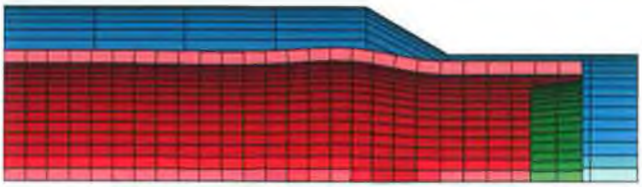

$t1=t0+dt, f1=f0+df1, p1=p0+dp1$
(normal expansion-no wrinkle)

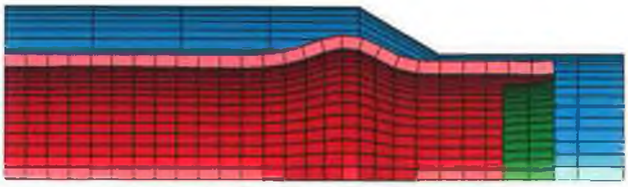

$t2=t1+dt, f2=f1+df2, p2=p1+dp2$
(formation of wrinkle)

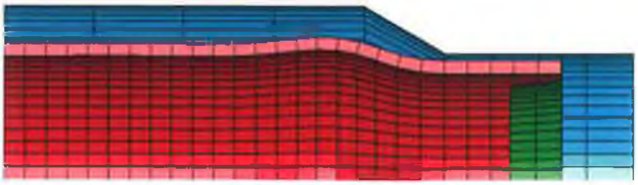

$t3=t2+dt, f3=f2+0, p3=p2+dp3$
(wrinkle suppressed due to increase in pressure)

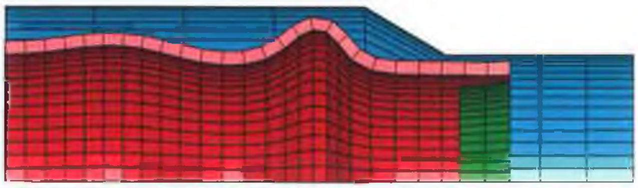

$t4=t3+dt, f4=f3+df4, p4=p3+dp4$
(formation of wrinkle due to excessive feed)

$t5=t4+dt, f5=f4+0, p5=p4+dp5$
(wrinkle suppressed due to further increase in pressure)

Fig 6.1.1 Wrinkle growth and it adjustment within the simulation process (one-eighth axisymmetric model)

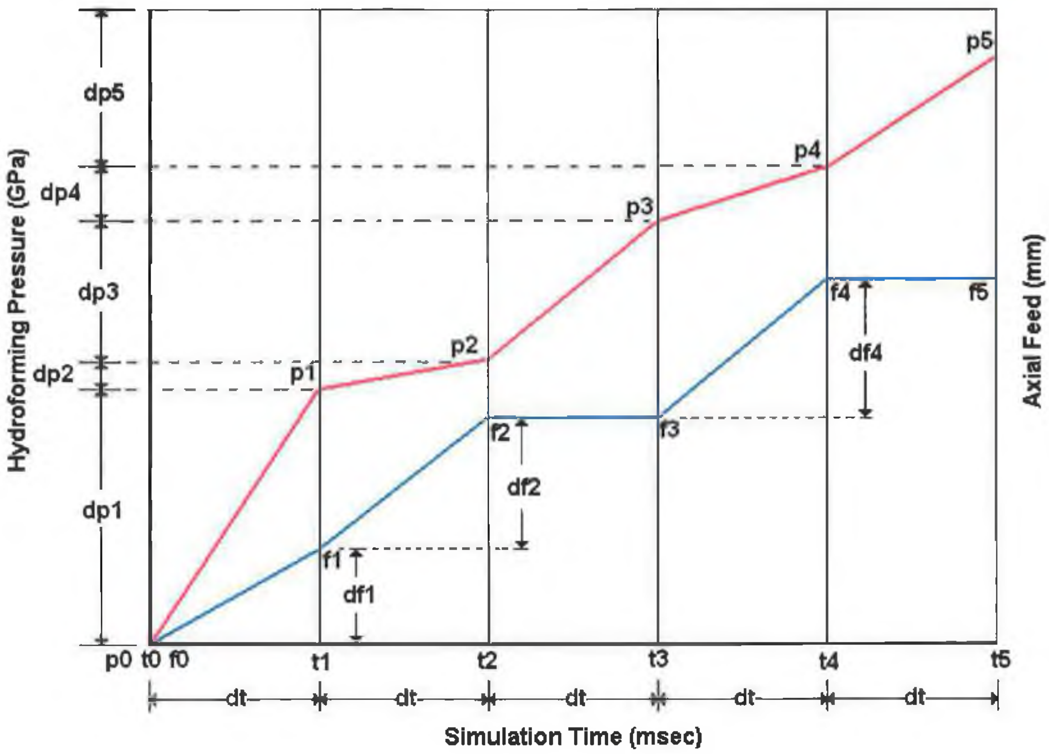

Time step (t0-t1): combined pressure (p1) and axial feeds (f1) are applied to yield the material and initiate the deformation.
Time step (t2-t1): further incremental pressure (dp2) and axial feeds (df2) are applied which results in development of wrinkle.
Time step (t3-t2): pressure is increased further (dp3) and feed is suspended to stop the wrinkle growth.
Time step (t4-t3): further incremental pressure (dp4) and axial feeds (df4) are applied which again results in wrinkle formation
Time step (t5-t4): the newly developed wrinkle is again suppressed by applying further incremental pressure (dp5) without any axial feed.

Fig 6.1.2 Schematic adaptive control procedure, for control of wrinkle growth during the process by adjustment of pressure and feed values with simultaneous part expansion

This chapter mainly discusses the development of different components such as part defect determination (wrinkle formation), and process parameter adjustment of the adaptive simulation approach and further development of a load control algorithm using fuzzy logic concepts. To develop the load control algorithm, a macro was written using ANSYS parametric design language script and was interfaced with the ANSYS/LS-DYNA pre-post processing tool and LS-DYNA solver. A couple of simple and complex part geometries were used in the study. The adaptive simulation at this stage is only capable of determining a feasible load part for circular tube hydroforming with straight or bent axis.

6.1.1. Adaptive simulation concept

The ultimate goal of the adaptive simulation approach is to eliminate trial-and-error simulation based approaches and to generate feasible process parameter curves with only a single continuous simulation.

In adaptive simulation, the process parameters (forming pressure and end feed) for the future simulation step are to be predicted to proper values (i.e. magnitude of incremental increase of pressure and feed) based on the forming part quality information collected from current simulation step (i.e. last simulation step). In other words, during a tube hydroforming process simulation run, the simulation intermediate results about forming part qualities (i.e. wrinkle growth, wall thickness change) up to the current time step are deduced using the simulation post-processing results and with mechanics of material, and then used to calculate appropriate process parameter values for the next simulation time step (simulation step). This is in contrast to the traditional application of finite element simulations where only the simulation results at the final step are considered and used to infer parameters adjustments for the next simulation step run in an attempt to improve the forming process behaviour.

In this study, the adaptive simulation used relies on an ability to detect the existence of defects such as wrinkles or excessive wall thinning in the part being formed and the ability to make appropriate adjustments of the relevant process parameters to correct these defects during the subsequent step simulation. The essential parameter adjustment strategy of the proposed method is to maximize as much possible end axial feed in the deforming zone so as to minimize tube wall thinning simultaneously applying as much pressure as required to expand the part while avoiding formation of wrinkles. Upon completion of all the step simulation runs, the evolution of the process parameters predicted by this methodology is the resultant feasible loading paths (pressure vs. time, and feed vs. time) and finally the forming pressure is defined as a function of the axial feed.

The adaptive simulation procedure stated above works on an intelligent load control algorithm, which senses the degree of wrinkle formation during the simulation and adjusts the forming pressure and axial feed as per requirement simultaneously, maintaining the level of tube wall thinning within the desirable safety limit. The process integration is explained schematically in the flowchart shown in fig 6.1.3.

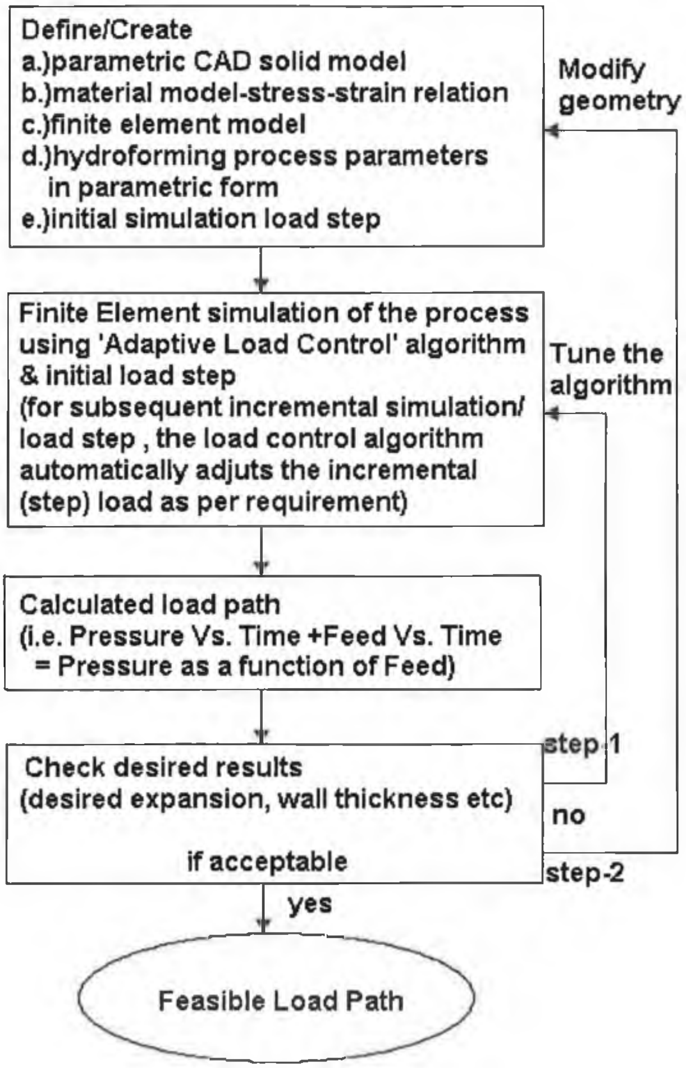

Fig 6.1.3 Flow chart for determination of feasible load path using finite element simulation and load control algorithm

For the above process, an intelligent process/load control algorithm is required which identifies the failure conditions within the simulation process itself and adjusts the load as per requirement. Thus, a fuzzy logic based load control algorithm was developed, which was integrated with the LS-DYNA 3D explicit finite element analysis solver.

The load control program required for the control of the process should be multi facet i.e. it should be able to detect failure and subsequently take the necessary corrective action to overcome the failure. The flow chart in fig 6.1.4 details the actual process integration and its operation control sequence with different sections illustrating a.) the failure detection and, b.) the corrective actions to be incorporated which can avoid the failures within the simulation process.

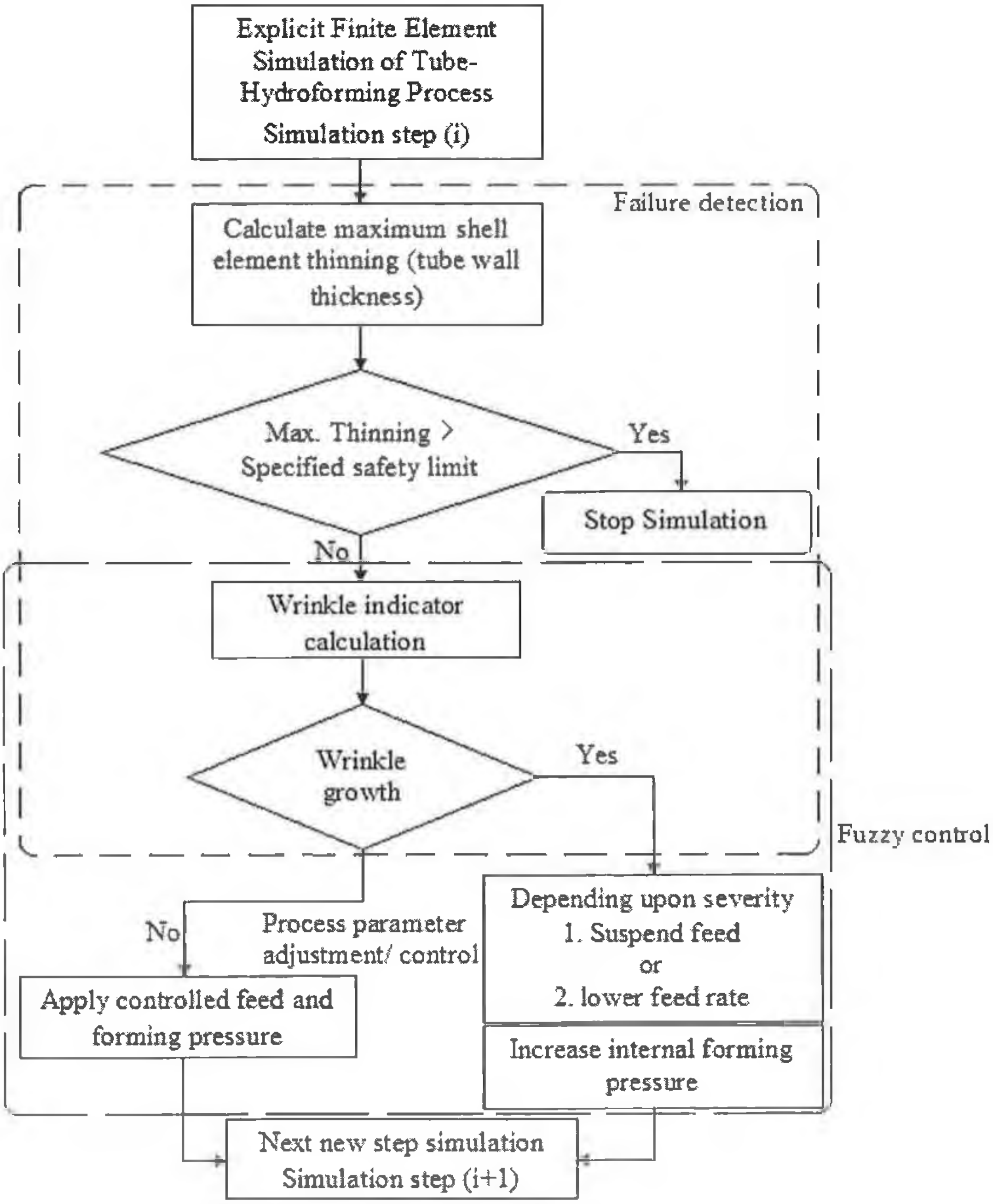

Fig 6.1.4 Process integration and control sequence

The subsequent sections detail the development of the fuzzy load control algorithm and its integration and application with ANSYS/LS-DYNA pre-post processor and LS-DYNA solver.

6.2. Development of 'Fuzzy Load Control Algorithm'

This section explains the development of the control system using fuzzy logic theory. For development of the load control algorithm, it is important to know the limiting process parameters, which demonstrate the failure conditions. These are usually termed as process control limits.

6.2.1. Process control limits

For a successful application of this process for manufacture of different components, prior knowledge of a suitable forming load path is of particular importance. As mentioned earlier, in hydroforming process where the thickness of the sheet is very small (as in the case of thin tube hydroforming), if the axial feed is too large with respect to the applied internal pressure then there is a chance of wrinkle growth in the unstable zone, subsequently leading to buckling of the tube. Conversely, if the pressure is too high with respect to the axial feed then there is chance of bursting of the tube due to excessive wall thinning. Thus, the forming load path has to be properly adjusted and tuned in order to obtain a successful component with this process. Based on these assumptions the adaptive load control algorithm was developed. From different simulation studies done by various researchers using finite element analysis, it has been shown that the explicit finite element formulations give very reliable results for the prediction of buckling, wrinkling and bursting conditions [56, 69, 84]. The theory and logic employed for the development of the load control algorithm to identify the formation of wrinkle or buckling of the tube during the course of simulation is explained in the following section.

In the finite element simulation with shell elements, growth of a wrinkle can be predicted by considering the strain difference across the element thickness. That is, if a wrinkle occurs or the tube is subjected to bending or buckling (fig 6.2.1), then the elements of the area subjected to wrinkle are strained differently on the outer ($\varepsilon 11$) and inner ($\varepsilon 15$) surfaces respectively (fig 6.2.2). The numerical difference ($\varepsilon 11 - \varepsilon 15 = \Delta\varepsilon$) of these two strain values (i.e. differential strain) can be used as the measure of the degree of bending

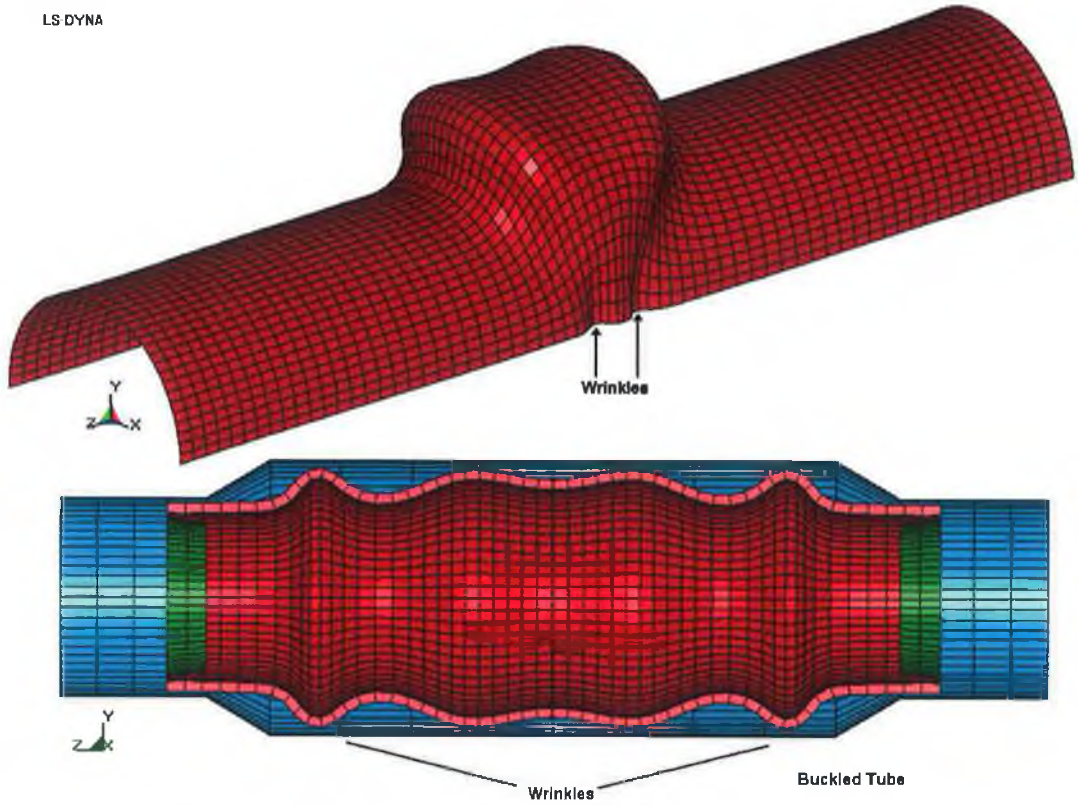

Fig 6.2.1 Half-symmetric wrinkled/buckled tubes (X-branch & an axisymmetric tube)

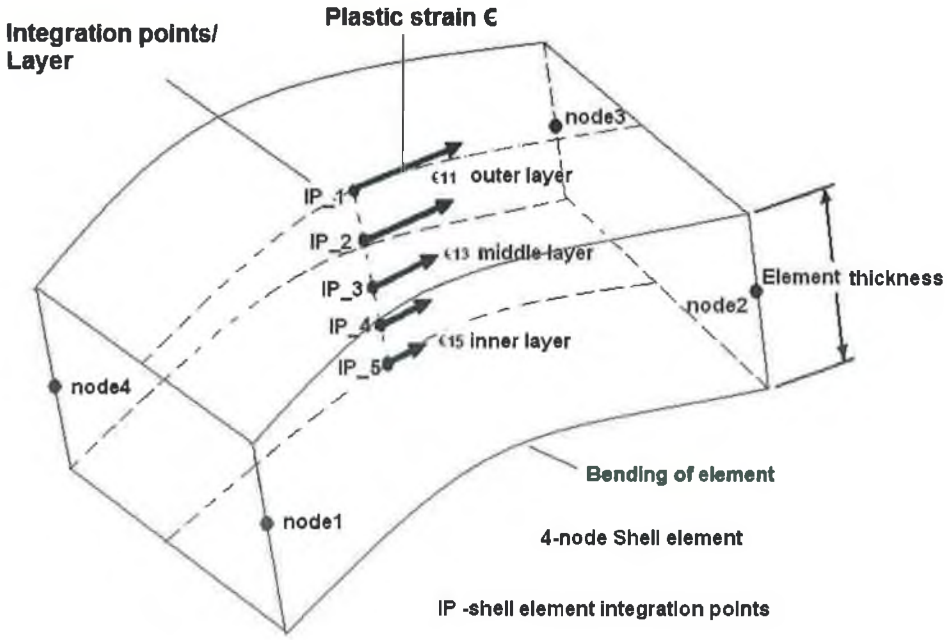

Fig 6.2.2 Strain distribution across the shell element thickness (an element subjected to bending)

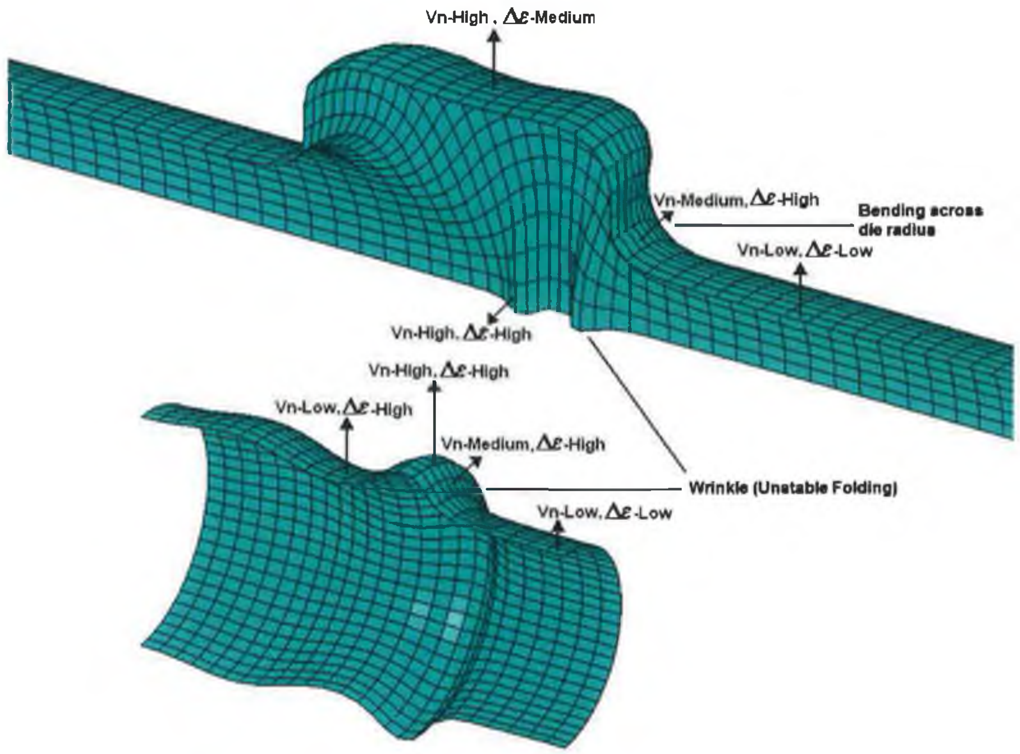

Fig 6.2.3 Not an allowable forming condition as per element strain difference and normal velocity distribution (Top–asymmetric expansion X-branch, bottom-axisymmetric expansion)

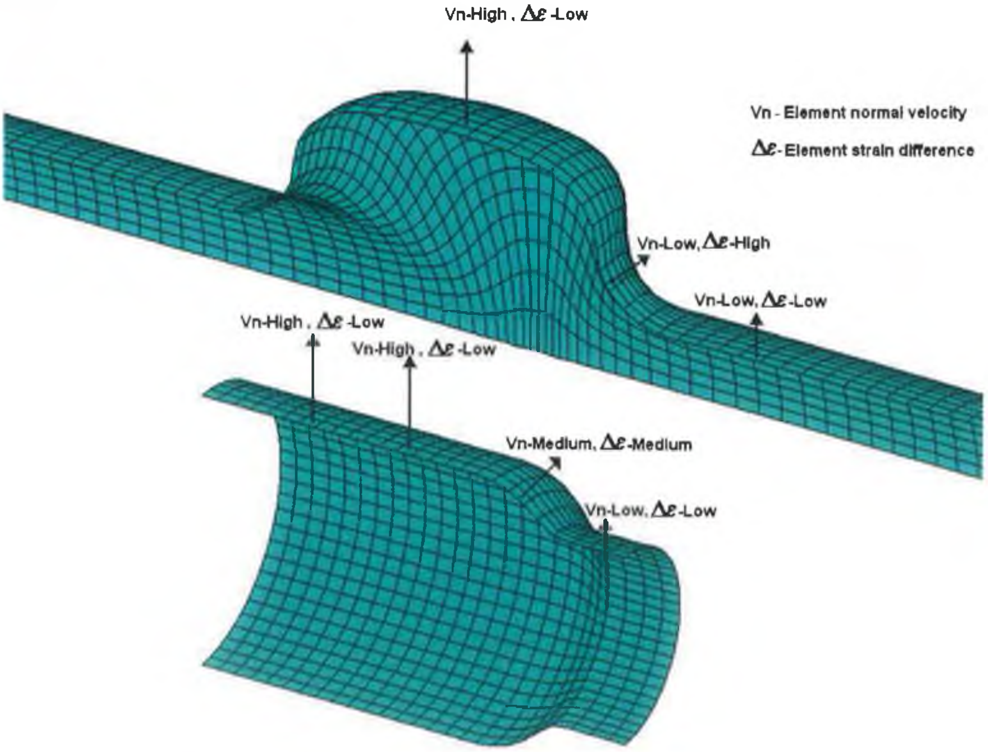

Fig 6.2.4 An allowable forming condition as per element strain difference and normal velocity distribution (Top–asymmetric expansion X-branch, bottom-axisymmetric expansion)

at a certain location. Additionally, the velocity (V_n) of the elements in the normal direction of the shell (tube wall) can also be used to assess whether the wrinkling or bending is desired or not, that is a.) whether the material is already in contact with the die surface (fig 6.2.4.) and has bent along the die radius, or b.) the wrinkle formed is an unstable folding (fig 6.2.3.) due to excessive axial feed and relatively low hydroforming pressure i.e. loss of contact of the element from the die surface. Because of the instability, a region of unstable folding or wrinkling has a much higher normal velocity than the free forming due to the internal pressure only. Fig 6.2.4 and fig. 6.2.3 differentiates between an allowable and an unallowable forming condition depending upon the strain difference ($\Delta\varepsilon$) and normal velocity distribution (V_n). In general a stable (without any wrinkle growth) and an unstable (with wrinkle growth) condition can be explained by considering element strain difference and normal velocity conditions of elements from different locations (fig 6.2.4 and fig 6.2.3) of the tube i.e. from wrinkled and non-wrinkled areas. Depending upon the geometry of the die two kind of wrinkle might occur i.e. in one case the wrinkle crest moves away from the die surface (fig 6.2.3 asymmetric case, X-branch) in such case normal velocity and strain difference both are negative and in the other case the wrinkle crest move towards the die surface (fig 6.2.3 axisymmetric case), in that case both normal velocity and strain difference are positive. Thus an element can be said to be unstable if above situation arise. Further there may be few elements, which may have high strain difference between the outer and inner surfaces with a low or almost negligible normal velocity. This kind of situation arises when the portion of the tube bends across a die radius or curve, thus this type of expansion can be termed as a normal bending. Similarly if it is a normal expansion without any bending or wrinkle in such case either the normal velocity may be high or low with low strain difference in both the cases. Different scenarios, such as cases of wrinkle growth, wrinkle suppression, bending and normal expansion can be approximately explained by considering different magnitudes of the strain difference and normal velocity of the elements. To understand all the above cases, it is important to first understand the type of strain difference and normal velocity acting on the elements. For this simple conventions can be used such as a strain difference is assumed to be +ve when the element outer surface (i.e. tube outer surface) strain is higher than inner surface and similarly element normal velocity is assumed to be +ve when the element moves outward or in other word the tube wall expands (fig 6.2.3 and fig 6.2.4). Thus different cases of the expansion can be explained, such as if the element strain difference is very high (+ve) and normal velocity is also high (+ve), then there are high chances of the element being subjected to wrinkle with a positive wrinkle crest. Similarly on the contrary, if the element strain difference is very high (-ve) and normal velocity is also high (-ve), then there are high chances of the element being subjected to wrinkle with a negative wrinkle crest. Few other situations can be detailed as, if the strain difference is medium or low and the normal velocity is high (+ve) or medium or low, then it can be termed as normal expansion. Similarly if the strain difference is high (-ve /+ve) and normal velocity is also high (+ve /-ve) this can be termed as suppression of wrinkle due to the nature of the loading and finally if the strain difference is high (-ve) and normal velocity is medium or low then it can be considered as a normal bending (might be along the die corner radius). Thus the above situation explains how combination of both strain difference and normal velocity can differentiate between different forming conditions.

Further the conditions can be explained in detail by considering two different hydroforming simulation cases of an axisymmetric type expansion. Table 6.2.1 and fig 6.2.5 show two different arbitrarily selected loading conditions for hydroforming simulation of this axisymmetric component. The first load path used resulted in formation of wrinkle and subsequent buckling of the tube (fig 6.2.6) whereas the second load path resulted in better part expansion (fig 6.2.9). Although the second load path resulted in better part expansion without any wrinkle growth however, this loading path cannot be considered as a perfect loading path, as it is not an optimized one. The two load paths were so selected that the starting and the end forming conditions (feed and pressure values) were identical. It was illustrated in Chapter 4 how different loading conditions affect the final part expansion characteristics. In this section, wrinkle development mechanism and the factors (element strain difference and normal velocities), which can

Table 6.2.1 Load path details for axisymmetric expansion

	Wrinkled Condition		Non Wrinkled Condition	
Simulation Time (msec)	Axial Feed (mm)	Forming Pressure (GPa)	Axial Feed(mm)	Forming Pressure (GPa)
0.00	0.0	0.0000	0.0	0.0000
0.75	5.0	0.0020	2.5	0.0155
1.50	8.0	0.0060	5.0	0.0240
2.25	9.5	0.0150	7.5	0.0300
3.00	10.0	0.0350	10.0	0.0350

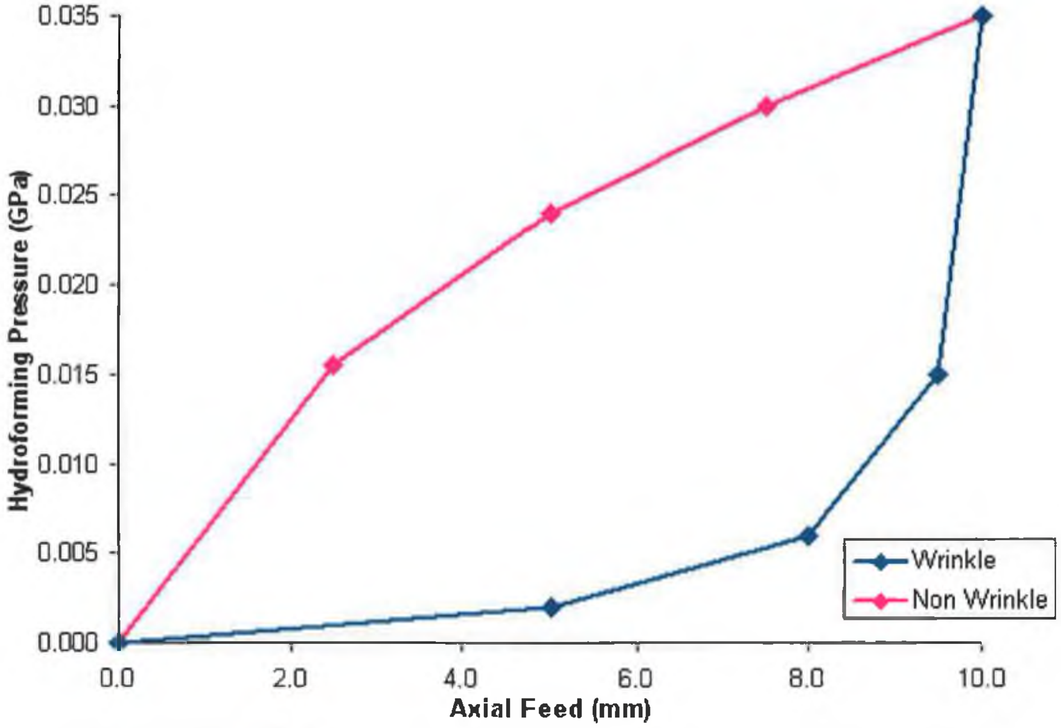

Fig 6.2.5 Load path plot pressure as a function of end feed for axisymmetric expansion (refer-Table 6.2.1)

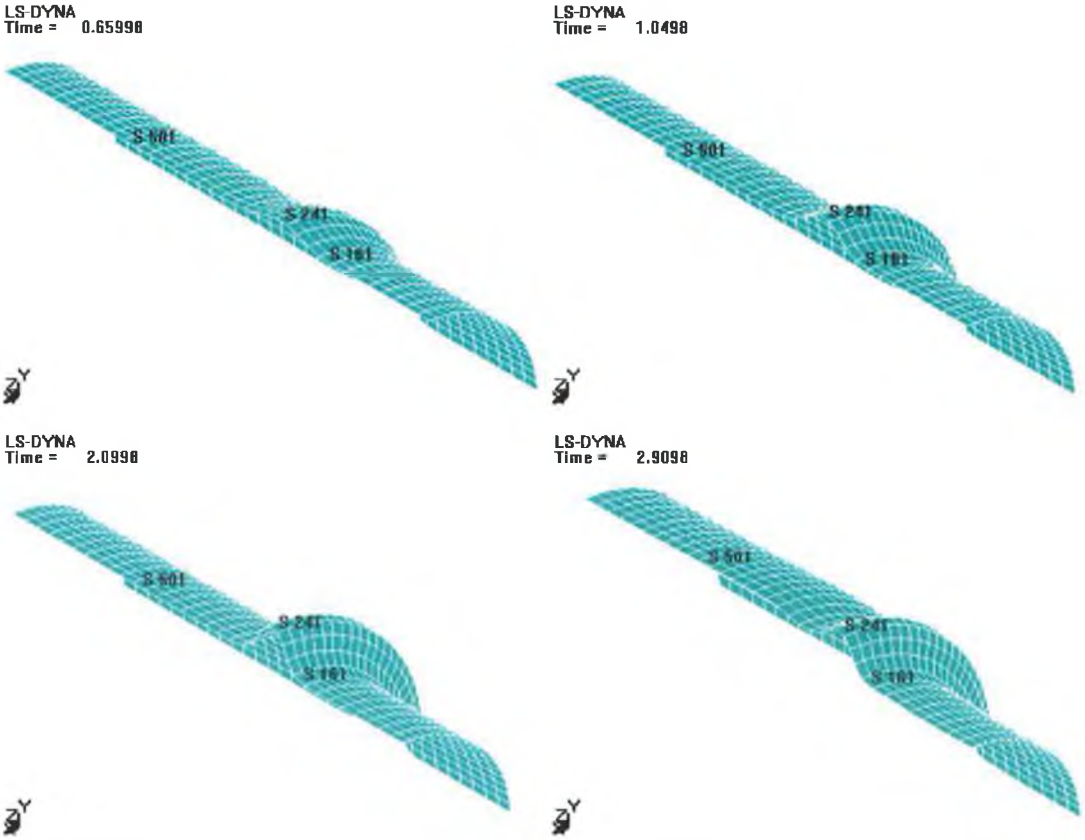

Fig 6.2.6 Axisymmetric expansion corresponding to wrinkle-load path at different phase of the simulation

identify this wrinkle growth are compared for the part with a stable and normal expansion (i.e. non-wrinkled) with a part with unstable forming condition (i.e. wrinkled).

Three different elements (element number 161, 241, 501) from different zones (i.e. bend along die corner radius, unstable zones/wrinkle and stable zone/non-wrinkle) of the wrinkled tube were selected for the comparison of the element strain difference and normal velocity variation over the simulation time with the identical elements for the non-wrinkled tube. Fig 6.2.7 and fig 6.2.8 show the element strain difference and the normal velocities for the wrinkled tube and fig 6.2.10 and fig 6.2.11 show the element strain difference and the normal velocities for the same elements in the non-wrinkled tube. It can be observed from the strain difference plots as well as from fig 6.2.6 for the wrinkled tube, that elements 161 and 241 have been subjected to either bending or wrinkle, due to which there is a steep rise in the strain difference whereas for element 501 the strain difference variation is minimal. Again comparing the element normal velocities (fig 6.2.8) it can be seen that the element normal velocity for element 241 is relatively high with respect to the other elements in the simulation time range of 0.5msec to 1.5msec with a maximum value of 5mm/msec whereas for element 161 and 501 it is almost zero. This shows that element 241 is subjected to wrinkle whereas element 161 is subjected to normal bending across the die radius or may be a bending at the base of a wrinkle. For element 501, both its strain difference and the normal velocity are low throughout most of the simulation time period, however there is a steady rise in the normal velocity at the later part of the simulation phase. Although the normal velocity is high at this stage but it can be considered as normal expansion without bending, as the strain difference is almost negligible. Furthermore, the development of the wrinkled surface and normal expansion can be better understood by referring to the non-wrinkled expansion (fig 6.2.9). It can be seen in this case, elements 241 and 501 are subjected to normal expansion whereas element 161 is subjected to minor bending. The element strain difference plots (fig 6.2.10) show that the maximum value of the strain difference for all the three elements are much lower as compared to the wrinkled case, and also the element normal velocities (fig 6.2.11) are nominal over the major part of simulation phase with a rise in the last stage of the simulation. The sudden rise in the velocity in the last stage of the simulation is due to the sudden transient expansion of the tube, which is due to rise in internal pressure (see fig 6.2.5 for feed range 8mm to 10mm). Thus the shell element strain difference and the normal element velocity provides a better understanding of the wrinkle growth during the forming process and utilizing this concept and the element behaviour, the intelligent load control algorithm was developed.

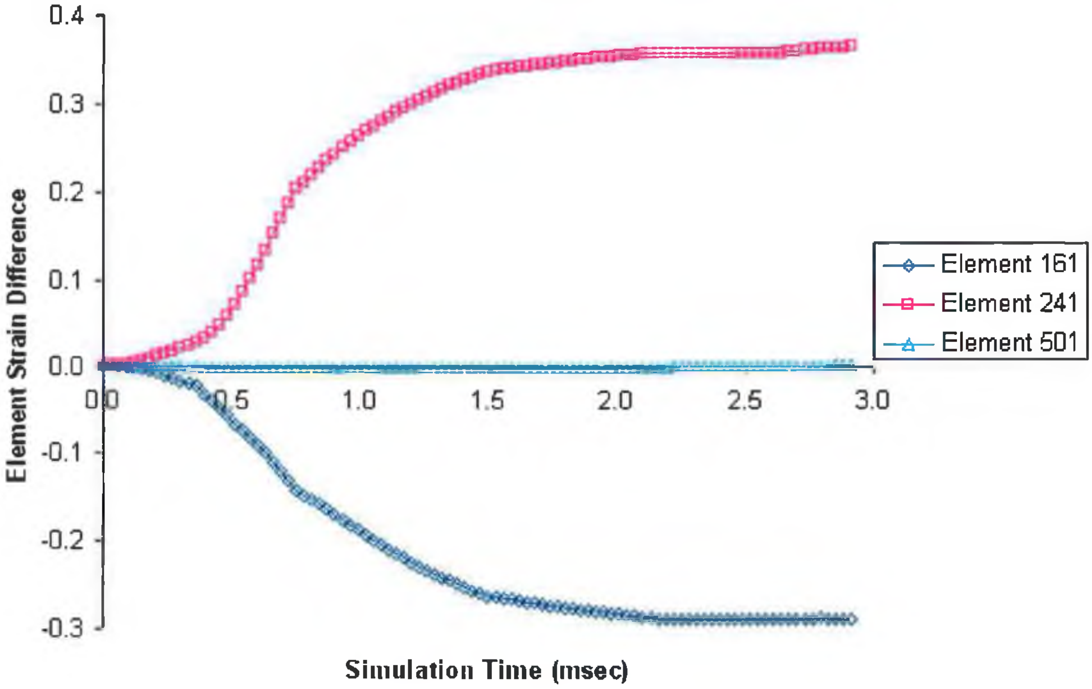

Fig 6.2.7 Development of element strain difference across element thickness (wrinkled axisymmetric expansion)

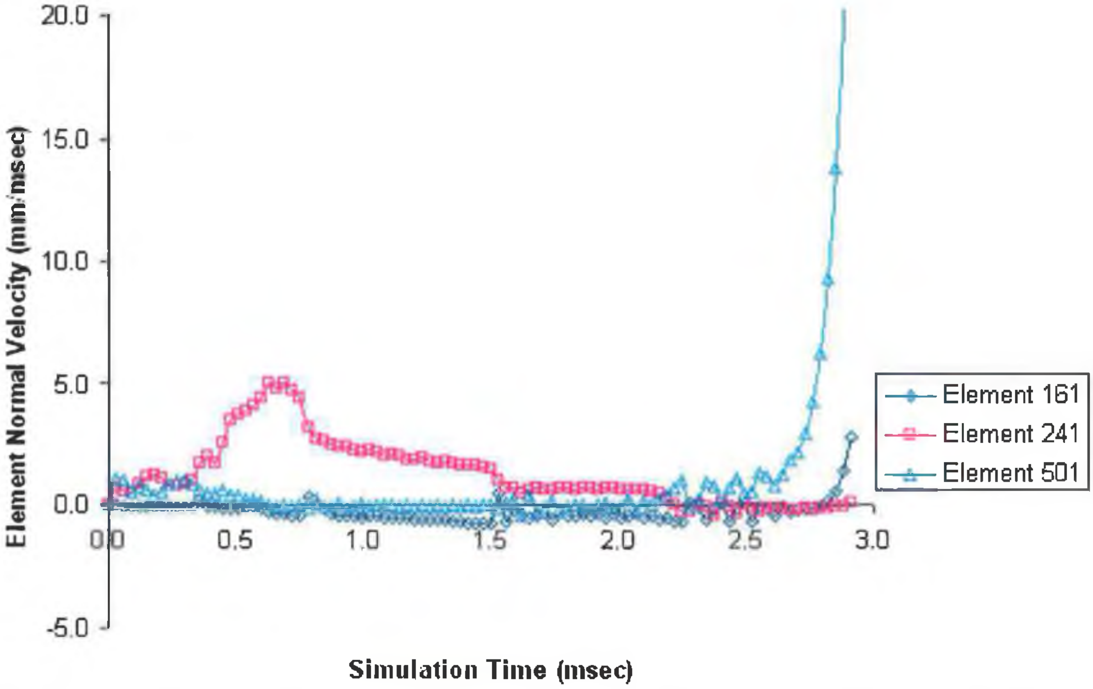

Fig 6.2.8 Development of element normal velocity (wrinkled axisymmetric expansion)

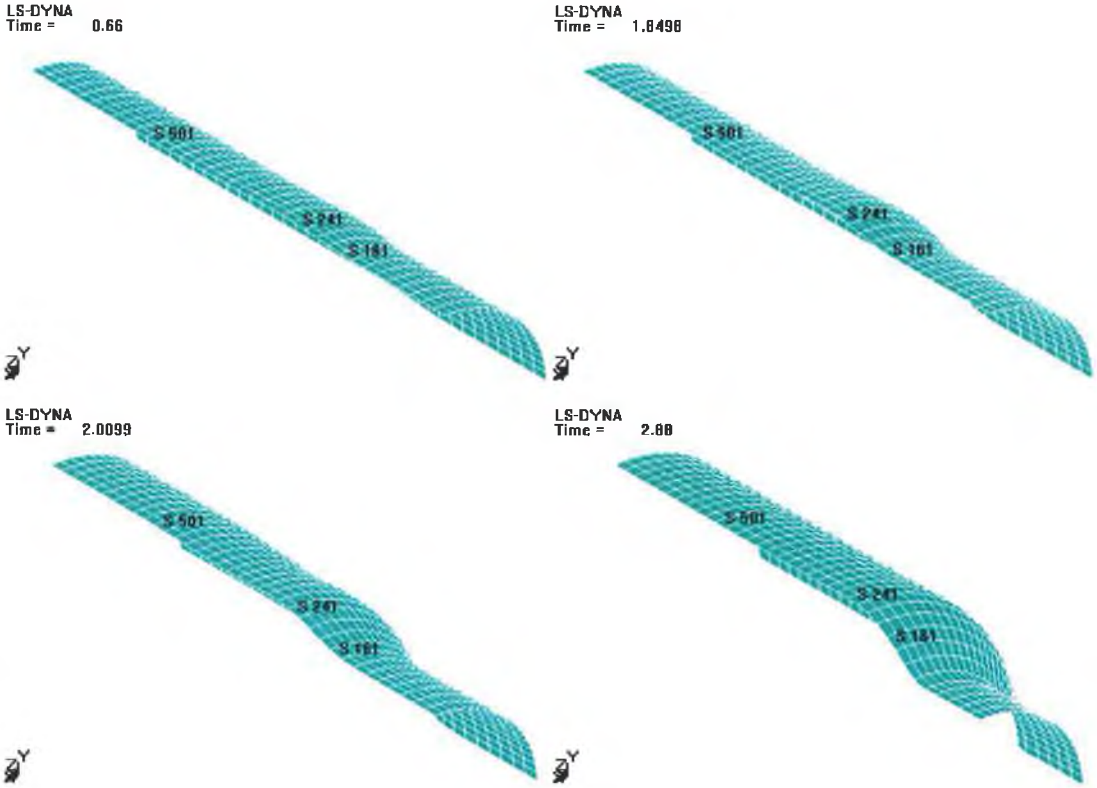

Fig 6.2.9 Axisymmetric expansion corresponding to non-wrinkle-load path at different phase of the simulation

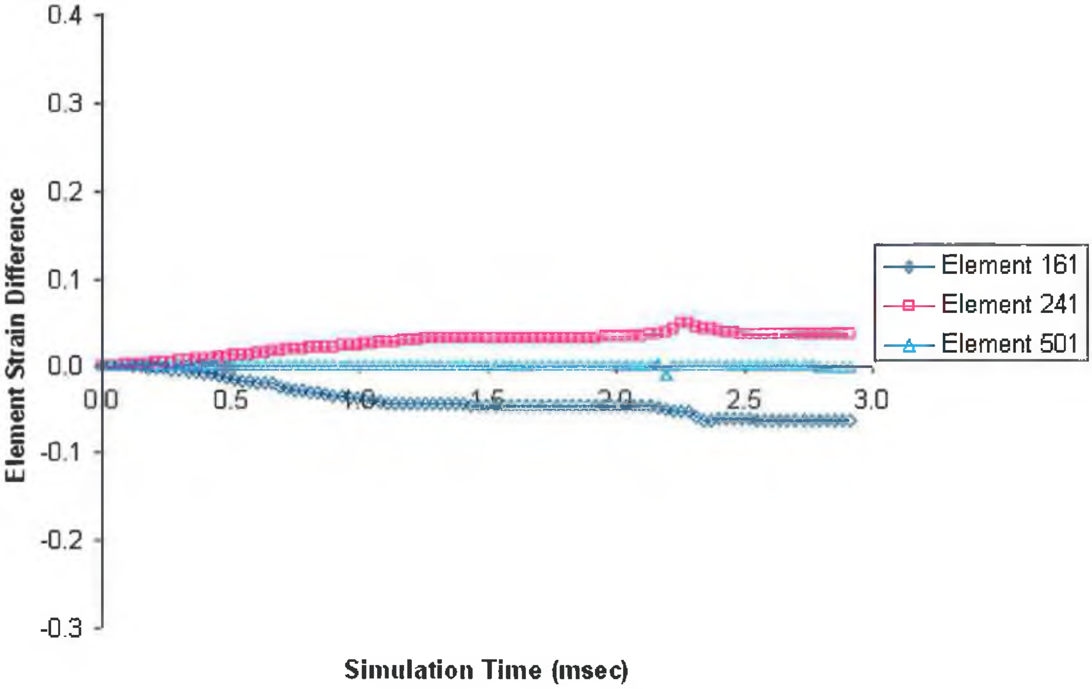

Fig 6.2.10 Development of element strain difference across element thickness (non-wrinkled axisymmetric expansion)

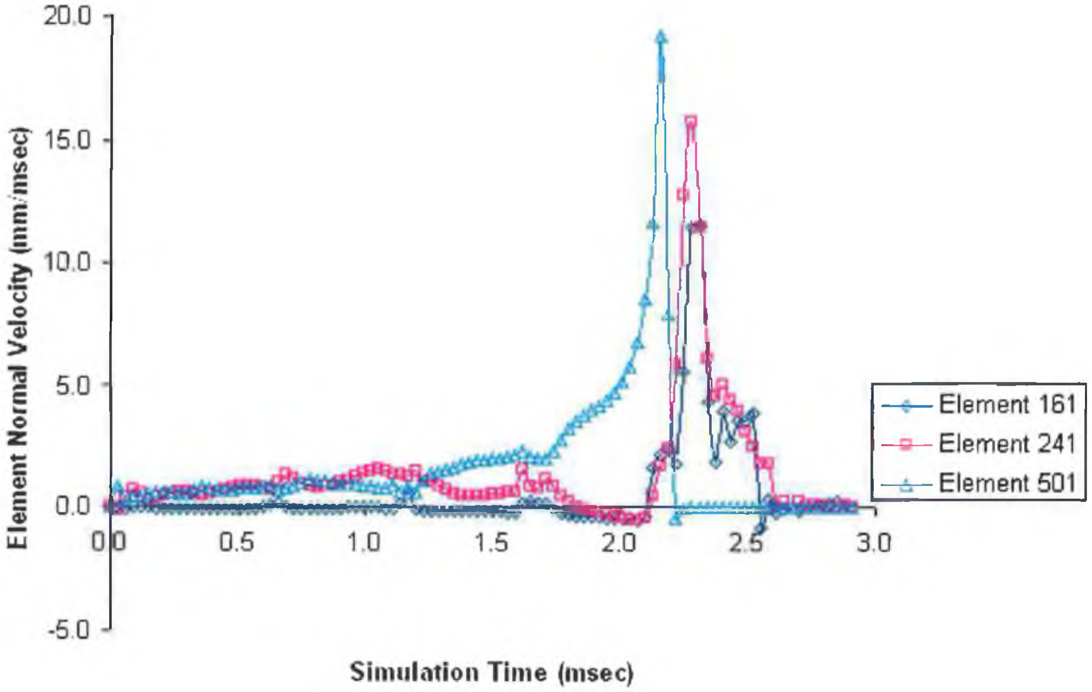

Fig 6.2.11 Development of element normal velocity (non-wrinkled axisymmetric expansion)

In hydroforming processes which involve combined end axial feed and internal hydroforming pressure, it is desired that the end axial feed over the process time should be as high as possible so that as much material as possible can be fed into the deforming zone, thereby decreasing the chance of failure due to excessive wall thinning or bursting. This extra material pushed into the deforming zone helps in maintaining the wall thickness near the highly strained areas within the desired limits. However, the value of actual axial feeding in the process is limited by the occurrence of wrinkles or buckling. Excess material pushed into the forming zone may result into either buckling or excessive wall thickening in certain zones. Thus, with the use of the intelligent load control algorithm the formation of a wrinkle can be detected in advance and controlled in the finite element simulation of the forming process itself. The intelligent load control algorithm developed here tries to provide as much possible axial feed to the tube ends, while simultaneously maintaining the internal pressure as low as necessary to prevent any wrinkle growth, buckling or bursting. Further, this control algorithm can also be tuned by adjusting different control parameters to maximize the part expansion. The flow chart in fig 6.2.12 shows the detail of the process and the implementation of the fuzzy load control algorithm in the finite element program LS-DYNA/explicit.

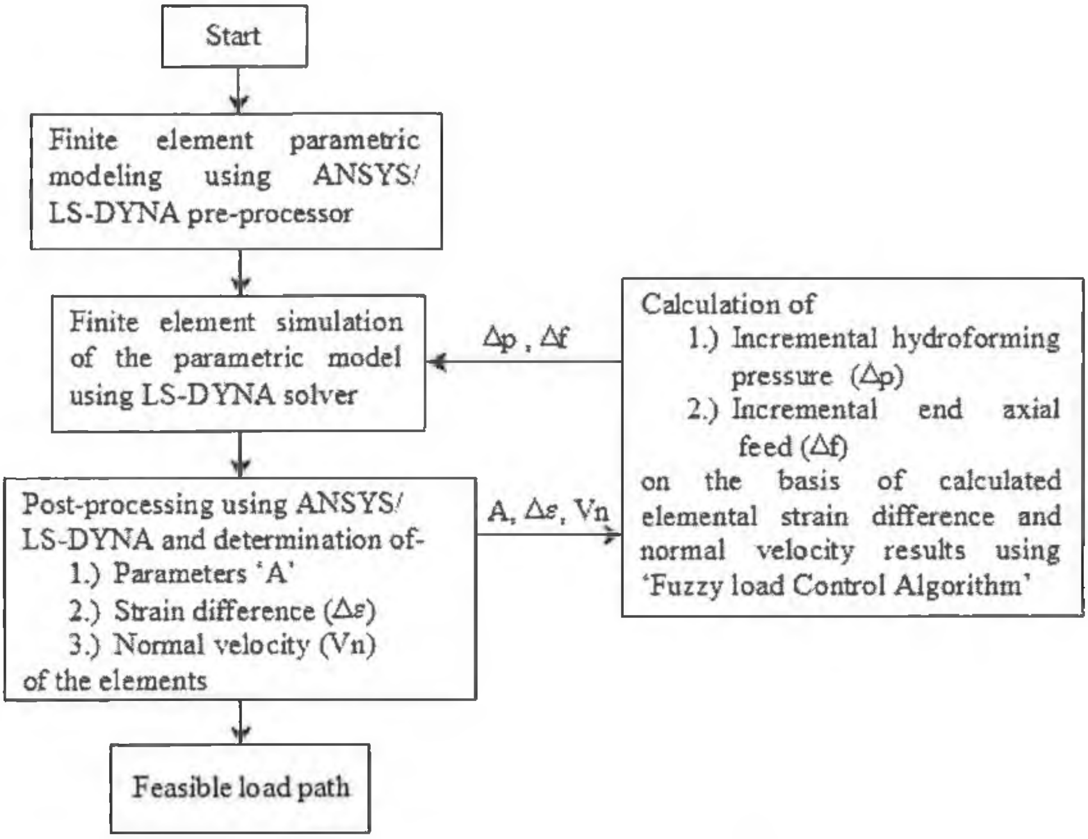

Fig 6.2.12 Integration of the fuzzy load control algorithm with the finite element code

6.2.2. Design of the load control algorithm

In the previous section, it was shown how the element strain difference between outer and inner surface and the normal velocities at the different phase of the simulation define the wrinkle growth, normal bending and normal part expansion for a simple axisymmetric type component. In this section, the same approach as illustrated above will be discussed again in further detail with a part with a different geometric configuration (asymmetric expansion– X-branch expansion) with an unstable loading. This is done with an objective to illustrate the detail design and development of the load control algorithm. In the later part of the chapter, the results obtained from the simulation of the same component (X-branch) using the developed load control algorithm will be presented and compared with the results obtained with the unstable loading. Again the objective is to study the effectiveness of the developed control algorithm in practical application for simulation of different part geometries. Table 6.2.2 shows the load path used for the study, which resulted in wrinkle formation, subsequently leading to buckling of the tube (X-branch expansion).

Table 6.2.2 Forming load path details for X-branch (wrinkled condition)

Simulation Time (msec)	Axial Feed (mm)	Forming Pressure (GPa)
0.00	0.00	0.0000
0.50	2.00	0.0020
1.00	6.00	0.0090
1.50	9.50	0.0185
2.00	12.50	0.0265

Fig 6.2.15 shows the variation of the strain difference between the outer and inner surface strains of the elements for five different elements (element number 625, 638, 648, 889, 912) during the forming of a X-branch with unstable loading. These elements are chosen from both wrinkled (unstable zone) and non-wrinkled (stable zone) surface as well as bend along die radius (fig 6.2.13) so as to clearly differentiate the element strain difference and normal velocity variation over the entire simulation period. To differentiate between a normal expansion and a wrinkled expansion, a critical limit value of +/-0.12 was defined for the strain difference, any element having strain difference (+ve or –ve) above the limits can be assumed to be severely wrinkled or bent. The limit was set by considering the element strain difference developed with respect to the wrinkle height. From experiments detailed in Chapter 3 it was observed that a minor wrinkle crest height was of the order of 0.5mm-0.9mm whereas the major wrinkle crest height was of the order of 3.0mm-3.5mm. Thus for the present analysis a wrinkle crest height which was above 0.5mm was considered to be a critical wrinkle. Fig 6.2.14 details the variation of strain difference (-ve in nature) with respect to negative wrinkle crest height for element number 912, which is subjected to wrinkle (fig 6.2.13).

At the beginning of the simulation at (time=0), it can be seen that the strain difference ($\Delta\varepsilon$) is within the assumed safety/cut-off limits (+/-0.12) for all the elements, however with the increase of the simulation time the strain difference increased steadily for some stable as well as unstable elements (element number 625, 912) this indicates bending. Either this may be due to the formation of a wrinkle or it may be a normal bending of the tube wall due to the die configuration in those locations. To distinguish this wrinkle growth from normal bending of the wall using the element strain difference values, as explained before the shell element normal velocity (V_n) has to be taken into account. Fig 6.2.16 shows the variation of shell (element) normal velocity pertaining to the highly strained elements (element 912, 625), initially at time=0, the normal velocities are low,

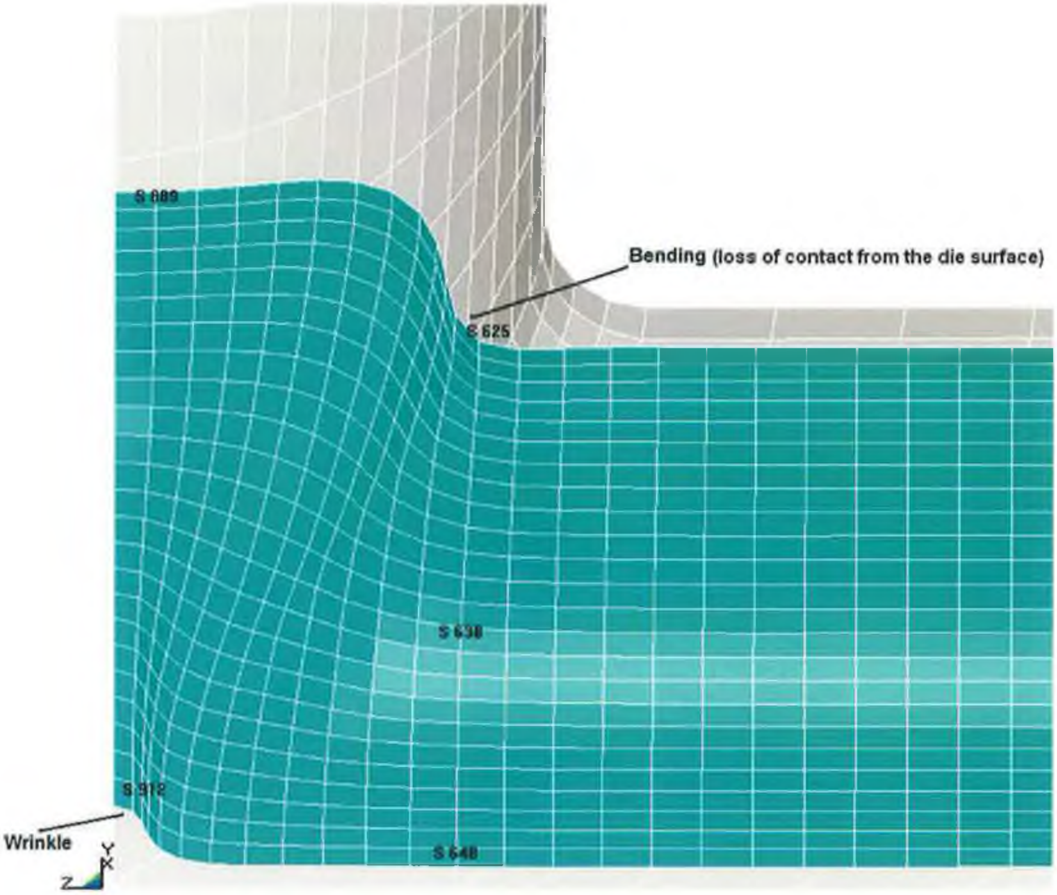

Fig 6.2.13 One-eighth symmetric, wrinkled X-branch hydroformed tube with element numbers shown on the tube surface

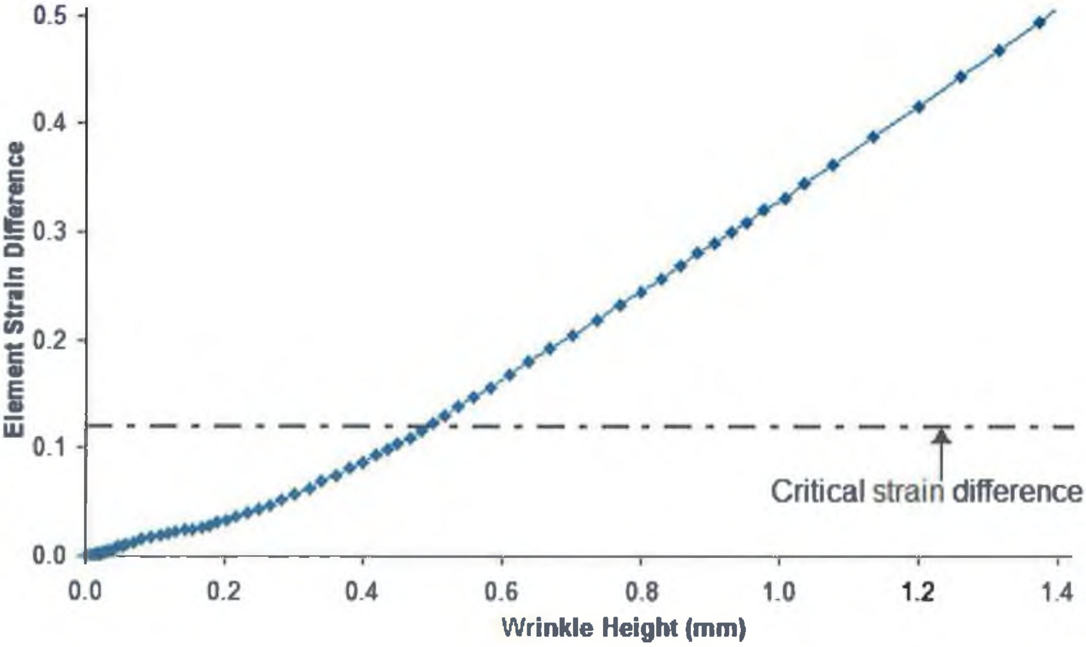

Fig 6.2.14 Variation of element strain difference with respect to wrinkle height for a negative wrinkle crest (for element 912 -refer fig 6.2.13).

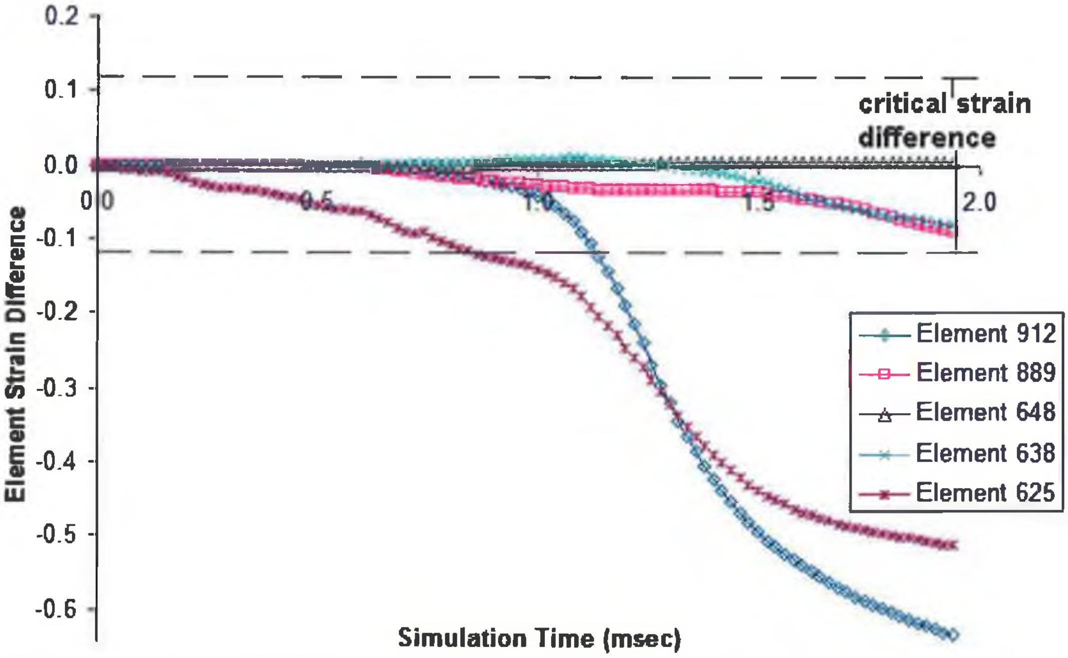

Fig 6.2.15 Development of element strain difference across element thickness (wrinkled X-branch forming)

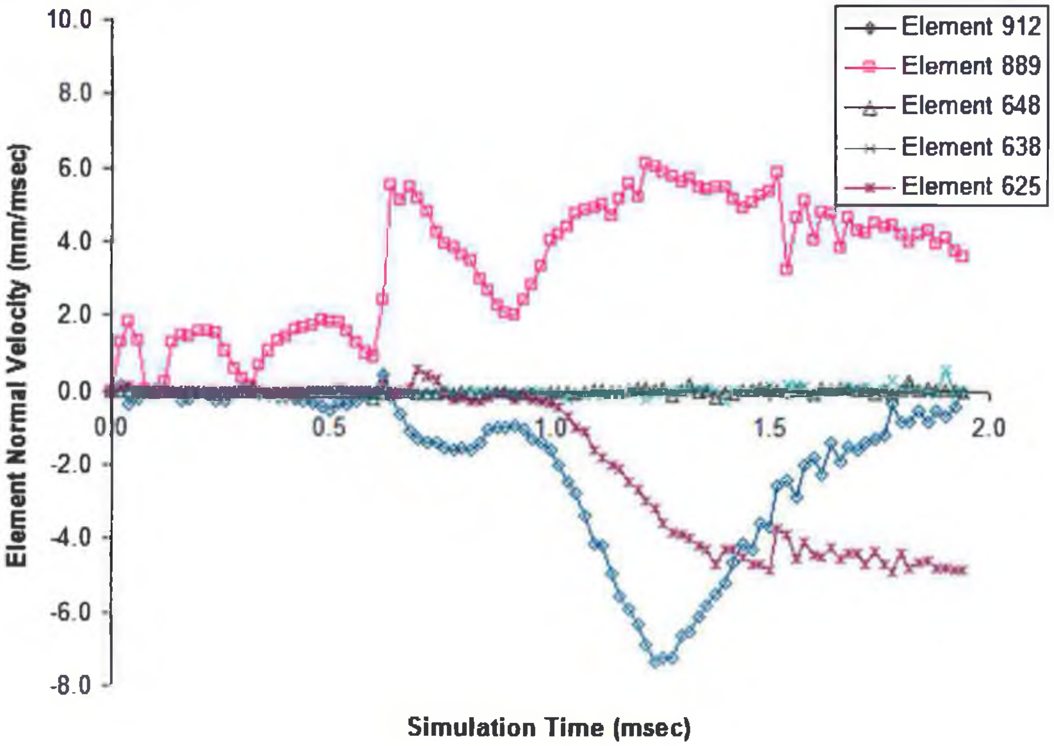

Fig 6.2.16 Development of element normal velocity (wrinkled X-branch forming)

however, with increase in simulation time the velocity rise was rapid, this indicates either formation of wrinkle or severe bending of the surface with subsequent loss of contact from the die surface. In this case element 912 can be categorized as subjected to wrinkle, whereas considering the die geometry (die radius), the state of element 625 can be defined as normal bending across the die radius in the initial phase of the simulation with subsequent loss of contact from the die surface due to buckling/ crushing of the tube, and hence there is a steep rise in the normal velocity. Had it been a normal bending across the die radius, in such case the element strain difference will be relatively high whereas the normal velocity will be considerably low. Form the simulation it was also observed that a wrinkling tendency started within a simulation time of 0.65msec-0.7msec, when axial feed was approximately 3.2mm with a visible wrinkle height of 0.15mm, which further increased with application of subsequent axial feed in the later part of the simulation.

Considering the other elements (element 889, 638, 648), it can be seen that the element strain difference for all these elements are nominal or very low (i.e. much below the strain cut-off limit) throughout the simulation and also for element 638 and 648 the normal velocity is almost zero, whereas for element 889 the velocity is fluctuating in nature throughout the simulation phase. Thus, all these cases can be considered as normal expansion of the tube wall as the element strain difference (between the outer and inner surfaces) is considerably low.

Thus in tube hydroforming processes, primarily these two terms, a.) strain difference and, b.) shell normal velocity, can describe the formation of a wrinkle or buckling of the part to be formed. In the course of the simulation, it is possible that some of the elements might be highly strained and the normal shell velocities might be high, but this does not prove that the portion is subject to wrinkling. If there is formation of a wrinkle then it starts within a small area in a relatively unstable zone, primarily with a few number of elements and it increases gradually. Therefore, it is very important to determine the area or segment where the wrinkle growth has started. Moreover in case of asymmetric components with protrusions such as 'T' or 'X' shapes, in those cases in the course of expansion the tube surface is bent into the bulged or protruded section. Thus, here it is relatively difficult to determine whether the tube surface has bent due to wrinkle or due to the die geometry/configuration (such as die bend/ die radius at the T or X junction). Thus, to determine the possibility and probable zone of formation of a wrinkle, a parameter 'A' as defined in Equation-(1) was used in the algorithm.

$$A = \frac{N_{CSE}}{N_{total}} \qquad (1)$$

Where N_{CSE} is the number of elements in a slice (fig 6.2.17), that exceeds a critical value of the strain difference '$\Delta\varepsilon$' over the tube sheet-thickness, and N_{total} is the total number of elements in the circumference of that particular slice of the model. These slices (set of elements or chain of elements along the circumference of the tube in the axial direction) were defined parametrically in the finite element mesh of the tube (fig 6.2.17). Apart from application with asymmetric components like X or T-branches, this parameter is of particular importance for parts with a bent centre line, as in those cases the possibility of wrinkle growth is maximum in the curved or bent portion of the tube corresponding to the inner curved radius (smaller radius) [56], this can be been seen from another simulation of a complex part presented in section 6.3.2. However, for axisymmetric components this parameter is not of much importance as in those cases the wrinkle growth is usually uniform along the entire circumference of the tube provided the tube inner and outer radius are uniform or in other term the wall thickness is constant and uniform throughout the length (i.e. no eccentricity in the centre of the outer and inner radii of the tube throughout the spline length). This parameter holds good for axisymmetric cases also if there is some non-uniformity in the wall thickness of the tube, in such cases wrinkles usually develop or buckling occurs at the thinner section of the tube due to structural instabilities (fig 6.2.18).

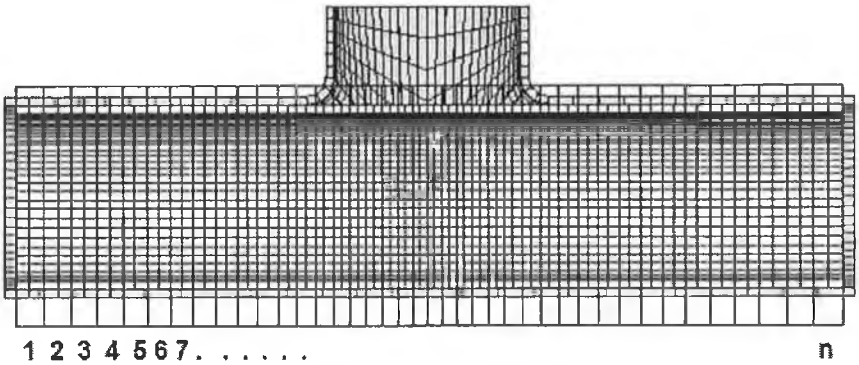

Fig 6.2.17 Tube elements divided in 'n' finite number of slices along the axis of the tube

By evaluating these variables '$\Delta\varepsilon$' (element strain difference), 'V_n' (shell element normal velocity) and 'A' (parameter defining relative number of strained elements in a particular slice) in an appropriate way in the control algorithm, it is generally possible to avoid failures due to buckling or wrinkles of any kind with in the finite element simulation of the process. Thus, the values of these three parameters can be used as physical signals for

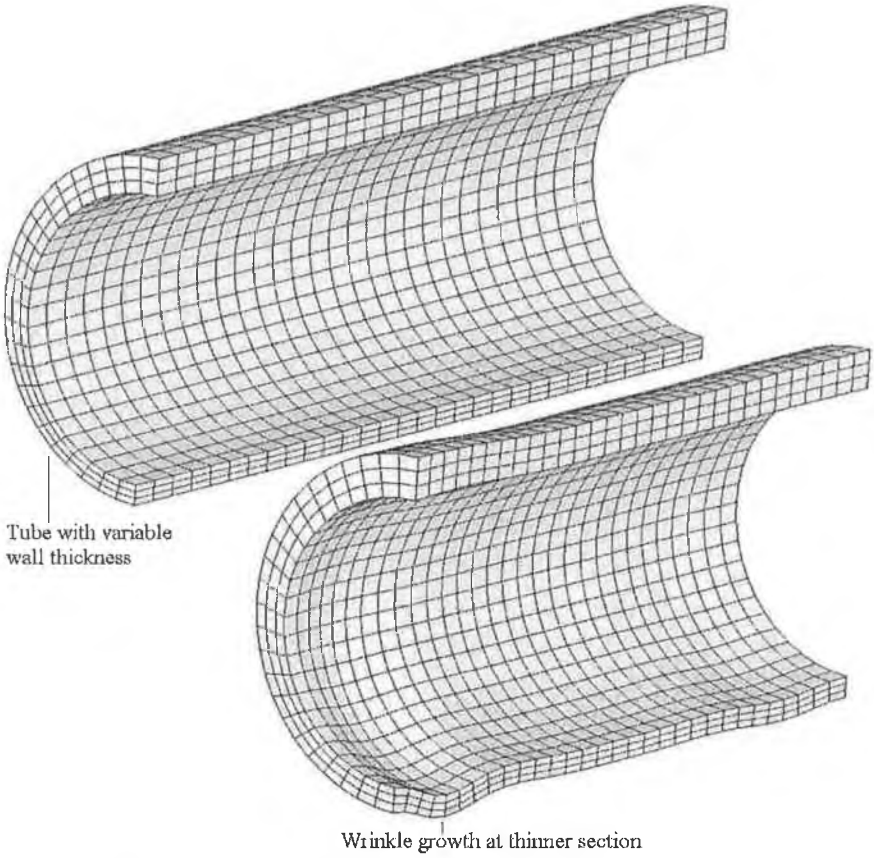

Fig 6.2.18 Wrinkle growth at the thinner section of the tube (half-symmetric axisymmetric component)

the control algorithm, which can indicate in advance the possible instability of the process. Hence, these three parameters can be used as the input for the load control algorithm. The difference between the conventional control applications and finite element simulation is that these values are obtained within the solution process of the finite element simulation. Because of the dynamic nature of the simulation process, the values of the element normal velocities and strain differences keep on oscillating or fluctuating over the entire simulation period (fig 6.2.15, fig 6.2.16). Therefore, a quantitative value for the classification "critical" or "not-critical" deformation or formation of wrinkle is difficult to define for different geometries. Thus, a definition of exact limit values that decide whether or not a wrinkle occurs is avoided here in the development of the control algorithm. Instead of exact terms as "wrinkle occurs during the forming process 'Yes' or 'No' " the criteria are evaluated in 'soft terms' and 'fuzzy rules'. The basic fuzzy rules incorporates a simple logical rule, based on "IF 'X' AND 'Y' THEN 'Z'" approach to solve any basic control problem rather than attempting to model the system mathematically, where 'X' and 'Y' are two different input conditions and 'Z' is the outcome or the output depending upon the inputs. Thus, a wrinkle formation (with the degree of severity) in this case can also be described in terms of logical rules and with linguistic terms. For example, formation of a severe wrinkle can be stated as "IF the portion of the tube surface is bent strong AND the surface is moving fast in the normal direction AND the surface is bent on the whole circumference THEN a critical wrinkle occurs". However, for defining the criteria for formation of wrinkle or buckling of the tube surface the parameters are defined in terms of "strain difference '$\Delta\varepsilon$', surface normal velocity 'V_n' and elemental slice parameter 'A'", i.e. the same can be defined in terms of these three parameters as, "IF the *strain difference* of an element is '*very high*' in a particular slice AND the element *normal velocity* is '*very high*' AND the *number* of such elements exceeding the strain cut off limit in that particular slice are '*many*' , THEN a *critical* wrinkle occurs". In a similar way the outputs i.e. the end axial feed and the internal pressure are determined. For example, "IF a '*very critical*' wrinkle occurs THEN lower the axial feed to '*minimum limit*' AND increase the internal pressure to '*maximum limit*'". Similarly, to avoid failure due to bursting, a simple logic stating the cut-off limits of maximum wall thinning was defined, "IF the maximum wall thickness is below certain cut-off limit THEN, stop the simulation run". Although these fuzzy terms are imprecise, still they are very descriptive of what must actually happen. Thus, to incorporate these kind of linguistic rules in the finite element code, fuzzy logic was used, which translates these rules into a control system. The inputs used for the control system are the calculated variables '$\Delta\varepsilon$', 'V_n', and 'A' (i.e. mechanical characteristics) and the outputs from the control system are the calculated incremental axial feed "Δf" and the internal forming pressure "Δp" (i.e. process parameters).

In general there are few distinct advantages of fuzzy logic such as:

- Fuzzy logic controller are inherently robust since it does not require precise, noise-free inputs
- Fuzzy logic controller processes user-defined rules governing the target control system, it can be modified and tweaked easily to improve the system performance
- Fuzzy logic can control nonlinear systems that would be difficult or impossible to model mathematically

- Because of the rule-based operation, any reasonable number of inputs can be processed and numerous outputs generated

Due to the above advantages of fuzzy logic control system, it can also be applied for control of the loading paths of complicated hydroforming processes where it is extremely difficult to establish the wrinkle growth during the forming operation as well as to model the process analytically.

6.2.2.1. Fuzzification of input variables and application of fuzzy rules

In order to define any input variable of a process controlled by fuzzy rules, first it is important to fuzzify or discretize the input variables prior to incorporating the logical rules in the control system. In the case of this control program, the rules were categorized with three input variables i.e. a.) $\Delta\varepsilon$- shell element strain difference (3-sets), b.) V_n - shell element normal velocity (3-sets) and, c.) 'A'- relative number of strained elements in the circumference with 3-different classes of strain difference (3-sets), all these inputs altogether activate 27-fuzzy rules, which judge whether the incremental axial feed (Δf) and internal pressure (Δp) have to be high, medium or low (fuzzy inference). This incremental axial feed and internal pressure values are calculated for each slice of the finite element model by the algorithm. For simplicity of the algorithm, only three different ranges or classes of input variables were used, however the control algorithm can be made much more robust by increasing the number of classes. Finally, a defuzzification program computes the output (Δp and Δf) as the weighted centre of the output set. With the parameters used in defuzzification, the control system allows and tunes the process to have small or moderate wrinkles during the simulation. A sample fuzzy rule matrix for the control algorithm is shown in table 6.2.3.

Table 6.2.3 Fuzzy rule matrix for strain difference vs. normal velocity

Fuzzy load control algorithm ($A \leq \alpha1$)	$\Delta\varepsilon$= (+ve high)	$\Delta\varepsilon$= (medium)	$\Delta\varepsilon$= (–ve high)
V_n = (+ve high)	Δp=very-low(α1) Δf=low(α1)	ΔP=low(α1) Δf=normal(α1)	Δp=normal(α1) Δf=normal(α1)
V_n = (medium)	Δp=low(α1) Δf=high(α1)	Δp=normal(α1) Δf=very high(α1)	Δp=high(α1) Δf=high(α1)
V_n = (-ve high)	Δp=normal(α1) Δf=normal(α1)	Δp=high(α1) Δf=normal(α1)	Δp=very high(α1) Δf=low(α1)

Similarly, 3 sets of rules were formulated for '$A \geq \alpha 2$' and '$\alpha 1 \leq A \leq \alpha 2$' respectively. Where very-low ($\alpha 1$), low ($\alpha 1$), normal ($\alpha 1$), high ($\alpha 1$) and very-high ($\alpha 1$) are the set of output membership functions for pressure and axial feed.

The boundaries for strain difference, velocity and the factor 'A' were defined from the preliminary data (for strain difference and normal velocity) obtained from simulation of a component which failed due to wrinkle. The development of the above boundaries for the control algorithm is entirely dependent on the type of part geometry. In the subsequent section the development of the boundaries of the X-branch expansion is detailed. The initial simulation results of the failed component give an approximate indication of element strain difference and normal velocity behaviour. Further the boundaries for strain difference (+ve high, medium and –ve high) and normal velocity (+ve high, medium and –ve high) were decided by considering the factor 'A' i.e. relative number of elements in a slice which were highly strained or in other word number of elements which have strain difference values above the +/-0.12 limit for X-branch expansion (refer section 6.2.2). Thus the first step is to categorize each slice of elements under three different classes ($A \leq \alpha 1$, $\alpha 1 < A < \alpha 2$ and $\alpha 2 \leq A$) to identify the susceptibility to wrinkle growth or the degree of wrinkle growth if any in each slice. For the present case the values of $\alpha 1$ and $\alpha 2$ were such that, with a slice containing 24 elements (as used for X-branch finite element model of tube i.e. 24 number of element in each slice where total number of slices in the tube blank is 38), if less than equal to 3 elements have strain difference above +/-0.12 (i.e. for case $A \leq \alpha 1$- with less than equal to 12.5% of the slice is wrinkle prone or have high strain difference values) then that slice will follow a set of fuzzy rules (i.e. set number 1, which is a set with relaxed values of strain difference and element normal velocity range used to define the range for +ve high, medium and –ve high domains, for calculation of the final input membership functions). Thus the above case is treated as a case with a minor or less severe risk of wrinkle growth. Similarly if a slice containing more than 3 and less than 8 elements have high differential strain above +/-0.12 (i.e. for case $\alpha 1 < A < \alpha 2$, with more than equal to 12.5% and less than 33.3% of the slice is wrinkle prone), then the slice will follow a set of fuzzy rules (i.e. set number 2, which is a set with much more tighter or stringent values of strain difference and element normal velocity range used to define the +ve high, medium and –ve high domains, for calculation of the final input membership functions). Thus this case can be treated as a case with medium or average risk of wrinkle. Finally if the number of elements with high differential strain is more than and equal to 8 (case $\alpha 2 \leq A$), then that slice will follow a set of fuzzy rules (i.e. set number 3, which is a set with most stringent values of strain difference and element normal velocity range used to define the +ve high, medium and –ve high domain, for calculation of the final input membership functions). Thus this case can be treated as a case with highest risk of wrinkle growth in the major part of the slice. Similarly the three different domains of the element strain difference and normal velocity for the three different ranges of parameter 'A' were defined considering the strain difference (fig 6.2.15) and normal velocity (fig 6.2.16) plots of element subjected to severe wrinkle as well as normal expansion. This can be explained by considering the case when $A \leq \alpha 1$. As explained above this is a case with minimum number of elements (less than equal to 3) either exceeds the critical winkle limit or none exceed the limit i.e. there is minor risk of wrinkle growth. Thus here the domain for the medium value of strain difference ($\Delta\varepsilon$= medium) was restricted within –0.055 to 0.00 to +0.055 (i.e. b-d-f, refer fig 6.2.19) and similarly for the positive high strain difference value ($\Delta\varepsilon$= +ve high) the domain was defined from + 0.025 to +0.085 to infinity (i.e. e-g-infinity, refer fig 6.2.19) and for negative high strain difference value ($\Delta\varepsilon$= -ve high) the domain was defined from -0.025 to -0.085 to -infinity (i.e. c-a-infinity, refer fig 6.2.19). Similarly considering the normal velocity distribution, the domain for the medium value of the element normal velocity (V_n=medium) was defined within –2.5msec to 1.0msec to 4.5msec (i.e. b-d-f, refer fig 6.2.19), for positive high normal velocity value (V_n= +ve high) the domain was defined from + 3.0msec to + 6.5msec to infinity (i.e. e-g-infinity, refer fig 6.2.19) and for negative high normal velocity value (V_n= -ve high) the domain was defined from –1.0msec to –4.5msec to -infinity (i.e. c-a-infinity, refer fig 6.2.19). the selection domain of the medium value of the strain difference and normal velocity with an assumption that in the initial stage or if there is no wrinkle or bending of any element , then the strain difference lies with the limit of +/-0.055 whereas the maximum variation in the normal velocity lies with in –2.5msec to 4.5msec. Thus with the above settings of the domains of $\Delta\varepsilon$ and V_n, most of the elements fall under the medium zone and follow the corresponding fuzzy rules which allows higher incremental pressure and axial feed at the end of the fuzzy processing. The domains for other conditions (strain difference and normal velocity) for $\alpha 1 < A < \alpha 2$ and $\alpha 2 \leq A$ were also defined in a similar fashion. The details of the control limits are defined in the control program listed in Appendix-C (refer section- fuzzy logic controller / load control algorithm). As explained above fuzzy logic does not require exact or precise values, thus a rough or approximate estimate of the control limit values reasonably works well with this kind of fuzzy control program.

6.2.2.2. Calculation of the membership function

The membership function is a representation of the magnitude of participation of each input variable. It associates a weighting with each of the inputs that are processed, define functional overlap between inputs, and ultimately determines an output response. The rules use the input membership values as the weighting factors to determine their influence on the fuzzy output sets of the final output conclusion. Once the functions are inferred, scaled and combined, they are defuzzified into a crisp output, which drives the logical control system. There are different ways of defining the fuzzy membership functions, here in this study for simplicity of the calculation, the fuzzy membership functions were defined with sets of linear functions (fig 6.2.19) however, Gaussian or Sigmodal functions can also be used for this purpose.

The membership functions formulation for the strain difference/shell normal velocity (input membership function) and incremental pressure/axial feed (output membership function) are shown in fig 6.2.19 and fig 6.2.20 respectively. The entire domain of the shell element normal velocity and strain difference were divided into 'three' different zones. The left portion defines the membership function for negative normal velocity/strain difference (-ve high) i.e. when the elements move inside towards the tube axis, the middle portion defines the membership function for the normal velocity/ strain difference (medium) i.e. when the normal velocity and strain difference is relatively small and, the right portion defines the membership function for the positive normal velocity/strain difference (+ve high) i.e. when the elements move away from the tube axis. Similarly, the output membership function for incremental pressure and axial feed were divided into 'five' different zones, i.e. very-low, low, normal, high and very-high.

6.2.2.3. Fuzzy inference, defuzzification and calculation of output parameters

Finally, to determine the firing strength of the fuzzy rules and to calculate the effective incremental pressure (Δp) and axial feed values (Δf), the results obtained from the rules were defuzzified to crisp numbers. In this case "the root-sum-square" method was used

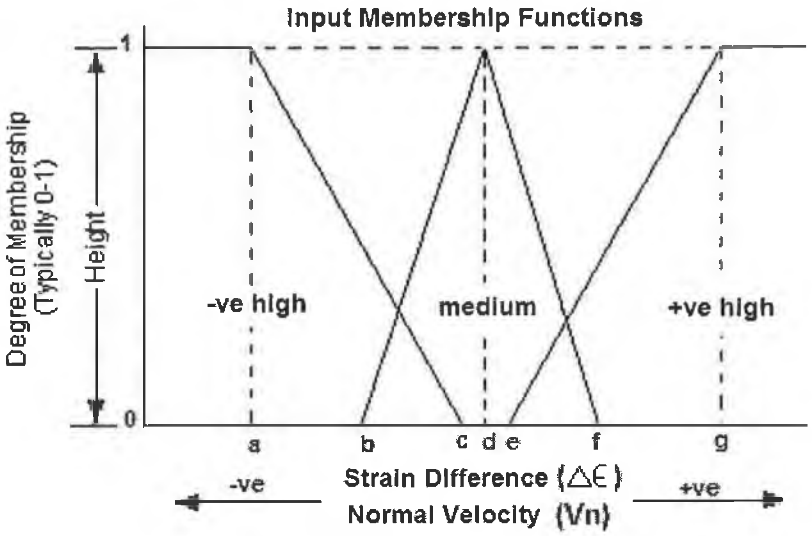

Fig 6.2.19 $\Delta\varepsilon$ and V_n input membership functions

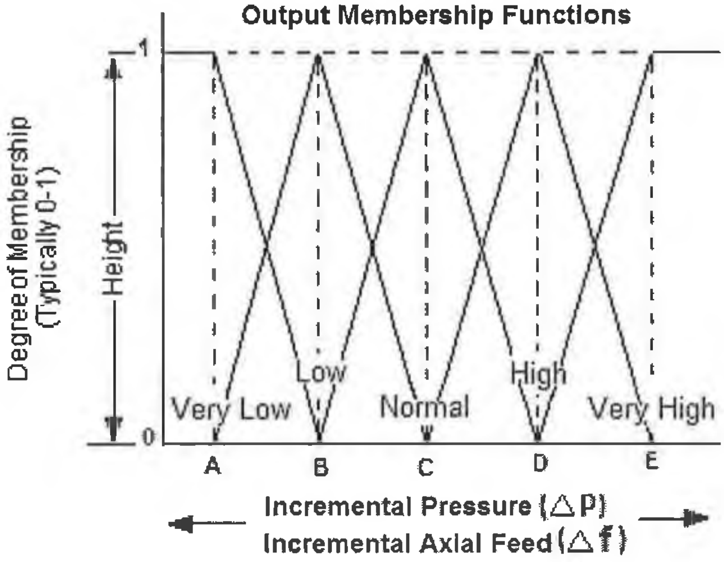

Fig 6.2.20 Δp and Δf output membership functions

for the defuzzification. This method computes the “fuzzy” centroid of the composite area. The root-sum-square method was chosen as it includes all contributing rules. For each element of a particular slice, from the strain difference and normal velocity data the input membership functions were calculated.

With the calculated input membership functions and associated fuzzy rules the output membership functions were calculated. Finally the crisp output values of the incremental pressure and the axial feed were calculated by taking the ratio of ‘the summation of the product of the weighted strengths of each output membership function area centroid with their respective membership function’ over ‘weighted membership function strengths’.

After calculation of 'Δp' and 'Δf' for each of the individual elements in a particular slice, it was averaged to determine the effective incremental pressure (Δp) and feed (Δf) for each slice and the minimum of the 'Δp' and 'Δf' for all the slices were selected as the final effective incremental pressure and axial feed for the entire geometry for the next set of simulation. The detail fuzzy load control algorithm employed in the finite element simulation program is shown in the flow chart in fig 6.2.21. The advantage of this type of control system is that within the simulation itself the element normal velocities are automatically adjusted by appropriately adjusting the hydroforming pressure and end axial feed, simultaneously maintaining proper deformation of the tube, by avoiding any

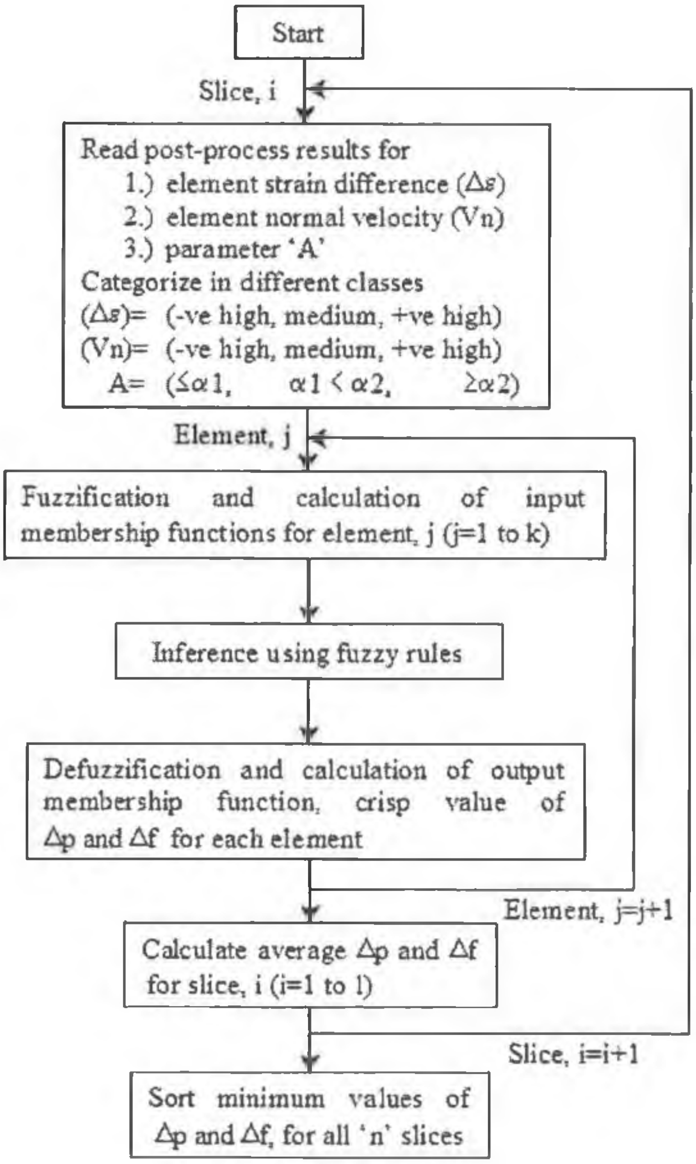

Fig 6.2.21 Details of the Fuzzy control algorithm and calculation of incremental pressure and feed values

failure due to wrinkle growth during the forming process. The final outcome of which is the desired optimal or feasible load path. Appendix-C details a sample control program (for X-branch forming) integrated with the LS-DYNA/explicit finite element simulation code.

Other than the development of the fuzzy load control program the following section details the extraction of required data and calculation procedure of the effective shell element thickness, normal velocity and strain difference.

1. Calculation of the shell element thickness

To determine the maximum thinning of the tube wall, a small post-processing routine was used in the control program which first sorts the element thickness at the last state of the step simulation particularly for all the elements of the tube blank elements at all location and then it sorts the minimum of all the sorted element thickness. The difference of this minimum value and the original shell thickness is the degree of tube wall thinning at the most stretched region of the tube. The detail of the program is illustrated in Appendix-C (in section- post-processing of results) and the flow chat (fig 6.2.22) detailed below outlines the calculation procedure of the shell element thickness and degree of wall thinning.

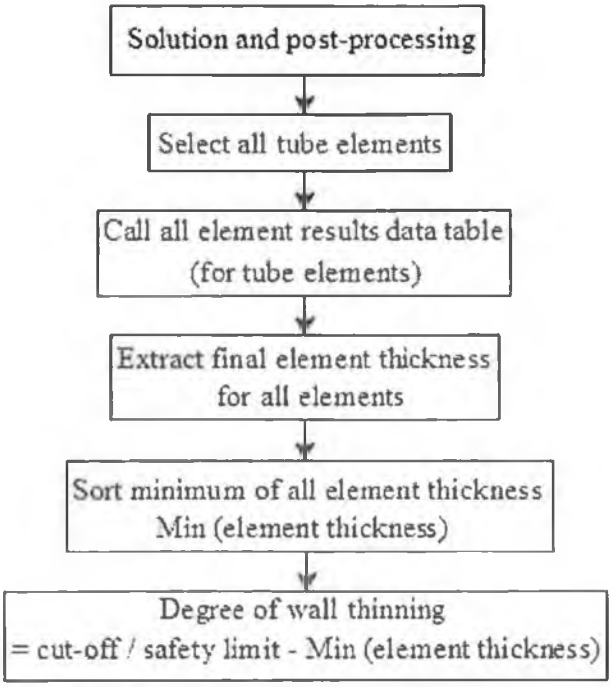

Fig 6.2.22 Flow chart for element thickness (tube wall thinning) calculation

2. Calculation of the shell element normal velocities

The ANSYS/LS-DYNA post-processor used in the control program does not support direct extraction of shell element normal velocities at the final stage of each step simulation. Thus, the normal velocities for the elements were calculated separately by using the nodal displacement results, direction cosine of the new elemental plane and the element velocities in the x, y and z direction with respect to the global coordinate system. The section below illustrates how the shell normal velocities for different time steps were calculated using 3D vector algebra.

During the forming process, in the course of expansion or wrinkle formation, the element normals for some of the elements vary with simulation time step, hence the element normal velocity also change accordingly. Fig 6.2.23 shows an element at two different time steps (i.e. at 'time=t' with initial nodal coordinates and element normal direction 'n' and at 'time=t+dt' with the new nodal coordinates and element normal direction 'n').

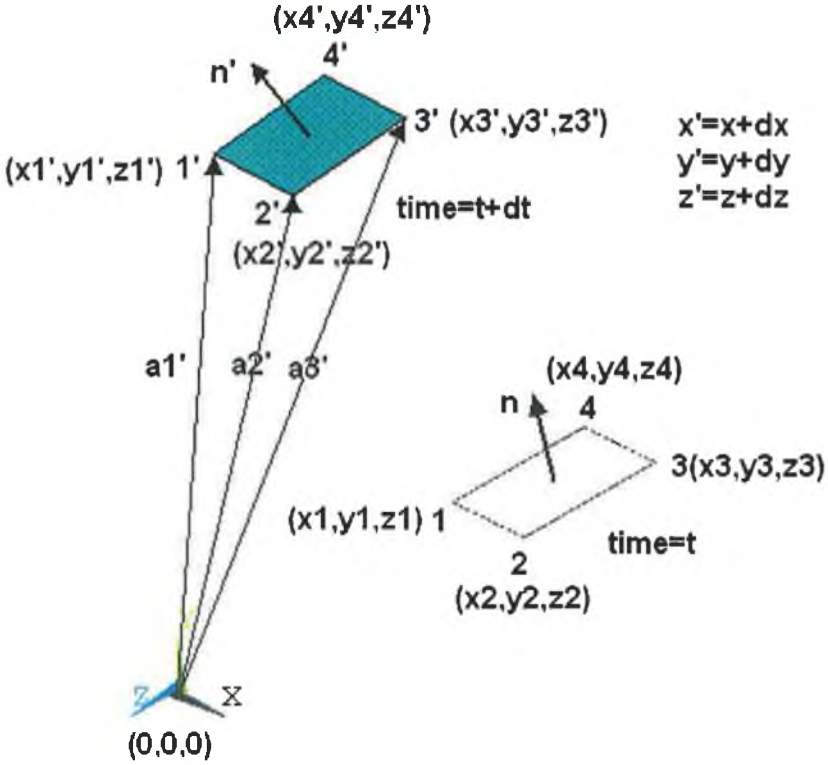

Fig 6.2.23 Element with nodal coordinate position at different time steps (t and t+dt)

The concept used here to calculate the element normal velocity requires the direction cosine values of the plane of the deformed element. For this the unit normal vector of the element was calculated from 3-positioned vectors ($a1', a2', a3'$) corresponding to the 3 nodes of the element, which defines the new elemental plane. The coefficient of i, j and k components i.e. a_x, a_y, a_z (along three coordinate axes) of the unit vector were used as the direction cosines of the new elemental plane. From the post-processing program the final coordinates of the nodes 1', 2' and 3' were calculated by extracting the initial nodal coordinates 1, 2 and 3 and the incremental displacement (dx, dy and dz) with respect to the initial coordinate of the nodes, and hence the unit normal vector was calculated. Finally, the normal velocity was calculated by taking the components of the x, y and z global velocities (*Vx, Vy* and *Vz*) of the element along the unit normal vector i.e. by taking the summation of the product of the global velocity in the individual axes with the direction cosine corresponding to that axis.

In terms of vector algebra the unit normal vector of the plane can be written as

$$\hat{n} = \frac{\vec{a}_{1'2'} \times \vec{a}_{1'3'}}{\left| \vec{a}_{1'2'} \times \vec{a}_{1'3'} \right|} = a_x \hat{i} + a_y \hat{j} + a_z \hat{k}$$

where,

$\hat{n}$ is the unit normal vector

$\vec{a}_{1'2'} \times \vec{a}_{1'3'}$ is the vector cross products of the two vectors

a_x, a_y, a_z are the direction cosine of the plane of the element

and the element normal velocity can be written as

$$V_n = V_x a_x + V_y a_y + V_z a_z$$

The details of the normal velocity calculations are illustrated in the program presented in Appendix-C (in section- post-processing of results).

3. Calculation of the shell element strain difference across the thickness

For calculation of the element strain difference (fig 6.2.24) across individual elements of the tube blank, another small post processing program was used which sorts the individual element effective strain values of the upper and the lower layers and finally calculates the difference of these two values, which is stored as the element strain difference for that particular element. The details of the post-processing program and calculations are presented in Appendix-C (in section- post-processing of results).

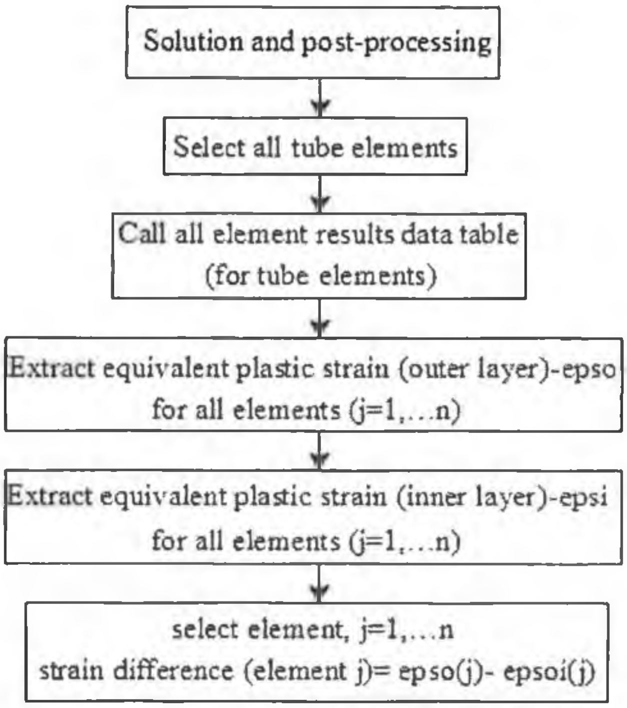

Fig 6.2.24 Flow chart for element strain difference calculation

6.3. Application of the load control algorithm for determination of feasible load paths

The developed load control program was used to simulate and calculate the feasible load paths from simple to complex geometries avoiding any failure due to wrinkle formation or buckling and excessive wall thinning. This was done with an objective to study the effectiveness of the algorithm and its control mechanism in determination of the feasible load path during the simulation process.

6.3.1. Asymmetric expansion -X and T-branch tube hydroforming processes

6.3.1.1. Finite element modelling, loading and solution

The finite element models used for the simulations were identical to the models used in Chapter 3 for validation of the model with experimental results of X and T-branch hydroforming processes except for, a.) the mesh density for the tube blank was increased here to detect even minor wrinkles or bending which is generally not possible with relatively larger element mesh size. Thus, the one-eighth model of the X-branch was meshed with 912 elements and one-fourth model of the T-branch was meshed with 1824 number of finite mapped meshed elements for the blank portion, whereas the die mesh was kept as it is. b.) the shell elements used were with 5-point integration. The 5-point integration of the shell element was assumed because for shell elements, stress-strain values are only calculated at the integration points across the thickness, not on the element surfaces. The 5-point integration shell elements give better strain output for the outer and the inner surfaces. If a shell has only 2 integration points (the default value of LS-DYNA code) then the stress-strain results are calculated for theoretical layers (outer and inner) which are at a distance of +/-0.5774 from the mid plane of the element, if the mid plane is considered to be at location '0' and the outermost or inner most surfaces are at a location '+/-1'. Whereas for 3-point integration the outermost and innermost strain values are calculated for layers at a distance of +/- 0.7746 and for 5-point integration the outputs are obtained for layers at a distance of +/-0.9062 from the element mid-plane. Thus, it is important to choose higher values of integration points for better stress-strain calculation for non-linear material across the element thickness. The modified ANSYS Parametric Design Language script for the X-branch forming is presented in Appendix-C. In the modified program script various changes were incorporated such as, a.) integration of the incremental simulation concept , b.) results post-processing, c.) calculation of the element normal velocities, strain difference and thickness change, d.) integration of the fuzzy load control program with the forming simulation.

In the control program the cut-off limit for the tube wall thickness reduction was set at 5% of the original wall thickness (cut-off limit 1.235mm), thus in the forming process if the thickness of any element reduces below this value then the program will assume failure due to excessive wall thinning. However, the load control program is so developed that it feeds as much material as possible so as to keep the wall thickness within or above the safety limit. The complete simulation of the process was done in 35-40 discrete step simulations, in each step the pressure and axial feed were adjusted by the load control algorithm as per requirement, which were calculated on the basis of the results of element strain difference, normal velocity values and relative numbers of highly strained element developed in the previous stage of the simulation (i.e. step simulation). The load control algorithm basically acts like a closed loop control system controlling the build up of the forming pressure and axial feed simultaneously avoiding any failure due to formation of wrinkles, buckling or excessive wall thinning of the tube.

6.3.1.2. Results

Fig 6.3.1, fig 6.3.2, fig 6.3.3 and fig 6.3.4 show the feasible piecewise load paths (pressure and feed curves) and fig 6.3.5 and fig 6.3.6 show the forming pressure as a function of axial feed for X and T-branch obtained from the simulation using the load control algorithm.

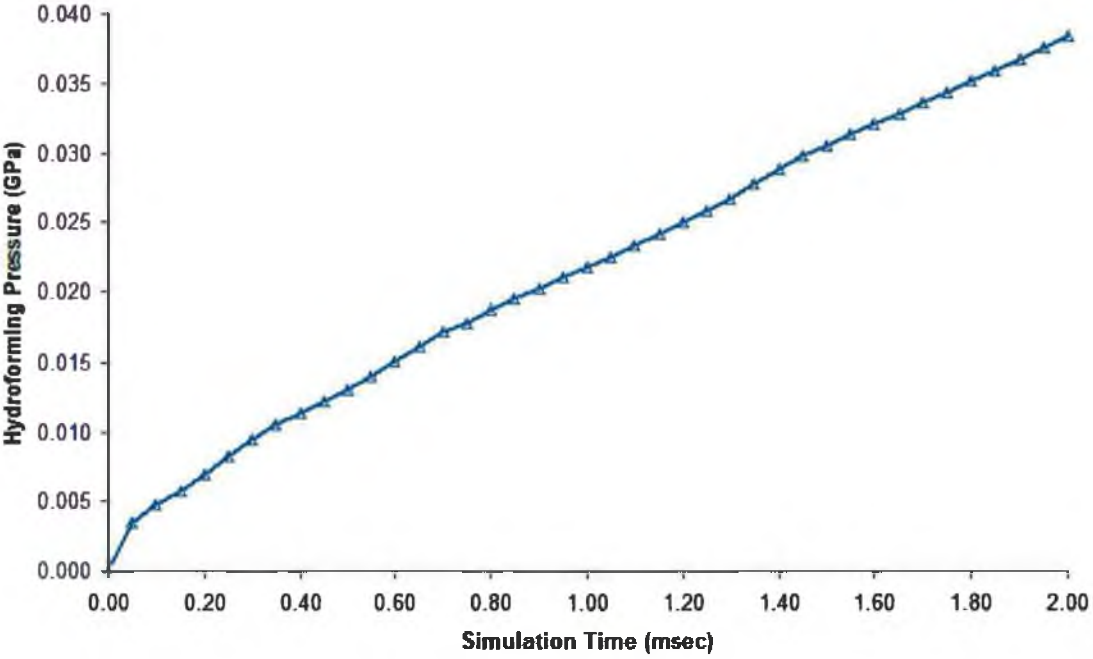

Fig 6.3.1 Pressure curve for X-branch forming obtained using load control algorithm

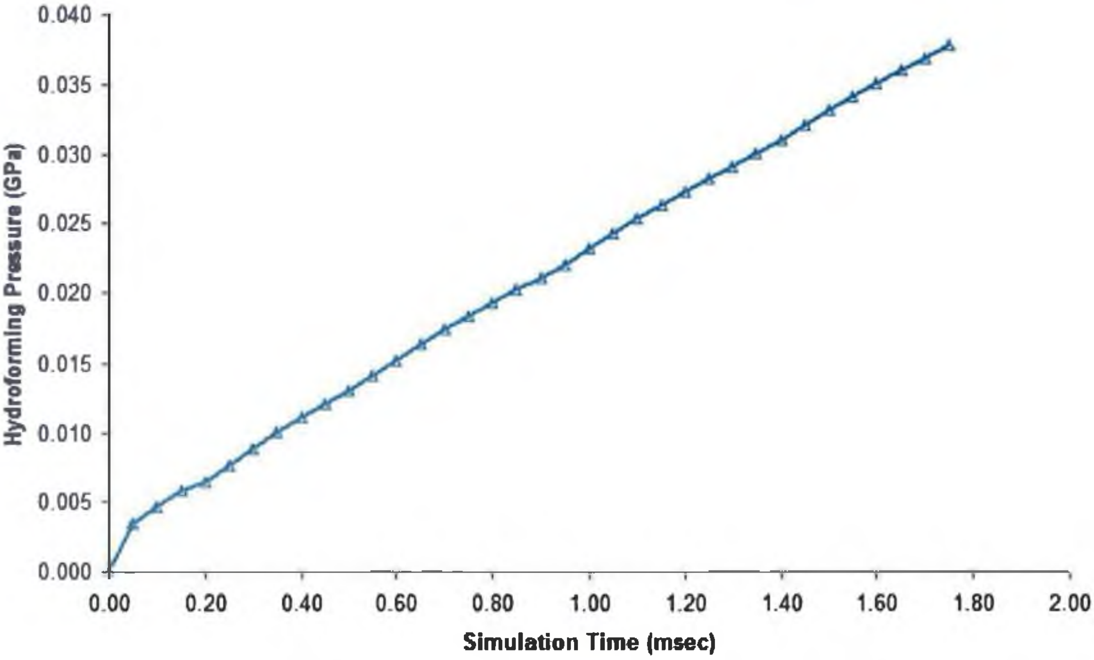

Fig 6.3.2 Pressure curve for T-branch forming obtained using load control algorithm

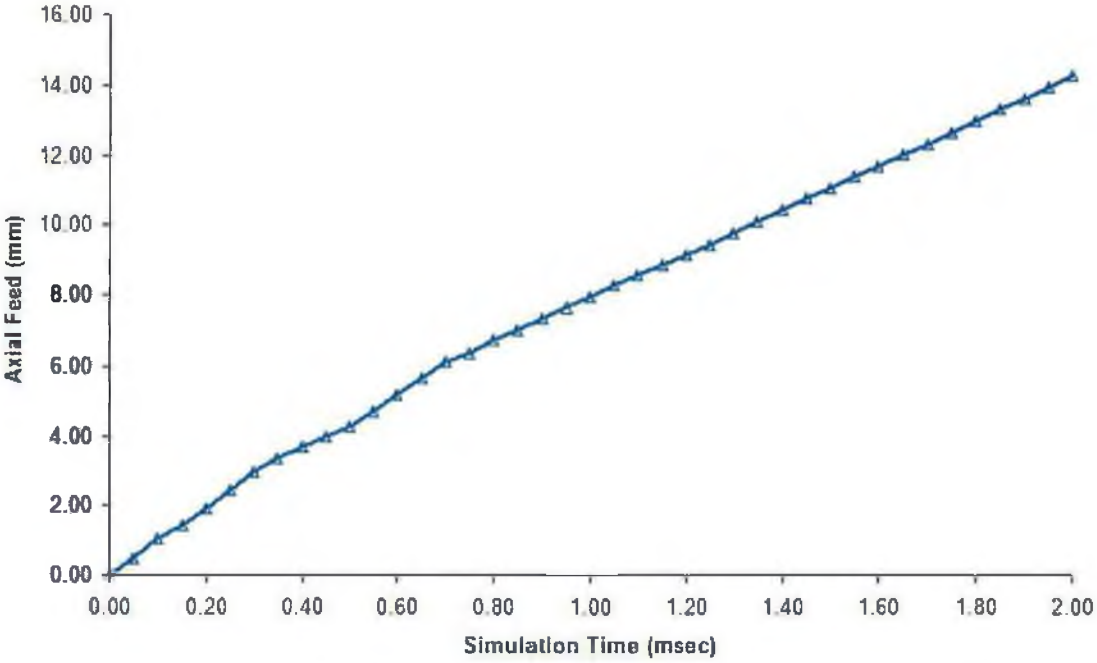

Fig 6.3.3 Feed curve for X-branch forming obtained using load control algorithm

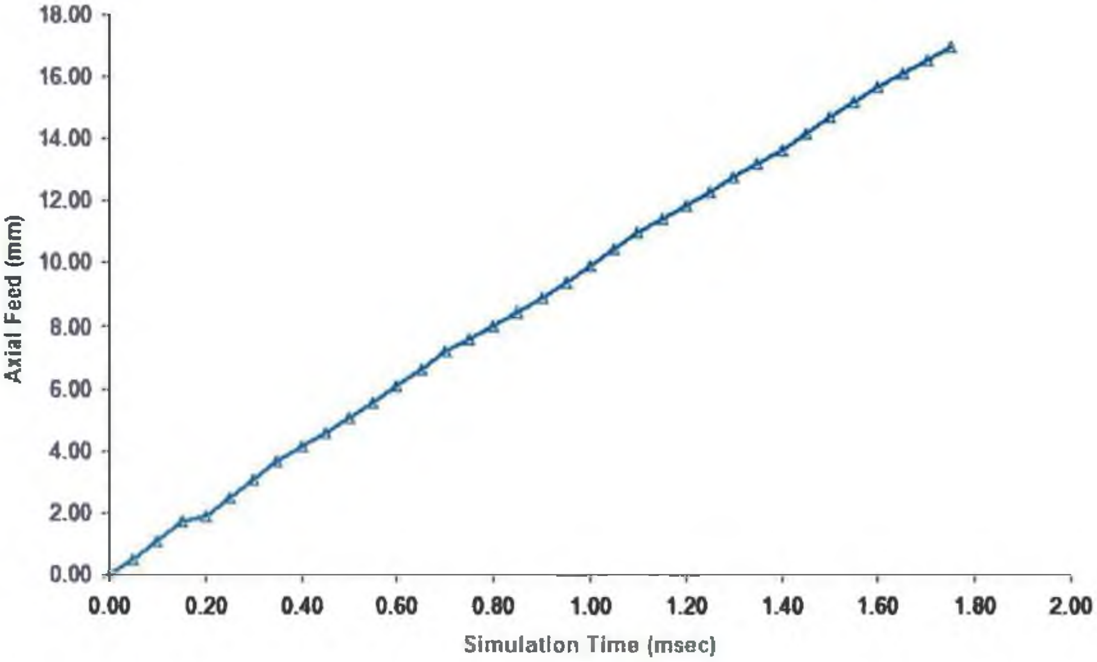

Fig 6.3.4 Feed curve for T-branch forming obtained using load control algorithm

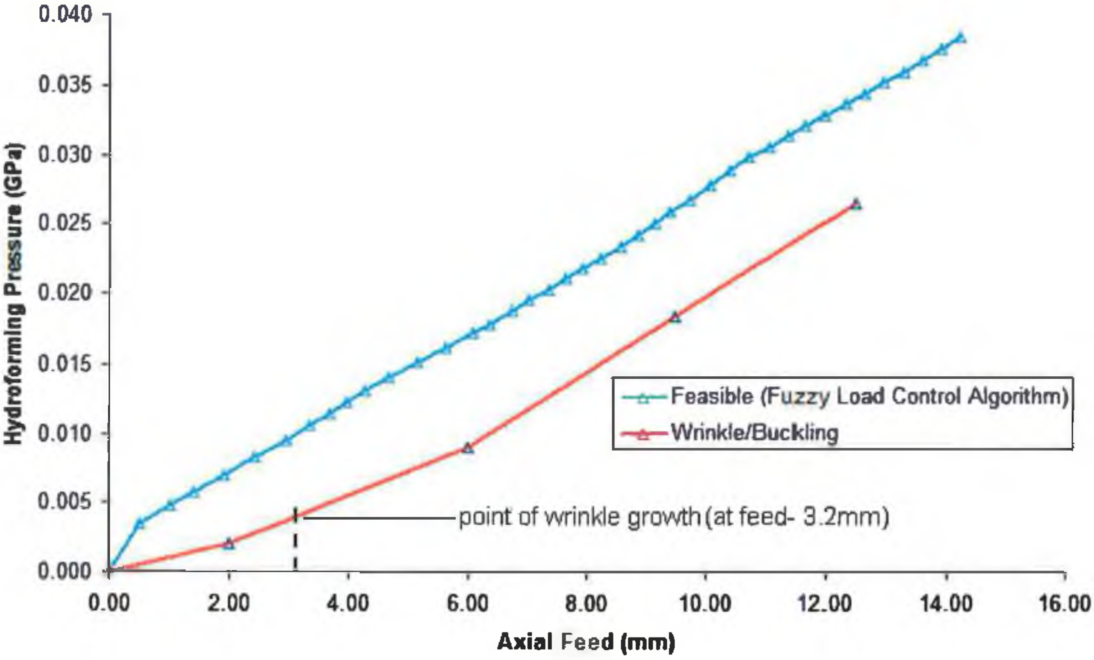

Fig 6.3.5 X-branch load paths – forming pressure as a function of end axial feed (feasible and failure)

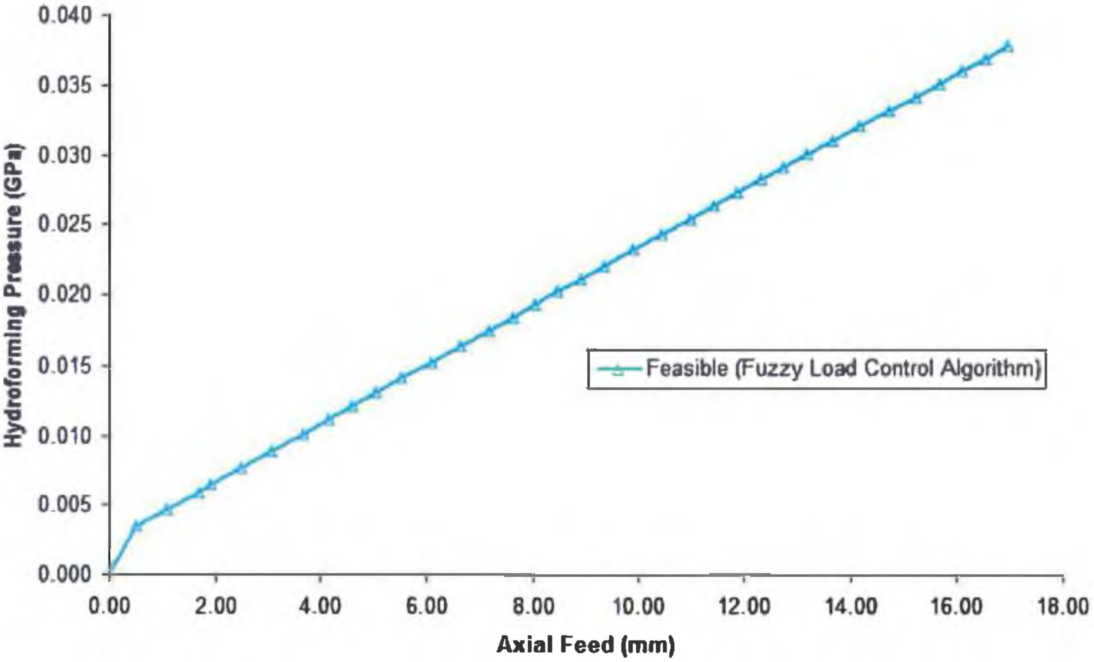

Fig 6.3.6 T-branch load path – forming pressure as a function of end axial feed (feasible)

It can be seen from the plots that the load paths obtained from the simulation for both X and T-branch were almost linear in nature for both pressure and feed curves, this linear nature of the load paths can be explained by considering the load control algorithm development basics (refer to appendix-c). As explained in section 6.2.2, for detection of a wrinkle and its severity a parameter 'A' was defined in the load control algorithm. This parameter defines the degree of wrinkle formation and was categorized under three different classes i.e. few, medium and large as per the number of elements subjected to wrinkle in a particular slice (fig 6.2.17) and as per this categorization the control algorithm selects the particular set of logical rules depending upon the wrinkle severity. In the case of X and T-branch for every step simulation the pressure and feed build up was linear in the initial stage with sufficient internal pressure due to which none or very few elements were subjected to wrinkle formation. Thus, the control algorithm usually selects the particular set of fuzzy rules pertaining to the group with 'less number of highly strained elements' for calculation of the subsequent load step.

To check the validity of the results obtained from the simulation using the load control algorithm, the element strain difference (fig 6.3.8) and normal velocity distribution (fig 6.3.9) profiles over the simulation period for the non-wrinkled X-branch hydroformed tube (fig 6.3.7) were compared with the strain difference and normal velocity profiles of the wrinkled X-branch formed tube with an unstable loading as shown in fig 6.2.15, fig 6.2.16 and fig 6.2.13. Again, the same set of five elements (912, 889, 648, 638 and 625) as selected in the previous section (wrinkled X-branch) was considered for the comparative study. It can be seen that throughout the simulation process the strain difference values for most of the elements were below the critical limits of +/-0.12 as set in the control algorithm except for few elements with a large bending. From the element strain difference plots (fig 6.3.8) it can be seen that element 625, which is subjected to bending across the die radius has developed a high strain difference over the simulation process exceeding the cut-off limit, however the normal velocity of this element is relatively low throughout the process this indicates that the tube surface is subjected to normal bending across the die radius, furthermore from time 0.5msec onwards there is an increase in normal velocity of this element in the negative direction, this proves that the element has lost contact from the die surface. This can be explained considering the dome shape of the bulged section, in the initial stage the element is in contact with the die surface until it bends across the die radius and subsequently with development of the bulge section or with increase in the dome height the element forms the part of the dome loosing contact with the die surface and hence, there is a minor increase in the normal velocity. Considering element 889, it can be seen that the strain difference is almost zero for the initial phase of the simulation with a minor increase in the later part again which is much below the cut-off limit, whereas considering the normal velocity, it can be seen that the velocity development was quite steep from the initial phase of the simulation and was high and fluctuating throughout the process, this condition illustrates pure stretching of the wall or in other terms it is normal expansion of the surface. For element 912 which was subjected to wrinkle in the previous simulation (fig 6.2.13), but in this case it is free from wrinkle that is there is no wrinkle growth in this section, but considering the element strain difference it can be seen that this element is also subjected to a minor bending with almost zero normal velocity, this minor bending is acceptable in comparison to the actual part expansion. Considering the element strain difference and normal velocities for elements 638 and 648, it can be concluded that these elements are subjected to either normal expansion or they are in constant touch with the die surface throughout the simulation period.

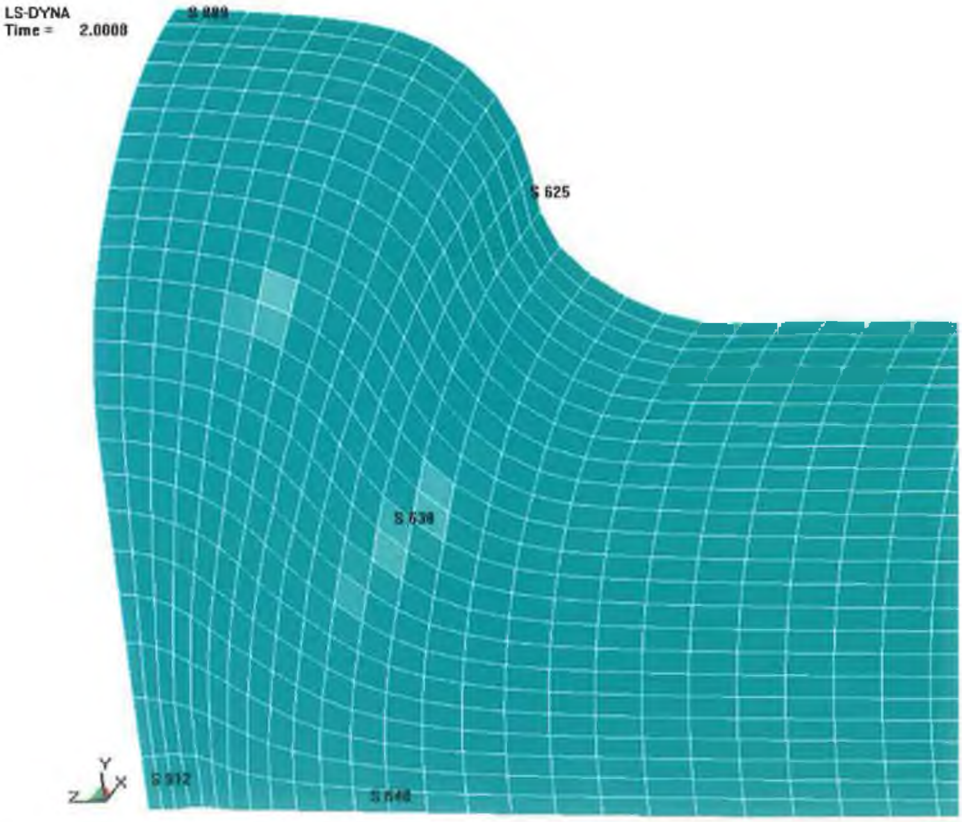

Fig 6.3.7 One-eighth symmetric, X-branch formed tube (simulated using load control algorithm) with element numbers shown on the tube surface

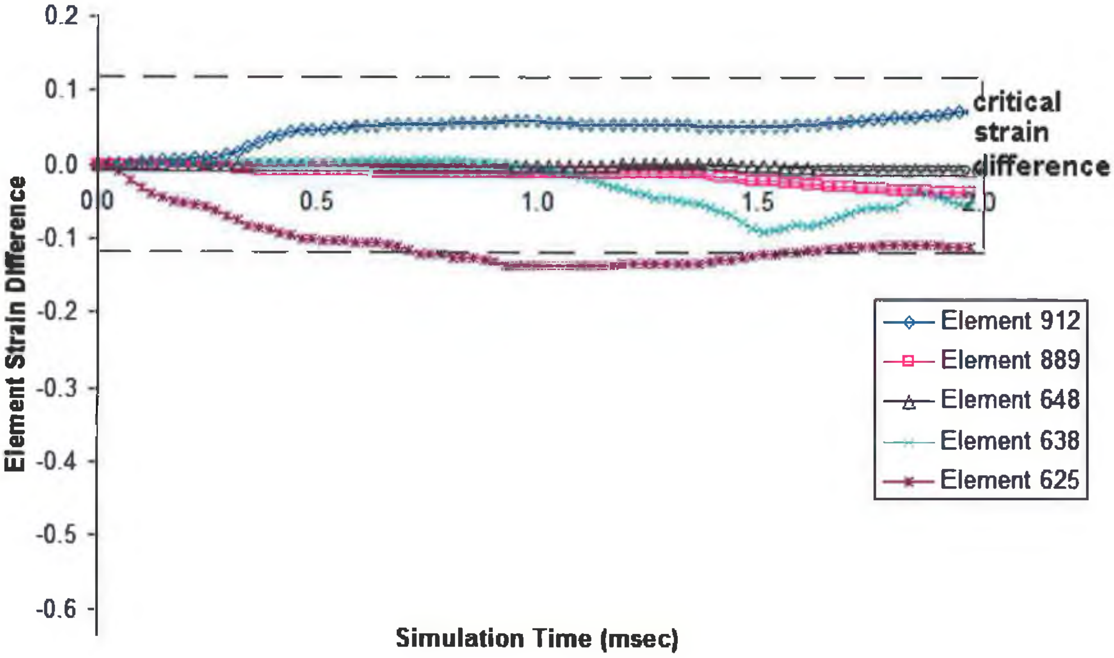

Fig 6.3.8 Development of element strain difference across element thickness (non-wrinkled X-branch expansion- simulated using load control algorithm)

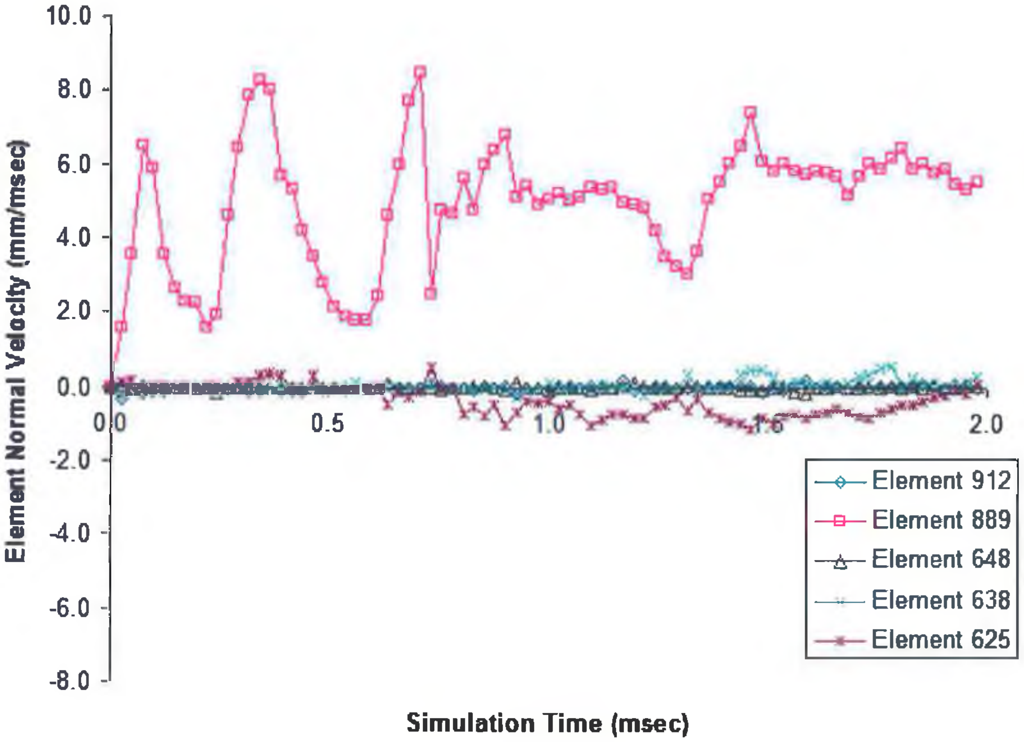

Fig 6.3.9 Development of element normal velocities (non-wrinkled X-branch expansion-simulated using load control algorithm)

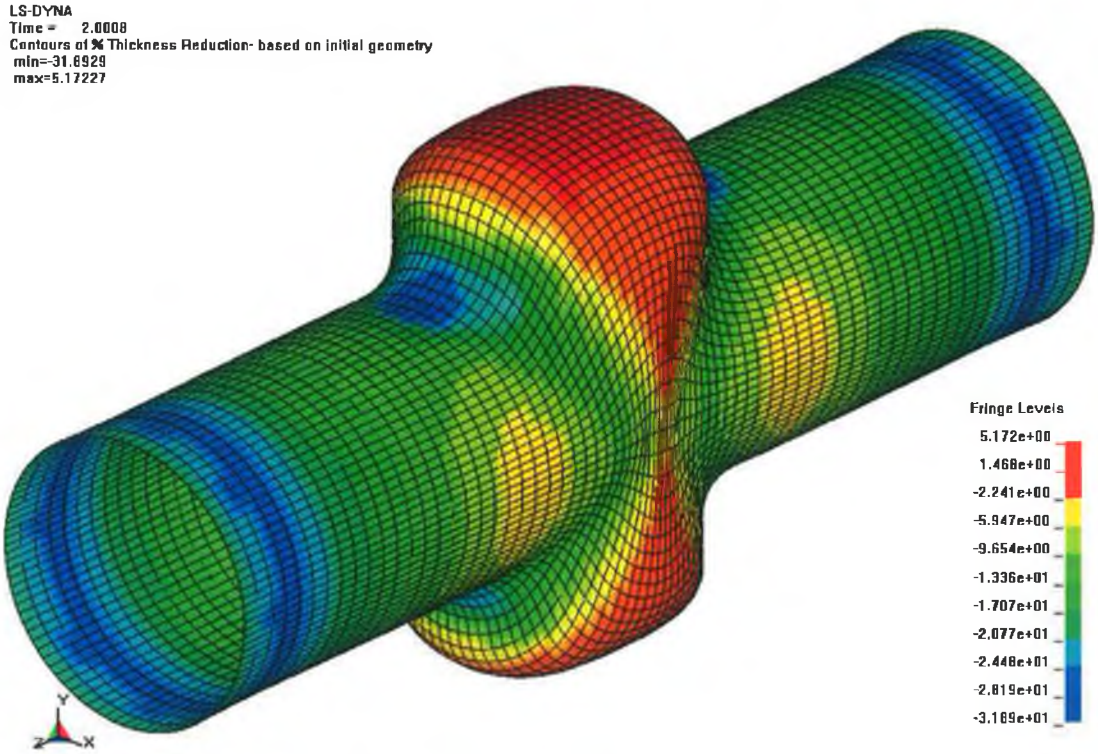

Fig 6.3.10 Contour plot of percentage of tube wall thinning with respect to initial wall thickness (X-branch)

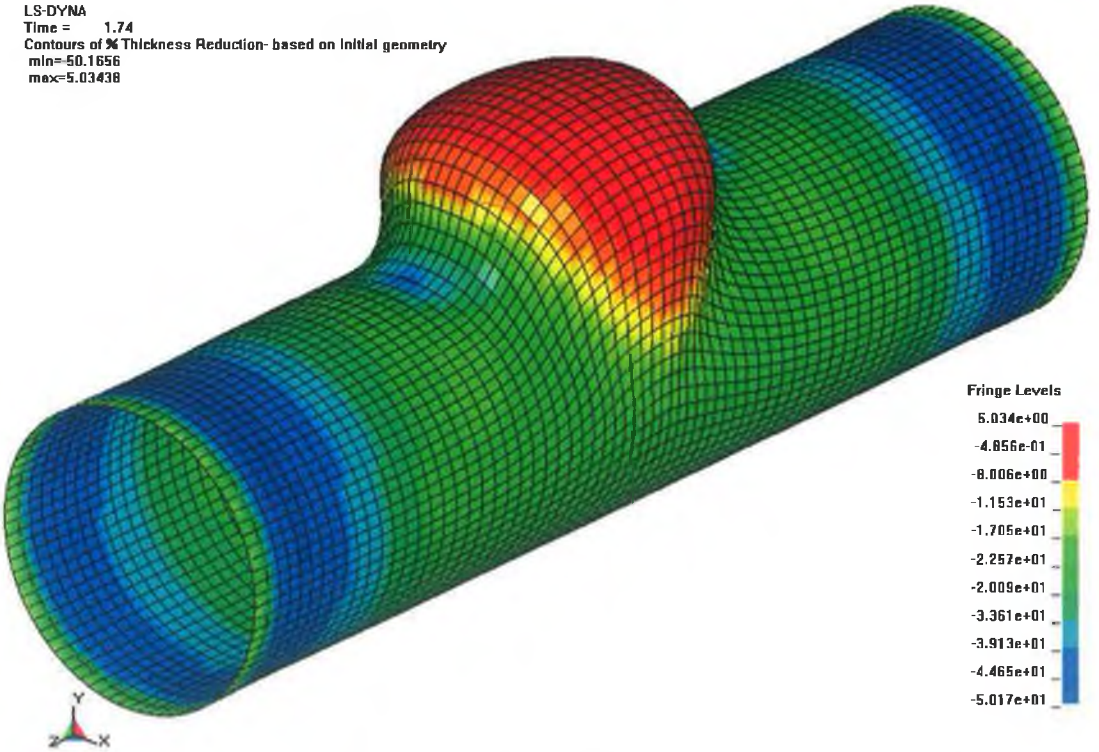

Fig 6.3.11 Contour plot of percentage of tube wall thinning with respect to initial wall thickness (T-branch)

Fig 6.3.10 and fig 6.3.11 show the contour plots of percentage of tube wall thickness reduction for the X and T-branch formed tubes. The maximum wall thickness reduction was approximately 5% of the initial value of tube wall thickness of 1.3mm for both the cases with a maximum developed branch height of 9.89mm with a corresponding end feed of 14.25mm for the X-branch and 9.91mm with a corresponding end feed of 16.87mm for the T-branch expansion. Although the algorithm does not maximize the branch height, however it tries to maximize the part expansion by feeding as much material as required simultaneously applying sufficient internal forming pressure to keep the part well expanded throughout the process, avoiding any wrinkle growth and simultaneously maintaining the wall thickness with in the specified / design safety limit.

6.3.2. Simulation of an automobile structural component with a complex geometry

The developed load control algorithm worked well for hydroforming of components (X and T-branch) from initial straight tubes, however to study its effectiveness for other configurations, a component with relatively complex geometry with variable rectangular cross section and a bent centre line was simulated. The part reflects the geometric configuration of automobile components such as sub-structures or cross-members. The details of the component with its finite element model and simulation results are presented in the subsequent sections.

6.3.2.1. Finite element modelling, loading and solution

The solid model of the die of the component was difficult to build using the present modelling capabilities of ANSYS modeller (pre-processor), hence it was built using Pro-Engineer CAD modelling tool and the model was translated as Initial Graphics Exchange Specification (IGES) file and imported into the ANSYS/LS-DYNA pre-processor. The solid model of the bent tube was built parametrically using the ANSYS modeller. Fig 6.3.12 shows the full model of the die and the initial bent tube.

For simulation of the process, certain assumptions were made. A pre-bent cylindrical steel AISI Type 1018 tube of 70mm (outer diameter), 3mm (thick) and 1001mm (curvilinear length) was used as the blank (fig 6.3.12) and the initial tube wall thickness was assumed constant throughout. By taking advantage of symmetry, a one-fourth symmetric finite element model was used for the simulation. The finite element model of the tube was built with four node 3D thin shell-elements with an assumption that, the material follows a bilinear isotropic hardening law, with Young's-modulus=200GPa, Yield-strength=0.310GPa, Tangent-modulus=0.763GPa, Poisson's ratio=0.27 and Density=7865Kg/m^3. The die surface (fig 6.3.12) which represented the shape of the final component was also built with 3D thin shell-elements with an assumption that a.) the die surface is rigid in nature (i.e. die is non-deformable) and b.) the material follows a linear elastic law. The four node explicit 3D shell elements used was with fully integrated Belytschko Wong Chiang element formulation. Due to the irregular shape of certain faces, the die was meshed with quadrilateral mapped as well as with a mixture of quadrilateral and triangular free mesh. The interface between the tube and the die was modelled with an automatic surface-to-surface contact algorithm with an elastic Coulomb's friction law with a coefficient of friction of 0.05 between the tube (slave) and die (master) surfaces. To avoid failures due to excessive wall thinning of the tube, the maximum allowable wall thinning was limited to 25 % of the initial tube wall thickness (3mm) in the finite element simulation.

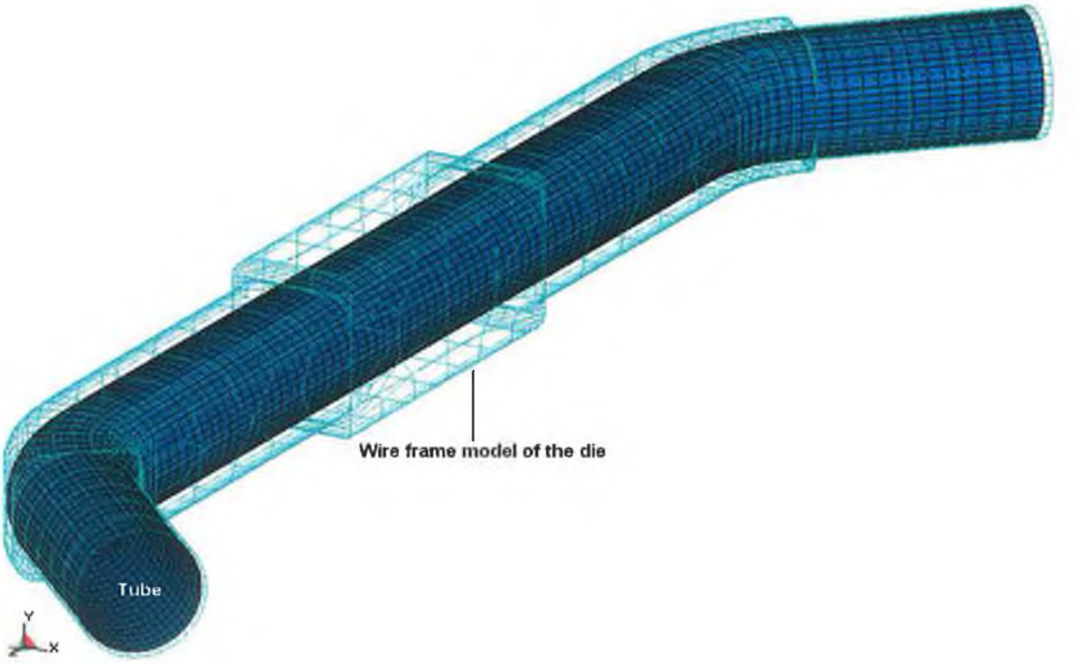

Fig 6.3.12 Finite element model of the pre-bent tube and the die (shape of the component to be hydroformed)

To set the control limits for the critical strain difference value, input membership function limits (strain difference and velocity values) in the load control algorithm, a simple load path was used to simulate the process, which resulted in failure of the part due to wrinkle growth. The elemental strain difference and normal velocities were calculated for different elements subjected to severe wrinkle, this facilitated the assumption of control limits of different input parameters.

The simulation with the load control algorithm was started with an initial small forming pressure and end feed. The forming load as usual was the internal hydraulic pressure along with tube end feeds. The pressure was applied as surface load on the tube inner surface and the end feed was applied as displacement to the tube ends along the tube axis. As the process is quasi-static in nature (illustrated in Chapter 2 and Chapter 3 the slow strain rate deformation in hydroforming processes) thus, to avoid any dynamic effect in the process, the incremental simulation time (load step size) was kept considerably high at 0.05msec. In the simulation, the actual yielding and expansion of the tube occurred when the forming pressure exceeded a value, given by equation-2 for yielding of thin wall tube subjected to internal pressure.

$$P_y = \sigma_y \frac{2t_i}{D_o - t_i} \qquad (2)$$

where,

P_y = minimum yielding pressure

σ_y = yield strength

D_o = initial outer diameter of the tube

t_i = initial thickness of the tube

6.3.2.2. Results

Fig 6.3.13 and fig 6.3.14 show the variation of hydroforming pressure and end feed with respect to the simulation time obtained from the simulation using the load control algorithm and fig 6.3.15 shows the calculated feasible load path (hydroforming pressure vs. end feed) for the successful component (fig 6.3.16) obtained from simulation using the control program and, an assumed load path which resulted in failure of the part due to wrinkle formation (Fig 6.3.17). By comparing the results of these two load paths, it can be concluded that the process is path dependent. Thus, for successful application of the process it is of primary importance to calculate a feasible load path in advance of physical forming of the component using this method of manufacture.

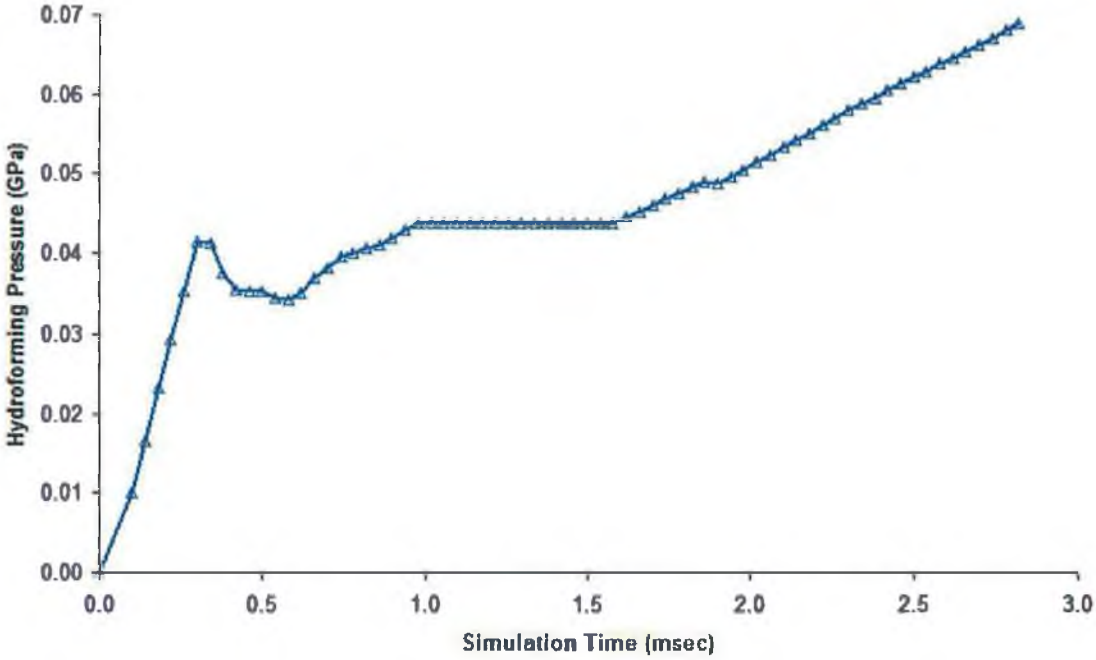

Fig 6.3.13 Pressure curve of the structural part obtained using load control algorithm

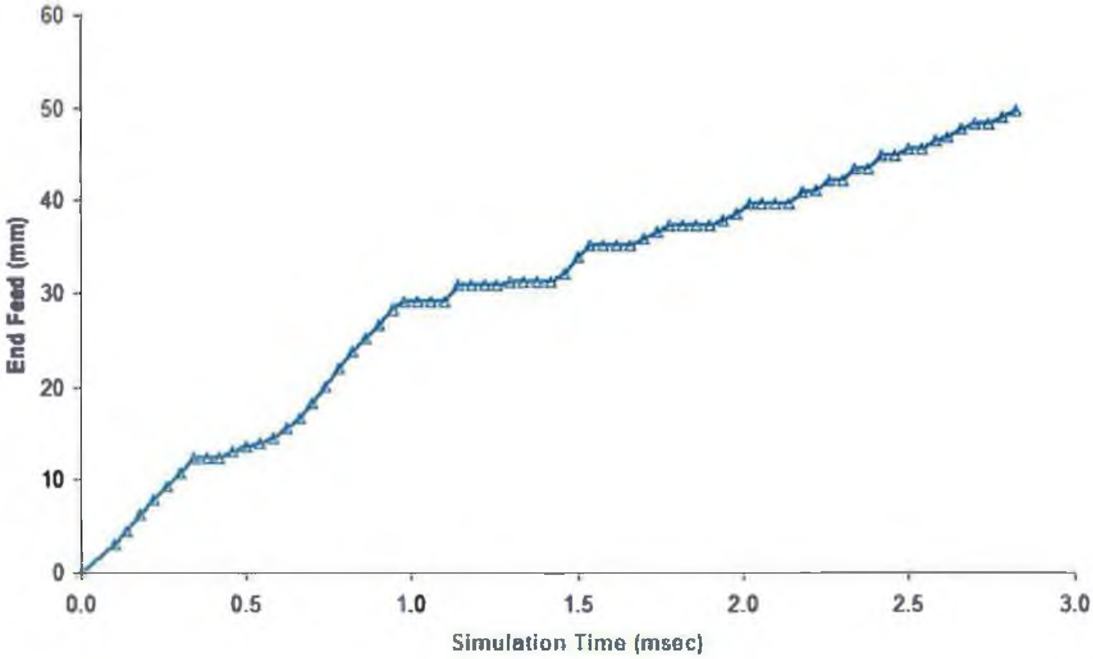

Fig 6.3.14 Feed curve of the structural part obtained using load control algorithm

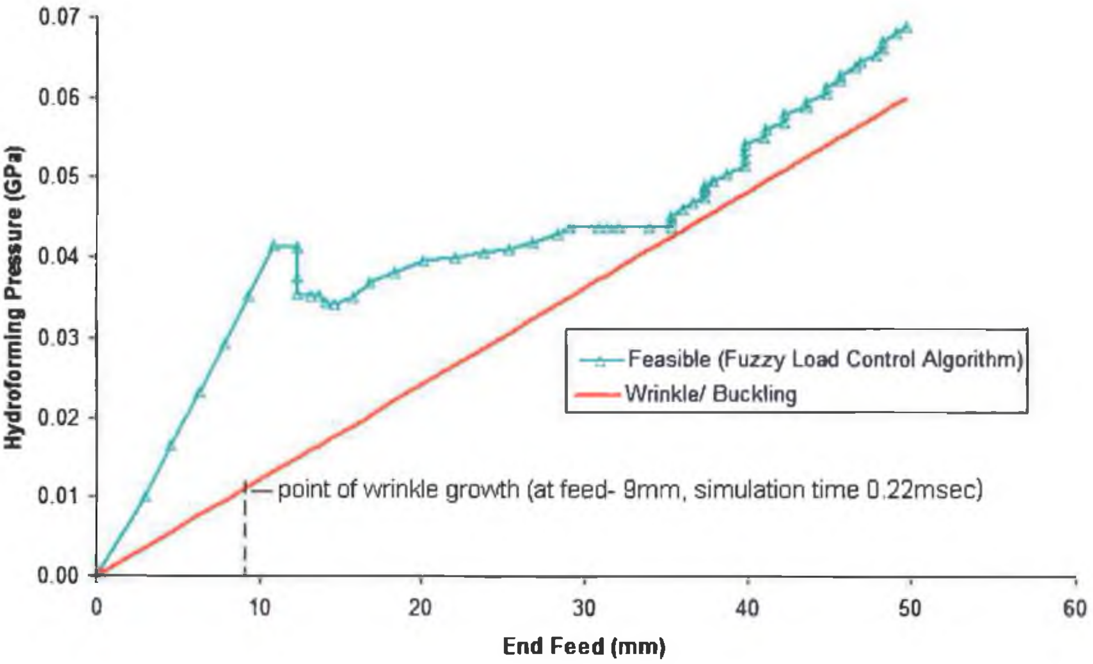

Fig 6.3.15 Forming load paths (hydroforming pressure vs. end feed) for the structural component (1. feasible load path, 2. load path leading to failure)

From the load path obtained using the load control algorithm it can be observed that in the initial stages of the simulation the pressure and the end feed both increased simultaneously, however in the later stages (within the simulation time 1.0msec to 1.6msec, refer fig 6.3.13 and fig 6.3.14) the increase in pressure was relatively low or almost there was no pressure rise as compared to the end feed, this indicates that the control algorithm allowed as much material as possible to be fed through the tube ends simultaneously avoiding formation of wrinkles and excessive tube wall thinning. In the simulation, it was observed that the actual expansion of the tube started when the hydroforming pressure exceeded 0.027GPa (minimum yielding pressure given by equation -2). Fig 6.3.16 shows the final hydroformed shape without any wrinkle, buckling or bursting failure with the contour plots of the final wall thickness distribution. The maximum wall thickness reduction was 21.4% of the initial tube wall thickness (3mm).

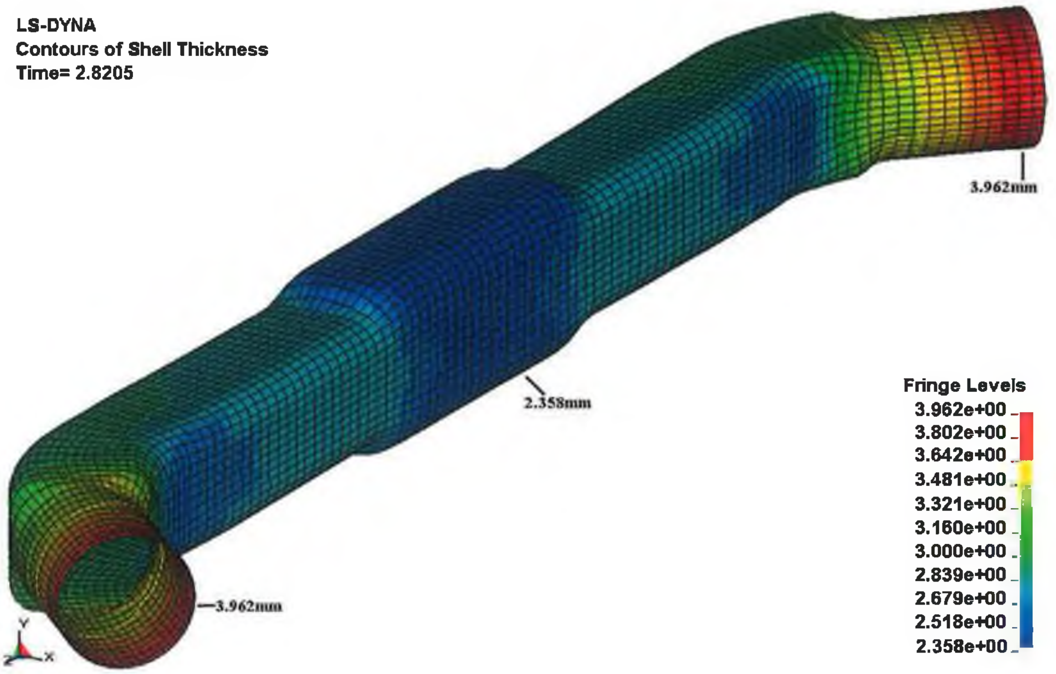

Fig 6.3.16 Contours plot of final tube wall thickness

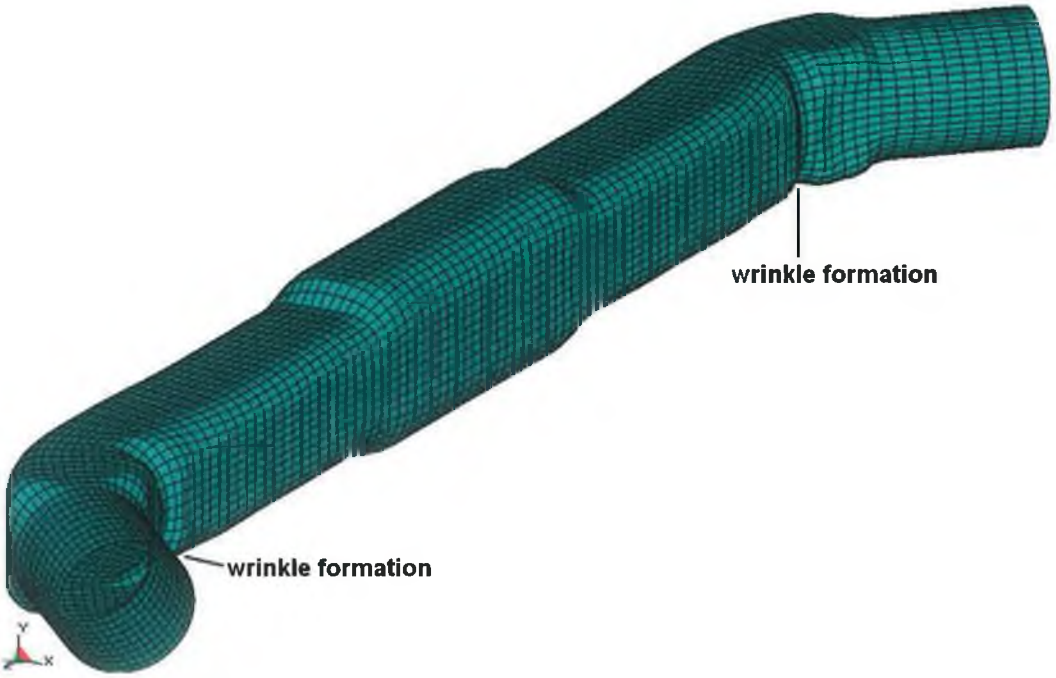

Fig 6.3.17 Failed part due to unstable loading

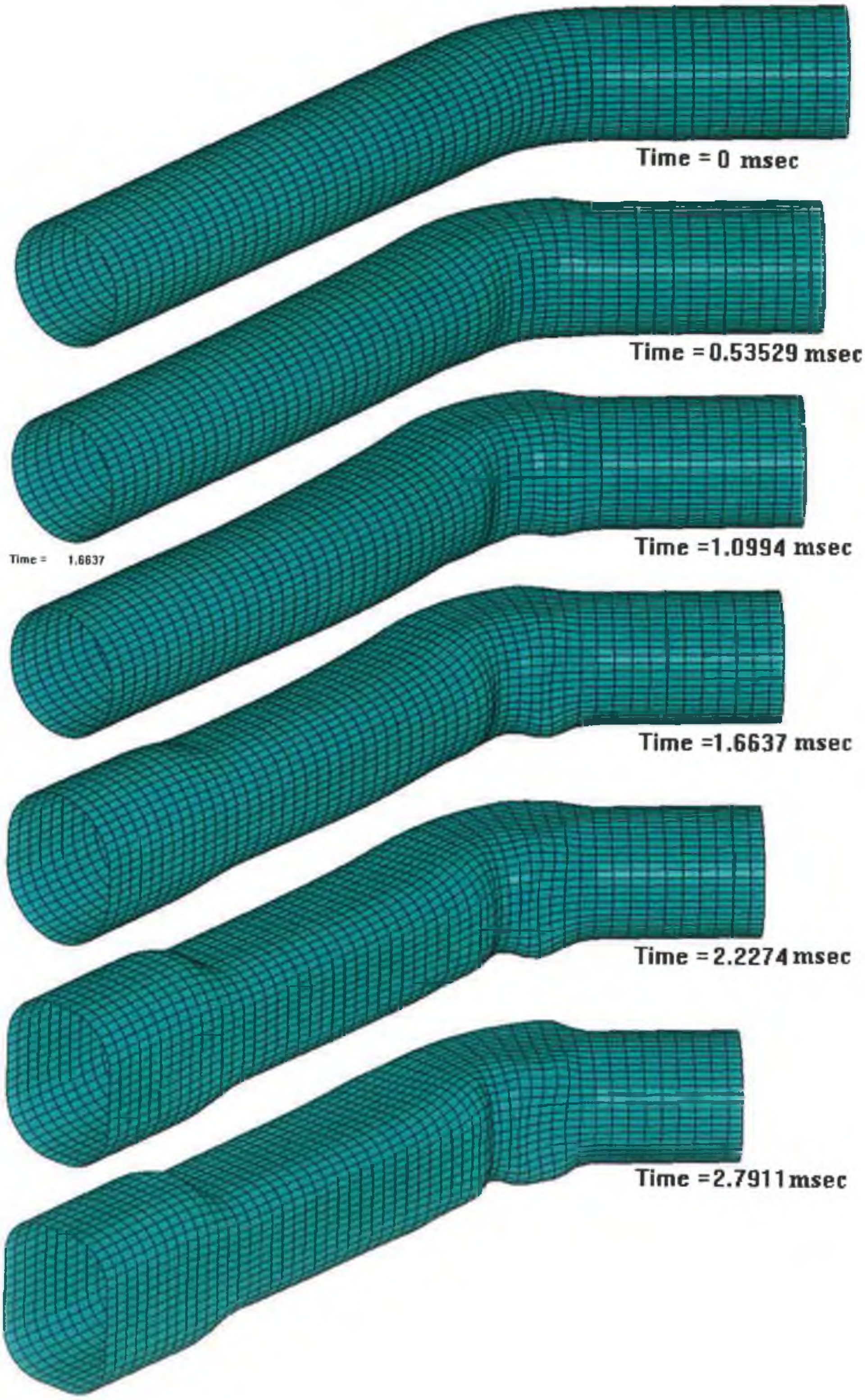

Fig 6.3.18 Development of wrinkle in the structural part (half symmetric model) at different phases of the simulation time (simulated using unstable loading)

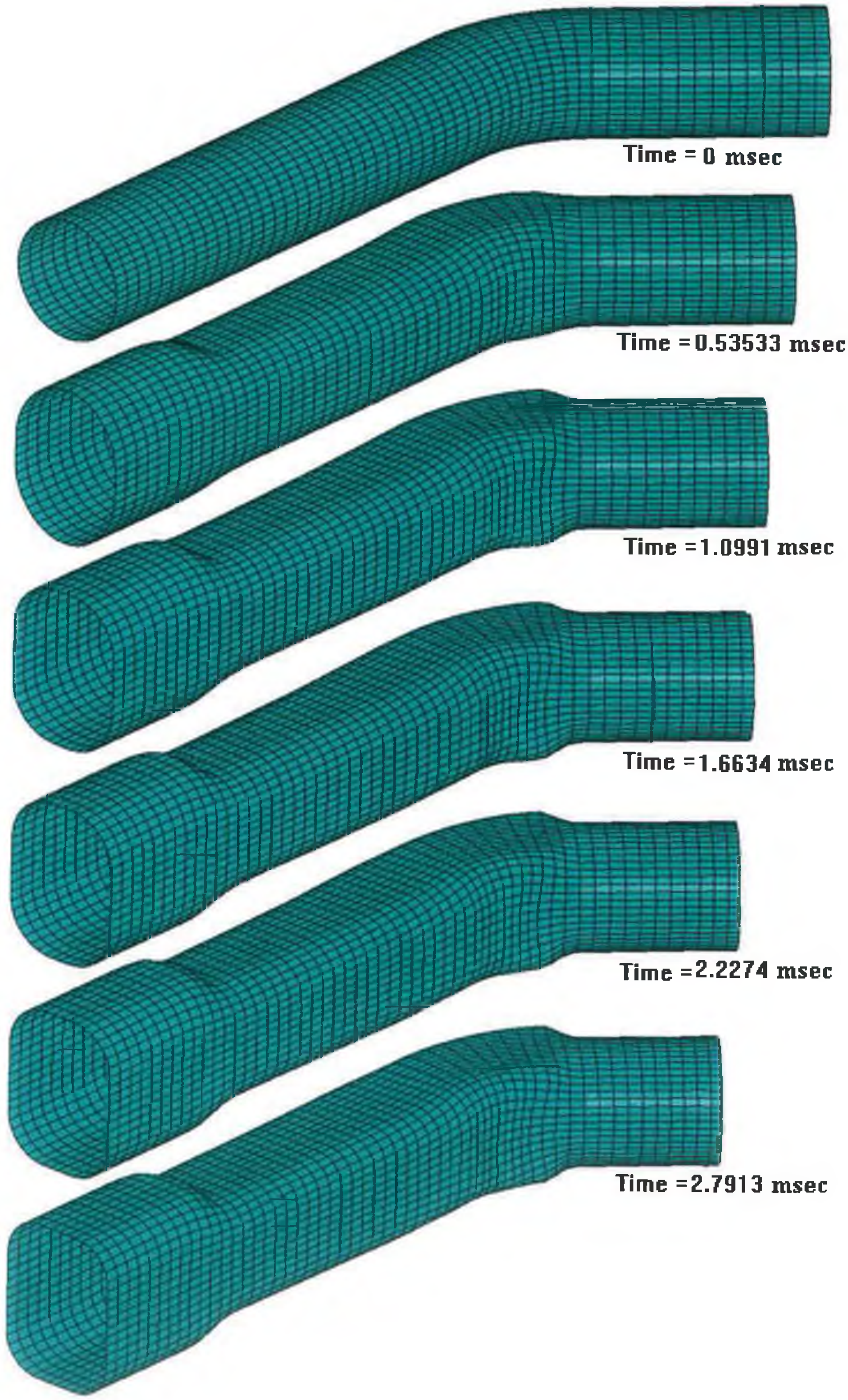

Fig 6.3.19 Non-wrinkled structural part with proper expansion (half symmetric model) at different phases of simulation time (simulated using load control algorithm)

Fig 6.3.18 and fig 6.3.19 illustrate the part expansion at different stages of the simulation phase for both wrinkled and non-wrinkled cases (simulation with load control algorithm). For the wrinkled case, it can be seen that the wrinkle growth started at the bend of the tube near the end in the initial phase of the simulation when the internal forming pressure was relatively low, however with increase of pressure in the subsequent step along with further axial feed, this could not be overcome. This proves that once the component becomes unstable to a certain extent (which depends upon the maximum wrinkle height developed at that instance) then irrespective of further pressure rise, the wrinkle growth cannot be stopped completely, if further axial feeding is not suspended at that instance. Thus, in certain cases, there is a possibility of a certain section of the tube becoming highly unstable and irrespective of further internal pressure rise, the developed wrinkle cannot be eliminated. It is thus very important that wrinkle growth should always be controlled in the initial phase of its development so that the tube remains stable throughout the rest of the process. From the simulation with the controlled load path, it can be seen that in the initial phase the pressure build up was relatively higher with respect to the linear load path (for wrinkle case), this ensures that the tube remains sufficiently expanded during the process, which is required to avoid any wrinkle growth in the initial phase of the simulation when the axial feed rate is relatively high.

With the successful simulation of this complex part with bends and relatively complex geometry with the load control algorithm, it can be assumed that the developed algorithm can work well with most hydroformed components.

6.4. Summary of Chapter 6

This chapter discusses the design and development of an adaptive load control program using fuzzy logic, which was further integrated with an explicit finite element simulation code (LS-DYNA 3D) for calculation of feasible forming load paths (i.e. relation between forming pressure and end axial feed) for different part configurations.

Chapter 7: Discussion

7.1. Experimental study and finite element simulation and analysis of 'X' and 'T'- branch tube hydroforming processes

Different experiments were conducted to hydroform simple asymmetric components such as X and T-branch and finite element simulation models representative of the experimental models were built to analyse the forming process numerically and compare the finite element simulation results with the experimental findings.

The experiments were conducted with different load/machine settings (i.e. with a predefined maximum forming pressure and end axial feed) on the partially automated and upgraded hydroforming machine, from which the actual build-up of internal forming pressure with respect to end axial feed applied to the tube ends during the forming operation (i.e. the forming load paths) were recorded by the LabView data acquisition system. Further the replicas of these experimental forming load paths after minor modification (i.e. smoothing of the values in the fluctuating zone, refer- fig 3.4.3 to fig 3.4.14) were used for finite element simulations along with similar geometric parameters (tube - length, diameter and thickness and die contact surface profiles- such as die corner radius) and material properties of the tube blank and die.

The different results, i.e. branch height (Table 3.4.1) obtained using different load setup/ loading conditions for both the X and T-branch (fig 3.4.3 to fig 3.4.14) show that the part expansion (i.e. branch height) was reasonably good for all the cases without any wrinkle growth on the tube surface. From the experimental load paths it can be observed that the machine setting for the forming process was such that, in most of the cases the build-up of forming pressure was relatively high with respect to the end axial feed in the initial stage of the forming, thus the forming pressure was sufficient enough to keep the part expanded throughout the forming operation. In actual practice, this kind of loading condition is not suitable or advisable as it involves the risk of failure due to excessive wall thinning and bursting. However for the cases presented in this study, there was no failure due to busting of the tube, but it can be seen from wall thickness plots (fig 3.4.19 to fig 3.4.24 – zx plane) corresponding to six different tests (test-a to test-f) for the X-branch expansion, the wall thickness at the X–junction (fig 3.3.4) and at the branch top has reduced substantially in comparison to rest of the tube wall thickness. This was due to large expansion of the tube or development of branch height with relatively less material flow in the deforming zone. This type of condition is not desirable in actual part manufacturing and can be avoided by using proper and balanced forming load paths (i.e. internal forming pressure and end axial feed). On the contrary with a different machine setting in which the initial axial feed was relatively high with respect to the build-up of internal forming pressure (fig 3.4.31), in this case the tube was subjected to wrinkle which could not be suppressed (fig 3.4.32) even with further increase in the internal forming pressure. Similarly from the wall thickness plots of T-branch expansion (fig 3.4.25 to fig 3.4.30), it can be seen that the wall thinning is always higher at the branch top, whereas at the T-junction the wall thickness has increased considerably, unlike X-branch where the possibilities of wall thinning are higher both at the X-junction and as well as at the branch top. Similarly with an initial low internal forming pressure and with relatively high axial feed, both X and T-branches were susceptible to wrinkle growth at the X and T-junctions (fig 3.4.32 and fig 3.4.38). Thus, for the forming operation to be successful (i.e. for proper part expansion without any failure or defects due to wrinkle growth or excessive wall thinning), it is important to set proper control limits (forming pressure and axial feed) at different stages (i.e. at intermediate and final stages) of forming as per the part expansion requirement, in other word for proper part expansion a controlled internal forming pressure with simultaneous controlled end axial feed should be applied.

The close adherence of the finite element simulation results (i.e. for the branch height development -Table 3.4.1 and wall thickness distribution along two different planes -zx and zy planes- fig 3.4.16 and fig 3.4.18 through the mid section of the tube) with experimental results, it can be concluded that the developed finite element model reasonably represent the physical experimental model and the process. The maximum deviation in the branch height predicted by finite element simulations for different tests for both X and T-branch were within +/-5.30% with respect to the experimental findings, whereas the maximum deviation in the wall thickness distribution was within +/-10% with respect to experimental results. The mismatch between the experimental and simulation results can be accounted for by considering the accuracy of the finite element modelling i.e. how accurately the physical geometrical parameters (i.e. tube length, diameter, wall thickness, die geometries, die radius, clearance between the die and tube contact surfaces), contact friction conditions, material properties (material plastic flow laws) of the tube blank and the forming loading conditions are represented or defined in the finite element simulation model. Further finite element simulations along with material formability diagrams can also aid in prediction of the possible zones of failure such as wrinkle growth or excessive wall thinning due to different kind of loadings conditions with corresponding part expansion. The formability diagrams plotted for X and T-branch part expansion were also in good agreement with the experimental findings in terms of the wrinkle detection and zones with excessive wall thinning.

7.2. Part and process design considerations of tube hydroforming components

For an effective numerical simulation and analysis of any physical process (in this case tube hydroforming processes) using finite element methods, the first and foremost important factor to be considered is the proper finite element modelling of the problem. Explicit finite element codes have various distinct advantages over implicit finite element codes, thus they are more suitable for analysis of quasi-static, large deformation metal forming analysis such as tube hydroforming processes.

As most tube hydroforming processes usually involves use of thin walled tube blanks, thus shell elements, which are usually used for analysis of sheet metal analysis, can also be used for analysis of tube hydroforming processes. Furthermore these shell elements have better failure detection capabilities such as wrinkle growth and excessive wall thinning. Furthermore for better wrinkle detection, the size of the element or mesh density also play an important role in sheet metal forming simulation, it can be seen from fig 4.2.2, 4.2.3 and fig 4.2.4, that the wrinkle growth (height of wrinkle) becomes more prominent with elements with finer mesh size or in other word with higher element mesh density. However, with the increase in the element mesh density in the finite element model, the element characteristic length also decreases proportionately, this leads to increase in the overall computation time for that particular simulation model.

The final part expansion characteristics, part geometric characteristics and process performance of any tube hydroforming part depends upon certain parameters which can be broadly categorized as, a.) geometric parameters and, b.) process parameters.

The geometric parameters, affecting the forming process of X or T type expansions are: a.) spline length of the tube, b.) initial tube wall thickness and, c.) die corner radius (at the X or T- blending region)

Different sets of simulations were conducted on X-branch forming to study the effects of the above geometric parameters on the final part features. The results of the simulations (fig 4.3.2, fig 4.3.3, fig 4.3.4 and fig 4.3.5) show that, increase in tube spline length affects the part expansion (branch height development) and also the final wall thickness distribution at the branch top and at the X-junction, and bending along die corner radius considerably. Tubes with larger spline lengths yield parts with shorter branch height with simultaneous increase in wall thinning at the branch top, however the wall thinning at the X-junction and wall thickening at bending along die corner radius show a reverse trend i.e. both decreased with increase in the tube spline length. Trend lines plotted for the variation of branch height, percentage wall thinning at the branch top and at X-junction with respect to the tube spline length show the variations are almost linear in nature (fig 7.2.1, fig 7.2.2 and fig 7.2.3). In other word the development of the branch height and wall thinning at the X-junction are inversely proportional to the initial tube length whereas the wall thinning at the branch top is directly proportional to the initial

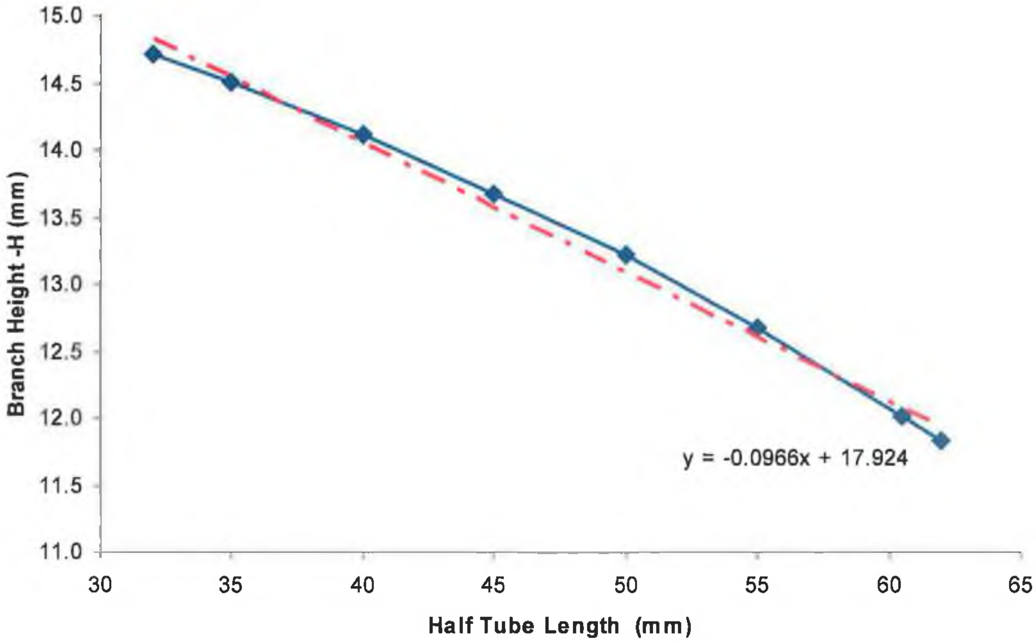

Fig 7.2.1 Variation of branch height with respect to half tube length with the trend line

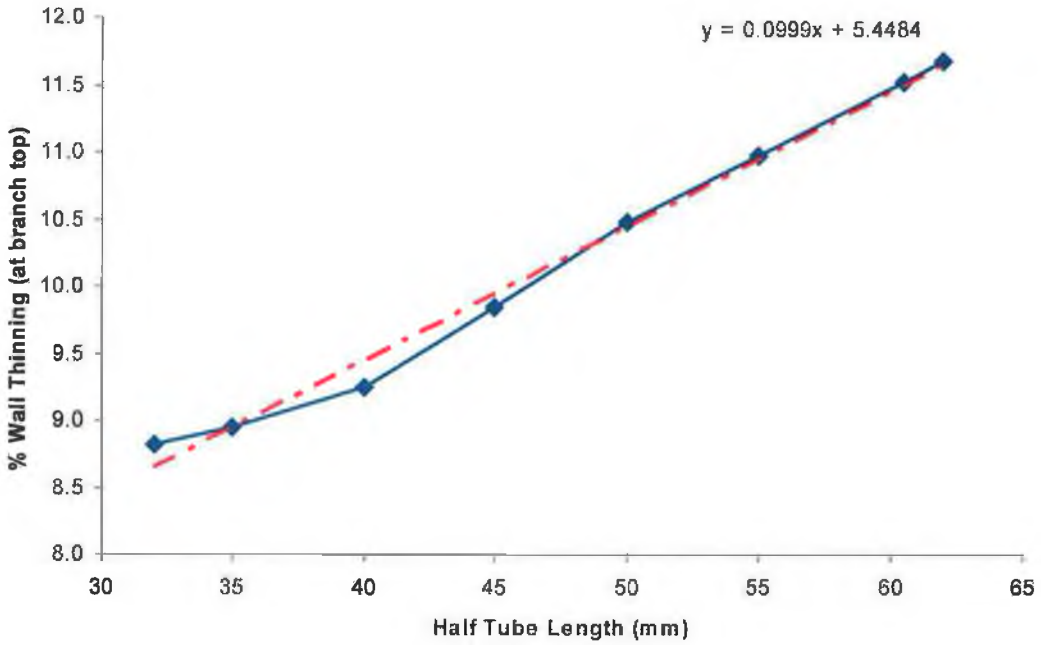

Fig 7.2.2 Variation of percentage wall thinning at branch top with respect to half tube length with the trend line

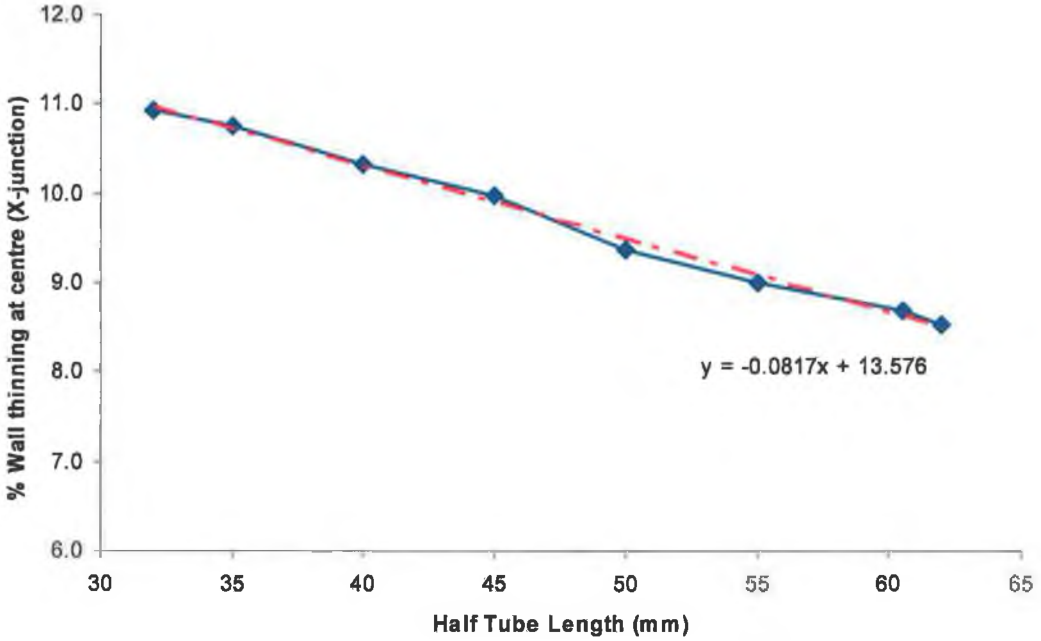

Fig 7.2.3 Variation of percentage wall thinning at X-junction with respect to half tube length with the trend line

tube length. Furthermore the experimental results (fig 4.4.2, fig 4.4.3, fig 4.4.4 and fig 4.4.5) also depict similar trends (i.e. decrease in branch height, increase in wall thinning at the branch top, decrease in wall thinning at the X-junction and along die corner radius with increase of tube spline length) as predicted by simulation results. Thus for a particular design of a part and its process, it is quite important to select the optimal initial length judiciously so that all the required objectives such as maximum branch height and final wall thickness at different locations can be maintained with in the desired design limits.

Similarly, the initial tube wall thickness also affects the final branch height and tube wall thinning. From fig 4.3.6 and fig 4.3.7 it can be seen that with an increase in tube wall thickness, the final developed branch height reduced to certain extent, the branch height variation follows approximately a power law relation (fig 7.2.4) with respect to the initial tube wall thickness. Furthermore increase of initial tube wall thickness is also associated with a lower wall thinning at the branch top, which is one of the desirable characteristics of any tube hydroforming processes. On the contrary increasing the initial tube wall thickness will also require higher internal forming pressure to deform the tube so as to achieve same level of part expansion as obtained with relatively thin walled tubes subjected to lower internal forming pressure.

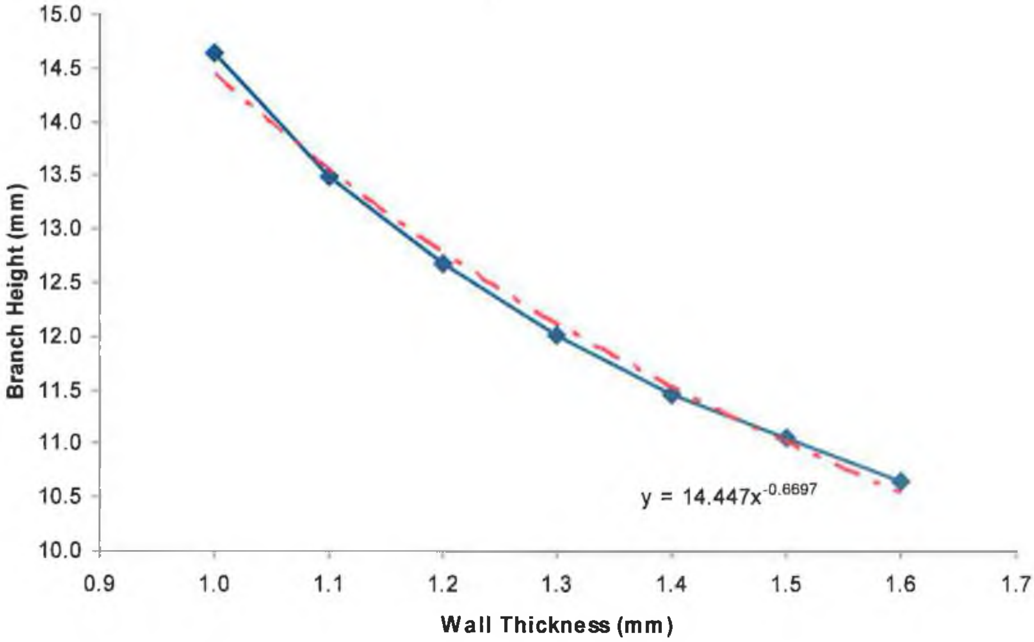

Fig 7.2.4 Variation of branch height with respect to wall thickness with the trend line

Apart from the blank parameters, the die configuration and its various radius and surface curvatures or profiles also have different effects on the part expansion. Fig 4.3.8 shows the effects of the die radius on the final branch height development, it can be seen that with increase of die corner radius, the final branch height also increased proportionately and approximately follow a linear relation (fig 7.2.5), the reason being with bigger radius it becomes easier for the material to flow to the bulged section along the die radius. Very similar results have also been reported by Koc et al [50] for T-branch expansion, where it was shown that with increase of die corner radius the final protrusion height of the T-section increased simultaneously. Thus for actual part design the critical die corner radius should be selected properly for effective flow of material in different zones.

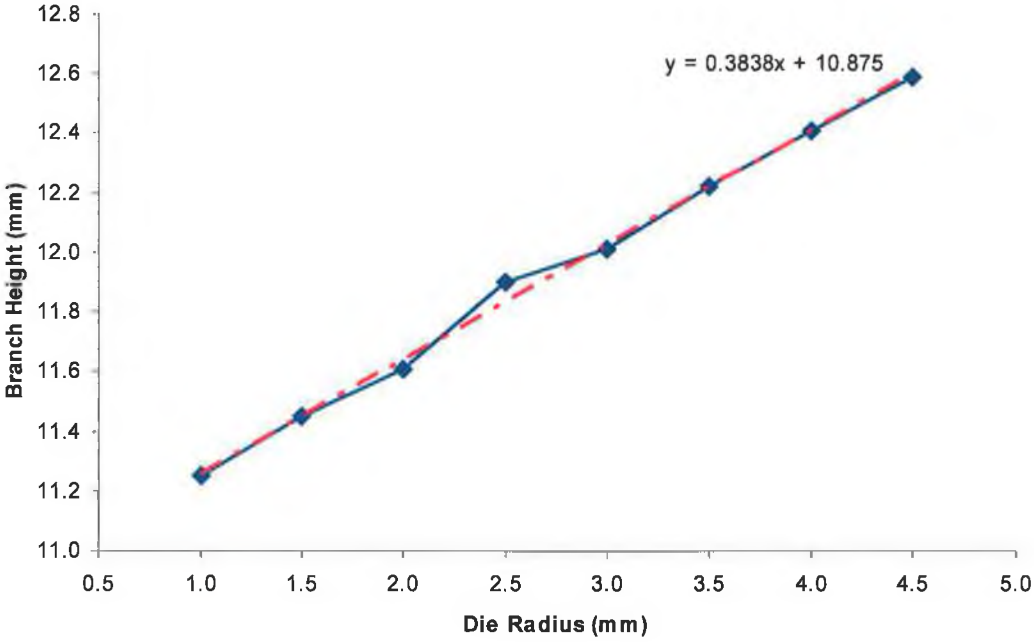

Fig 7.2.5 Variation of branch height with respect to die radius with the trend line

Other than geometric parameters, the process parameters affecting the forming process are mainly:

a.) friction between the die and the tube interface, b.) load paths i.e. pressure and feed curves with respect to time.

Further different sets of simulations on X-branch expansion were conducted to study the effects of various process parameters on the part expansion and final part features. From the simulation results it was observed that the contact surface friction has a negative effect on the final part expansion, i.e. with increase of friction the developed branch height reduced substantially (fig 4.3.9), due to the fact that increased surface frictional

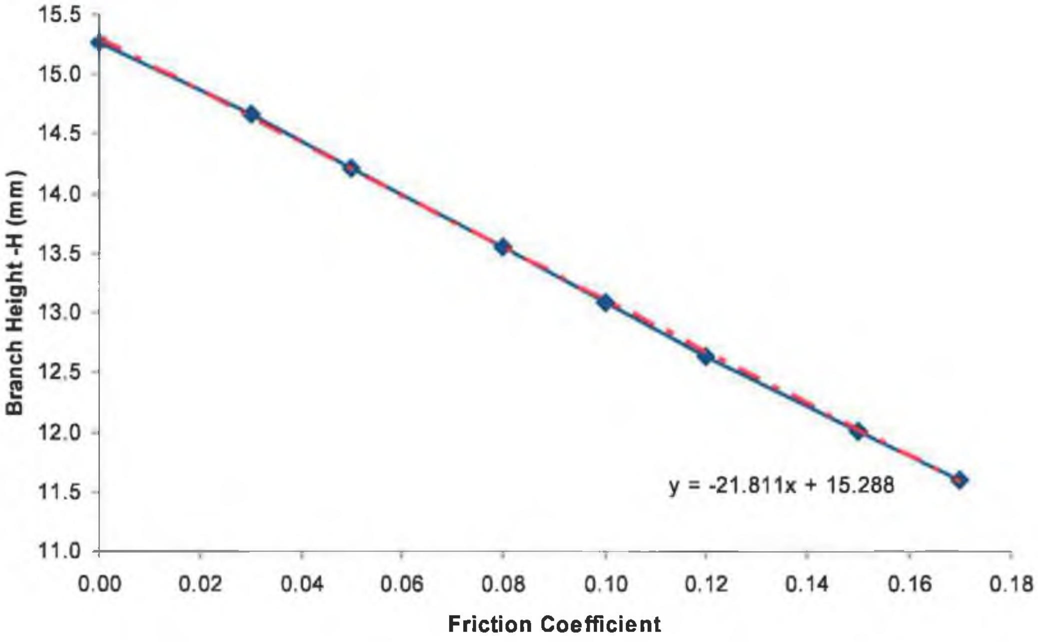

Fig 7.2.6 Variation of branch height with respect to friction coefficient with the trend line

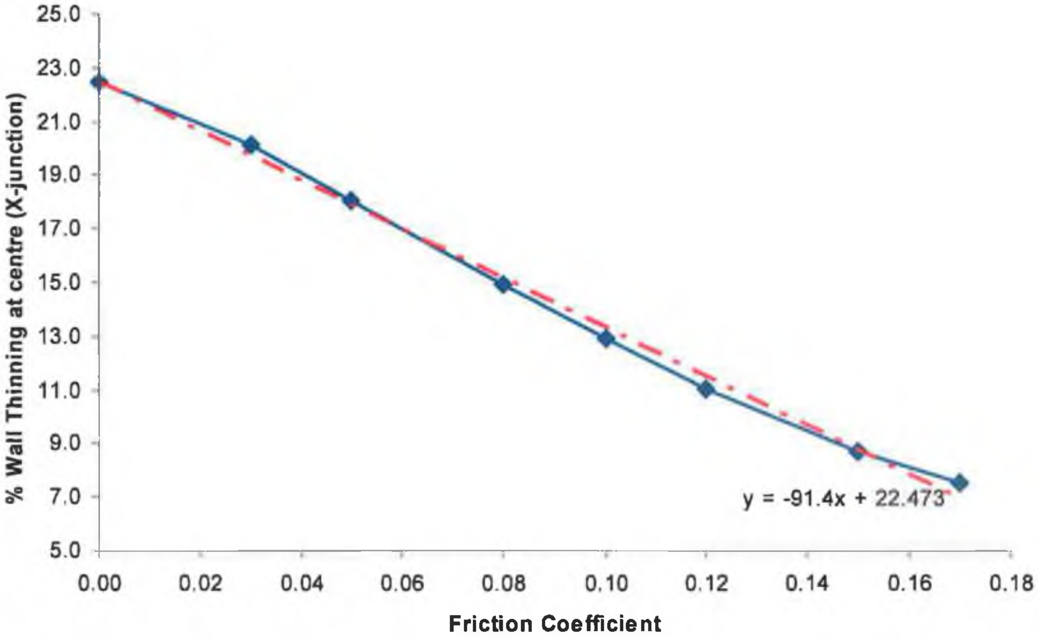

Fig 7.2.7 Variation of percentage wall thinning at X-junction with respect to friction coefficient with the trend line

forces hinders the plastic flow of the material which results in poor branch height development as well as severe thinning in certain parts of the tube especially in the branch top (fig 4.3.10), where the portion expands due to stretching of the tube wall. Whereas with increase of friction coefficient the final wall thinning at the X-junction shows a reverse trend, i.e. the wall thinning decreased in this case (fig 4.3.11). In both the cases it was observed that the variation trend follow a linear relation (fig 7.2.6 and fig 7.2.7). Similarly the wall thickening characteristic at the tube bending along the die radius shows a different trend, it can be seen from the wall thickness plot (fig 4.3.12) in the initial stage (i.e. at lower friction values) the wall thickness increased with increase in friction coefficient and after reaching a peak then starts decreasing in the later part. Thus from all the simulations with varying friction coefficient it can be concluded that proper lubrication condition should be selected so that the wall thinning remain uniform throughout the part.

The part expansion, wall thickness variation and part failure conditions (fig 4.3.14) for a X-branch expansion with different loading conditions (fig 4.3.13) illustrates that the tube hydroforming process is dependent on the forming load path i.e. to avoid any kind of failure and to obtain a proper part expansion (as per the forming die shape) of the part, it is quite important to select proper internal forming pressure and axial feed curves with respect to the operation or process time. The main failures associated with the tube hydroforming processes are either wrinkle formation which subsequently leads to buckling (if further axial feed is applied once the wrinkle has become unstable – fig 3.4.37) or excessive tube wall thinning, subsequently leading to bursting or development of crack (if further forming pressure is applied once the wall has thinned severely- fig 3.4.29). These failures are mainly caused either due to large axial feed with respect to forming pressure or due to high forming pressure with respect to axial feed. From fig 4.3.13 and fig 4.3.14 it can be seen that corresponding to load path-1 the axial feed is too high with respect to the forming pressure and it leads to development of wrinkle at a certain part of the tube (i.e. at the X-junction), associated with wall thickening at the branch top and relatively poor branch height development. Corresponding to load path–7, the loading condition was entirely different in comparison to load path-1 (i.e. almost opposite), as in this case the build-up of the forming pressure was relatively higher with respect to the end axial feed. Thus, the part expansion was reasonably good with maximum developed branch height and without any wrinkle growth, however the wall thinning at the branch top as well as at the X-junction was also maximum for this case. From load path-4 it can be seen that the build-up of forming pressure and increase of end axial feed was quite uniform in nature, and throughout the process there was almost negligible wrinkle growth and resulted in a better part expansion. Thus, it can be concluded that the selection of suitable forming load path is quite important for proper part expansion and to avoid different forming failures or defects.

7.3. Determination of optimal loading paths using finite element simulation and optimization technique

Different optimization techniques can be used to optimize the part expansion of a tube hydroforming process simultaneously eliminating any failure due to wrinkle growth or bursting due to excessive wall thinning during the forming process. The main objective of the optimization of tube hydroforming process is to calculate or determine the optimal or feasible loading path with in the forming zone, which can be further used for design of the process and its toolings. In the present study a subproblem optimization method was used to optimize the process parameters i.e. to determine the optimal relation between the internal forming pressure and end axial feed (defined as design variables) which can maximize the part expansion by maximizing the branch height (defined as objective function) simultaneously maintaining the wall thickness (defined as design constraints) within the specified safety limit avoiding any wrinkle growth (defined as design constraints). For optimization of the loading path for maximizing part expansion during the forming process, piecewise linear (4 linear sets) load paths for forming pressure and end feed were assumed with respect to the simulation time which reasonably captures the load curve profiles for X and T-branch type expansions.

From the optimization results for the X and T- branches, it can be seen that the optimal load paths (forming pressure vs. feed plots- fig 5.5.4 and fig 5.5.11) curves tend to take a profile in which the build-up of forming pressure is relatively high with respect to applied axial feed (resembling load path-5 and 6 illustrated in Chapter 4 in section 4.3.2.2- fig 4.3.13), from this it is quite evident that throughout the process the part remains pressurised so that the chances of formation of wrinkles are minimum. Further for both X and T-branch expansion, the final hydroforming pressure and axial feed values have increased substantially from the initial design values (fig 5.5.2, fig 5.5.3, fig 5.5.9 and fig 5.5.10), from this it is quite evident that the optimization algorithm allowed as much possible internal pressure and end feed to maximize the part expansion simultaneously maintaining the required design constraints such as wall thickness and wrinkle depth below the design or cut-off limits.

Although for the optimization of the process parameters a built-in optimization algorithm with the finite element code was used, however it successfully predicts the optimal load paths for the process within the specified design variable limits simultaneously satisfying the design constraint limits. Further this optimization algorithm can also be used with other design methods such as probabilistic design methods to determine the most important geometric parameter, which can influence the part expansion to the maximum extent (for a particular loading condition) when uncertainties or design variables (as shown in Chapter 4, different parameters affecting the part characteristics such as - initial length of tube, initial tube wall thickness, die corner radius, contact surface friction condition etc.) are numerous.

7.4. Determination of feasible loading paths using adaptive simulation concepts

As demonstrated by experimental study and with finite element simulations of X and T–branch forming, how the actual forming load paths (hydroforming pressure with respect to end axial feed) influence the process performance as well as the physical part expansion (branch height) and part characteristics (wall thinning, wrinkle growth) of the final formed component. Thus it is quite important to determine or estimate a feasible load path in advance for successful application of this process.

A code/macro using ANSYS Parametric Design Language (APDL) script and fuzzy logic concepts was used to develop an intelligent adaptive load control program, which can calculate the feasible load path for tube hydroforming processes with different initial configurations of the tube blank (i.e. from simple straight axisymmetric to complex asymmetric components with axial bends) avoiding all failure modes such as wrinkling and bursting of the tube during the forming process. The developed adaptive load control calculates the feasible loading path in incremental steps by avoiding any wrinkle growth or excessive wall thinning. The control algorithm sense the differential strain across element thickness (i.e. strain difference between the outer and inner surfaces) and normal velocity values of the elements to predict the degree of a wrinkle growth in advance and as per that estimates the required incremental forming pressure and end axial feed for proper part expansion simultaneously eliminating or suppressing any wrinkle growth.

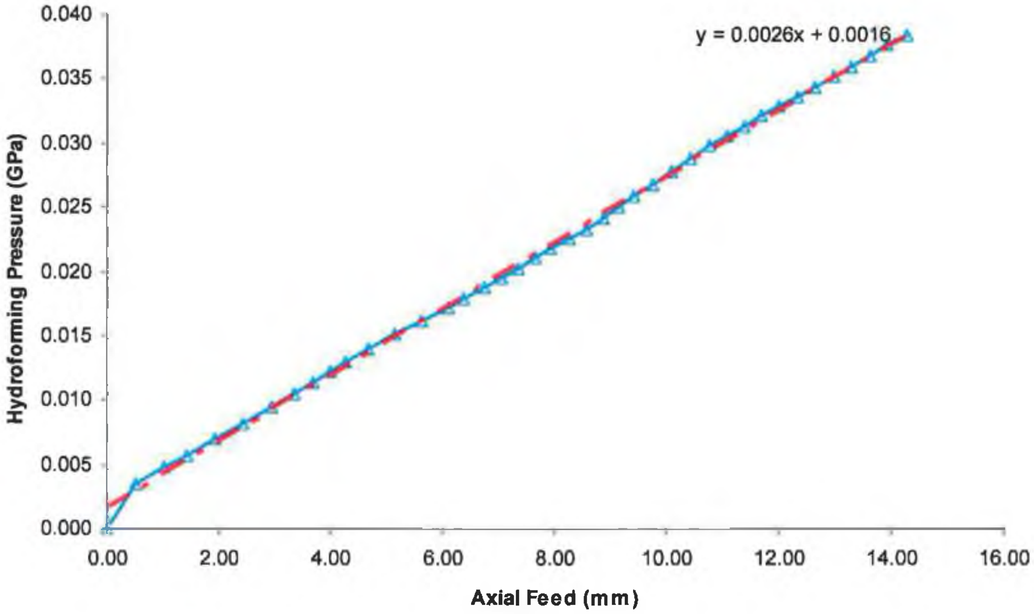

Fig 7.4.1 X-branch feasible load path with trend line

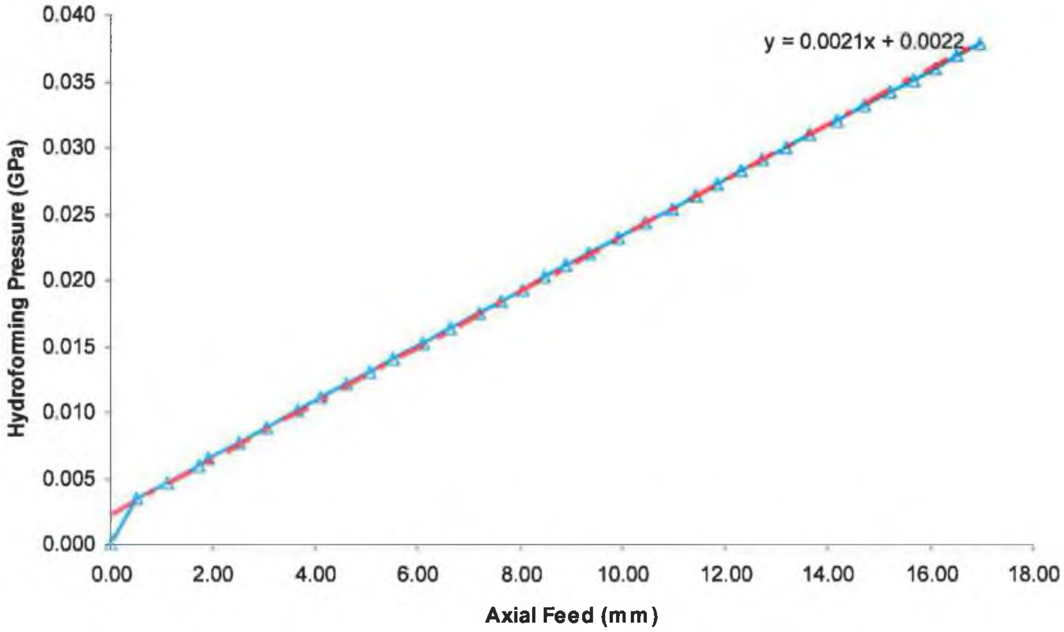

Fig 7.4.2 T-branch feasible load path with trend line

From the calculated load paths for the X and T–branch, it can be seen that both the load paths are linear in nature (fig 7.4.1 and fig 7.4.2) and are comparable with the assumed load path (linear relation between pressure and feed) fig 4.3.13 used in Chapter 4, section 4.3.2.2 (load paths 3 and 4). As it was shown with the simulations, how this type of load path with a relatively higher slope (pressure rise relatively faster than feed rise) usually avoids formation of wrinkle as well as aid in proper part expansion with relatively less wall thinning at the final stage of the process.

Further to study the effectiveness of the developed load control algorithm for other shapes with complex geometries, it was used to calculate the feasible load path for a complex part with axial bends resembling an automobile chassis component. The initial simulation of the part was done with a linear load path (fig 6.3.15). With this load path the part failed due to severe wrinkling near the tube bends and resulted in a poor part expansion. Simulations with the load control algorithm calculated an entirely different load path (fig 6.3.15) with an initial linear relation between the forming pressure and end axial feed over a period of simulation time, however in the later case the pressure rise was relatively low in comparison to the axial feed and for a certain range the pressure remained fixed with further axial feed. Thus, the algorithm maintained as much pressure as required to keep the part expanded simultaneously feeding an adequate amount of material from the tube ends to avoid wrinkle growth or excessive wall thinning. With the load path obtained using the load control algorithm it was possible to eliminate the wrinkles near the tube bends.

With the developed load control algorithm, it was possible to calculate the initial feasible load paths for the hydroforming processes. Once the feasible load paths are obtained then it can be further tuned or refined to make the path optimal by setting the individual objectives. In other words, once the key points of the load curve are obtained from this adaptive simulation using the intelligent load control algorithm, then it can be used as an initial design load path and optimization algorithms (as illustrated in Chapter 5) can be used to further maximize the part expansion with different objectives functions or functional requirements. The objectives may differ depending upon the part configuration, such as it may be the maximum branch height in the case of a X or T-branch type expansion, or it may be the total volume in case of axisymmetric components.

From all the above studies, it can be concluded that for a successful application of any tube hydroforming process it is quite important to understand the actual process behaviour which is mainly affected due to variation of different process (loading paths, contact interface friction etc.) and geometric (length, diameter, wall thickness of tube, die corner radius etc.) parameters. Thus, this calls for selection of proper a.) forming process parameters and, b.) tube and die geometric parameters, and hence require proper design and optimization of the process and it parameters in advance. Thus experimental analysis and numerical simulations coupled with advanced optimization algorithm and adaptive load control programs can provide better insight of the actual process, its design and optimization in greater detail.

8.1. Conclusions

1. Experimental study and finite element simulation and analysis of 'X' and 'T'- branch tube hydroforming processes

- Experimental and numerical studies on hydroforming of X and T-branches show, for proper part expansion without failure due to wrinkle growth or excessive wall thinning it is important to apply proper controlled internal forming pressure along with end axial feed.
- In case of X-branches the chances of wall thinning are higher at the X-junction and at branch top, whereas for T-branches the chances of wall thinning are higher at the branch top when the part expansion occurs mainly due to initial high forming pressure with relatively low axial feed.
- In case of both X and T-branches the chances of wrinkle growth are higher at the X and T-junctions respectively when the part expansion occurs mainly due to initial low forming pressure with relatively high axial feed.
- Finite element simulations coupled with forming limit diagrams can determine the possible failure zones of a tube hydroforming process for different loading conditions with corresponding part expansion.

2. Part and process design considerations for tube hydroforming components

- Thin shell elements have better solution and analysis capabilities and better defect prediction capability for sheet metal forming operations.
- Shell element size (i.e. mesh density) has a considerable effect on defect determination and, in particular, on simulation of wrinkle growth. With higher mesh densities wrinkles can be more effectively determined.
- Initial tube length has a considerable effect on the final part expansion (branch height). With increased tube length the branch height decreases with simultaneous increase in wall thinning at the branch top and decrease in wall thinning at the X-junction.
- Initial tube wall thickness also has certain effect on the part expansion, with thinner walled tubes it is possible to achieve higher branch height at the cost, however, of relatively higher wall thinning at the branch top.

- Varying the die corner radius also has an effect on the part expansion. With larger die radius the metal flow into the bulged section is much better with higher branch height. However selection of die radius is limited by the part geometry requirement.
- The contact interface friction has a considerable effect on the flow of material and part expansion. With increased friction coefficient, the developed branch height reduces considerably along with increases in wall thinning at the branch top and a simultaneous decrease in wall thinning at the X-junction.
- Combined axial feed and internal pressure are required for proper expansion of the tube to avoid any defects due to wrinkling or bursting during the forming process. Thus a balanced loading is required for the process. A very high pressure at the initial stage of the process with respect to low axial feed can result in bursting failure due to excessive wall thinning, similarly a high axial feed at the initial stage of the forming process with respect to low forming pressure can cause wrinkle or buckling of the tube.

From the above it can be concluded that for a better design of a tube hydroforming part and its process and, for a successful application of the process for manufacture of a sound component, prior knowledge of effects of different geometric parameters of tube and die, and process parameters (interface friction and loading paths) are quite important.

3. Determination of optimal loading paths using finite element simulations and optimization techniques.

- With the successful application of the subproblem approximation method coupled with finite element simulation for hydroforming process optimization, (i.e. determination of optimal forming pressure vs. axial load relation) by maximizing the part expansion subjected to various design constraints such as wrinkle height and wall thinning, it can be concluded that conventional optimization techniques/algorithms can also be used to optimize hydroforming process parameters.
- From the optimal load paths obtained for X and T-branch forming with numerical optimization it can be seen that for both the load paths the hydroforming pressure build-up rate was relatively higher with respect to end axial feed. This kind of load path usually avoids or arrests wrinkle growth while simultaneously maintaining wall thinning.

- The failure criteria used for the optimization process were wrinkle growth and wall thinning. For optimisation purposes the possible location of formation of the wrinkle was assumed to be at the X or T-junction (fig 3.4.23, fig 3.4.25, fig 3.4.30) which was determined from prior experiments and simulations of X and T-branch components. However this concept may not hold good for hydroforming of other geometries where the possible zones of wrinkle growth may not be exactly known.

4. Determination of feasible loading paths using adaptive simulation concepts

- Element strain difference across thickness (i.e. strain difference between the outer and inner surface) along with the normal velocity during the deformation process can be useful to predict the stability (i.e. wrinkling tendency, wrinkled or non-wrinkled) of a particular area during the forming process subjected to combined internal forming pressure and end axial feed. A wrinkle growth can be defined by considering these two factors (strain difference and normal velocity) such as if an element has a very high strain difference between its outer and inner surfaces and is subjected to a very high normal velocity then it can be said that the element is subjected to wrinkle.
- Logical terms can be used to define the severity or degree of a wrinkle growth on a tube surface based on the element strain difference and normal velocity. These terms can also define possible corrective action to be taken in terms of adjustment of process parameters (forming pressure and end feed) to overcome or suppress the developed wrinkle.
- Using the logical terms and fuzzy rules, an intelligent adaptive load control program was developed which can estimate wrinkle growth in advance and simultaneously adjust the process parameters to suppress wrinkle growth in the course of the numerical simulation of the forming process.
- The developed load control algorithm is capable of calculating feasible forming load paths for simple to complex asymmetric hydroformed part geometries.

With the successful application of the adaptive load control algorithm to calculate the feasible loading paths of parts with different geometries and shapes, it can be concluded that the developed load control algorithm can also determine feasible load paths for other tube hydroforming parts with various complex part geometries or configurations.

8.2. Thesis contribution

Tube hydroforming is a relatively new manufacturing processes and due to its distinct advantages over conventional manufacturing process, it has recently being widely used in the automotive, aerospace and other industries for manufacture of seamless, lightweight and near-net-shape components. The application ranges from simple tubular joints to complex automotive chassis. The understanding of the process to date has been very limited and important aspects such as effects of various geometric parameters of the tube blank and the forming die and, effects of process parameters, on the final part expansion and deformation process have been largely unknown. As a result, part defects and failures in the process have been common and are of major concern to industries using such manufacturing processes. These part defects can be avoided to a major extent by selecting proper forming loading conditions as well as by optimizing the process and part design parameters. The finite element simulations of the hydroforming processes, application of the optimization methods for process parameter optimization and the development of an intelligent process control algorithm to calculate the feasible load paths in advance will contribute significant knowledge in this area for tube hydroforming part and its process parameter design and optimization. In particular the research contributions that are associated with this work are:

1.) Detailed experimental study of the process with different part configurations and analysis of the process behaviour, part expansion, final part features and failure modes of hydroformed parts. This study will facilitate better understanding of the forming process and part expansion characteristics of asymmetric type expansion in greater detail.
2.) Finite element modelling of the parts using similar experimental loading, boundary conditions and material properties of the tube blank to simulate the actual forming process and further validate the finite element results with experimental results so as to develop a better understanding, coherence of the actual forming process with the numerical simulation and also to develop a standard for development of finite element simulation models for further analysis and optimization of the process.
3.) Process and part design parameters of a X or T-branch part to be considered for design and manufacture by this method. These concepts can also be used as design guidelines for other parts to be manufactured by this method.
4.) Application of optimization concepts for optimization of processes parameters of tube

hydroforming processes such as X and T-branch. The optimization procedure and concepts can also be used for design of process parameters for other part geometries.

5.) Development of an adaptive load control program using fuzzy logic and explicit finite element simulations for calculation of feasible hydroforming load paths for different part configurations. The program can be used to calculate feasible hydroforming load paths avoiding all failure modes for parts with axisymmetric or asymmetric configuration from straight tubes or tubes with a pre-bent centre line.

With the above study it is possible to reduce the design and prototyping lead time of any tube hydroforming process considerably.

8.3. Future work

1. Modification and new improvements in the adaptive control program

Although the developed fuzzy load control algorithm works well for certain configuration of tubes and can calculate the feasible load paths, further improvement can be done or certain additional features can be added to the algorithm so that it can detect all failure conditions and calculate the feasible load paths more accurately. Further improvements that can be made or incorporated in the control program are as detailed below:

1.1. Simple improvements without any additional new features

The present algorithm uses a concept in which all the new additional load steps are added to the original load path and again the entire simulation is run with the appended load path. Improvements can be done by taking advantage of the LS-DYNA 'Restart' program capabilities so that instead of running the entire or full simulation with the appended load path, only part of the new additional load step simulation can be run. This would result in a considerable saving of computation time and costs for simulation of components with a relatively large finite element mesh.

1.2. Complex improvements with additional new features

Integration of the optimization tool with the adaptive simulation control program i.e. develop a methodology in which objective functions with design constraints can be incorporated in the program (such as maximizing the part expansion simultaneously maintaining the wall thickness within the safety limits for a partial load path) and the control program can calculate the load path simultaneously controlling the wrinkle formation and excessive wall thinning. This can be repeated for the development of the entire or complete load path.

2. Other new concepts of development of adaptive control program using metal plasticity theory

A more global way to determine the feasible and optimal loading path can be done by using the failure mode analysis of the hydroforming process, using the forming limit diagram and forming limit curve of the deforming tube/sheet. An optimization algorithm or controller can be developed using fuzzy logic, which can calculate the load-steps, based on the current element state in the forming limit diagram (i.e. whether the element is subject to wrinkle or have wrinkling tendency, or the element is highly thinned and susceptible to bursting failure or development of crack) of the tube blank during the hydroforming process.

3. Application in other sheet metal forming processes

The concepts used for development of the adaptive control of hydroforming process and the new concept stated above using (future work 2) can be used for optimization of other sheet metal forming processes such as deep drawing of circular or rectangular cups.

4. Complete automation of the hydroforming machine in the R & D lab of Dublin City University

As shown in this research study proper control of forming load path is one of the important aspects of tube hydroforming process. The present capability of the machine does not allow applying controlled forming pressure with respect to axial feed in other word a predefined load path with intermediate control points (i.e. pressure and feed values) cannot be used in the machine. Further for more effective control of the axial feed, the axial feed force value is of much importance, however the machine does not allow recording of the actual feed force acting on the tube ends. Considering all these limitation of the machine, the machine can be further upgraded and automated to fulfil all the above requirements. Chart in fig 8.3.1 details the present capabilities, limitations and possible upgrades required to fully automate the machine.

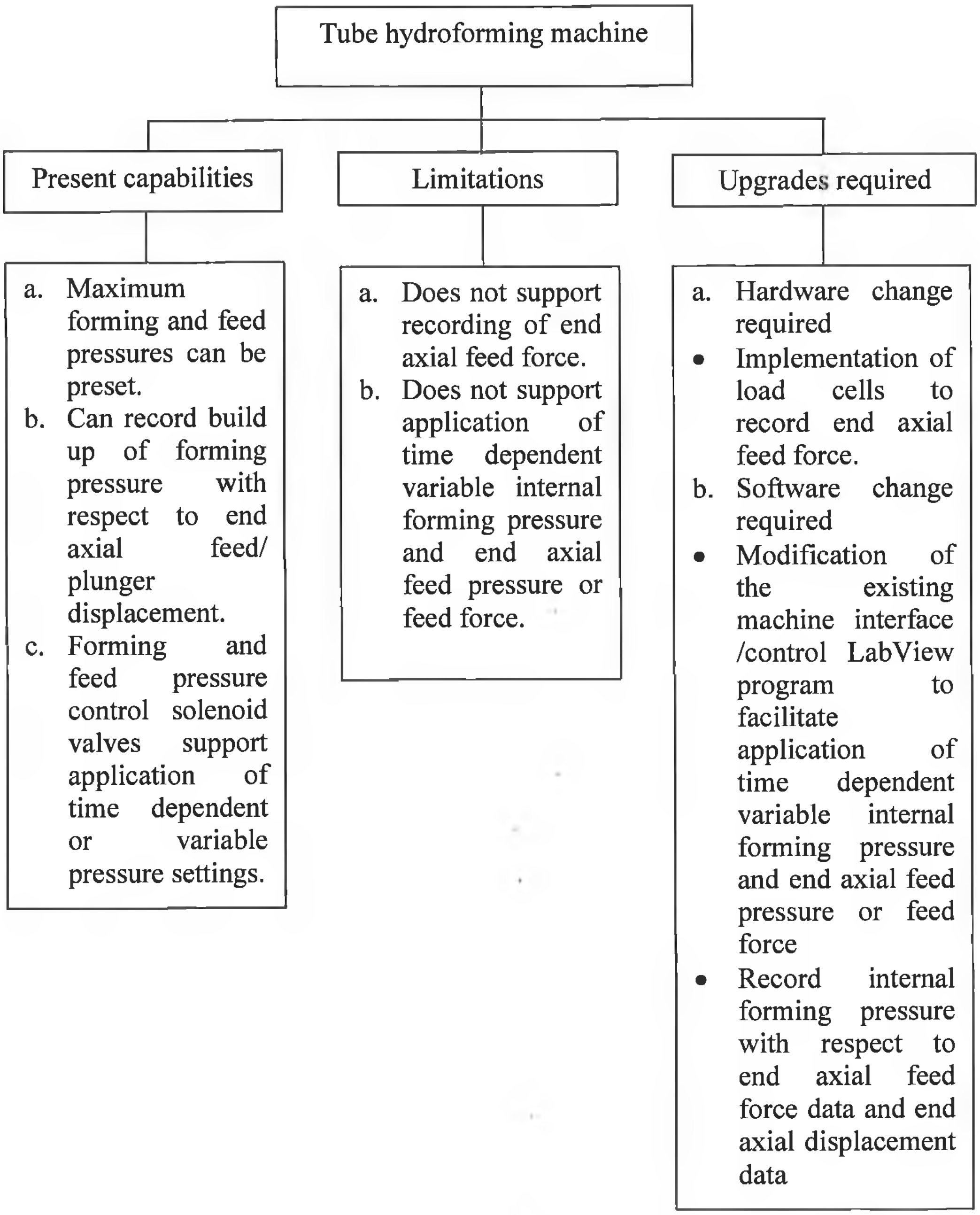

Tube hydroforming machine

Present capabilities

a. Maximum forming and feed pressures can be preset.
b. Can record build up of forming pressure with respect to end axial feed/ plunger displacement.
c. Forming and feed pressure control solenoid valves support application of time dependent or variable pressure settings.

Limitations

a. Does not support recording of end axial feed force.
b. Does not support application of time dependent variable internal forming pressure and end axial feed pressure or feed force.

Upgrades required

a. Hardware change required
- Implementation of load cells to record end axial feed force.

b. Software change required
- Modification of the existing machine interface /control LabView program to facilitate application of time dependent variable internal forming pressure and end axial feed pressure or feed force
- Record internal forming pressure with respect to end axial feed force data and end axial displacement data

Fig 8.3.1 Tube hydroforming machine- present capabilities, limitations and upgrades required.

References

[1] American Iron and Steel Institute, www.autosteel.org/pdfs/ gdis_2002_honda_civic.pdf, (Accessed on January 1, 2005)

[2] Vari-Form, www.vari-form.com/bins/site/content/documents/ ABCs_Hydro.pdf, (Accessed on February 1, 2005)

[3] J. E. Grey, A. P. Deveraux and W. M. Parker, Apparatus for making wrought metal T's , U.S.A. Patents office , filed June 1939, patent no 2,203,868

[4] R.E. Crawford, Solder Fittings, Industrial Progress, May 1948, 33-36

[5] P.B. Mellor, Tensile instability in thin walled tubes, Journal of Mechanical Engineering. Sciences, Vol. 4, No. 3, 1962, 251-256

[6] R.P. Felgar, Plastic analysis of the instability of pressure vessels subjected to internal pressure and axial load, Trans. ASME, J. Basic Eng., Vol. 84, 1962, 62-72

[7] N.A. Weil, Tensile instability of thin-walled cylinders of fmite length, International Journal of Mechanical Sciences, Vol. 5, 1963, 487-506

[8] B.H. Jones and P.B. Mellor, Plastic flow and instability behaviour of thin walled cylinders subjected to constant ratio tensile stress, J. Strain Analysis, Vol.2, 1967, 62-72

[9] J. Remmerswaal and A. Verkaik, Use of compensation forces and stress in difficult metal forming operations, Int. Conf. of Manufacturing Technology, ASME, 1967, 1171-1180

[10] J. Stalter, Method of Forming Complex Tubular Shapes, UK Patent Office, Filed March 1968, Patent No. 1,181,611

[11]T. Ogura and T. Ueda, Liquid Bulge Forming, Metalworking Production, 1968, 73-81

[12] H.A. Al-Qureshi, P.B. Mellor and S. Garber, Application of Polyurethane to the Bulging and Piercing of Thin-walled Tubes, Advances in Mach. Tool Des. Res. Pergammon Press, 1969, 318-338.

[13] Al-Qureshi, Forming Technique and Hydraulic Forming Process, Sheet Metal Industry, 47, 1970, 607-612

[14] M.Limb, J. Chakrabarty, S.Garber and P .B.Mellor, The forming of axisymmetric and asymmetric components from a tube, Proc. 14th International MTDR Conference, 1973,799

[15] M. Limb, J. Chakrabarty and S. Garber, The axisymmetric tube forming process, Int. Inst. for Prod. Eng .Research Conf, Tokyo, 1974,280-283

[16] M. Limb, J. Chakrabarty, S. Garber and W.T. Roberts, Hydraulic forming of tubes, Sheet Metal Industries, 1976,418-424

[17] S. Kandil, Hydrostatic metal tube bulging as a basic process, Metallurgy and Metal Forming, 1976, 152-155

[18] D.M. Woo, Tube Bulging Under Internal Pressure and Axial Force, Journal of Engineering Materials and Technology, 1978, 421-425

[19] W.J. Sauer, A Goetra, F. Robb and P. Huang, Free bulging of tubes under internal pressure and axial compression, Trans. of NAMRC VI, SME, 1978, 228-235

[20] D.M. Woo and A.C. Lua, Plastic Deformation of Anisotropic Tubes in Hydraulic Bulging, Journal of Engineering Materials and Technology, 1978, 421-425

[21] D.M. Woo, Development of a bulge forming process, Sheet Metal Industries, 1978, 623-624 and 628

[22] V.L. Lukanov, V.V. Klechkov, V.P. Shateev and L.V. Orlov, Hydromechanical Stamping of Tees with Regulated Liquid Pressure, Forging and Stamping Industry, Vol. 3, 1980, 5-7

[23] A.R. Ragab, Producing superplastic tubular tee joints by thermoforming, Proc. Int. MTDR Conf., 1980, 223-230

[24] M.S.J.Hashmi, Radial thickness distribution around a hydraulically bulge formed annealed copper T-joint: experimental and theoretical predictions, 22nd Int. M.T.D.R Conf, 1981,507-516

[25] T. Ueda, Differential gear casing for automobiles by liquid bulge forming processes part 1, Sheet Metal Industries, Vol. 60, part 3/4, 1983, 181-185

[26] T. Ueda, Differential gear casing for automobiles by liquid bulge forming processes part 2, Sheet Metal Industries, Vol. 60, part 4, 1983, 220-224

[27] M. S. J. Hashmi, Forming of tubular components from straight tubing using combined axial load and internal pressure: Theory and experiment, Proc. of Int. Conf. on Dev. on Drawing of Metals, Metals Society, 1983, 146-155

[28] L.A.M. Filho and H.A. Al-Quershi, Unconventional Tee Forming on Metal Tubes, J. Eng. Ind., 107, 1985, 392-396

[29] M. S. J. Hashmi and R. Crampton, Hydraulic Bulge Forming of Axisymmetric and Asymmetric Components: Comparison of Experimental Results and Theoretical Predictions, Proc. 25th Int. MTDR Conf., Birmingham, (1985) 541-549

[30] F. Dohmann and F. Klass, Liquid Bulge Forming of Tubular Workpieces, Strips Sheets Tubes, Vol. 4, part 1, 1987, 7-10

[31] M. I. Hutchinson, R. Crampton, M. S. Ali, M. S. J. Hashmi, The hydraulic bulge forming of tubular components- The effect of changing the tube blank material, Proc. 4th Nat. Conf. in Prod. Res, Sheffield 1988,439-444

[32] M. I. Hutchinson, R. Crampton, W. Rushton and M. S. J. Hashmi, The hydraulic bulge forming of tubular components- The effect of changing the plungers applying compressive axial load, Proc. 6th Irsih manufacturing committee conf., Dublin 1989, 248-254

[33] S. Thiruvarudchelvan and F.W. Travis, Tube Bulging with a Urethane Rod, Journal of Materials and Proc. Technology, 23, 1990, 152-209

[34] S. Thiruvarudchelvan, A Theory for the Bulging of Aluminium Tubes Using a Urethane Rod, Journal of Materials and Processing Technology, 41, 1994, 311-330

[35] S. Thiruvarudchelvan, A Theory for Initial Yield Conditions in Tube Bulging with a Urethane Rod, Journal of Materials and Processing Technology, 42, 1994, 61-74

[36] F. Dohmann and C. Hartl, Liquid Bulge Forming as a Flexible Production Method, Journal of Materials and Processing Technology, Vol. 45, 1994, 377-382

[37] L.A.M. Filho, J. Menezes and H.A. Al-Quereshi, Analysis of Unconventional Tee Forming on Metal Tubes, Journal of Materials and Processing Technology, Vol. 45, 1994, 383-388

[38] S. Sheng and W. Tonghai, Research into the Bulge Forming of a Tube Under Axial-Radial Compound Forces and It's Application, Journal of Materials and Processing Technology, Vol. 51, 1995, 346-357

[39] J. Tirosh, A. Neuberger and A. Shirizly, On tube expansion by internal fluid pressure with additional compressive stress, International Journal of Mechanical Sciences, Vol. 38, No. 8, 1996, 839-851

[40] F. Dohmann and C. Hartl, Hydroforming – A Method to Manufacture Light Weight Parts, Journal of Materials and Processing Technology, Vol. 60, 1996, 669-676

[41] J.O. Hallquist and D.J. Benson, Explicit Finite Element Methods for Impact Engineering, Proc. of the first Australasian Congress on Applied Mechanics, Melbourne, 1996, 11-16.

[42] F. Dohmann and C.Hartl, Tube Hydroforming—Research and Practical Application, Journal of Materials Processing Technology, Vol 71, Issue 1, 1997, 174-186

[43] M.Ahmed, M.S.J.Hashmi, Finite element analysis of bulge forming applying pressure and in-plane compressive load, Journal of Material Processing Technology , Vol. 77 ,1998, 95-102

[44] E. Doege, R. Kosters and C. Ropers, Determination of optimised control parameters for internal high pressure forming processes with the FEM, Proceedings of the International Conference Sheet metal'98, Twente, The Netherlands 1998, 119-128

[45] N. Asnafi, Analytical modelling of tube hydroforming, Thin-Walled Structures, Vol.34, 1999, 295-330

[46] M. Ahmed and M. S. J. Hashmi , Finite element simulation of bulge forming of an elbow of box section from circular tube, Journal of Materials Processing Technology, Vol. 92-93, 1999, 410-418

[47] O. Ghouati, H. Lenoir, J.C. gelin and M.Baida, Design and control of forming processes using optimization techniques. Proceedings of the ASME design engineering technical conferences, Las Vegas, Nevada ,1999

[48] N. Asnafi and A. Skogsgårdh, Theoretical and experimental analysis of stroke-controlled tube hydroforming, Materials Science and Engineering A, Vol. 279, 2000, 95-110

[49] B.J.Mac Donald, M.S.J.Hashmi, Finite element simulation of bulge forming of a cross-joint from a tubular blank, Journal of Material Processing Technology, Vol. 103, 2000, 333-342

[50] M. Koc, T. Allen, S. Jiratheranat, T. Altan, The use of FEA and design of experiments to establish design guidelines for simple hydroformed parts, International Journal of Machine Tools & Manufacturing, Vol. 40, 2000, 2249-2266

[51] L. P. Lei, J. Kim, B. S. Kang, Analysis and design of Hydroforming process for automobile rear axle housing by FEM, Vol. 40, 2000, 1691-1708

[52] M. Ahmetoglu, K. Sutter, X. J. Li and T. Altan, Tube hydroforming-current research, applications and need for training, Journal of Materials Processing Technology, Vol.98, 2000, 224-231

[53] M. Ahmetoglu and T. Altan, Tube hydroforming: state-of-the-art and future trends. Journal of Materials Processing Technology, Vol 98, 2000, 25-33

[54] W Rimkus, H Bauer, M J A Mihsein, Design of load curves for hydroforming applications. Journal of Materials Processing Technologies, Vol.108, 2000, 97-105

[55] M. Ahmed and M. S. J. Hashmi ,Three-dimensional finite-element simulation of bulge forming, Journal of Materials Processing Technology, Vol. 119, 2001,387-392

[56] B. G. Teng, S. J. Yuan and Z. R. Wang, Experiment and numerical simulation of hydro-forming toroidal shells with different initial structure, International Journal of Pressure Vessels and Piping, Vol.78, 2001, 31-34

[57] T Murao, K Mori, A Takagi and H Okubo, Finite element simulation of redrawing process of cup without blankholder, Proceeding of the 7th International

Conference on Numerical Methods in Industrial Forming Processes, Numiform2001 Toyohashi Japan, 2001, 789-794

[58] M. Koç and T. Altan, An overall review of the tube hydroforming (THF) technology, Journal of Materials Processing Technology, Vol 108, 2001, 384-393

[59] H. U. Lücke, Ch. Hartl and T. Abbey, Hydroforming, Journal of Materials Processing Technology, Vol 115, 2001, 87-91

[60] J. B. Yang, B. H Jeon and S. I. Oh, Design sensitivity analysis and optimization of the hydroforming process, Journal of Materials Processing Technology, Vol 113, 2001, 666-672

[61] M. Koç and T. Altan, Prediction of forming limits and parameters in the tube hydroforming process, International Journal of Machine Tools and Manufacture, Vol. 42, 2002, 123-138

[62] S. Kim, Y. Kim, Analytical study for tube hydroforming , Journal of Material Processing Technology, 128, 2002, 232-239

[63] M. Koc, T.Altan, Application of two dimensional (2D) FEA for the tube hydroforming process, International Journal of Machine Tools & Manufacturing Vol. 42 , 2002, 1285-1295

[64] B. J. Mac Donald and M. S. J. Hashmi, Three-dimensional finite element simulation of bulge forming using a solid bulging medium, Journal of Materials Processing Technology, Vol. 120, 2002,341-347

[65] K. Manabe, M. Amino, Effects of process parameters and material properties on deformation process in tube hydroforming, Journal of Material Processing Technology, Vol 123, 2002, 285-291

[66] B. J. Mac Donald and M. S. J. Hashmi, Analysis of die behaviour during bulge forming operations using the finite element method, Finite Elements in Analysis and Design, Vol. 39, 2002, 137-151

[67] G. Nefussi and A. Combescure, Coupled buckling and plastic instability for tube hydroforming. International Journal of Mechanical Sciences, Vol 44, 2002,899-914

[68] N. Boudeau, A. Lejeune and J. C. Gelin, Influence of material and process parameters on the development of necking and bursting in flange and tube hydroforming. Journal of Materials Processing Technology, Vol 125-126, 2002, 849-855

[69] X.M. Chen, K. Palanisamy and X.H.Zhu, Process parameter sensitivity study on tube hydroforming, Proceedings of 7th international LS-DYNA users conference, Dearborn, Michigan 2002, 35-45

[70] J. C. Gelin and C. Labergere, Application of optimal design and control strategies to the forming of thin walled metallic components, Journal of Materials Processing Technology, Vol 125-126, 2002, 565-572

[71] M. Koc, Investigation of the effect of loading path and variation in material properties on robustness of the tube hydroforming process, Journal of Materials Processing Technology, Vol.133, 2003, 276-281

[72] A. Shirayori, S. Fuchizawa, H. Ishigure and M. Narazaki, Deformation behavior of tubes with thickness deviation in circumferential direction during hydraulic free bulging , Journal of Materials Processing Technology, Vol.139, 2003,58-63

[73] K. Manabe, S. Miyamoto and H. Koyama, Application of Database-Assisted Fuzzy Adaptive Process Control System to Tube Hydroforming Process, Intelligence in a material world, selected papers from IPMM-2001, CRC Press, Boca Raton, FL, 2003, 537-543

[74] A. Lejeune, N. Boudeau and J. C. Gelin, Influence of material and process parameters on bursting during hydroforming process, Journal of Materials Processing Technology, Vol 143-144, 2003, 11-17

[75] G. T. Kridli, L. Bao, P. K. Mallick and Y. Tian, Investigation of thickness variation and corner filling in tube hydroforming . Journal of Materials Processing Technology, Vol 133, 2003, 287-296

[76] K. J. Fann and P. Y. Hsiao, Optimization of loading conditions for tube hydroforming. Journal of Materials Processing Technology, Vol 140, 2003, 520-524

[77] W Rust and K Schweizerhof, Finite element limit load analysis of thin-walled structures by ANSYS (implicit), LS-DYNA (explicit) and in combination. Thin Walled Structures, Vol 41, 2003, 227-244

[78] MSC.Software Corporation, http://www.mscsoftware.com/ (Accessed on April 15, 2004)

[79] S. Jirathearanat and T. Altan, Optimization of Loading Paths for Tube Hydroforming, AIP Conference Proceedings-712,. NUMIFORM , Columbus, Ohio, 2004, 1148-1153

[80] N. Abedrabbo, N. Zafar, R. Averill, F. Pourboghrat and R. Sidhu, Optimization of a Tube Hydroforming Process, AIP Conference Proceedings-712, NUMIFORM , Columbus, Ohio, 2004, 1172-1177

[81] K. I. Johnson, B. N. Nguyen, R. W. Davies, G. J. Grant and M. A. Khaleel , A numerical process control method for circular-tube hydroforming prediction, International Journal of Plasticity, Vol. 20, 2004, 1111-1137

[82] S. Yoshihara, B. J. MacDonald, H. Nishimura, H. Yamamoto and K. Manabe, Optimisation of magnesium alloy stamping with local heating and cooling using the

finite element method, Journal of Materials Processing Technology, Vol. 153-154, 2004, 319-322

[83] T. J. Barlow, The Hydraulic Bulge Forming of Tubular Components, PhD thesis, Sheffield City Polytechnic (1986)

[84] M. I. Hutchinson, Bulge Forming of Tubular components, PhD thesis, Sheffield City Polytechnic (1988)

[85] Z. Merciniak and J.L.Duncan, The Mechanics of Sheet Metal Forming, Edward Arnold , 1992

[86] M Ahmed, Finite element modelling and simulation of metal flow in bulge forming, PhD thesis, Dublin City University (1997)

[87] F Deb, Optimization for Engineering Design Algorithms and Examples, Prentice-Hall India, 1998

[88] B J Mac Donald, Non Linear Finite Element Simulation of Complex Bulge Forming Processes, PhD thesis, Dublin City University (2000)

[89] S Mc Donnell, Automation of a Bulge Forming Machine, Final year project report, Dublin City University (2003)

[90] ANSYS, Inc Theory Reference, Design Optimization , Version 8.1, 2004

[91] ANSYS LS-DYNA User's Guide, ANSYS Inc, Version 8.1, 2004

Bibliography

G. H. Ryder, Strength of Materials, Macmillan Press LTD, 1969

W. Johnson and P. B. Mellor, Engineering Plasticity, Ellis Horwood Limited, 1983

J. O. Hallquist, LS-DYNA3D Theoretical Manual, Livermore Software Technology Corporation, California, USA, 1993

K. J. Bathe, Finite Element Procedures, Prentice-Hall International, 1996

LS-DYNA User's Manual, Nonlinear Dynamic Analysis of Structures, Livermore Software Technology Corporation

LS-DYNA Keyword User's Manual, Volume-2, Livermore Software Technology Corporation

Appendix: A

Finite Element Simulation Using Implicit Finite Element Code

1. Introduction

In chapter 4, X and T-branch components were simulated using explicit finite element code (LS-DYNA 3D). However, as explained before due to the quasi-static nature of the problem it can also be simulated using implicit finite element code (ANSYS). Although the implicit simulation is not so computationally cost-effective, however it helps to understand the process to some basic extent. In this section finite element simulation results using ANSYS implicit solver are presented and compared with the experimental results already presented in Chapter 4. The objective of this chapter is to detail the finite element modelling concepts for simulation with implicit solver.

2. CAD and finite element modelling of X and T-branch

The CAD models built for the simulations were similar in all respect to the solid models used for building the finite element models as explained in Chapter 3, except for the blank portion, i.e. instead of the curved surface of the tube corresponding to the mean diameter of the tube as used in case of simulation with LS-DYNA, here the entire 3D solid geometry was built. The solid 3D model of the tube blank was built, as in this case the simulation was done with 3D solid brick elements. Fig A1.1 and fig A1.2 show the CAD geometry of the die surface and the solid blank for X and T-branch respectively. Taking advantage of symmetry, one-eighth and one-fourth symmetric CAD models were built for the X and T-branch respectively. The finite element models were built by meshing the solid tube with fully integrated eight-node SOLID185 hexagonal mapped mesh elements. This solid element is suitable for 3-D modelling of solid structures and has three degrees of freedom at each node i.e. translations in the nodal x, y, and z directions. The element has plasticity and large strain capabilities. In the finite element model, only the tube blank was assumed to be deformable. Fig A1.3 and fig A1.4 show the finite element model of the tube and the die. The detail of the contact surface modelling is explained in the later part of the section. The tube blank was meshed with two layers of solid elements with 900 and 1800 finite elements for the X and T-branch respectively.

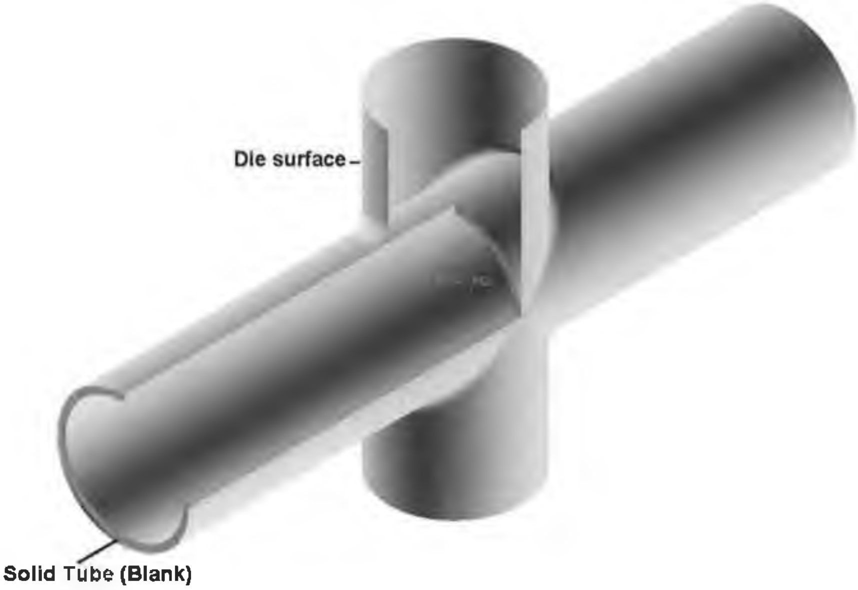

Fig A1.1 Cut away CAD solid model of X-branch

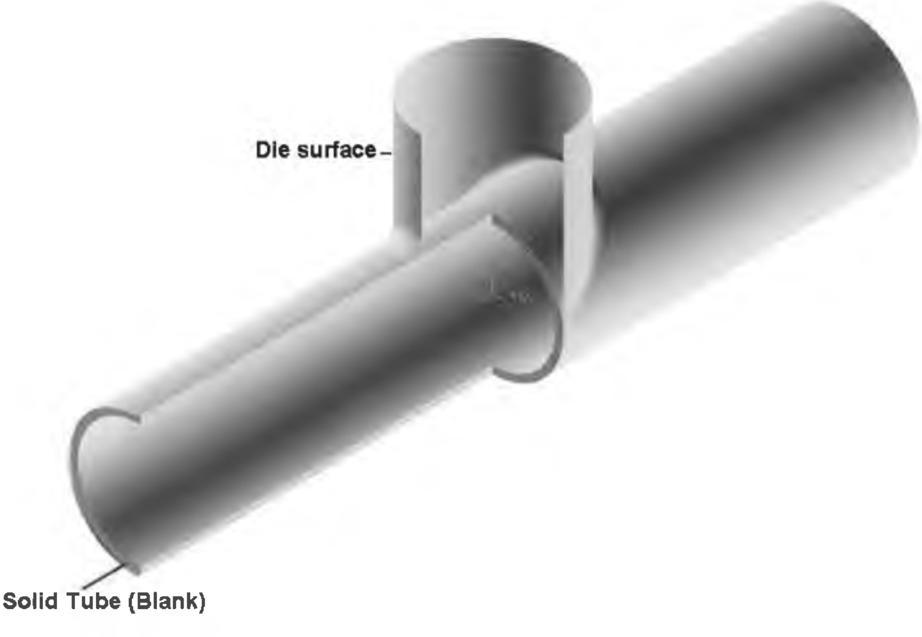

Fig A1.2 Cut away CAD solid model of T-branch

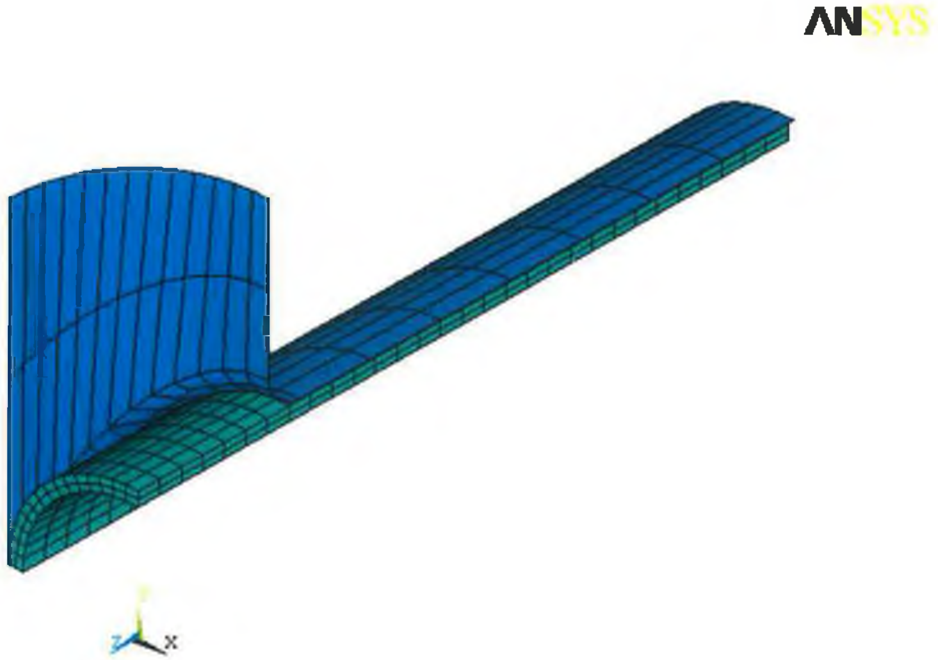

Fig A1.3 One-eighth symmetric finite element model of X-branch (solid elements used for the tube blank)

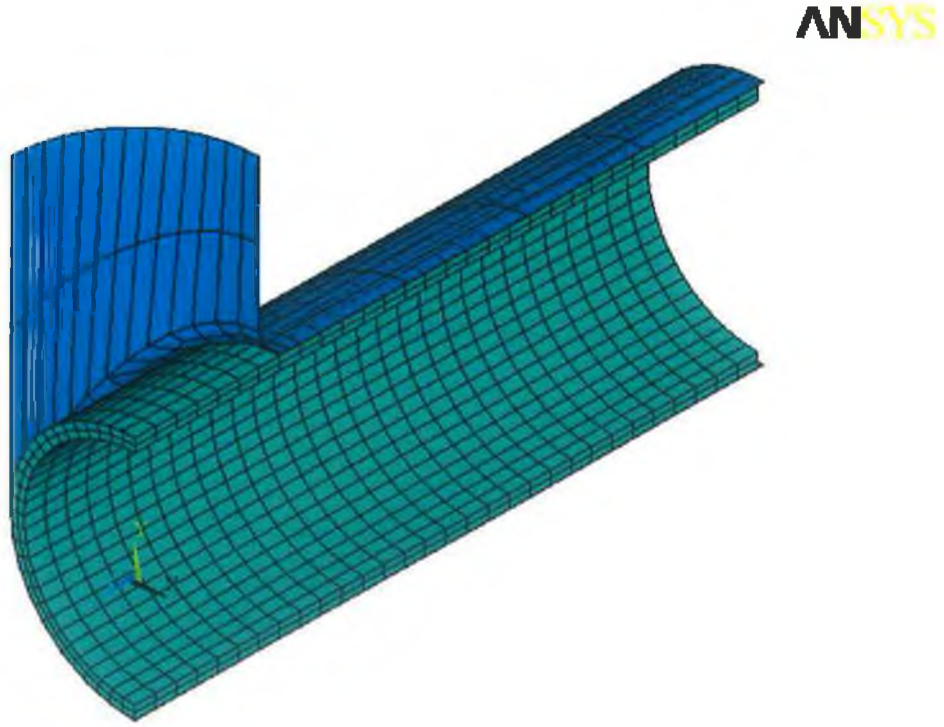

Fig A1.4 One-fourth symmetric finite element model of T-branch (solid elements used for the tube blank)

3. Material model

A piecewise linear plasticity law corresponding to a power law plasticity material model ($\sigma = 0.4257\varepsilon^{0.2562}$ GPa) with strength coefficient (k=0.4257GPa) and hardening exponent (n=0.2562) was used for the copper tube blank. As the die surface was assumed to be rigid and non-deformable in nature, hence no material model was defined for the die portion. The die surface (termed as target surface in contact pair creation) is automatically assumed to be a rigid surface (with constraints in all direction of freedom) while creating the surface-to-surface contact pair with ANSYS program provided it is defined as non-deformable surface and also no additional material model is required for meshing with contact pair elements (target elements).

4. Contact definition

The contact pair definition used for this implicit finite element simulation is entirely different from the contact pair definition used in explicit finite element simulation. In this case, a semi-automatic, surface-to-surface type contact pair algorithm was used between the interfaces of the tube and the die contact surfaces with an assumed elastic Coulomb friction coefficient of 0.15 between the tube (contact) and die (target) surfaces. The die was assumed to be rigid and it was meshed with rigid Target-170 type contact surface elements, and the tube outer surface in contact with the die was meshed with flexible Contact-174 type contact surface elements. To ensure proper working of the contact pair algorithm, it is important to check the contact pair normal directions/ orientation and any gap between the contact and target surfaces. Thus, the contact pair surface normal directions were checked properly so that the normal of the tube contact surface elements points towards the die and the normal of the die contact elements points towards the tube during the course of simulation. To reduce the simulation time and also to increase the chance of convergence of the solution within the maximum iteration steps of 25 (default value of ANSYS program), few controls in the contact pair were also altered from the default value as there was too much penetration of the contact surface with the target surface, which was due to the tight tolerances of the die and tube used in the solid modelling. Thus in the model the penalty stiffness factor was set to 0.5 from a default value of 1.0, contact penetration depth tolerance was set to 0.3mm from the default value of 0.1mm. Fig A1.5 shows a contact pair with element normal and fig A1.6 and fig A1.7

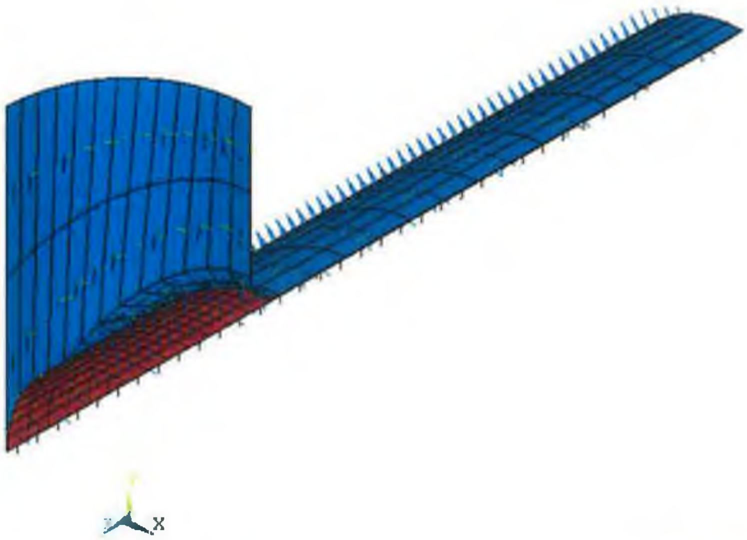

Fig A1.5 Contact pair X-branch

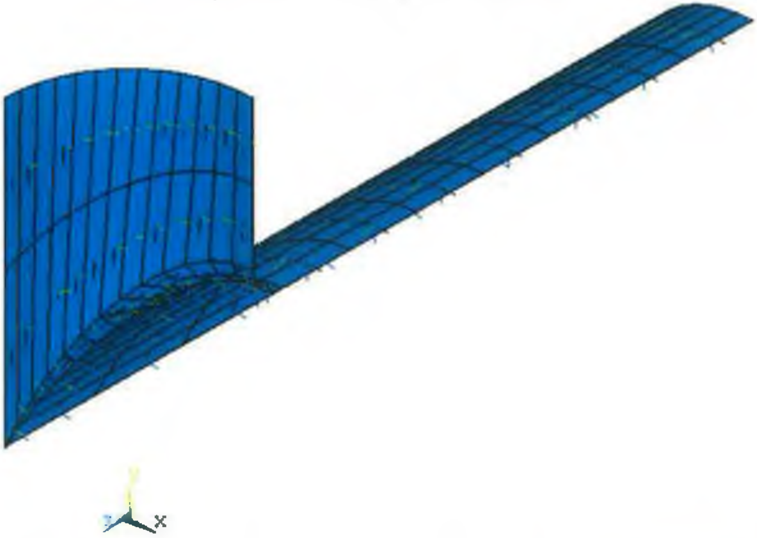

Fig A1.6 Target surface of contact pair with normal pointing towards blank

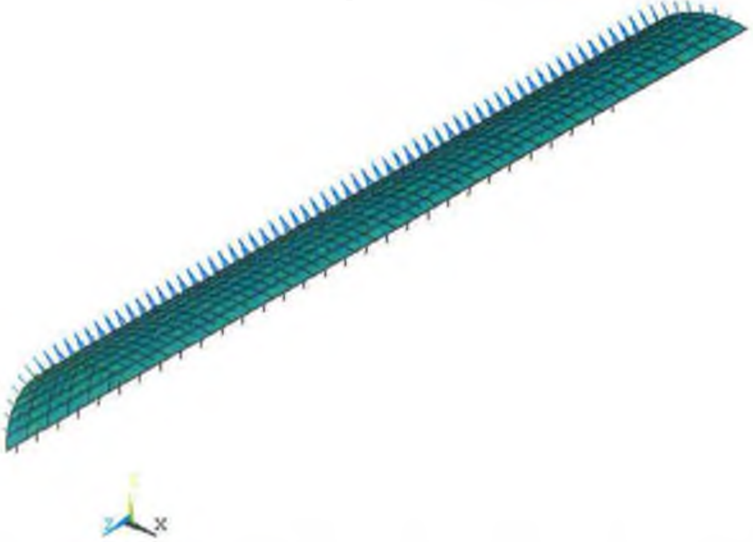

Fig A1.7 Contact surface of contact pair with normal pointing towards die show the element normal of the rigid target surface and flexible contact surface and its direction.

5. Constraints, boundary conditions and loading

Mirror or reflecting symmetric boundary conditions were applied to the symmetric areas of the tube (one-eighth model of X-branch and one-fourth model of T-branch). The tube ends nodes were constrained for all degrees of freedom except it were allowed to move along the axial direction of the tube (Z-axis). This was done with an assumption that the tube ends axial feeds are being applied by end punches and the tube ends nodes cannot move along the radial direction to the tube (towards the centre of the tube), as in this case the punch was not modelled. The load in this case i.e. internal forming pressure and end axial feed were applied as a function of time in four discrete steps using an inbuilt function editor. Linear equations were assumed for the four load steps. Fig A1.8 and fig A1.9 show the load path for two different tests for the X and T-branch. The loading between the steps were assumed to be a ramped loading, this ramped loading helps in gradual increment of the load within the time step. The solution control preference was set for 'large deformation type analysis', as the analysis is basically a sheet metal forming analysis which involves large deformation or stretching of some of the elements during the simulation process. The pressure load was applied as a surface load on the tube inner

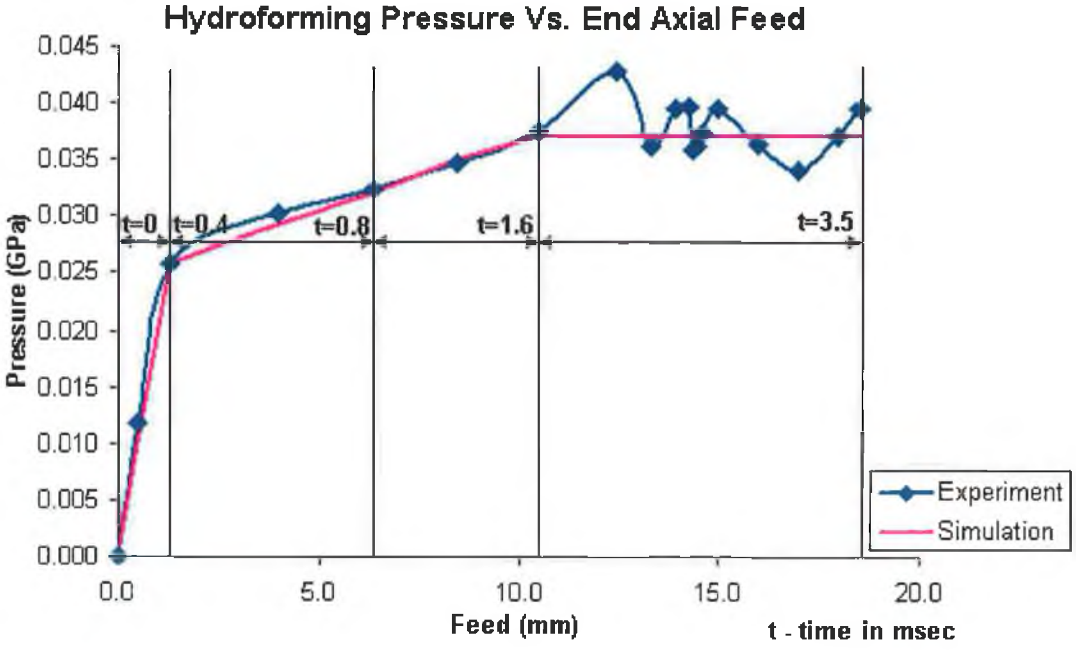

Fig A1.8 Load path X-branch (test-b)

surface with normal directing outwards towards the die and the end axial feed was applied as a displacement load to the tube end nodes in the positive Z-direction.

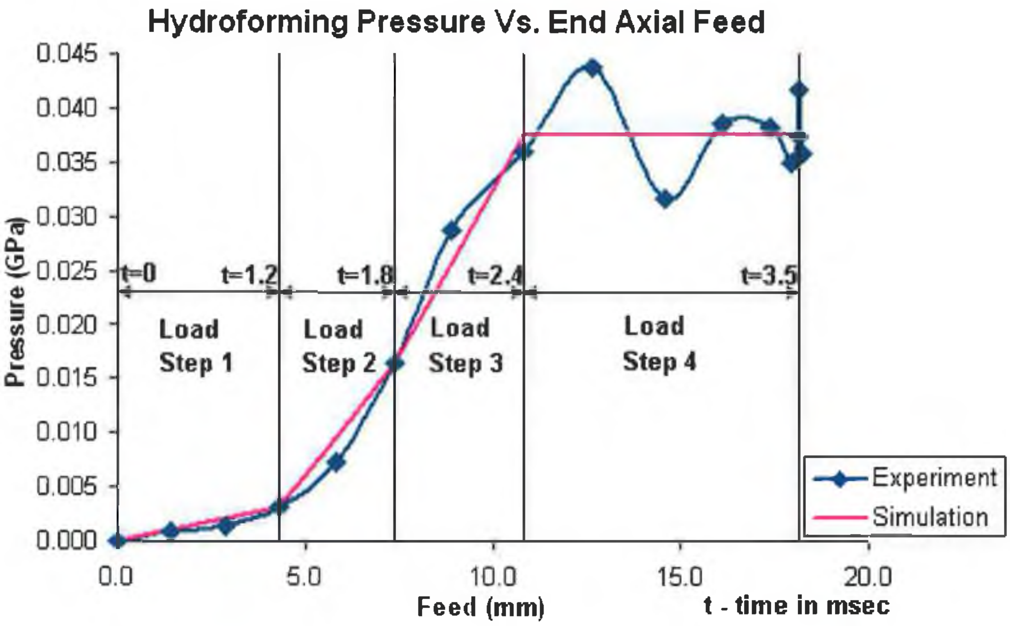

Fig A1.9 Load path T-branch (test-b)

6. Solution, results and discussion

The finite element results obtained were compared with the experimental results details in Chapter 3. Table A1.1 details the branch height comparison of the simulation and experimental results.

Table A1.1 Branch height comparison–experiment and simulation results

Branch type	**X- Branch (Test-b)**	**T-Branch (Test-b)**
Maximum- internal pressure (GPa)	0.0370	0.0375
Maximum-feed (L) (mm)	18.50	18.22
Branch height (H) (mm) (Experiment)	**14.75**	**12.70**
Branch height (H) (mm) (Simulation)	**15.46**	**12.29**
Percentage deviation (Simulation results w.r.t experiment)	-4.81	+3.22

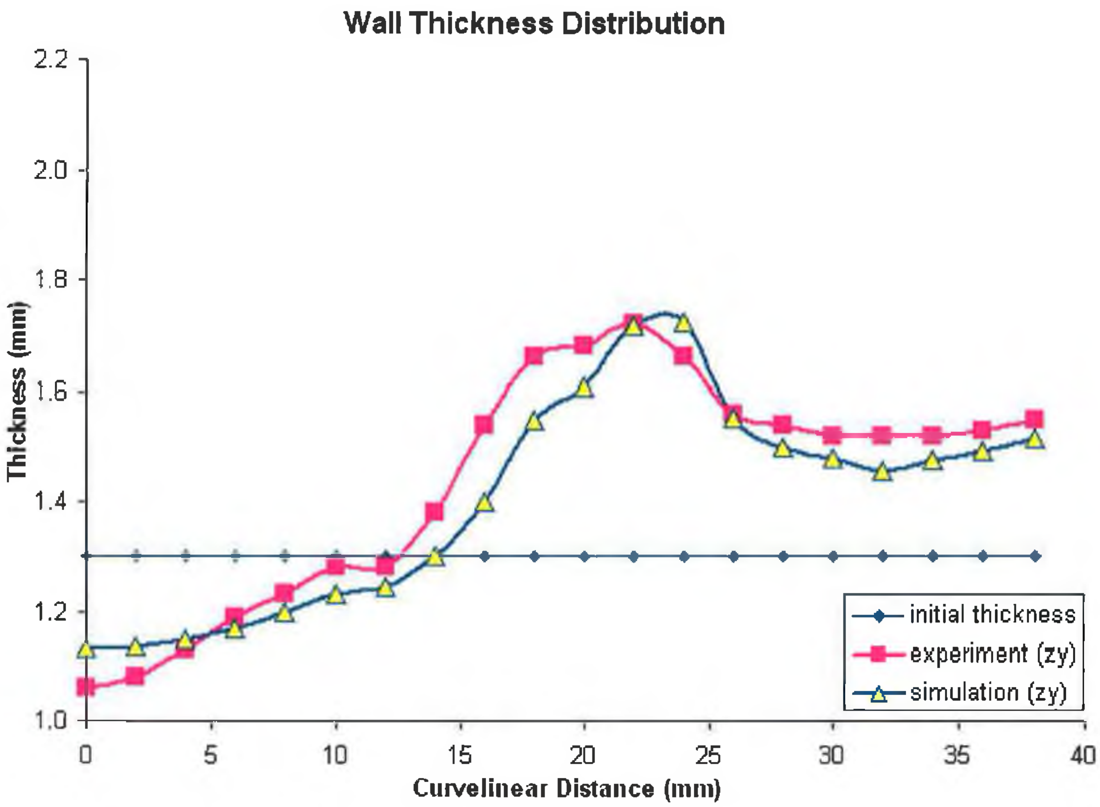

Fig A1.10 Wall thickness distribution plot along zy-plane of the tube, X-branch (test-b)

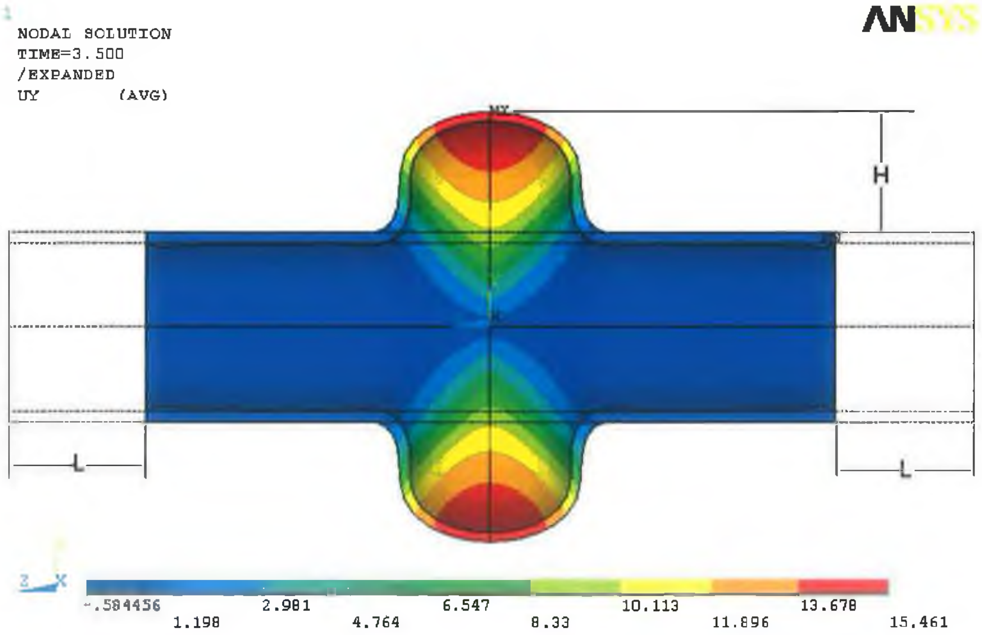

Fig A1.11 X-branch formed tube illustrating total end feed (L) and maximum developed branch height (H)

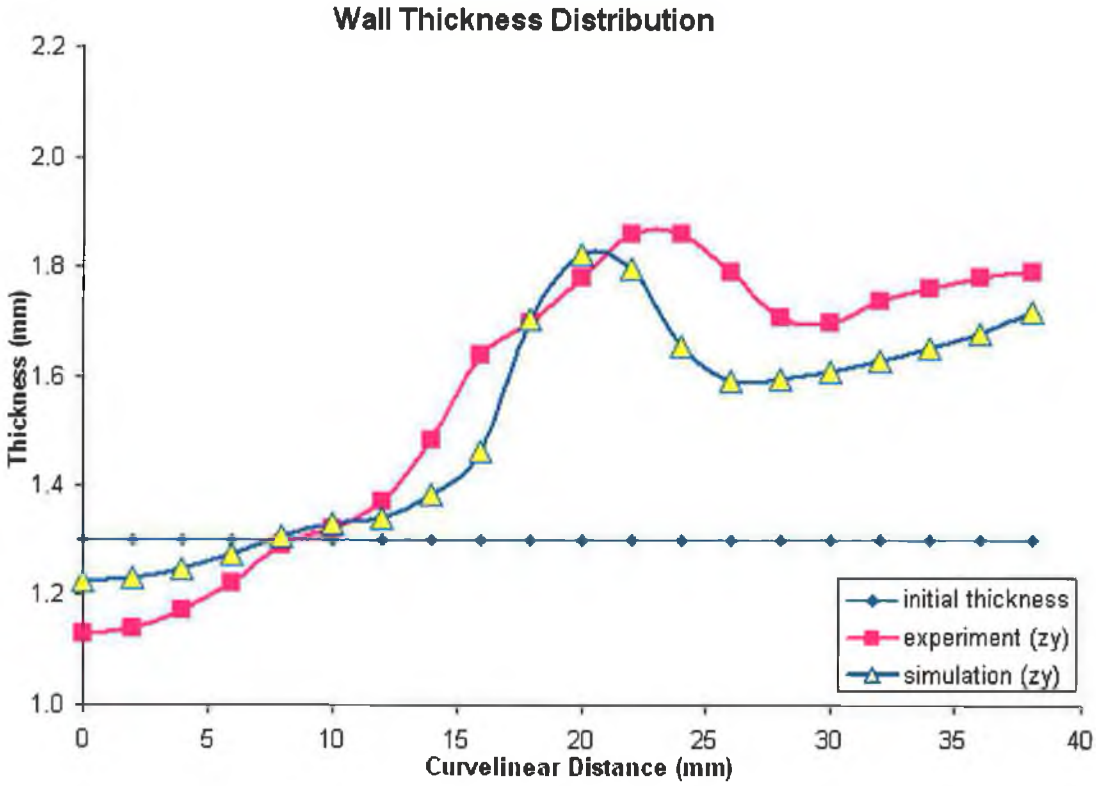

Fig A1.12 Wall thickness distribution plot along zy-plane of the tube, T-branch (Test-b)

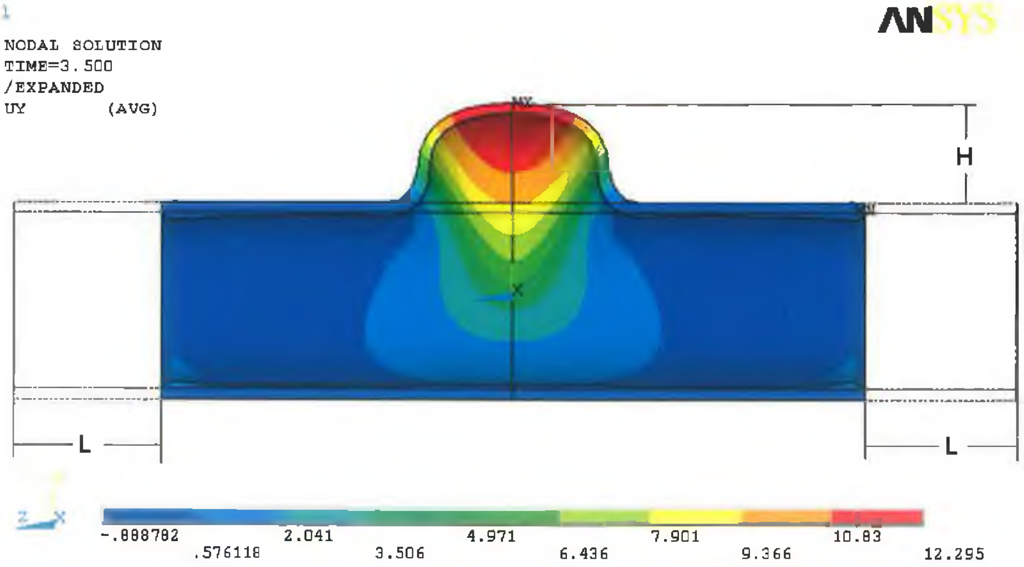

Fig A1.13 T-branch formed tube illustrating, total end feed (L) and maximum developed branch height (H)

It was observed that the simulation branch height was in good agreement with the experimental results with a minor deviation. The simulation and experimental wall thickness distribution trend along the zy-plane from the top central node (node at the highest bulged region) along the curvilinear length of the tube to the tube end were reasonably in good agreement for both the cases. The deviation observed in the thickness distribution along the curvilinear length is due to the deviation in the branch height and amount of plastic flow of material during the process. It was shown in Chapter-4 how the plastic flow of the material for tube hydroforming process is dependent on the actual loading, boundary conditions as well as the dynamic friction forces acting between the tube and the die contact interfaces. From the simulations as well as from the experimental findings, it was observed that the maximum thinning of the tube wall for the T-branch occurred at the tube top bulge portion along the zy-plane whereas maximum thickening of the tube wall was observed along the radius of the X or T junction. The reason for maximum thickening at the curved section or radius of the die can be explained by considering the physical behaviour of the process. During the forming, the tube ends are subjected to axial compressive force, whereas the portion of the tube which has already deformed (bulged section) and has entered the X or T junction is subjected to tensile stresses due to expansion, however in this zones the rate of flow of material due to the tensile force is much less than the rate of flow of material due to compressive axial force. This results in deposition of excess material in the curved section as well as also leads to thickening of the portion of the tube inside the straight die cavity along the tube axis.

The results obtained from the implicit finite element simulation with solid elements were comparable with the explicit finite element simulation with shell elements detailed in Chapter 3. However, there are certain limitations associated with implicit simulations, which are as follows:

a.) The solution iteration convergence is difficult due to existence of various non-linearities such as complex contact conditions, contact failure or change in element normal direction of contact-target interface during simulation, non-linear material properties and due to steep loading conditions, i.e. rate of application of axial feed.

b.) Usually solid elements are the best choice for 3D implicit simulation of metal forming processes as the solution convergence is relatively easy and better in such cases as compared to shell elements. For solution convergence, the criterion used in case of solid element is the force convergence norm whereas for shell elements both the force and moment convergence norms are used. Thus the solution convergence with implicit shell elements is very difficult for certain non-linear cases.

c.) Solution time is much longer as compared to explicit simulation with similar type and number of elements (i.e. mesh densities) due to convergence difficulties associated with large deformation of the material.

7. Summary

This appendix presents the finite element modelling details and comparison of simulation results with experimental results for asymmetric type expansions using implicit finite element code and shows how 3D implicit simulations can also be used for basic analysis of quasi-static metal forming processes such as tube hydroforming processes.

Appendix: B

Parametric Finite Element Modelling and Optimization Using Subproblem Optimization Method

```
!X-Branch
!tube parameters
!wall thickness =1.3mm => shell thickness= 2 x 0.65 mm
!length=121 mm
!diameter (od)=24.1mm , mean diameter of tube =(24.1+24.1-2x1.3)/2=22.8mm
!units mm,Kg,msec
!pressure- GPa
!density- Kg/mm-cube
!feed- mm

!PRE-PROCESSING
/PREP7

!feed parameters
F1=0                                    !fixed point
F2=2.5
F3=5.0
F4=7.5
F5=10.0

!pressure parameters
P1=0                                    !fixed point
P2=0.0085
P3=0.0150
P4=0.0200
P5=0.0270

L=60.5                                  !half tube spline length
T=1.3/2                                 !half tube wall thickness
R=3                                     !die blend radius
F=0.15                                  !coefficient of friction

/DSCALE,1,1.0                           !plot ctrl, style, displacement scaling, set to true scale
/REPLOT

!X-die and tube solid modeling
CYLIND,12.05+T, ,0,-(L+0.5),90,180,     !create cylinder (die lower-die portion along tube length)
CYLIND,12.05-T, ,0,-L,90,180,           !create cylinder (tube )

WPRO,,-90.000000,                       !work plane x_offset by -90deg

CYLIND, 12.05+T, , 0,30,90,180,         !create cylinder (die upper-die portion perpendicular to the tube)

WPCSYS, -1                              !align work plane with active coordinate system
WPSTYLE,,,,,,,0

VADD, 1,3                               !add die volumes
VDELE, 4                                !delete all volumes- die and tube keeping the surface areas
VDELE, 2
ADELE, 23, , ,1                         !delete areas not required in the final model
ADELE, 21, , ,1
ADELE, 20, , ,1
ADELE, 18, , ,1
ADELE, 17, , ,1
ADELE, 16, , ,1
ADELE, 12, , ,1
ADELE, 10, , ,1
ADELE, 9, , ,1
ADELE, 7, , ,1
```

```
ADELE, 6, , ,1
ADELE, 2, , ,1
ADELE, 1, , ,1

BOPTN,VERS,RV52                         !tolerance limit set to 0.0001
BTOL,0.0001,

AFILLT,22,19,R,                         !area fillet (die blend radius)

BOPTN,VERS,RV52                         !tolerance limit set to original value
BTOL,0.00001,

NUMMRG,ALL, , , ,LOW                    !merge all coinciding entities
NUMCMP,ALL                              !compress numbers

! punch solid modeling
CONE,12.05-T-T-(T-0.01),9.5,-(L-10.5),-(L+0.01),90,180,          !create conical part of the punch
CYLIND,12.05,12.05-T-T-(T-0.01),-(L+0.01),-(L+4.5),90,180,       !create cylindrical part of the punch
VDELE,1
VDELE,2
ADELE,     6, , ,1
ADELE,     9, , ,1
ADELE,     8, , ,1
ADELE,     5, , ,1
ADELE,    10, , ,1
ADELE,    14, , ,1
ADELE,    15, , ,1
ADELE,    12, , ,1
ADELE,    13, , ,1

NUMMRG,ALL, , , ,LOW
NUMCMP,ALL

!element selection
ET,1,SHELL163,12                        !element type belytschko-wong chiang-advance shell element
                                        formulation
R,1                                     !real constant
RMODIF,1,1,5/6,3,2*T,2*T,2*T,2*T,       !shear factor 5/6, no of integration point 3
!material selection
MP,DENS,1,8.9E-006                      !material model for tube blank
MPDE,EX,1
MP,EX,1,119.86
MPDE,NUXY,1
MP,NUXY,1,0.31
TBDE,PLAW,1
TB,PLAW,1,,,2,
TBDAT,1,0.4257                          !power law plasticity
TBDAT,2,0.2562

EDMP,RIGI,2,7,7                         !material model for die
MP,DENS,2,7.9E-6
MP,EX,2,210
MP,NUXY,2,0.3
EDMP,RIGI,3,4,7                         !material model for punch
MP,DENS,3,7.9E-6
MP,EX,3,210
MP,NUXY,3,0.3

!meshing
LX1=20                                  !number of element division in the  tube
LX2=36

HX1=1                                   !biasing ratio
HX2=1

LESIZE,4,,,LX1,HX1                      !tube element division
LESIZE,5,,,LX1,HX1
```

```
LESIZE,7,,,LX2,HX2
LESIZE,8,,,LX2,HX2

LESIZE,1,,,4                            !die element division
LESIZE,3,,,12
LESIZE,11,,,12
LESIZE,9,,,6
LESIZE,13,,,6
LESIZE,2,,,15
LESIZE,6,,,15
LESIZE,12,,,15
LESIZE,10,,,15

LESIZE,15,,,15                          !plunger element division
LESIZE,14,,,15
LESIZE,18,,,15
LESIZE,16,,,2
LESIZE,17,,,2
LESIZE,20,,,1
LESIZE,19,,,1

MSHAPE,0,2D                             !area mapped meshing for all areas
MSHKEY,1

!material attributes for die , tube , punch and meshing
ASEL, , , ,4
AATT,1,1,1,0,
ASEL, , , ,1
AATT,2,1,1,0,
ASEL, , , ,2
AATT,2,1,1,0,
ASEL, , , ,3
AATT,2,1,1,0,
ASEL, , , ,4
AMESH,4
ASEL, , , ,1
AMESH,1
ASEL, , , ,3
AMESH,3

MSHKEY,0
ASEL, , , ,2
AMESH,2
MSHAPE,0,2D
MSHKEY,1

ASEL, , , ,5
AATT,3,1,1,0,
ASEL, , , ,6
AATT,3,1,1,0,
ASEL, , , ,5
AMESH,5
ASEL, , , ,6
AMESH,6
ALLSEL,ALL                              !select every thing

/VIEW, 1 ,1,1,1                         !isometric view
/ANG, 1
/REP,FAST
EDPART,CREATE                           !create parts

!contact definition- automatic surface to surface type
EDCGEN,ASTS, 1,2,F,F,0.5,0.116/1.732,20, , , , ,0,10000000,0,0
EDCGEN,ASTS, 1,3,F,F,0.5,0.116/1.732,20, , , , ,0,10000000,0,0

!advanced contact controls
EDCONTACT,0.1,0,2,2,1,2,1,4,1           !penetration check on, shell thickness change included
```

```
EDSP,ON,     1,     2,1,

!hourglass control
EDMP,HGLS,1,0,0.1,1.5,0.06, , ,

!shell thickness change activation
EDSHELL,20,-1,1,2,1,1

!feed, pressure and time array definition in parametric form
*DIM,ADISPLACEMENT,ARRAY,5,1,1, , ,
*DIM,APRESSURE,ARRAY,5,1,1, , ,
*DIM,ATIME,ARRAY,5,1,1, , ,

ADISPLACEMENT(1,1,1) =F1
ADISPLACEMENT(2,1,1) =F2
ADISPLACEMENT(3,1,1) =F3
ADISPLACEMENT(4,1,1) =F4
ADISPLACEMENT(5,1,1) =F5
APRESSURE(1,1,1) =-P1
APRESSURE(2,1,1) =-P2
APRESSURE(3,1,1) =-P3
APRESSURE(4,1,1) =-P4
APRESSURE(5,1,1) =-P5
ATIME(1,1,1) =0.00000
ATIME(2,1,1) =0.75000
ATIME(3,1,1) =1.50000
ATIME(4,1,1) =2.25000
ATIME(5,1,1) =3.00000

!component creation
LSEL,S, , ,     4
NSLL,S,1
CM,TUBE_END,NODE

ASEL,S, , ,     4
ESLA,S
CM,PR_SURF,ELEM

ALLSEL,ALL                                  !select all
!constraints
DL,8, ,UX,0                                 !symmetric constraints-displacement and rotational on nodes
DL,8, ,ROTY,0
DL,8, ,ROTZ,0
DL,7, ,UY,0
DL,7, ,ROTX,0
DL,7, ,ROTZ,0
DL,5, ,UZ,0
DL,5, ,ROTX,0
DL,5, ,ROTY,0

!boundary conditions
EDLOAD,ADD,PRES,0,PR_SURF,ATIME,APRESSURE,0,,,,,
                                            !pressure load on tube inner surface
EDLOAD,ADD,RBUZ,0, 3,ATIME,ADISPLACEMENT,0,,,,,
                                            !displacement load on tube end plunger
EDLOAD, ADD, UZ, 0,TUBE_END,ATIME,ADISPLACEMENT,0,,,,
                                            !displacement load on tube end nodes
EPLOT                                       !plot elements

!solution time control
TIME,3.0,                                   !solution time in milli sec
EDRST,100,                                  !number of result file steps
EDHTIME,200,                                !number of history file steps
EDDUMP,1,
EDINT,3,4,                                  !save solution for all layers for shell
EDOPT,ADD,BLANK,BOTH                        !results file type ansys and lsdyna
!end of pre-processing
```

```
!SOLUTION
/SOL
/STATUS,SOLU
SOLVE

!GENERAL POST-PROCESSOR
/POST1
SET, , ,1, , , ,101,
PARTSEL,'S',1, , ,                                  !select tube for post-processing of results

!calculation of maximum branch height
*GET,YMAX,NODE,58,U,Y

!calculation of wrinkle height (for nodes susceptible to wrinkle formation)
*GET,XMAX22,NODE,22,U,X
*GET,XMAX57,NODE,57,U,X
*GET,XMAX56,NODE,56,U,X
*GET,XMAX55,NODE,55,U,X
*GET,XMAX54,NODE,54,U,X
*GET,XMAX53,NODE,53,U,X
*GET,XMAX52,NODE,52,U,X
*GET,XMAX51,NODE,51,U,X
*GET,XMAX50,NODE,50,U,X

!root mean square wrinkle height calculation
RMSWRINKLE=SQRT(((XMAX22*XMAX22)+(XMAX57*XMAX57)+(XMAX56*XMAX56)+(XMAX55*XMAX
55)+(XMAX54*XMAX54)+(XMAX53*XMAX53)+(XMAX52*XMAX52)+(XMAX51*XMAX51)+(XMAX50*XM
AX50))/9)

!sort element with minimum thickness for blank
AVPRIN,0, ,
ETABLE, ,NMISC, 4
ESORT,ETAB,NMIS4,0,0, ,
*GET,ELEMTHKMIN,SORT,,MIN

OBJFUN=40-YMAX                                      !objective function calculation

ALLSEL,ALL
FINISH
!end of post-processing

!START OF DESIGN OPTIMIZATION LOOP
/OPT
!define the optimization analysis file with optimization parameters
OPANL,'X_LSDYNA-SUB-OPT-LOADPATH','INP',' '

!design variables with lower and upper limits
OPVAR,F2,DV,0.05,3.5, ,
OPVAR,F3,DV,3.5,7.5, ,
OPVAR,F4,DV,7.5,12.0, ,
OPVAR,F5,DV,10.0,19.0, ,
OPVAR,P2,DV,0.0050,0.0150, ,
OPVAR,P3,DV,0.0150,0.0200, ,
OPVAR,P4,DV,0.0200,0.0250, ,
OPVAR,P5,DV,0.0250,0.0350, ,

!state variables
OPVAR,ELEMTHKMIN,SV,1.17,1.85, ,                    ! minimum allowable wall thickness-1.17mm
OPVAR,RMSWRINKLE,SV,0,0.095, ,                      ! maximum allowable wrinkle height-0.095mm
!objective function
OPVAR,OBJFUN,OBJ, , ,1.5,
OPKEEP,ON                                           !save best design
OPTYPE,SUBP                !optimization method type-subproblem approximation.
OPSUBP,30,7,
OPEXE
!end of design optimization loop
```

Appendix: C

Adaptive Load Control Algorithm

```
!X-Branch
!start the program in drive-d:, folder-ansys-lsdyna, path-D:\ansys-lsdyna\x-branch\
!tube parameters
!wall thickness =1.3mm => shell thickness= 2 x 0.65 mm
!length=121 mm
!diameter (od)=24.1mm , mean diameter of tube =(24.1+24.1-2x1.3)/2=22.8mm
!units mm,kg,msec
!pressure- GPa
!density- Kg/mm-cube
!feed- mm

!PRE-PROCESSING
/PREP7
L=60.5                                    !half tube spline length
T=1.3/2                                   !half tube wall thickness
R=3                                       !die blend radius
F=0.15                                    !coefficient of friction
/DSCALE,1,1.0                             !plot ctrl, style, displacement scaling, set to true scale
/REPLOT
 !X-die and tube solid modeling
CYLIND,12.05+T, ,0,-(L+0.5),90,180,       !create cylinder (die lower-die portion along tube length)
CYLIND,12.05-T, ,0,-L,90,180,             !create cylinder (tube )
WPRO,,-90.000000,                         !work plane x_offset by -90deg
CYLIND, 12.05+T, , 0,30,90,180,           !create cylinder (die upper-die portion perpendicular to the tube)
WPCSYS, -1                                !align work plane with active coordinate system
WPSTYLE,,,,,,,0

VADD, 1,3                                 !add die volumes
VDELE, 4                                  !delete all volumes- die and tube keeping the surface areas
VDELE, 2
ADELE, 23, , ,1                !delete areas not required in the final model
ADELE, 21, , ,1
ADELE, 20, , ,1
ADELE, 18, , ,1
ADELE, 17, , ,1
ADELE, 16, , ,1
ADELE, 12, , ,1
ADELE, 10, , ,1
ADELE, 9, , ,1
ADELE, 7, , ,1
ADELE, 6, , ,1
ADELE, 2, , ,1
ADELE, 1, , ,1
BOPTN,VERS,RV52                !tolerance limit set to 0.0001
BTOL,0.0001,

AFILLT,22,19,R,                !area fillet (die blend radius)

BOPTN,VERS,RV52                !tolerance limit set to original value
BTOL,0.00001,
NUMMRG,ALL, , , ,LOW           !merge all coinciding entities
NUMCMP,ALL                     !compress numbers

!punch solid modeling
CONE,12.05-T-T-(T-0.01),9.5,-(L-10.5),-(L+0.01),90,180,             !create conical part of the punch
CYLIND,12.05,12.05-T-T-(T-0.01),-(L+0.01),-(L+4.5),90,180,          !create cylindrical part of the punch

VDELE,1
VDELE,2
ADELE,     6, , ,1
ADELE,     9, , ,1
```

```
ADELE,    8, , ,1
ADELE,    5, , ,1
ADELE,   10, , ,1
ADELE,   14, , ,1
ADELE,   15, , ,1
ADELE,   12, , ,1
ADELE,   13, , ,1
NUMMRG,ALL, , , ,LOW
NUMCMP,ALL

!element selection
ET,1,SHELL163,12                        !element type Belytschko-Wong Chiang-advance shell element
                                        formulation
R,1                                     !real constant
RMODIF,1,1,5/6,5,2*T,2*T,2*T,2*T,       !shear factor 5/6, integration points 5

!material selection
MP,DENS,1,8.9E-006                      !material model for tube blank
MPDE,EX,1
MP,EX,1,119.86
MPDE,NUXY,1
MP,NUXY,1,0.31
TBDE,PLAW,1
TB,PLAW,1,,,2,
TBDAT,1,0.4257                          !power law plasticity
TBDAT,2,0.2562
EDMP,RIGI,2,7,7                         !material model for die
MP,DENS,2,7.9E-6
MP,EX,2,210
MP,NUXY,2,0.3
EDMP,RIGI,3,4,7                         !material model for punch
MP,DENS,3,7.9E-6
MP,EX,3,210
MP,NUXY,3,0.3

!mesh size selection
LX1=24                                  !number of element division in the TUBE
LX2=38
HX1=1/1.5                               !biasing ratio
HX2=1/1.5
LESIZE,4,,,LX1,HX1                      !tube element division
LESIZE,5,,,LX1,HX1
LESIZE,7,,,LX2,HX2
LESIZE,8,,,LX2,HX2
LESIZE,1,,,4                            !die element division
LESIZE,3,,,12
LESIZE,11,,,12
LESIZE,9,,,6
LESIZE,13,,,6
LESIZE,2,,,15
LESIZE,6,,,15
LESIZE,12,,,15
LESIZE,10,,,15
LESIZE,15,,,15                          !plunger element division
LESIZE,14,,,15
LESIZE,18,,,15
LESIZE,16,,,2
LESIZE,17,,,2
LESIZE,20,,,1
LESIZE,19,,,1

MSHAPE,0,2D                             !area mapped meshing for all areas
MSHKEY,1

!material attributes and meshing of die ,tube and punch
ASEL, , , ,4
AATT,1,1,1,0,
```

```
ASEL, , , ,1
AATT,2,1,1,0,
ASEL, , , ,2
AATT,2,1,1,0,
ASEL, , , ,3
AATT,2,1,1,0,
ASEL, , , ,4
AMESH,4
ASEL, , , ,1
AMESH,1
ASEL, , , ,3
AMESH,3

MSHKEY,0
ASEL, , , ,2
AMESH,2
MSHAPE,0,2D
MSHKEY,1

ASEL, , , ,5
AATT,3,1,1,0,
ASEL, , , ,6
AATT,3,1,1,0,
ASEL, , , ,5
AMESH,5
ASEL, , , ,6
AMESH,6
ALLSEL,ALL                              !select every thing

/VIEW, 1 ,1,1,1                         !isometric view
/ANG, 1
/REP,FAST

EDPART,CREATE                           !create parts for explicit dynamic analysis
PARTSEL,'s',1, , ,                      !select part, tube is selected
*get,z,ELEM,,count,                     !get number of elements in the tube blank= z elements
ALLSEL,ALL

!contact definition- automatic surface to surface type
EDCGEN,ASTS, 1,2,F,F,0.5,0.116/1.732,20, , , , ,0,10000000,0,0
EDCGEN,ASTS, 1,3,F,F,0.5,0.116/1.732,20, , , , ,0,10000000,0,0

!advanced contact controls
EDCONTACT,0.1,0,2,2,1,2,1,4,1       !penetration check on, shell thickness change included
EDSP,ON,     1,     2,1,
!hourglass control
EDMP,HGLS,1,0,0.1,1.5,0.06, , ,
!shell thickness change activation
EDSHELL,20,-1,1,2,1,1

!create arrays for storing element strain difference, normal velocity data
*DO,u,1,LX2,1                                     !total number of slice=lx2=38
*DIM,z_strain_diff_slice%u%,ARRAY,z/LX2,1,1, , ,
*DIM,z_vel_norm_slice%u%,ARRAY,z/LX2,1,1, , ,
*ENDDO
*DO,x,2,40,1                                      !for 40 nos. of step simulations
!feed, pressure and time array definition in parametric form
*DIM,ADISPLACEMENT,ARRAY,x,1,1, , ,     !feed array
*DIM,APRESSURE,ARRAY,x,1,1, , ,                   !pressure array
*DIM,ATIME,ARRAY,x,1,1, , ,                       !time array
d%2%=0.5                                          !initial/1st load step
p%2%=0.0035
t%2%=0.05

*DO,y,2,x,1
ADISPLACEMENT(y,1,1) = d%y%     !define/edit displacement step
APRESSURE(y,1,1) = -p%y%                !define/edit pressure step
```

```
ATIME(y,1,1) = t%y%                     !define/edit time step
*ENDDO

!component creation
LSEL,S, , ,     4
NSLL,S,1
CM,TUBE_END,NODE

ASEL,S, , ,     4
ESLA,S
CM,PR_SURF,ELEM
ALLSEL,ALL                              !select all

!constraints
DL,8, ,UX,0                             !symmetric constraints-displacement and rotational on nodes
DL,8, ,ROTY,0
DL,8, ,ROTZ,0
DL,7, ,UY,0
DL,7, ,ROTX,0
DL,7, ,ROTZ,0
DL,5, ,UZ,0
DL,5, ,ROTX,0
DL,5, ,ROTY,0

!boundary conditions
EDLOAD,ADD,PRES,0,PR_SURF,ATIME,APRESSURE,0,,,,,
                                        !pressure load on tube inner surface
EDLOAD,ADD,RBUZ,0, 3,ATIME,ADISPLACEMENT,0,,,,,
                                        !displacement load on tube end plunger
EDLOAD,ADD,UZ,0,TUBE_END,ATIME,ADISPLACEMENT,0,,,,
                                        !displacement load on tube end nodes
EPLOT                                   !plot elements

!solution time control
TIME,t%x%,                              !total solution time
EDRST,100,                              !number of result file steps
EDHTIME,200,                            !number of time history file steps
EDDUMP,1,
EDINT,5,4,                              !save solution for all 5-layers for shell
EDCTS,1.5E-04,0.9,
EDOPT,ADD,BLANK,BOTH                    !results file type ansys and lsdyna
SAVE,abc%x%,db,D:\ansys-lsdyna\x-branch\  !save database
FINISH
!end of pre-processing

!SOLUTION PHASE
/SOLU
EDWRITE,ANSYS,abc,k,                    !write the lsdyna key word file
/STATUS,SOLU
SOLVE                                   !solve- start simulation

!POST-PROCESSING OF RESULTS
/POST1
INRES,ALL
FILE,abc,rst,
SET,LIST
SET,,, ,,, ,98

!calculation of minimum element thickness                (refer section 6.2.2.3, fig 6.2.22)
!sorting element with minimum thickness for tube blank
PARTSEL,'s',1, , ,                      !select part 1
AVPRIN,0, ,
ETABLE, ,NMISC, 6                       !sort element thickness result
ESORT,ETAB,NMIS6,0,0, ,
*get,elemthkmin,sort,,min
ALLSEL,ALL
```

```
!Element normal velocity calculation                    (refer section 6.2.2.3. fig 6.2.23)
!create element table data to extract element global velocities
ETABLE,vx,V,X
ETABLE,vy,V,Y
ETABLE,vz,V,Z

*DO,u,1,LX2,1                                     !total no of slice=38
*DO,w,1,z/LX2,1

!finds the node number for particular element (1st,2nd and 3rd node)
*GET,z_node1,ELEM,%w+(u-1)*LX1%,NODE,1
*GET,z_node2,ELEM,%w+(u-1)*LX1%,NODE,2
*GET,z_node3,ELEM,%w+(u-1)*LX1%,NODE,3

!finds the initial location of the nodes in the global coordinate system
*GET,XCOORDNODE%z_node1%I,NODE,z_node1,LOC,X
*GET,YCOORDNODE%z_node1%I,NODE,z_node1,LOC,Y
*GET,ZCOORDNODE%z_node1%I,NODE,z_node1,LOC,Z
*GET,XCOORDNODE%z_node2%I,NODE,z_node2,LOC,X
*GET,YCOORDNODE%z_node2%I,NODE,z_node2,LOC,Y
*GET,ZCOORDNODE%z_node2%I,NODE,z_node2,LOC,Z
*GET,XCOORDNODE%z_node3%I,NODE,z_node3,LOC,X
*GET,YCOORDNODE%z_node3%I,NODE,z_node3,LOC,Y
*GET,ZCOORDNODE%z_node3%I,NODE,z_node3,LOC,Z

!finds the relative displacement of the nodes at the end of timestep from the initial position (at time =0)
*GET,XDISPLNODE%z_node1%I,NODE,%z_node1%,U,X
*GET,YDISPLNODE%z_node1%I,NODE,%z_node1%,U,Y
*GET,ZDISPLNODE%z_node1%I,NODE,%z_node1%,U,Z

*GET,XDISPLNODE%z_node2%I,NODE,%z_node2%,U,X
*GET,YDISPLNODE%z_node2%I,NODE,%z_node2%,U,Y
*GET,ZDISPLNODE%z_node2%I,NODE,%z_node2%,U,Z
*GET,XDISPLNODE%z_node3%I,NODE,%z_node3%,U,X
*GET,YDISPLNODE%z_node3%I,NODE,%z_node3%,U,Y
*GET,ZDISPLNODE%z_node3%I,NODE,%z_node3%,U,Z

!absolute displacement of the nodes or actual position of the nodes in the global coordinate system at the end of
timestep
XC%z_node1%F=XCOORDNODE%z_node1%I + XDISPLNODE%z_node1%I          !x1
YC%z_node1%F=YCOORDNODE%z_node1%I + YDISPLNODE%z_node1%I          !y1
ZC%z_node1%F=ZCOORDNODE%z_node1%I + ZDISPLNODE%z_node1%I          !z1
XC%z_node2%F=XCOORDNODE%z_node2%I + XDISPLNODE%z_node2%I          !x2
YC%z_node2%F=YCOORDNODE%z_node2%I + YDISPLNODE%z_node2%I          !y2
ZC%z_node2%F=ZCOORDNODE%z_node2%I + ZDISPLNODE%z_node2%I          !z2
XC%z_node3%F=XCOORDNODE%z_node3%I + XDISPLNODE%z_node3%I          !x3
YC%z_node3%F=YCOORDNODE%z_node3%I + YDISPLNODE%z_node3%I          !y3
ZC%z_node3%F=ZCOORDNODE%z_node3%I + ZDISPLNODE%z_node3%I          !z3

!calculation of direction cosine of the plane containing the element with new nodal coordinates
node1(x1,y1,z1),node2(x2,y2,z2),node3(x3,y3,z3)
!vector a12=i(x2-x1) + j(y2-y1) + k(z2-z1)
!vector a13=i(x3-x1) + j(y3-y1) + k(z3-z1)
!cross product of vector a12xa13= i[(y2-y1)(z3-z1)-(y3-y1)(z2-z1)] + j[-(x2-x1)(z3-z1)+(x3-x1)(z2-z1)] + k[(x2-
x1)(y3-y1)-(x3-x1)(y2-y1)]
!IA12A13=[(y2-y1)(z3-z1)-(y3-y1)(z2-z1)]
!JA12A13=[-(x2-x1)(z3-z1)+(x3-x1)(z2-z1)]
!KA12A13=[(x2-x1)(y3-y1)-(x3-x1)(y2-y1)]

IA12A13=((YC%z_node2%F-YC%z_node1%F)*(ZC%z_node3%F-ZC%z_node1%F)-(YC%z_node3%F-
YC%z_node1%F)*(ZC%z_node2%F-ZC%z_node1%F))

JA12A13=(-(XC%z_node2%F-XC%z_node1%F)*(ZC%z_node3%F-C%z_node1%F)+(XC%z_node3%F-
XC%z_node1%F)*(ZC%z_node2%F-ZC%z_node1%F))

KA12A13=((XC%z_node2%F-XC%z_node1%F)*(YC%z_node3%F-C%z_node1%F)-(XC%z_node3%F-
XC%z_node1%F)*(YC%z_node2%F-YC%z_node1%F))
```

```
!modulus of vector a12Xa13
MODA12A13=SQRT(IA12A13*IA12A13+JA12A13*JA12A13+KA12A13*KA12A13)

!direction cosine of the plane containing the element
DCX=IA12A13/MODA12A13
DCY=JA12A13/MODA12A13
DCZ=KA12A13/MODA12A13

!extract element velocities in x,y,z directions with reference to global coordinate system
*GET,zvel_x,ELEM,%w+(u-1)*LX1%,ETAB,VX
*GET,zvel_y,ELEM,%w+(u-1)*LX1%,ETAB,VY
*GET,zvel_z,ELEM,%w+(u-1)*LX1%,ETAB,VZ

!calculation of velocity of the element in its normal direction
z_vel_norm_slice%u%(w,1,1)=(zvel_x)*(DCX)+(zvel_y)*(DCY)+(zvel_z)*(DCZ)

*set,zvel_x,                            !deletion of redundant parameters after calculation
*set,zvel_y,
*set,zvel_z,
*SET,DCX,
*SET,DCY,
*SET,DCZ,
*SET,XCOORDNODE%z_node1%I,
*SET,YCOORDNODE%z_node1%I,
*SET,ZCOORDNODE%z_node1%I,
*SET,XCOORDNODE%z_node2%I,
*SET,YCOORDNODE%z_node2%I,
*SET,ZCOORDNODE%z_node2%I,
*SET,XCOORDNODE%z_node3%I,
*SET,YCOORDNODE%z_node3%I,
*SET,ZCOORDNODE%z_node3%I,
*SET,XDISPLNODE%z_node1%I,
*SET,YDISPLNODE%z_node1%I,
*SET,ZDISPLNODE%z_node1%I,
*SET,XDISPLNODE%z_node2%I,
*SET,YDISPLNODE%z_node2%I,
*SET,ZDISPLNODE%z_node2%I,
*SET,XDISPLNODE%z_node3%I,
*SET,YDISPLNODE%z_node3%I,
*SET,ZDISPLNODE%z_node3%I,
*SET,XC%z_node1%F,
*SET,YC%z_node1%F,
*SET,ZC%z_node1%F,
*SET,XC%z_node2%F,
*SET,YC%z_node2%F,
*SET,ZC%z_node2%F,
*SET,XC%z_node3%F,
*SET,YC%z_node3%F,
*SET,ZC%z_node3%F,
*SET,IA12A13,
*SET,JA12A13,
*SET,KA12A13,
*set,z_node1,
*set,z_node2,
*set,z_node3,

!element strain difference calculation                    (refer section 6.2.2.3, fig 6.2.24)
layer,1                  !data for upper (outermost) layer of the element
ETABLE,plastic_strain1,EPPL,EQV
*GET,z_layer1_element_strain,ELEM,%w+(u-1)*LX1%,ETAB,plastic_strain1          !element plastic strain data
for element no 'w' for layer 1

layer,2                  !data for lower (innermost) layer of the element
ETABLE,plastic_strain2,EPPL,EQV
*GET,z_layer2_element_strain,ELEM,%w+(u-1)*LX1%,ETAB,plastic_strain2          !element plastic strain data
for element no 'w' for layer 2
```

```
z_strain_diff_slice%u%(w,1,1)=z_layer1_element_strain-z_layer2_element_strain

*SET,z_layer1_element_strain,
*SET,z_layer2_element_strain,

*ENDDO
*ENDDO

SAVE,abc_new%x%,db,D:\ansys-lsdyna\x-branch\
finish

!wall thinning check
THK=1.235                    !safety limit for wall thinning 1.235mm

*if,elemthkmin,LE,THK, then
SAVE,abc_new%x%,db,D:\ansys-lsdyna\x-branch\          !if element thinning is severe , then save the
                                                      database file and stop the simulation run
*ENDDO
*endif

!FUZZY LOGIC CONTROLLER/LOAD CONTROL ALGORITHM
!start of fuzzy logic controller

delta_aa=0.12                          !define critical strain difference -parameter A

!no. of elements having strain value greater than  ' delta_aa' in a slice= dj%u%
s1=8
s2=3

*DO,u,1,LX2,1                !number of slice=lx2

dj%u%=0
*DO,w,1,LX1,1

*IF,ABS(z_strain_diff_slice%u%(w,1,1)),GE,delta_aa,THEN
g%w%=1
*ELSE
g%w%=0
*ENDIF
dj%u%=dj%u%+g%w%

*SET,g%w%,
*ENDDO

*IF,dj%u%,GE,s1,THEN
                             !(case for large number of elements having strain difference greater than delta_aa)
!categories of pressure increment on element
p_v_h=5
p_h=4
p_n=3
p_l=0.5
p_v_l=-1.5
!categories of displacement increment on tube end nodes
d_v_h=2.5
d_h=1.5
d_n=1
d_l=-2

z_press=0
z_displ=0

        *DO,w,1,LX1,1

!strain mf of element no_%u%%w%
!for strain mf
s_a=-0.020
s_b=-0.0075
```

```
s_c=-0.0055
s_d=0
s_e=0.0055
s_f=0.0075
s_g=0.020

s_x=z_strain_diff_slice%u%(w,1,1)
*IF,s_x,GE,s_g,THEN
mf_convex%u%%w%=1
*ELSEIF,s_x,LE,s_e,THEN
mf_convex%u%%w%=0
*ELSE
mf_convex%u%%w%=(s_x-s_e)/(s_g-s_e)
*ENDIF
*IF,s_x,GE,s_c,THEN
mf_concave%u%%w%=0
*ELSEIF,s_x,LE,s_a,THEN
mf_concave%u%%w%=1
*ELSE
mf_concave%u%%w%=1-(s_x-s_a)/(s_c-s_a)
*ENDIF

*IF,s_x,LT,s_f,AND,s_x,GE,s_d,THEN
mf_flat%u%%w%=1-(s_x-s_d)/(s_f-s_d)
*ELSEIF,s_x,LT,s_d,AND,s_x,GT,s_b,THEN
mf_flat%u%%w%=(s_x-s_b)/(s_d-s_b)
*ELSE
mf_flat%u%%w%=0
*ENDIF

!for velocity mf
v_a=-1.5
v_b=-0.75
v_c=-0.5
v_d=0
v_e=0.5
v_f=0.75
v_g=1.5

v_x=z_vel_norm_slice%u%(w,1,1)

*IF,v_x,GE,v_g,THEN
mf_positive_high%u%%w%=1
*ELSEIF,v_x,LE,v_e,THEN
mf_positive_high%u%%w%=0
*ELSE
mf_positive_high%u%%w%=(v_x-v_e)/(v_g-v_e)
*ENDIF

*IF,v_x,GE,v_c,THEN
mf_negative_high%u%%w%=0
*ELSEIF,v_x,LE,v_a,THEN
mf_negative_high%u%%w%=1
*ELSE
mf_negative_high%u%%w%=1-(v_x-v_a)/(v_c-v_a)
*ENDIF

*IF,v_x,LT,v_f,AND,v_x,GE,v_d,THEN
mf_medium%u%%w%=1-(v_x-v_d)/(v_f-v_d)
*ELSEIF,v_x,LT,v_d,AND,v_x,GT,v_b,THEN
mf_medium%u%%w%=(v_x-v_b)/(v_d-v_b)
*ELSE
mf_medium%u%%w%=0
*ENDIF
                  !rule1-if strain is 'concave' and velocity is 'negative_high' then pressure is 'p_high_high' and displ is
                  'd_low'
                  mf_strain1%u%%w%=mf_concave%u%%w%
```

```
mf_vel1%u%%w%=mf_negative_high%u%%w%
*if,mf_strain1%u%%w%,LE,mf_vel1%u%%w%,then
mf_rule1=mf_strain1%u%%w%
*else
mf_rule1=mf_vel1%u%%w%
*endif

!rule2-if strain is 'flat' and velocity is 'negative_high' then pressure is 'p_high' and displ is 'd_normal'
mf_strain2%u%%w%=mf_flat%u%%w%
mf_vel2%u%%w%=mf_negative_high%u%%w%

*if,mf_strain2%u%%w%,LE,mf_vel2%u%%w%,then
mf_rule2=mf_strain2%u%%w%
*else
mf_rule2=mf_vel2%u%%w%
*endif

!rule3-if strain is 'convex' and velocity is 'negative_high' then pressure is 'p_normal' and displ is 'd_normal'
mf_strain3%u%%w%=mf_convex%u%%w%
mf_vel3%u%%w%=mf_negative_high%u%%w%

*if,mf_strain3%u%%w%,LE,mf_vel3%u%%w%,then
mf_rule3=mf_strain3%u%%w%
*else
mf_rule3=mf_vel3%u%%w%
*endif

!rule4-if strain is 'concave' and velocity is 'medium' then pressure is 'p_high' and displ is 'd_high'
mf_strain4%u%%w%=mf_concave%u%%w%
mf_vel4%u%%w%=mf_medium%u%%w%

*if,mf_strain4%u%%w%,LE,mf_vel4%u%%w%,then
mf_rule4=mf_strain4%u%%w%
*else
mf_rule4=mf_vel4%u%%w%
*endif

!rule5-if strain is 'flat' and velocity is 'medium' then pressure is 'p_normal' and displ is 'd_high_high'
mf_strain5%u%%w%=mf_flat%u%%w%
mf_vel5%u%%w%=mf_medium%u%%w%

*if,mf_strain5%u%%w%,LE,mf_vel5%u%%w%,then
mf_rule5=mf_strain5%u%%w%
*else
mf_rule5=mf_vel5%u%%w%
*endif

!rule6-if strain is 'convex' and velocity is 'medium' then pressure is 'p_low' and displ is 'd_high'
mf_strain6%u%%w%=mf_convex%u%%w%
mf_vel6%u%%w%=mf_medium%u%%w%

*if,mf_strain6%u%%w%,LE,mf_vel6%u%%w%,then
mf_rule6=mf_strain6%u%%w%
*else
mf_rule6=mf_vel6%u%%w%
*endif

!rule7-if strain is 'concave' and velocity is 'positive_high' then pressure is 'p_normal' and displ is 'd_normal'
mf_strain7%u%%w%=mf_concave%u%%w%
mf_vel7%u%%w%=mf_positive_high%u%%w%

*if,mf_strain7%u%%w%,LE,mf_vel7%u%%w%,then
mf_rule7=mf_strain7%u%%w%
```

```
                *else
                mf_rule7=mf_vel7%u%%w%
                *endif

                !rule8-if strain is 'flat' and velocity is 'positive_high' then pressure is 'p_low' and displ is 'd_normal'
                mf_strain8%u%%w%=mf_flat%u%%w%
                mf_vel8%u%%w%=mf_positive_high%u%%w%

                *if,mf_strain8%u%%w%,LE,mf_vel8%u%%w%,then
                mf_rule8=mf_strain8%u%%w%
                *else
                mf_rule8=mf_vel8%u%%w%
                *endif

                !rule9-if strain is 'convex' and velocity is 'positive_high' then pressure is 'p_low_low' and displ is 'd_low'
                mf_strain9%u%%w%=mf_convex%u%%w%
                mf_vel9%u%%w%=mf_positive_high%u%%w%
                *if,mf_strain9%u%%w%,LE,mf_vel9%u%%w%,then
                mf_rule9=mf_strain9%u%%w%
                *else
                mf_rule9=mf_vel9%u%%w%
                *endif

mf_p_v_h=SQRT(mf_rule1**2)
mf_p_h=SQRT(mf_rule2**2+mf_rule4**2)
mf_p_n=SQRT(mf_rule3**2+mf_rule5**2+mf_rule7**2)
mf_p_l=SQRT(mf_rule6**2+mf_rule8**2)
mf_p_v_l=SQRT(mf_rule9**2)

mf_d_v_h=SQRT(mf_rule5**2)
mf_d_h=SQRT(mf_rule4**2+mf_rule6**2)
mf_d_n=SQRT(mf_rule2**2+mf_rule3**2+mf_rule7**2+mf_rule8**2)
mf_d_l=SQRT(mf_rule1**2+mf_rule9**2)

press%u%%w%=(p_v_h*mf_p_v_h+p_h*mf_p_h+p_n*mf_p_n+p_l*mf_p_l+p_v_l*mf_p_v_l)/(mf_p_v_h+mf_p_h+mf_p_n+mf_p_l+mf_p_v_l)
displ%u%%w%=(d_v_h*mf_d_v_h+d_h*mf_d_h+d_n*mf_d_n+d_l*mf_d_l)/(mf_d_v_h+mf_d_h+mf_d_n+mf_d_l)

z_press=z_press+press%u%%w%
z_displ=z_displ+displ%u%%w%
*SET,mf_convex%u%%w%,
*SET,mf_flat%u%%w%,
*SET,mf_concave%u%%w%,
*SET,mf_positive_high%u%%w%,
*SET,mf_medium%u%%w%,
*SET,mf_negative_high%u%%w%,
*SET,press%u%%w%,
*SET,displ%u%%w%,

*DO,P,1,9,1
*SET,mf_strain%P%%u%%w%,
*ENDDO

*DO,P,1,9,1
*SET,mf_vel%P%%u%%w%,
*ENDDO

*DO,P,1,9,1
*SET,mf_rule%P%,
*ENDDO

*SET,mf_p_v_h,
*SET,mf_p_h,
*SET,mf_p_n,
*SET,mf_p_l,
*SET,mf_p_v_l,
```

```
*SET,mf_d_v_h,
*SET,mf_d_h,
*SET,mf_d_n,
*SET,mf_d_l,

        *ENDDO

press%u%=z_press/LX1
displ%u%=z_displ/LX1

*SET,p_v_h,
*SET,p_h,
*SET,p_n,
*SET,p_l,
*SET,p_v_l,
*SET,d_v_h,
*SET,d_h,
*SET,d_n,
*SET,d_l,
*SET,z_press,
*SET,z_displ,

*ELSEIF,dj%u%,LE,s2,THEN
                                                   !(case for few no. of elements having strain difference greater than delta_aa)
!categories of pressure increment on element
p_v_h=5
p_h=4
p_n=3
p_l=1.5
p_v_l=0
!categories of displacement increment on tube end nodes
d_v_h=3
d_h=2
d_n=1
d_l=0
z_press=0
z_displ=0

        *DO,w,1,LX1,1
!strain mf of element no_%u%%w%
!for strain mf
s_a=-0.085
s_b=-0.055
s_c=-0.025
s_d=0
s_e=0.025
s_f=0.055
s_g=0.085

s_x=z_strain_diff_slice%u%(w,1,1)

*IF,s_x,GE,s_g,THEN
mf_convex%u%%w%=1
*ELSEIF,s_x,LE,s_e,THEN
mf_convex%u%%w%=0
*ELSE
mf_convex%u%%w%=(s_x-s_e)/(s_g-s_e)
*ENDIF

*IF,s_x,GE,s_c,THEN
mf_concave%u%%w%=0
*ELSEIF,s_x,LE,s_a,THEN
mf_concave%u%%w%=1
*ELSE
mf_concave%u%%w%=1-(s_x-s_a)/(s_c-s_a)
*ENDIF
```

```
*IF,s_x,LT,s_f,AND,s_x,GE,s_d,THEN
mf_flat%u%%w%=1-(s_x-s_d)/(s_f-s_d)
*ELSEIF,s_x,LT,s_d,AND,s_x,GT,s_b,THEN
mf_flat%u%%w%=(s_x-s_b)/(s_d-s_b)
*ELSE
mf_flat%u%%w%=0
*ENDIF

!for velocity mf
v_a=-4.5
v_b=-2.5
v_c=-1
v_d=1
v_e=3
v_f=4.5
v_g=6.5

v_x=z_vel_norm_slice%u%(w,1,1)
*IF,v_x,GE,v_g,THEN
mf_positive_high%u%%w%=1
*ELSEIF,v_x,LE,v_e,THEN
mf_positive_high%u%%w%=0
*ELSE
mf_positive_high%u%%w%=(v_x-v_e)/(v_g-v_e)
*ENDIF

*IF,v_x,GE,v_c,THEN
mf_negative_high%u%%w%=0
*ELSEIF,v_x,LE,v_a,THEN
mf_negative_high%u%%w%=1
*ELSE
mf_negative_high%u%%w%=1-(v_x-v_a)/(v_c-v_a)
*ENDIF

*IF,v_x,LT,v_f,AND,v_x,GE,v_d,THEN
mf_medium%u%%w%=1-(v_x-v_d)/(v_f-v_d)
*ELSEIF,v_x,LT,v_d,AND,v_x,GT,v_b,THEN
mf_medium%u%%w%=(v_x-v_b)/(v_d-v_b)
*ELSE
mf_medium%u%%w%=0
*ENDIF

            !rule1-if strain is 'concave' and velocity is 'negative_high' then pressure is 'p_high_high' and displ is
            'd_low'
            mf_strain1%u%%w%=mf_concave%u%%w%
            mf_vel1%u%%w%=mf_negative_high%u%%w%

            *if,mf_strain1%u%%w%,LE,mf_vel1%u%%w%,then
            mf_rule1=mf_strain1%u%%w%
            *else
            mf_rule1=mf_vel1%u%%w%
            *endif

            !rule2-if strain is 'flat' and velocity is 'negative_high' then pressure is 'p_high' and displ is
            'd_normal'
            mf_strain2%u%%w%=mf_flat%u%%w%
            mf_vel2%u%%w%=mf_negative_high%u%%w%

            *if,mf_strain2%u%%w%,LE,mf_vel2%u%%w%,then
            mf_rule2=mf_strain2%u%%w%
            *else
            mf_rule2=mf_vel2%u%%w%
            *endif

            !rule3-if strain is 'convex' and velocity is 'negative_high' then pressure is 'p_normal' and displ is
            'd_normal'
            mf_strain3%u%%w%=mf_convex%u%%w%
```

```
mf_vel3%u%%w%=mf_negative_high%u%%w%

*if,mf_strain3%u%%w%,LE,mf_vel3%u%%w%,then
mf_rule3=mf_strain3%u%%w%
*else
mf_rule3=mf_vel3%u%%w%
*endif

!rule4-if strain is 'concave' and velocity is 'medium' then pressure is 'p_high' and displ is 'd_high'
mf_strain4%u%%w%=mf_concave%u%%w%
mf_vel4%u%%w%=mf_medium%u%%w%

*if,mf_strain4%u%%w%,LE,mf_vel4%u%%w%,then
mf_rule4=mf_strain4%u%%w%
*else
mf_rule4=mf_vel4%u%%w%
*endif

!rule5-if strain is 'flat' and velocity is 'medium' then pressure is 'p_normal' and displ is
'd_high_high'
mf_strain5%u%%w%=mf_flat%u%%w%
mf_vel5%u%%w%=mf_medium%u%%w%

*if,mf_strain5%u%%w%,LE,mf_vel5%u%%w%,then
mf_rule5=mf_strain5%u%%w%
*else
mf_rule5=mf_vel5%u%%w%
*endif

!rule6-if strain is 'convex' and velocity is 'medium' then pressure is 'p_low' and displ is 'd_high'
mf_strain6%u%%w%=mf_convex%u%%w%
mf_vel6%u%%w%=mf_medium%u%%w%

*if,mf_strain6%u%%w%,LE,mf_vel6%u%%w%,then
mf_rule6=mf_strain6%u%%w%
*else
mf_rule6=mf_vel6%u%%w%
*endif

!rule7-if strain is 'concave' and velocity is 'positive_high' then pressure is 'p_normal' and displ is
'd_normal'
mf_strain7%u%%w%=mf_concave%u%%w%
mf_vel7%u%%w%=mf_positive_high%u%%w%
*if,mf_strain7%u%%w%,LE,mf_vel7%u%%w%,then
mf_rule7=mf_strain7%u%%w%
*else
mf_rule7=mf_vel7%u%%w%
*endif

!rule8-if strain is 'flat' and velocity is 'positive_high' then pressure is 'p_low' and displ is 'd_normal'
mf_strain8%u%%w%=mf_flat%u%%w%
mf_vel8%u%%w%=mf_positive_high%u%%w%

*if,mf_strain8%u%%w%,LE,mf_vel8%u%%w%,then
mf_rule8=mf_strain8%u%%w%
*else
mf_rule8=mf_vel8%u%%w%
*endif

!rule9-if strain is 'convex' and velocity is 'positive_high' then pressure is 'p_low_low' and displ is
'd_low'
mf_strain9%u%%w%=mf_convex%u%%w%
mf_vel9%u%%w%=mf_positive_high%u%%w%

*if,mf_strain9%u%%w%,LE,mf_vel9%u%%w%,then
mf_rule9=mf_strain9%u%%w%
*else
```

```
                    mf_rule9=mf_vel9%u%%w%
                    *endif

mf_p_v_h=SQRT(mf_rule1**2)
mf_p_h=SQRT(mf_rule2**2+mf_rule4**2)
mf_p_n=SQRT(mf_rule3**2+mf_rule5**2+mf_rule7**2)
mf_p_l=SQRT(mf_rule6**2+mf_rule8**2)
mf_p_v_l=SQRT(mf_rule9**2)

mf_d_v_h=SQRT(mf_rule5**2)
mf_d_h=SQRT(mf_rule4**2+mf_rule6**2)
mf_d_n=SQRT(mf_rule2**2+mf_rule3**2+mf_rule7**2+mf_rule8**2)
mf_d_l=SQRT(mf_rule1**2+mf_rule9**2)

press%u%%w%=(p_v_h*mf_p_v_h+p_h*mf_p_h+p_n*mf_p_n+p_l*mf_p_l+p_v_l*mf_p_v_l)/(mf_p_v_h+mf_p_h+
mf_p_n+mf_p_l+mf_p_v_l)
displ%u%%w%=(d_v_h*mf_d_v_h+d_h*mf_d_h+d_n*mf_d_n+d_l*mf_d_l)/(mf_d_v_h+mf_d_h+mf_d_n+mf_d_l)

z_press=z_press+press%u%%w%
z_displ=z_displ+displ%u%%w%

*SET,mf_convex%u%%w%,
*SET,mf_flat%u%%w%,
*SET,mf_concave%u%%w%,
*SET,mf_positive_high%u%%w%,
*SET,mf_medium%u%%w%,
*SET,mf_negative_high%u%%w%,
*SET,press%u%%w%,
*SET,displ%u%%w%,

*DO,P,1,9,1
*SET,mf_strain%P%%u%%w%,
*ENDDO

*DO,P,1,9,1
*SET,mf_vel%P%%u%%w%,
*ENDDO

*DO,P,1,9,1
*SET,mf_rule%P%,
*ENDDO

*SET,mf_p_v_h,
*SET,mf_p_h,
*SET,mf_p_n,
*SET,mf_p_l,
*SET,mf_p_v_l,
*SET,mf_d_v_h,
*SET,mf_d_h,
*SET,mf_d_n,
*SET,mf_d_l,
        *ENDDO

press%u%=z_press/LX1
displ%u%=z_displ/LX1

*SET,p_v_h,
*SET,p_h,
*SET,p_n,
*SET,p_l,
*SET,p_v_l,
*SET,d_v_h,
*SET,d_h,
*SET,d_n,
*SET,d_l,
*SET,z_press,
*SET,z_displ,
```

```
*ELSE

            !IF,dj%u%,LT,s1,AND,dj%u%,GT,s2,THEN (case for medium number of elements having strain difference
            greater than delta_aa)
!categories of pressure increment on element
p_v_h=5
p_h=4
p_n=3
p_l=0
p_v_l=-0.5
!categories of displacement increment on tube end nodes
d_v_h=3
d_h=2
d_n=1
d_l=-1

z_press=0
z_displ=0

            *DO,w,1,LX1,1

!strain mf of element no_%u%%w%
!for strain mf
s_a=-0.05
s_b=-0.03
s_c=-0.01
s_d=0
s_e=0.01
s_f=0.03
s_g=0.05

s_x=z_strain_diff_slice%u%(w,1,1)

*IF,s_x,GE,s_g,THEN
mf_convex%u%%w%=1
*ELSEIF,s_x,LE,s_e,THEN
mf_convex%u%%w%=0
*ELSE
mf_convex%u%%w%=(s_x-s_e)/(s_g-s_e)
*ENDIF

*IF,s_x,GE,s_c,THEN
mf_concave%u%%w%=0
*ELSEIF,s_x,LE,s_a,THEN
mf_concave%u%%w%=1
*ELSE
mf_concave%u%%w%=1-(s_x-s_a)/(s_c-s_a)
*ENDIF

*IF,s_x,LT,s_f,AND,s_x,GE,s_d,THEN
mf_flat%u%%w%=1-(s_x-s_d)/(s_f-s_d)
*ELSEIF,s_x,LT,s_d,AND,s_x,GT,s_b,THEN
mf_flat%u%%w%=(s_x-s_b)/(s_d-s_b)
*ELSE
mf_flat%u%%w%=0
*ENDIF

!for velocity mf
v_a=-2.5
v_b=-1.5
v_c=-0.5
v_d=0.5
v_e=1.5
v_f=2.5
v_g=3.5
v_x=z_vel_norm_slice%u%(w,1,1)
```

```
*IF,v_x,GE,v_g,THEN
mf_positive_high%u%%w%=1
*ELSEIF,v_x,LE,v_e,THEN
mf_positive_high%u%%w%=0
*ELSE
mf_positive_high%u%%w%=(v_x-v_e)/(v_g-v_e)
*ENDIF

*IF,v_x,GE,v_c,THEN
mf_negative_high%u%%w%=0
*ELSEIF,v_x,LE,v_a,THEN
mf_negative_high%u%%w%=1
*ELSE
mf_negative_high%u%%w%=1-(v_x-v_a)/(v_c-v_a)
*ENDIF

*IF,v_x,LT,v_f,AND,v_x,GE,v_d,THEN
mf_medium%u%%w%=1-(v_x-v_d)/(v_f-v_d)
*ELSEIF,v_x,LT,v_d,AND,v_x,GT,v_b,THEN
mf_medium%u%%w%=(v_x-v_b)/(v_d-v_b)
*ELSE
mf_medium%u%%w%=0
*ENDIF
```

```
!rule1-if strain is 'concave' and velocity is 'negative_high' then pressure is 'p_high_high' and displ is 'd_low'
mf_strain1%u%%w%=mf_concave%u%%w%
mf_vel1%u%%w%=mf_negative_high%u%%w%

*if,mf_strain1%u%%w%,LE,mf_vel1%u%%w%,then
mf_rule1=mf_strain1%u%%w%
*else
mf_rule1=mf_vel1%u%%w%
*endif

!rule2-if strain is 'flat' and velocity is 'negative_high' then pressure is 'p_high' and displ is 'd_normal'
mf_strain2%u%%w%=mf_flat%u%%w%
mf_vel2%u%%w%=mf_negative_high%u%%w%
*if,mf_strain2%u%%w%,LE,mf_vel2%u%%w%,then
mf_rule2=mf_strain2%u%%w%
*else
mf_rule2=mf_vel2%u%%w%
*endif

!rule3-if strain is 'convex' and velocity is 'negative_high' then pressure is 'p_normal' and displ is 'd_normal'
mf_strain3%u%%w%=mf_convex%u%%w%
mf_vel3%u%%w%=mf_negative_high%u%%w%

*if,mf_strain3%u%%w%,LE,mf_vel3%u%%w%,then
mf_rule3=mf_strain3%u%%w%
*else
mf_rule3=mf_vel3%u%%w%
*endif

!rule4-if strain is 'concave' and velocity is 'medium' then pressure is 'p_high' and displ is 'd_high'
mf_strain4%u%%w%=mf_concave%u%%w%
mf_vel4%u%%w%=mf_medium%u%%w%

*if,mf_strain4%u%%w%,LE,mf_vel4%u%%w%,then
mf_rule4=mf_strain4%u%%w%
*else
mf_rule4=mf_vel4%u%%w%
*endif
```

```
                    !rule5-if strain is 'flat' and velocity is 'medium' then pressure is 'p_normal' and displ is
                    'd_high_high'
                    mf_strain5%u%%w%=mf_flat%u%%w%
                    mf_vel5%u%%w%=mf_medium%u%%w%

                    *if,mf_strain5%u%%w%,LE,mf_vel5%u%%w%,then
                    mf_rule5=mf_strain5%u%%w%
                    *else
                    mf_rule5=mf_vel5%u%%w%
                    *endif

                    !rule6-if strain is 'convex' and velocity is 'medium' then pressure is 'p_low' and displ is 'd_high'
                    mf_strain6%u%%w%=mf_convex%u%%w%
                    mf_vel6%u%%w%=mf_medium%u%%w%

                    *if,mf_strain6%u%%w%,LE,mf_vel6%u%%w%,then
                    mf_rule6=mf_strain6%u%%w%
                    *else
                    mf_rule6=mf_vel6%u%%w%
                    *endif

                    !rule7-if strain is 'concave' and velocity is 'positive_high' then pressure is 'p_normal' and displ is
                    'd_normal'
                    mf_strain7%u%%w%=mf_concave%u%%w%
                    mf_vel7%u%%w%=mf_positive_high%u%%w%

                    *if,mf_strain7%u%%w%,LE,mf_vel7%u%%w%,then
                    mf_rule7=mf_strain7%u%%w%
                    *else
                    mf_rule7=mf_vel7%u%%w%
                    *endif
                    !rule8-if strain is 'flat' and velocity is 'positive_high' then pressure is 'p_low' and displ is 'd_normal'
                    mf_strain8%u%%w%=mf_flat%u%%w%
                    mf_vel8%u%%w%=mf_positive_high%u%%w%

                    *if,mf_strain8%u%%w%,LE,mf_vel8%u%%w%,then
                    mf_rule8=mf_strain8%u%%w%
                    *else
                    mf_rule8=mf_vel8%u%%w%
                    *endif

                    !rule9-if strain is 'convex' and velocity is 'positive_high' then pressure is 'p_low_low' and displ is
                    'd_low'
                    mf_strain9%u%%w%=mf_convex%u%%w%
                    mf_vel9%u%%w%=mf_positive_high%u%%w%

                    *if,mf_strain9%u%%w%,LE,mf_vel9%u%%w%,then
                    mf_rule9=mf_strain9%u%%w%
                    *else
                    mf_rule9=mf_vel9%u%%w%
                    *endif

mf_p_v_h=SQRT(mf_rule1**2)
mf_p_h=SQRT(mf_rule2**2+mf_rule4**2)
mf_p_n=SQRT(mf_rule3**2+mf_rule5**2+mf_rule7**2)
mf_p_l=SQRT(mf_rule6**2+mf_rule8**2)
mf_p_v_l=SQRT(mf_rule9**2)

mf_d_v_h=SQRT(mf_rule5**2)
mf_d_h=SQRT(mf_rule4**2+mf_rule6**2)
mf_d_n=SQRT(mf_rule2**2+mf_rule3**2+mf_rule7**2+mf_rule8**2)
mf_d_l=SQRT(mf_rule1**2+mf_rule9**2)

press%u%%w%=(p_v_h*mf_p_v_h+p_h*mf_p_h+p_n*mf_p_n+p_l*mf_p_l+p_v_l*mf_p_v_l)/(mf_p_v_h+mf_p_h+
mf_p_n+mf_p_l+mf_p_v_l)
displ%u%%w%=(d_v_h*mf_d_v_h+d_h*mf_d_h+d_n*mf_d_n+d_l*mf_d_l)/(mf_d_v_h+mf_d_h+mf_d_n+mf_d_l)
```

```
z_press=z_press+press%u%%w%
z_displ=z_displ+displ%u%%w%

*SET,mf_convex%u%%w%,
*SET,mf_flat%u%%w%,
*SET,mf_concave%u%%w%,
*SET,mf_positive_high%u%%w%,
*SET,mf_medium%u%%w%,
*SET,mf_negative_high%u%%w%,
*SET,press%u%%w%,
*SET,displ%u%%w%,

*DO,P,1,9,1
*SET,mf_strain%P%%u%%w%,
*ENDDO

*DO,P,1,9,1
*SET,mf_vel%P%%u%%w%,
*ENDDO
*DO,P,1,9,1
*SET,mf_rule%P%,
*ENDDO

*SET,mf_p_v_h,
*SET,mf_p_h,
*SET,mf_p_n,
*SET,mf_p_l,
*SET,mf_p_v_l,
*SET,mf_d_v_h,
*SET,mf_d_h,
*SET,mf_d_n,
*SET,mf_d_l,

         *ENDDO
press%u%=z_press/LX1
displ%u%=z_displ/LX1
*SET,p_v_h,
*SET,p_h,
*SET,p_n,
*SET,p_l,
*SET,p_v_l,
*SET,d_v_h,
*SET,d_h,
*SET,d_n,
*SET,d_l,
*SET,z_press,
*SET,z_displ,

*ENDIF
*SET,dj%u%,

*ENDDO

*DO,u,1,LX2,1

*IF,displ%u%,LE,0,THEN
         displ%u%=0
*ELSE
         displ%u%=displ%u%
*ENDIF
*ENDDO

!sorting the minimum for feed and pressure
*do,u,1,LX2-1,1

*if,displ%u%,LE,displ%u+1%,then
displ%u+1%=displ%u%
```

```
*else
displ%u+1%=displ%u+1%
*endif

*if,press%u%,LE,press%u+1%,then
press%u+1%=press%u%
*else
press%u+1%=press%u+1%
*endif

displ_min=displ%u+1%
press_min=press%u+1%

*enddo

*do,u,1,LX2,1
*set,displ%u%,
*set,press%u%,
*enddo

/PREP7
z_d=displ_min
z_p=press_min
d%x+1%=d%x% + z_d*0.18
p%x+1%=p%x% + z_p*0.00042
t%x+1%=t%x%+0.05

*DEL,,3
*DEL,,2
*DEL,,1

*ENDDO
finish
```

Appendix: D

List of Publications

[1] P. Ray and B.J. MacDonald, Determination of the optimal load path for tube hydroforming processes using a fuzzy load control algorithm and finite element analysis, in: Finite Elements in Analysis and Design, Volume 41, Issue 2, November 2004, Pages 173-192

[2] P.Ray , B.J.MacDonald, Intelligent control of tube hydroforming processes using finite element analysis in: Proc. of 8th International Conference on Numerical Methods in Industrial Forming Processes (Materials Processing and Design: Modeling, Simulation and Applications NUMIFORM 2004 -Columbus Ohio, U.S.A)

[3] P.Ray , B.J.MacDonald, An Overview of Finite Element Simulation of Hydroforming Processes, Proc. of International Conference on –Advances in Materials and Processing Technologies, Dublin, Ireland (2003), Vol.1, 433-436

[4] P.Ray , B.J.MacDonald, Optimisation of Process Parameters of Tube Hydroforming Processes using Fuzzy Logic & Finite Element Analysis, Proc. of International Conference on –Advances in Materials and Processing Technologies, Dublin, Ireland(2003), Vol.1, 437-440